

Hybridisation of High Penetration Photovoltaic, Anaerobic Digestion Biogas Power Plant and Electrical Energy Storage

Thesis submitted for the degree of Doctor of Philosophy

Department of Engineering Science, University of Oxford

Chun Sing Lai

St Cross College

Supervisor: Professor Malcolm D. McCulloch

Trinity Term 2017

Contents

List of mnemonics, abbreviations and acronyms ..... **vi**

List of Figures ..... **xvi**

List of Tables ..... **xxi**

Abstract ..... **xxiii**

Acknowledgements ..... **xxiv**

1 Introduction **1**

1.1 Why renewable energy? The challenge to reduce carbon dioxide emissions 2

1.1.1 Why solar PV? The motivation and obstacles 6

1.2 Research context and scope 10

1.3 Mechanism to relieve the issues: Electrical energy storage 13

1.4 Thesis roadmap 14

1.5 Novelty and knowledge contribution 18

2 Literature review **20**

2.1 PV system global development 20

2.1.1 U.S.A 22

2.1.2 China 22

2.1.3 India 23

2.1.4 Australia 24

2.1.5 Germany 24

2.1.6 Japan 24

2.2 Application and selection of EES for PV system 27

2.2.1 EES costs 27
2.2.2 Grid storage growth 28
2.3 Overview of different EES for PV system 32
2.3.1 Redox flow battery 32
2.3.2 Lead-acid battery 33
2.3.3 Lithium-ion (Li-ion) battery 34
2.3.4 Sodium-Sulphur (NaS) battery 34
2.3.5 Nickel-Cadmium (Ni-Cd) battery 34
2.4 Research gaps 36
2.4.1 LCOE for solar PV and electrical energy storage 36
2.4.2 Clearness Index cluster analysis for PV system sizing 45
2.4.3 Efficient method for PV-AD-EES system sizing 47
2.4.4 Operating regime for PV-AD-EES system and EES degradation costs analysis 52
2.5 Summary 58
3 Levelized cost of electricity for solar photovoltaic and electrical energy storage 60
3.1 Levelized cost of electricity for solar PV 61
3.2 Cost calculation methodology 62
3.2.1 Electrical energy storage 65
3.2.2 Solar PV and storage system 67
3.3 Case studies 67
3.3.1 Data acquisition 67
3.3.2 Cost and asset specification 70
3.3.3 Marginal levelized cost of electricity 70
3.3.4 LCOD and $\mathrm{LCOE_{System}}$ for VRB and Li-ion battery 76
3.4 Summary 79

4 Daily Clearness Index profiles cluster analysis 80

4.1 Clearness Index development 81

4.1.1 Clear-sky solar irradiance model 81

4.1.2 Clearness Index 82

4.2 Clustering methods 85

4.2.1 Distribution-based clustering 85

4.2.2 Partition-based clustering 86

4.2.3 Comparison of computational complexities 90

4.3 Cluster analysis and discussions 91

4.3.1 Clustering of daily Clearness Index profiles 91

4.3.2 Fuzzy decision making 93

4.3.3 Reduction of clusters with centroid evaluation 98

4.3.4 Centroids comparison with real-life CI profiles 104

4.4 Clearness Index and weather conditions analysis 107

4.5 Summary 111

5 Hybrid system sizing 112

5.1 Optimal sizing problem 113

5.2 Comparison of optimisation methods 114

5.3 Hybrid system sizing with the complete solar irradiance dataset 119

5.3.1 Sizing of solar panels 121

5.3.2 Sizing of storage 125

5.3.3 Sizing of inverter and solar charge controller 127

5.4 Hybrid system sizing with the cluster dataset 128

5.4.1 Sizing of solar panels 132

5.4.2 Sizing of storage 135

5.5 Levelized cost of electricity 137
5.5.1 Levelized cost of electricity for system 138
5.5.2 Cost analysis for PV hybrid and AD-only systems 139
5.6 Summary 141
6 Operating regime and EES degradation cost analyses 142
6.1 Problem context and operating regime 142
6.1.1 Problem context 142
6.1.2 Operating regime 144
6.1.3 Case study 147
6.2 Operational cost models for AD and EES 149
6.2.1 AD operational cost model 150
6.2.2 $LiCoO_2$ degradation cost model and number of replacements 151
6.3 Levelized cost of electricity 156
6.3.1 LCOE for PV 156
6.3.2 LCOE for AD 157
6.3.3 LCOS 158
6.3.4 LCOD 158
6.3.5 LCOE for system 159
6.4 LCOE analyses and discussion 160
6.4.1 Levelized cost for system components 160
6.4.2 EES capital costs sensitivity analysis 162
6.4.3 LCOE with PV and EES capacity variation 163
6.5 Summary 164
7 Conclusions and future work 165
7.1 Research novelty 165

7.2 Future research areas 166

7.3 Publications 168

References 170

List of mnemonics, abbreviations and acronyms

$\Delta\mathrm{SOC}$	Change in State of Charge (%)
Δh	Hour interval (hr)
η_{EES}	EES round-trip efficiency (%)
σ	PV array efficiency (%)
ε	Solar irradiance (Wm^{-2})
ε_{c}	Correction factor to mean solar distance
γ_{s}	Solar altitude angle (degrees)
δ_{r}	Rayleigh optical depth
δ	Solar declination angle (degrees)
ϕ	Latitude (degrees)
ω	Solar hour angle (degrees)
μ_i	Mean vector for component i
μ_{fuzz}	Normalized membership for each solution
Σ_i	Covariance matrices for component i
a, b, c	Quadratic fuel cost function constants for biogas generator
a_{ees}	Parameter for the capacity fade model
AD	Anaerobic Digestion
B	Expected value of the log likelihood function
$C_{\mathrm{AD_{Fuel}}}$	Fuel cost for biogas generator ($)
$C_{\mathrm{AD_{Labour}}}$	Labour cost for operating the biogas power plant (0.05 $/kWh)
C_{Asset}	Net present value of asset, i.e., PV, AD, EES, solar charge controller or inverter ($)

$C_{\mathrm{Asset}_{\mathrm{O\&M}_{\mathrm{Fixed}}}}$	Fixed operation and maintenance cost for asset, i.e., AD, PV and EES ($/kW)
$C_{\mathrm{Asset}_{\mathrm{O\&M}_{\mathrm{Total}}}}$	Total O&M cost for asset, i.e., AD, PV, EES, solar charge controller and inverter ($)
$C_{\mathrm{Asset}_{\mathrm{O\&M}_{\mathrm{Var}}}}$	Variable operation and maintenance cost for asset, i.e., AD or EES ($/kWh)
$C_{\mathrm{Asset}_{\mathrm{Storetotal}}}$	Net present value of electricity production from asset, i.e., AD or PV to be stored in EES ($)
$C_{\mathrm{Cap}_{\mathrm{Asset}}}$	Capital cost for asset, i.e., AD, PV, EES, solar charge controller and inverter (Unit is asset dependent)
$C_{\mathrm{Case}(k)_t}$	Cost for the PV array for Case *k*, year t ($)
C_{Direct_t}	Costs for generating electricity for direct consumption ($)
C_{EES}	Net present value of electrical energy storage ($)
$C_{\mathrm{EES}_{\mathrm{Replacement}}}$	Replacement cost per discharge cycle ($)
$C_{\mathrm{EES}_{\mathrm{DegkWh}}}$	EES degradation cost due to energy discharge ($)
C_{Gas}	AD gas cost (6.97 $/mcf)
C_{In_t}	Cost for delivering the PV power into EES at year *t* ($)
$C_{\mathrm{Inst}_{\mathrm{Asset}}}$	Installation cost for asset, i.e., PV, solar charge controller, and inverter (Unit is asset dependent)
$C_{\mathrm{O\&M}_{\mathrm{Asset}}}$	Operation and maintenance cost for asset, i.e., AD, PV, EES, solar charge controller and inverter (Unit is asset dependent)
$C_{\mathrm{O\&M}_{\mathrm{PVpro}}}$	Operation and maintenance cost for PV per hour ($/hr)
C_{PVdirect}	Net present value of PV generation for direct consumption ($)
$C_{\mathrm{PVsurplus}}$	Net present value of PV generation for storage ($)

C_{Storage_t}	The combined capital, operation and maintenance costs for electrical energy storage at year t (\$)
C_{Surplus_t}	Combined costs, i.e., capital and O&M costs for generating surplus electrical energy at year t (\$)
C_{System_t}	Cost of the hybrid system at year t (\$)
C_t	Cost at year t (\$)
$C_{\text{Total}_{\text{case(k)}}}$	Net present value of the system for Case k (\$)
CC	Computational Complexity
CF	Capacity Factor (%)
CF	Net cash flow (\$)
CHP	Combined Heat and Power
CI	Clearness Index
CSP	Concentrated Solar Power
d	Dimension of Clearness Index vector
D	Distance metric function
d_{CHP}	Degradation rate for CHP (%)
d_{ees} , e_{ees} and f_{ees}	Three-parameter equation constants for EES rated cycle-life at deep discharges
d_{EES}	Degradation rate for EES (%)
d_{PV}	Degradation rate for PV (%)
D_{Total}	Total intra-cluster distance
DBA	Dynamic Time Warping Barycentre Averaging
DOD	Depth of Discharge (%)
DTW	Dynamic Time Warping

$E_{\mathrm{Asset}_{\mathrm{Directtotal}}}$	Net present value of electricity produced by asset, i.e., AD or PV for direct consumption (kWh)
E_{AD}	Electricity production of biogas generator (MWh)
$E_{\mathrm{AD}_{\mathrm{Total}}}$	Net present value of electricity production of biogas generator (kWh)
$E_{\mathrm{Case}(k)_t}$	Electricity production from the PV array for Case *k*, year t (MWh)
E_{Deficit}	Deficit energy in the hybrid system (MWh)
E_{In_t}	Input energy to the EES at year *t* (MWh)
E_{EES}	Net present value for EES electricity output (kWh)
$E_{\mathrm{EES}_{\mathrm{Store}}}$	Electricity to be stored in EES (MWh)
$E_{\mathrm{EES}_{\mathrm{Rated}}}$	Rated energy capacity of EES (MWh)
$E_{\mathrm{EES}_{\mathrm{S}(X)}}$	Electricity discharged by EES at stage *X*, $X \in \{1,2\}$ (MWh)
E_{PV}	Net present value of electricity generated by PV farm (kWh)
E_{Storage_t}	Electricity output from electrical energy storage at year t (MWh)
E_{Surplus}	Surplus electricity generated by PV system (MWh)
E_{System_t}	Electricity production from the hybrid system at year t (MWh)
E_t	Energy output at year t (MWh)
E_{tCHP}	Rated annual electricity production from CHP (MWh)
E_{tPV}	Rated annual electricity production from PV (MWh)
$E_{\mathrm{Total}_{\mathrm{case(k)}}}$	Net present value of electricity output at Case k (kWh)
ED	Euclidean distance
EES	Electrical Energy Storage
EM	Expectation-Maximisation
EMCL	Minimum Emissions-Compliant Load
F_{CHP}	Annual fuel cost of the CHP unit ($)

f_i	The solutions in the i^{th} objective function
F_t	Interest expenditure at year t (\$)
FCM	Fuzzy C-Means
F-gases	Fluorinated gases
g	Gaussian mixture densities
GA	Genetic Algorithm
GAIP	Genetic Algorithm with Interior Point method
GDP	Gross Domestic Product
GMM	Gaussian Mixture Model
h	Time interval of the system operation (hr)
HFCs	Hydrofluorocarbons
$h_{n_{\mathrm{v}}}$	Number of elements in the vector $x_{n_{\mathrm{v}}}$
H_{R}	8400 (metres)
i	Interest rate for the hybrid system with 100 % debt financing (%)
I	Total installation cost including PV, battery and the CHP module (\$)
I_{o}	Initial investment cost (\$)
$I_{\mathrm{Construct}}$	Constructed solar irradiance from centroids (Wm^{-2})
I_{d}	Diode current (Ampere)
I_{SC}	Short circuit current (Ampere)
I_{Model}	Solar model clear-sky solar irradiance (Wm^{-2})
$I_{\mathrm{Pyranomter}}$	Real-life solar irradiance (Wm^{-2})
I_{Solar}	Solar constant (1367 Wm^{-2})
IEA	International Energy Agency
IP	Interior Point method

IRR	Internal Rate of Return (%)
j'	Julian day angle (degree)
J_{Julian}	Julian day
k	Case number in Chapter 3, $k = \{1,2,3\}$
K	Cluster number
$L(\theta)$	Log likelihood function with parameter θ
LB	Lower Bound
LCOD	Levelized Cost of Delivery ($/kWh)
LCOE	Levelized Cost of Electricity ($/kWh)
$\text{LCOE}_{\text{Asset}}$	Levelized Cost of Electricity for generation asset, i.e., PV or AD biogas generator ($/kWh)
$\text{LCOE}_{\text{Basecase}}$	LCOE for PV system in Case 1 ($/kWh)
$\text{LCOE}_{\text{Marginal(a-b)}}$	Marginal LCOE for Cases a and b ($/kWh)
$\text{LCOE}_{\text{System}}$	Levelized Cost of Electricity for system ($/kWh)
LCOS	Levelized Cost of Storage ($/kWh)
LHV	Lower Heating Value (905 btu/ft^3) of biogas
Li-ion	Lithium-ion
LULUCF	Land-Use, Land-Use Change, and Forestry
m	Number of EES cycles
m_{c}	Number of mixture components
m_{fuzz}	Fuzzifier for FCM (constant)
m_{Nondom}	The number of non-dominated solutions
m_{Optic}	Optical air mass corrected for station height
M_t	Maintenance costs at year t ($)

MD	Manhattan distance
MSE	Mean Square Error
n	System lifetime (years)
N_{Con}	Number of solar charge controllers
$\widehat{N}_{\mathrm{Direct}}$	Average number of panels for generating electricity for direct consumption
N_{dB}	Decibel scale for PV capacity installation
NF_3	Nitrogen trifluoride
N_{EES}	Number of EES replacements
N_{Inv}	Number of inverters
n_{Obj}	Number of objective functions
$N_{\mathrm{PV_{Day}}}$	Number of solar panels for different days
$\widehat{N}_{\mathrm{Surplus}}$	Average number of panels for surplus electricity for storage
N_{Store}	Number of PV panels for generating electricity for storage
N_{Surplus_h}	Number of PV panels at hour *h* for generating surplus electricity for storage
N_{Direct_h}	Number of PV panels at hour *h* for generating electricity for direct consumption
N_{Total}	Total number of PV panels
NaS	Sodium-Sulphur
NDC	Normalised Discharge Capacity (%)
Ni-Cd	Nickel-Cadmium
NPV	Net Present Value
NREL	National Renewable Energy Laboratory

n_{v}	Number of Clearness Index profiles
O	Operation cost ($)
O&M	Operation and Maintenance
P_{AD}	Output power of biogas power plant (MW)
$P_{\mathrm{AD_{Max}}}$	Rated power capacity of biogas power plant (MW)
$P_{\mathrm{AD_{Min}}}$	Minimum output power of biogas power plant (MW)
$P_{\mathrm{Asset_{Direct}}}$	Power generated with asset, i.e., AD or PV for direct consumption (MW)
$P_{\mathrm{Asset_{Store}}}$	Power generated with asset, i.e., AD or PV for storage (MW)
P_{Con}	Rated power of solar charge controller (kW)
P_{Deficit}	Deficit power in the hybrid system (MW)
$P_{\mathrm{EES_{S(X)}}}$	EES power discharge at stage *X*, $X = \{1,2\}$ (MW)
PFCs	Perfluorocarbons
$P_{\mathrm{Generation}}$	Power generation (MW)
P_{Inv}	Rated power of inverter (kW)
P_{Load}	Power demand (MW)
$P_{\mathrm{Panel_rated}}$	Rated power capacity per solar panel (kW)
P_{Solar}	Solar farm output power (MW)
$P_{\mathrm{Solarfarm}}$	Solar farm rated capacity (MW)
P_{Surplus}	Surplus power generated by PV farm (MW)
p/p_{o}	Pressure correction for station height
PrV	Present Value
PS	Pattern Search
PSO	Particle Swarm Optimisation

PSOIP	Particle Swarm Optimisation with Interior Point method
PV	Photovoltaic
r	Discount rate (%)
Ratedcycle	Rated cycle-life of EES
RFB	Redox flow battery
S_t	Rated electrical generator output at year t (kWh)
SA	Simulated Annealing
SF_6	Sulfur hexafluoride
SOC	State of Charge (%)
SOC_{Lower}	The minimum SOC value of a cycle (%)
SOC_{Max}	Maximum SOC (%)
SOC_{Mean}	Mean SOC (%)
SOC_{Min}	Minimum SOC (%)
$SOC_{Threshold}$	SOC threshold (%)
SOC_{Upper}	The maximum SOC value of a cycle (%)
SSR	Self-Sufficiency Ratio
t	Year
t_{it}	Iteration number
T	Cycle
TLK or T_{LK}	Linke turbidity factor
UB	Upper Bound
v_K	Centroid vector for cluster K
w_i	Mixture weight for component i
w_{ij}	Fuzzy-partition matrix

W_Y	PV installation capacity in year Y (W)
W_{Yref}	Installed PV capacity in reference year (W)
$x_{n_{\mathrm{v}}}$	Clearness Index profile vector for vector n_{v}
z	Site elevation above sea level (metre)
Zn-Br	Zinc-Bromine
Zn-Fe	Zinc-Iron

List of Figures

Figure 1.1. Global emissions intensity and CO_2 emissions [3]. 3

Figure 1.2. Greenhouse gas emissions in 2010 [6]. 4

Figure 1.3. Power capacities for renewables (excluding hydropower) as of 2015 [7]. 5

Figure 1.4. Energy shares for global electricity production as of 2015 [7]..... 6

Figure 1.5. A simple equivalent circuit model for a solar cell, reproduced from [13]. 7

Figure 1.6. The global long-term average of daily and annual solar insolation map in $kWhm^{-2}$, reproduced with permission from [15]. 8

Figure 1.7. PV power curve and scaled-down national load in Kenya. 9

Figure 1.8. Daily solar irradiance in Kenya in November 2011..... 10

Figure 1.9. Power curves of hybrid system. 12

Figure 1.10. Hybrid system schematic and key parameters. 16

Figure 1.11. Research framework. 17

Figure 2.1. Trends for global penetration of solar PV systems [39, 40]. 21

Figure 2.2. Solar PV system power capacity in various countries and continents.[58]. 25

Figure 2.3. Solar PV system power capacity in various countries and continents at base 10 logarithmic scale. 26

Figure 2.4. Blended price projections for EES in grid scale applications [73, 74]. 27

Figure 2.5. Global storage installation capacity (electrochemical only) [74, 76]..... 28

Figure 2.6. India energy storage installation capacity (all types) [77]..... 28

Figure 2.7. U.K. energy storage installation capacity (excluding pumped storage) [78]. 29

Figure 2.8. U.S.A. electrochemical energy storage installation capacity (Residential, Non-Residential and Utility) [79]. 29

Figure 2.9. Simple flowcharts for zero-charge and full cycle-charge strategies. 53

Figure 3.1. Energy flow diagram of the PV system and electrical energy storage..... 64

Figure 3.2. Solar irradiance between 1st Jan. to 6th Jan. in 2009–2012 at Johannesburg. 69

Figure 3.3. A representative daily national load curve for Kenya and Johannesburg. 69

Figure 3.4. Solar and load curve for Cases 1, 2, and 3 73

Figure 3.5. Solar and load power curves for Case 1 in sensitivity analysis. 74

Figure 3.6. Solar and load power curves for a 5 MW nameplate PV farm. 74

Figure 3.7. Marginal LCOE, LCOD and $\mathrm{LCOE}_{\mathrm{System}}$ with respect to PV capacity. 75

Figure 3.8. LCOD for Li-ion and VRB at various discount rates. 78

Figure 3.9. $\mathrm{LCOE}_{\mathrm{System}}$ for Li-ion and VRB at various discount rates. 78

Figure 4.1. Solar irradiance for clear-sky model and real-life (pyranometer) data in Johannesburg. 83

Figure 4.2. Clearness Index for the four seasons in Johannesburg. 84

Figure 4.3. Clearness Index for the four seasons in Kenya. 84

Figure 4.4. Original and warped CI profiles for Cluster 1 for winter, Kenya. 88

Figure 4.5. Original and warped CI profiles for Cluster 4 for winter, Kenya. 89

Figure 4.6. Association table in DBA for winter, Kenya. 90

Figure 4.7. Total intra-cluster distance for different number of clusters for Johannesburg. 92

Figure 4.8. Fuzzy decision making for the four seasons for Johannesburg. 94

Figure 4.9. Centroids for different clustering techniques for winter, Johannesburg. 95

Figure 4.10. Centroids for different clustering techniques for summer Johannesburg. 95

Figure 4.11. Centroids for different clustering techniques for autumn, Johannesburg. 96

Figure 4.12. Centroids for different clustering techniques for spring, Johannesburg. 96

Figure 4.13. Centroids for different clustering techniques for winter, Kenya. 97

Figure 4.14. Centroids for different clustering techniques for summer, Kenya. 97

Figure 4.15. Centroids for different clustering techniques for autumn, Kenya. 98

Figure 4.16. Centroids for different clustering techniques for spring, Kenya. 98

Figure 4.17. CI profiles in respective centroids for FCM DTW for winter, Johannesburg. . 100
Figure 4.18. CI profiles in respective centroids for FCM DTW for summer, Johannesburg. 100
Figure 4.19. CI profiles in respective centroids for FCM DTW for autumn, Johannesburg. 101
Figure 4.20. CI profiles in respective centroids for FCM DTW for spring, Johannesburg. . 102
Figure 4.21. CI profiles in respective centroids for FCM DTW for spring, Kenya. 102
Figure 4.22. CI profiles in respective centroids for FCM DTW for summer, Kenya..... 103
Figure 4.23. CI profiles in respective centroids for FCM DTW for autumn, Kenya..... 103
Figure 4.24. CI profiles in respective centroids for FCM DTW for winter, Kenya. 104
Figure 4.25. MSE between centroids and real profiles with K-Means MD for winter, Kenya. 105
Figure 4.26. MSE between centroids and real profiles with FCM for winter, Kenya. 105
Figure 4.27. MSE between centroids and real profiles with K-Means ED for winter, Kenya. 106
Figure 4.28. MSE between centroids and real profiles with GMM for winter, Kenya..... 106
Figure 4.29. MSE between centroids and real profiles with FCM DTW for winter, Kenya. 107
Figure 5.1. Objective function with solar panel area variation for 27th Dec. 2012 lower bound (LB) case, Johannesburg..... 115
Figure 5.2. PV system sizing for June 2012 LB case, Johannesburg. 116
Figure 5.3. Optimisation method comparison for 22nd June 2012 LB, Johannesburg. 117
Figure 5.4. PV system sizing for June 2012 UB case, Johannesburg. 118
Figure 5.5. Optimisation method comparison for 22nd June 2012 UB, Johannesburg. 118
Figure 5.6. Optimisation results for the daily case PV system sizing, Johannesburg..... 120
Figure 5.7. Optimisation results for the daily case PV system sizing, Kenya..... 120
Figure 5.8. Count for daily case solar panel sizing, Johannesburg..... 123

Figure 5.9. Count for daily case solar panel sizing, Kenya. 124

Figure 5.10. Solar irradiance curves for 2009–2012 at maximum E_{Deficit}, Johannesburg. .. 125

Figure 5.11. Solar irradiance curves for 2011–2014 at maximum E_{Deficit}, Kenya. 126

Figure 5.12. Constructed irradiance from centroids in FCM DTW for winter, Johannesburg. 128

Figure 5.13. Constructed irradiance from centroids in FCM DTW for summner, Johannesburg. 129

Figure 5.14. Constructed irradiance from centroids in FCM DTW for autumn, Johannesburg. 129

Figure 5.15. Constructed irradiance from centroids in FCM DTW for spring, Johannesburg. 130

Figure 5.16. Constructed irradiance from centroids in FCM DTW for winter, Kenya. 130

Figure 5.17. Constructed irradiance from centroids in FCM DTW for summer, Kenya..... 131

Figure 5.18. Constructed irradiance from centroids in FCM DTW for autumn, Kenya..... 131

Figure 5.19. Constructed irradiance from centroids in FCM DTW for spring, Kenya..... 132

Figure 5.20. Optimisation results for PV panel sizing, Johannesburg. 133

Figure 5.21. PV farm rated capacity (15 % solar cell efficiency) with different clustering techniques, Johannesburg. 133

Figure 5.22. Optimisation results for PV panel sizing, Kenya. 134

Figure 5.23. PV farm rated capacity (15 % solar cell efficiency) with different clustering techniques, Kenya. 134

Figure 5.24. Histogram for system energy deficit for four years of daily case study, Johannesburg. 136

Figure 5.25. Histogram for system energy deficit for four years of daily case study, Kenya. 137

Figure 6.1. Proposed hybrid system operating regime. 146

Figure 6.2. System's power output for winter. 147

Figure 6.3. System's power output for autumn. 148

Figure 6.4. EES SOC for 0 % and 100 % $SOC_{Threshold}$ in summer and spring. 149

Figure 6.5. Fuel consumption curve for AD [227]. 150

Figure 6.6. $LiCoO_2$ cycle-life function for discharge from 100 % SOC. 153

Figure 6.7. Comparison of Li-ion EES degradation costs and cycle-life for discharge from 100 % SOC. 154

Figure 6.8. Number of lifetime EES replacements for different $SOC_{Threshold}$. 155

Figure 6.9. System's lifetime SOCs and SOC differences for $SOC_{Threshold}$ at 0 % and 100 %. 156

Figure 6.10. LCOE for AD, EES and system at different $SOC_{Threshold}$ values. 160

Figure 6.11. System LCOE with and without storage degradation cost. 161

Figure 6.12. System LCOE with different EES capital costs. 162

Figure 6.13. System LCOE with different EES and PV rated capacities. 163

List of Tables

Table 1.1. Rated capacity and discharge time for various energy storage technologies [27]. 13

Table 2.1. Top 10 largest solar farms across the globe as of 2016. 26

Table 2.2. The top 10 largest EES under commission or in operation as of 2016 [82]. 31

Table 2.3. Technical specifications for different EES technologies [2, 29, 95-100]. 35

Table 2.4. Current typical capital and operation and maintenance costs for different EES technologies [2, 95, 96, 99, 100]. 35

Table 2.5. A summary on commercial-socio based information for VRB and Li-ion battery in grid scale application. 36

Table 3.1. Cost and technical specification of the system components for the case study. 70

Table 4.1. Algorithm for reduction of redundant centroids. 99

Table 4.2. Optimal number of clusters for Johannesburg. 101

Table 4.3. Optimal numbers of clusters for Kenya. 104

Table 4.4. Data structure for time, irradiance, weather conditions and CI. 108

Table 4.5. Algorithm for calculating the total percentage of 'clear days' with weather data. 109

Table 4.6. Percentage of 'clear days' with cluster analysis and weather analysis for Kenya. 110

Table 4.7. Percentage of 'clear days' with cluster analysis and weather analysis for Johannesburg. 110

Table 5.1. Panel area for the LB and UB optimisation cases for 22nd June 2012..... 117

Table 5.2. Parameters for PSOIP for daily case optimisation. 120

Table 5.3. Annual case sizing results, Johannesburg. 121

Table 5.4. Annual case sizing results, Kenya. 122

Table 5.5. Percentage day covered at different power ratings, Johannesburg. 124

Table 5.6. Percentage day covered at different power ratings, Kenya..... 124

Table 5.7. Maximum E_{Deficit} for 2009–2012, Johannesburg. 125

Table 5.8. Maximum E_{Deficit} for 2011–2014, Kenya. 126

Table 5.9. Summary of optimal size for the hybrid system. 127

Table 5.10. E_{Deficit} with Johannesburg and Kenya clustered irradiance data. 135

Table 5.11. System component cost specification and values..... 137

Table 5.12. AD only case. 140

Table 5.13. Hybrid system with VRB at lower bound cost, Johannesburg..... 140

Table 5.14. Hybrid system with VRB at upper bound cost, Johannesburg..... 140

Table 5.15. Hybrid system with VRB at lower bound cost, Kenya..... 140

Table 5.16. Hybrid system with VRB at upper bound cost, Kenya..... 140

Table 6.1. Component costs and sizes. 144

Abstract

This thesis presents the development of methodologies for the hybridisation of an energy system with a solar Photovoltaic (PV), an Anaerobic Digestion biogas power plant (AD) and an electrical energy storage (EES). This includes the system sizing and operating regime. The key aspect is to evaluate the Levelized Cost of Electricity (LCOE) for the system and the generation assets.

The challenge arises in analysing the economic projections on PV and EES hybrid systems. EES does not produce electricity as it is not a conventional generation source. Commonly, the cost of a generating asset or the power system is evaluated using LCOE. Levelized Cost of Delivery (LCOD) has been proposed to calculate the LCOE for the EES.

A deterministic approach for sizing an off-grid PV and EES with AD biogas power plant to meet a proportional scaled-down demand of the national load has been implemented. The aim is to achieve a minimal LCOE for the system while minimising the energy imbalance between generation and demand due to both AD and PV generator constraints.

To reduce the amount of irradiance data and to provide a standardised methodology for PV system design and analysis, feature extraction technique has been used to discover Clearness Index (CI) patterns and to construct centroids for the daily CI profiles. Fuzzy C-Means with Dynamic Time Warping has been used for daily CI profiles' classification.

An operating regime has been proposed for the hybrid system, and the EES degradation cost has been considered via a capacity fade model.

The work presented in this thesis has been supported with case studies from real-life solar irradiance and national load data. The proposed methodologies have contributed to a more efficient and cost-effective method for PV-AD-EES hybrid system sizing and operation.

Acknowledgements

Firstly, I would like to express my sincere gratitude to my supervisor, Professor Malcolm D. McCulloch for his guidance and support through the duration of my research. His invaluable suggestions and useful advice were necessary to complete this research.

I am very much indebted to Professor Zhao Xu, who has given me an opportunity to have a visiting Ph.D. studentship at The Hong Kong Polytechnic University and under his supervision.

I would also like to express my appreciation to my friends and colleagues at the Smart Grid Lab, The Hong Kong Polytechnic University, and Energy and Power Group, University of Oxford for their friendship and companionship. In particular Dr Youwei Jia, Dr Jun Cao and Dr Richard T.K. Wong, for their insights and constructive comments in my research work. I am also indebted to Professor Richard McMahon and Dr Daniel J. Rogers for examining the thesis and provided invaluable comments.

I am grateful to my parents Li Rong Li and Loi Lei Lai, sisters Qi Ling Lai and Qi Hong Lai, and girlfriend Yingshan Tao for their love, unending support and encouragement.

Last but not least, this thesis is dedicated to the memory of my beloved grandmother, Shun Yi Chen, who has inspired me to be diligent.

Chapter 1

Introduction

The aim of this thesis is to develop the sizing and operating methodologies for an off-grid hybrid energy system comprising a solar Photovoltaic (PV), an Anaerobic Digestion biogas power plant (AD), and an Electrical Energy Storage (EES); to minimise the Levelized Cost of Electricity (LCOE) and to maximise the use of solar energy. The primary objective comprises the off-grid system, but with methodologies similar to the one developed in this thesis, the work can be applied to a grid-connected system.

Section 1.1 presents the reasons behind the motivation to reduce global warming due to the use of fossil fuels, which is strongly linked to environmental pollution. Fossil fuel power station burns natural gas, coal, or petroleum to produce electricity.

Typical agents of environmental pollutions resulting from burning fossil fuels are nitrogen oxides, sulphur oxide, carbon dioxide, carbon monoxide, and particulate matter [1]. This issue can be alleviated by deploying solar photovoltaic power, and the incentives and challenges associated with the same have also been presented. The research motivations and context are described in Section 1.2. Due to the operational constraints, Section 1.3 discusses how EES can be potentially used to mitigate the issues. Section 1.4 establishes the set of criteria that must be fulfilled to develop the useful techniques for the sizing, operation and techno-economic analysis for the renewable hybrid system. Section 1.5 presents the novelty value of the work.

1.1 Why renewable energy? The challenge to reduce carbon dioxide emissions

Renewable energy has been used by humanity for several millennia. In fact, hydro, wind, solar and biofuel powers were the only available energy sources during ancient times. The Industrial Revolution in the 18th century introduced a new era of energy conversion and consumption methods. This had a tremendous positive effect on the development and advancement of civilisation. However, significant environmental adverse impacts became noticeable in the last several decades. Burning fossil fuels, i.e., coal, oil and gas emits carbon dioxide. Consequently, generating fossil fuel-based power causes global warming due to carbon emission and a significant increase in environmental pollution levels. In the recent decades, governments from several countries realised the severe issues. There is a need to reassess the ways in which electricity is generated and consumed to minimise pollution from emissions, planetary global warming rate and to mitigate nuclear accidents risks [2]. Figure 1.1 presents the trend for global CO_2 emissions and the emission intensity of fossil-fuel use from the past two decades. The emission intensity is the ratio of the emitted greenhouse gas to the Gross Domestic Product (GDP) of a country. It is evident that there is an increase in global CO_2 emission although there is a decline in emission intensity. This is due to the increasing energy requirement around the globe, particularly for the developing countries. The reduction in emission intensity is due to the growth of non-carbon sources, e.g., renewable generations and change in generation mix. Reducing the emission intensity alone is not sufficient to reduce the global carbon emission, but it also requires the deployment of renewable energy sources to substitute the carbon emitting plants.

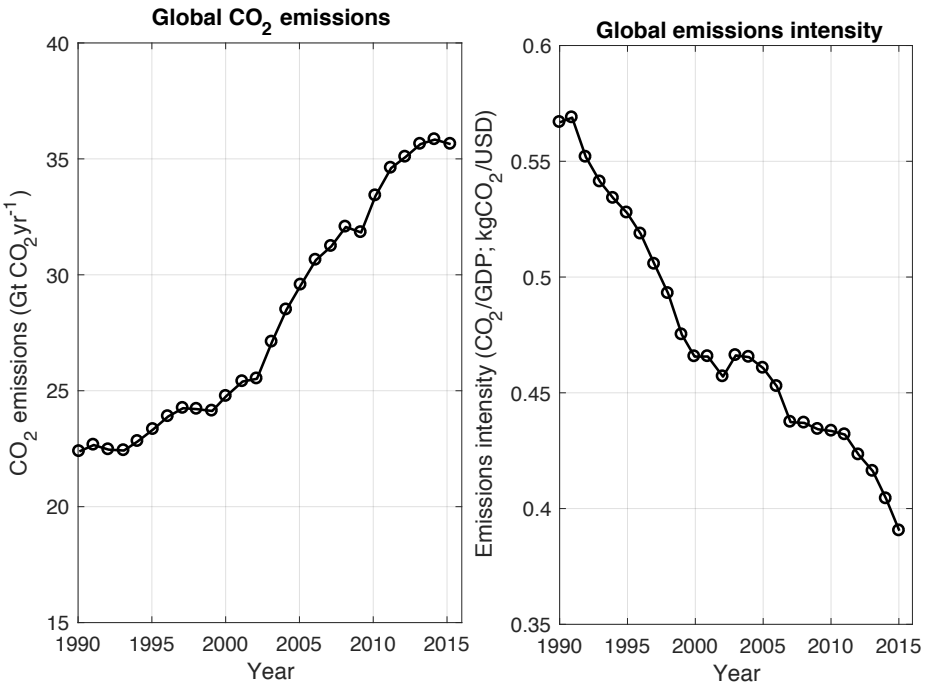


Figure 1.1. Global emissions intensity and CO_2 emissions [3].

The breakdown of greenhouse gas emission for the World, China, U.S.A., and the countries in the E.U. is provided in Figure 1.2. For countries with high GDP, i.e., China, U.S.A., and the countries in the E.U., more than three quarters of the gas emissions are related to the industrial processes and the direct burning of fossil fuel. Land-Use, Land-Use Change and Forestry (LULUCF) contribute to 10 % global greenhouse emission. Fluorinated gases (F-gases) occupy a small share of the global greenhouse gas emission. F-gases are man-made gases that consists of four types, namely perfluorocarbons (PFCs), nitrogen trifluoride (NF_3), hydrofluorocarbons (HFCs) and sulphur hexafluoride (SF_6), with HFCs being the most common ones containing fluorine, carbon, and hydrogen. These gases are used in several products such as air-conditioning systems, refrigeration, heat pump equipment, aerosol propellants, and fire extinguishers. PFCs are the compounds containing fluorine and carbon. They are widely used in electronics, cosmetics, and pharmaceutical industries as well as in refrigeration when combined with other gases [4].

The methane (CH_4) emissions are both naturally occurring and man-made. Man-made activities such as production and transport of natural gas, coal, and oil release methane into the atmosphere. Methane is also produced from livestock and decay of organic waste in urban solid waste landfills. It is emitted by termites, wetlands, grasslands, lakes, and coal beds [5].

An effective approach to tackle the global emission is to promote industries' use of clean energy such as solar energy. Additionally, the proper collection and treatment, i.e., with AD, of organic waste in LULUCF can reduce direct release of greenhouse gases into the atmosphere.

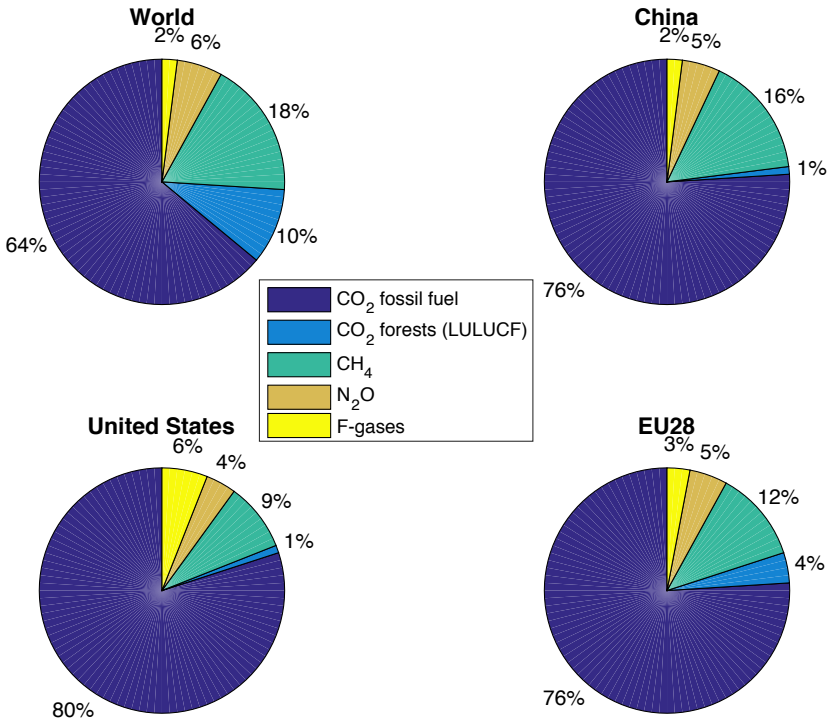


Figure 1.2. Greenhouse gas emissions in 2010 [6].

As there is a need for global adoption of renewable energy, Figure 1.3 shows the installed capacities for different renewable sources as of 2015. With the exclusion of hydro, wind power occupies the largest share of the installed renewable power capacities except in Japan and Italy. The promotion of a particular renewable greatly depends on the location of resources and other factors such as the capital and maintenance costs of the technology. The global power output from renewables excluding hydro reached a new peak of 800 GW by the end of 2015 with China contributing a quarter of the total share. Bio-power such as anaerobic digestion comes

third in the renewable share behind wind and solar. There is a potential for further uptake of this technology, especially in agriculture and remote areas. Ocean power, geothermal power, and Concentrated Solar Power (CSP) constitute a small percentage of the renewables share.

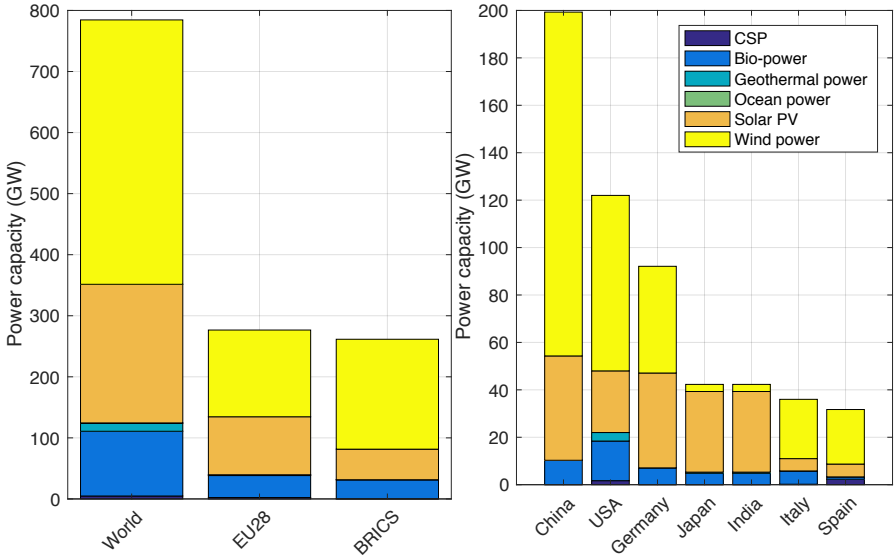


Figure 1.3. Power capacities for renewables (excluding hydropower) as of 2015 [7].

Figure 1.4 depicts a comparison of the global renewable energy shares and shares of non-renewables and renewable electricity generation as of 2015. It is worth mentioning that the calculated total percentage is affected by the decimal rounding error. The global hydropower capacity is more than four times larger than that of wind. Bio-power such as biomass is widely deployed in developing countries such as Kenya [8]. The general forms of biomass are 'wood and agricultural products', 'solid waste', 'landfill gas and biogas', and 'alcohol fuels: ethanol and biodiesel'. People combust wood for heating and cooking. Solid wastes such as garbage are combusted in many communities to produce electricity in waste-to-energy plants. Gasohol and ethanol fuel are used to power motors by mixing ethanol with petrol. Biogas digesters create methane with the breakdown of organic matter, e.g., manure and plants, in the absence of oxygen. This process is known as anaerobic digestion. Biogas digesters are airtight containers made of bricks or steel. Methane is produced in landfills due to anaerobic digestion

and collected by landfill gas collection systems. Methane can generate electricity in internal combustion engines [9].

Solar PV currently has only 1.2 % of the renewable share. It is expected that the share will increase at a rapid rate due to the improvement of solar cell technologies and the lowering of capital costs.

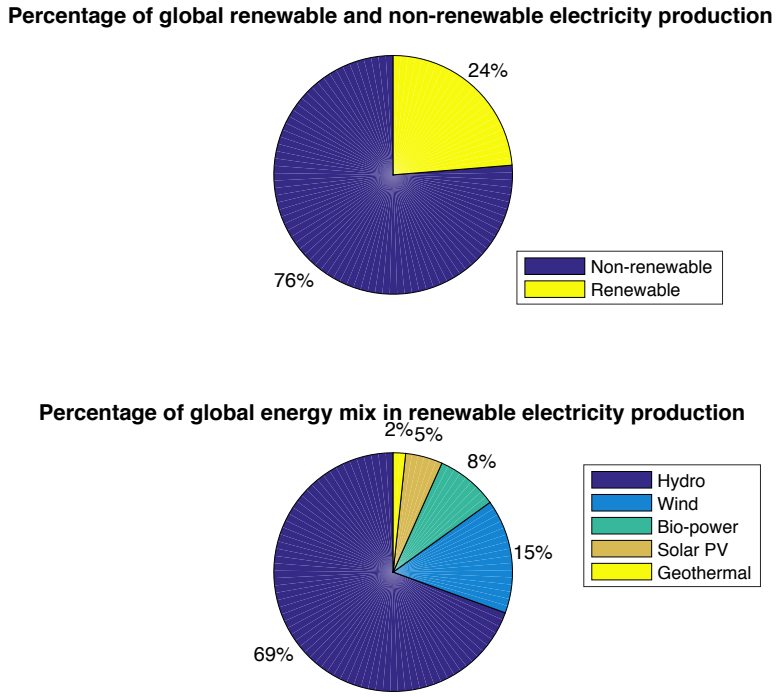


Figure 1.4. Energy shares for global electricity production as of 2015 [7].

1.1.1 Why solar PV? The motivation and obstacles

Solar energy is a sustainable and clean source of renewable energy. With clear sky irradiance assumptions and available land area, the maximum potential annual solar energy amount reaching the earth's surface before energy conversion was estimated to be $50 * 10^{21}$J [10]. The potential does not consider conversion efficiency. It is assumed that 3.6 billion hectares are available for solar energy with the assumption that ten percent of the 4 billion hectares of unused land is used for infrastructure and habitation [10].

The solar resource potential is significantly larger than the total annual world energy consumption in 2012, which was $0.376 * 10^{21}$J [11]. The global solar energy production is

significantly greater than the global energy demand [12]. However, due to the diurnal and stochastic nature of solar energy, integrating solar power into the power system is challenging. The PV effect was first discovered in 1839 by a French physicist named Edmund Becquerel. The phenomenon was discovered when a potential difference was generated in a weak electrolyte solution with an illuminated metal electrode [13]. However, the first PV cell was only built forty years after the first discovery by Adams and Day. The cell was based on selenium with one to two percent efficiency [14].

Semiconductors are used for building PV cells to convert sunlight, i.e., photons into electricity. The study of semiconductor physics involving band gap energy and doping of intrinsic semiconductors is crucial for PV cell development. The simplest equivalent circuit model for a PV cell consists of a current source and a real diode as shown in Figure 1.5. The current is delivered by the ideal current source which is proportional to the exposed solar irradiance. The short-circuit current, I_{SC}, is the largest current that may be delivered by the solar cell. I_d represents the diode current.

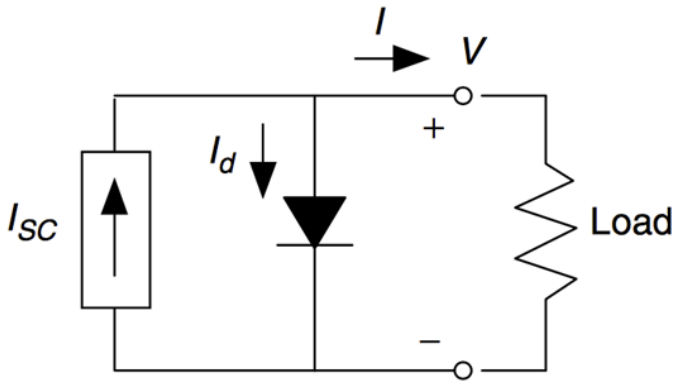


Figure 1.5. A simple equivalent circuit model for a solar cell, reproduced from [13].

Solar power generation is directly proportional to the solar irradiance. This signifies that there regularly adjusting the power output of dispatchable generators, e.g., coal, fire or gas power plant is required to avoid fluctuations. Consequently, it poses challenges in determining the adequate system reserve economically for secure and reliable operation. When PV systems

constitute a larger share of generation capacity, i.e., increase in penetration, increasing system flexibility should thus become a priority for policy and decision makers.

Figure 1.6 presents the long-term average daily and annual solar irradiance received by the earth. Africa and Australia receive the highest proportion of solar irradiance compared to other continents. In general, countries near the equator will benefit more from the solar resource. Subject to governmental policy, global connection of PV and energy sources will be a feasible solution to improve asset management and to fully utilise resources for countries with abundant solar irradiance.

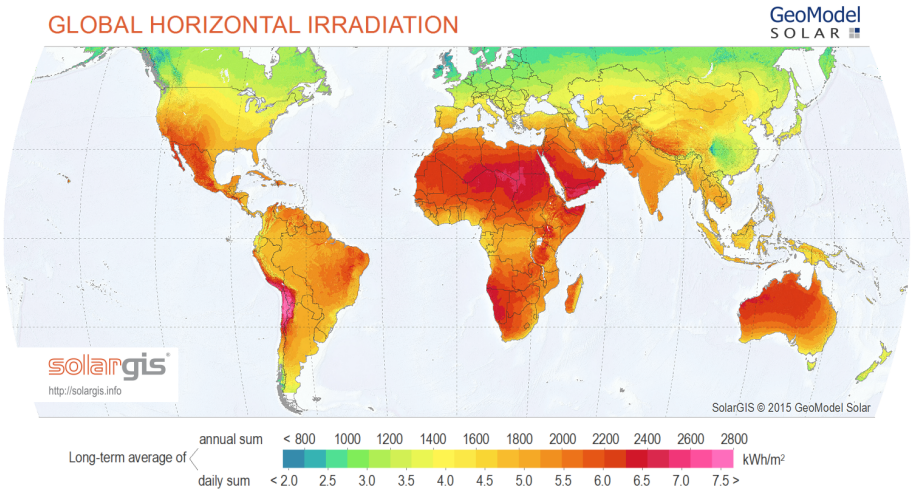


Figure 1.6. The global long-term average of daily and annual solar insolation map in $kWhm^{-2}$, reproduced with permission from [15].

To maximise the available power generation and use of renewables, it is essential to include "Energy Internet". The term has been proposed for residential distribution systems to achieve adaptable energy sharing for consumers with renewable energy sources and energy storage devices [16]. For "Global Energy Internet", the power imbalance between generation and demand is in a global scale. In the future, more countries will participate in electricity trading and sharing to overcome the energy imbalance between supply and demand. For instance, Africa generates surplus electricity at noon and Europe's electricity demand is high during that time. Hence, Europe can benefit from the renewable electricity produced in Africa with its

abundant solar resource. However, advanced transmission systems are needed to transmit power. An ultra-high voltage AC/DC system and a smart grid technology are the basis for the development of global energy internet and interconnection [17]. This is out of the scope of the thesis and is an area of focus for future research and development.

To illustrate the issues with PV power, Figure 1.7 presents a scaled-down national load curve for Kenya and a PV power curve was constructed from real-life solar irradiance in Johannesburg for a 5 MW solar farm. The PV output rarely matches the load demand except for a very few instances. Moreover, surplus electrical energy is generated during midday when the solar array receives the highest amount of solar irradiance. As shown in Figure 1.8, the issue worsens when the shape and magnitude of the daily irradiance is different for 30 days in November 2011 (each colour denotes a day).

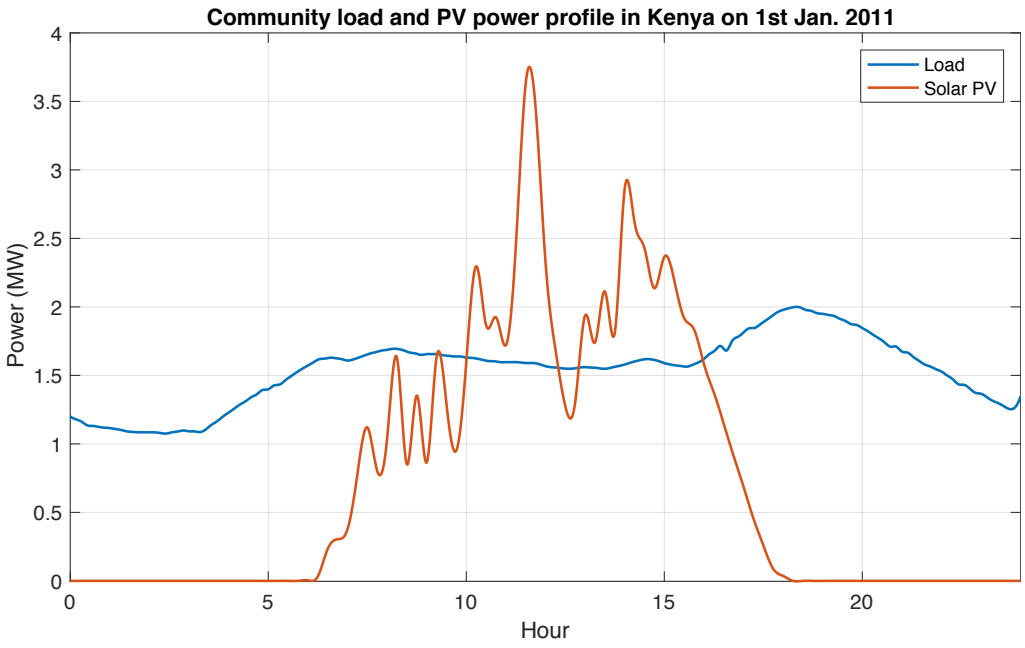


Figure 1.7. PV power curve and scaled-down national load in Kenya.

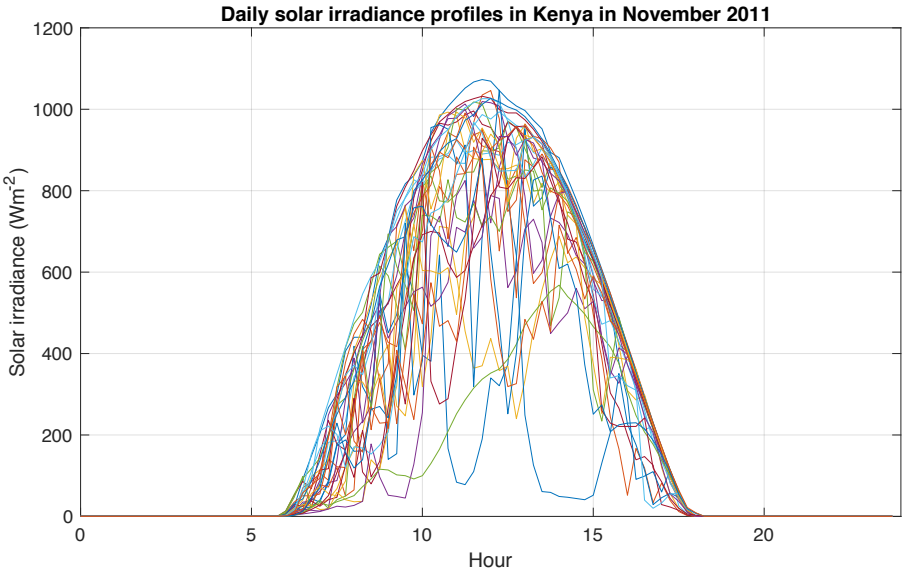


Figure 1.8. Daily solar irradiance in Kenya in November 2011.

1.2 Research context and scope

Access to modern energy services has significant links to economic development, poverty alleviation and improved health. Despite these links, over 590 million people in sub-Saharan Africa remain without access to electricity [18]. Two significant aspects of the African context motivated this study:

1. Africa has abundant solar resource. Presently, it is harnessed only for small-scale applications (i.e., solar home systems).

2. Biogas power plants powered by anaerobic digestion can be used to facilitate the integration of intermittent renewable sources such as solar and wind power by offsetting diurnal fluctuations in the output power.

Generally, off-grid hybrid renewable energy systems perform better with multiple energy sources compared to those with a single energy source [19]. This can be explained by the fact that different energy sources have different technical constraints and may be used to complement each other and to maximise the supply's security. The generation costs could also be potentially reduced. However, the control, design and optimisation of such systems is a

complicated matter. Many of these systems were generally designed. aiming to minimise the total generation cost such as the LCOE [19, 20].

Optimal sizing and operation have become a complicated issue due to the diurnal, stochastic effect of solar irradiance and the operational constraints from the AD. The hybrid system aims to dispatch the maximum available solar power first to meet the load demand. The problem arises when solar power starts increasing and decreasing during the morning and afternoon, respectively as this changes the required output from the AD.

A technical constraint for partial load operation of reciprocating combustion engine power plants is the Minimum Emissions-Compliant Load (EMCL). This is the lowest output at which the engine can operate and still meet environmental limits for nitrous oxides (N_2O) and carbon monoxide (CO) emissions. Operation at lower loads can cause reduced combustion temperature , resulting in less conversion of CO to CO_2, and potential emissions permit exceedances [21].

To enable a wider range of gas engine outputs, manufacturers have introduced control systems designed to extend emissions-compliant turndown while minimising efficiency impacts at part load [22]. Part-load is when the generator is at certain specified load values below 100 % of its rated capacity. Gas engines can develop ash deposits with insufficient cylinder pressure, a reduced detonation margin and damaged engine components. One of the approaches to reduce the emission constraint at low loads is to produce higher combustion temperatures to enhance the conversion of CO to CO_2. Currently, reciprocating gas engines can achieve emissions-compliant turndown to about 40 % of the baseload power [22].

NO_X emission increases with higher combustion temperature. At part load, particulate matter formation is insignificant but NO_X is still produced. Recirculating a portion of an engine's exhaust gas back to the engine cylinders is useful to reduce NO_X emission at part load for spark ignition engines [23].

It is most likely that there will be surplus energy in the afternoon. This energy should be stored and used to meet energy demands. In the late afternoon, the solar irradiance reduces and there is a need to increase the AD output to meet the load. Excluding the consideration of solar PV fluctuations at midday, there are two notable occasions when there is insufficient energy supply from both PV and AD. AD shuts down due to the operating constraint and when insufficient solar irradiance is available. Figure 1.9 presents a typical solar power curve from real-life irradiance data, the AD and a down-sized load curve. The AD is used to compensate for the energy deficiency when solar energy is not available before sunrise and after sunset. The surplus and deficit energy are highlighted in green and purple, respectively.

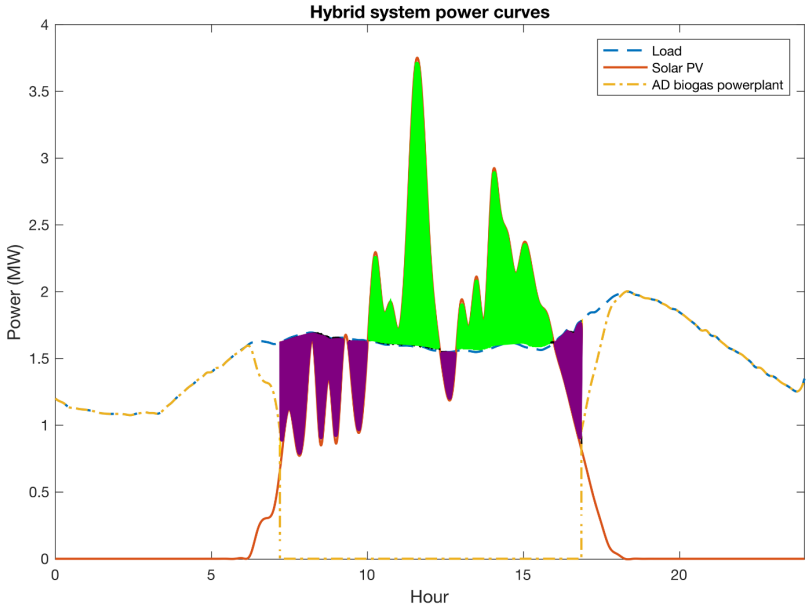


Figure 1.9. Power curves of hybrid system.

Motivated by the research context, the scope of this thesis focuses on tropical climate locations. It is worth mentioning that the developed methodologies may be applicable to solar irradiance in other climate locations, e.g., the Polar and Antarctic regions. The biomass-to-biogas conversion process of anaerobic digestion for electrical power generation is not a focus in this work.

1.3 Mechanism to relieve the issues: Electrical energy storage

AD biogas power plants act as a 'long-term' storage for a hybrid system. The waste organic material that is used for the anaerobic digestion process contains stored energy. The bacterial hydrolysis process is initiated to begin the digestion process. The digester can store the biogas for a long time to be used and to dispatch for electricity generation. On the contrary, 'short-term' storage where stored energy can be retained for a shorter duration, i.e., EES, can be of significance. The presence of EES is essential in any hybrid renewable energy system to utilise the surplus energy and to perform load balancing [24]. This is achieved by performing short-term scheduling to the dispatchable generators and the electrical storage [25]. EES can be charged or discharged at a given time instance while fulfilling constraints such as the State of Charge (SOC). Large-scale, i.e., kW-to-MW EES has received significant attention in the past few years. This is essentially due to the sharp cost decline and the maturity of the electrical storage technology [26, 27]. As of year 2011, there are several types of EES which can be utilised for a renewable hybrid system as shown in Table 1.1. Since then, several technology breakthroughs have occurred in energy storage technologies. This leads to an increase in system power ratings as depicted in Table 2.2 for 2016. The choice of EES depends on the type of grid application such as Uninterruptible Power Supply (UPS) and Transmission and Distribution (T&D) grid support.

		UPS / power quality		**T & D grid support / load shifting**			**Bulk power management**	
Discharge time at rated power	**Hours**	Flow batteries					Pumped hydro	
					NaS battery		Compressed air energy storage	
	Minutes	High-energy supercapacitors		Advanced lead-acid battery				
		Li-ion battery						
		Lead-acid battery						
		NiCd						
		NiMH						
	Seconds	High-power flywheels						
		High-power supercapacitors						
		1 kW	**10 kW**	**100 kW**	**1 MW**	**10MW**	**50 MW**	**100 MW**	**1 GW**
		System power ratings						

Table 1.1. Rated capacity and discharge time for various energy storage technologies [27].

1.4 Thesis roadmap

The objective of this research is twofold. The first is to study the economic projection of the hybrid system, and the second is to develop optimal sizing and operating regime for the hybrid system with high penetration PV. The proposed methodologies focus on stand-alone systems but may be applicable for grid-connected systems.

To successfully address the objective, a set of key criteria and the necessary conditions to be fulfilled have been raised. The responses to these criteria are part of the research and will be presented in the chapters of this thesis.

Refinement in the levelized cost calculation for PV-AD-EES system

Accurate economic analysis is of critical importance to the hybrid system sizing and operation. LCOE has primarily been used as an indicator to compare the costs of power generation methods. It can also be used as an objective function to minimise the system generation cost. However, the literature suggests that most cost calculation methods are oversimplified. For instance, capacity factors are used to represent the power generation of solar PV. This may not be applicable to intermittent generations and obscures the actual generation costs by ignoring the PV variability. To address this, Chapter 3 provides the improved calculation methods for the LCOE of PV and EES.

EESs have been used in hybrid systems, and the LCOE for EES has received significant attention. The cost of storage can be affected by both the application, i.e., frequency regulation, renewable integration, back-up purposes etc., and the type of EES employed. The term Levelized Cost of Storage (LCOS) has recently been studied by industries such as Lazard (financial advisory and asset management firm) and in academia [28, 29]. However, the metric does not reflect the actual storage costs as it does not consider the energy production costs. Hence, a variation of the LCOS metric will be proposed in Chapter 3 and will be studied for

the hybrid system. The marginal LCOE will also be proposed to understand the levelized cost implications for increasing the PV power capacity and adopting EES.

For the first time, a cell capacity fade model has been used to consider the Depth of Discharge (DOD) for a hybrid system in the LCOE calculation presented in Chapter 6. This will reflect a more accurate LCOE by considering the degradation of the EES due to irregular cycling.

Solar irradiance dataset reduction for PV system sizing

With the increasing number of distribution generation PV systems, it is necessary to reduce the amount of irradiance dataset generated from the pyranometer for PV system sizing. This will potentially reduce the computational requirement for PV system analysis, and the benefits will be of significance when the study involves collecting irradiance data from multiple locations. Data analytics will play a crucial role in studying the features of the solar irradiance datasets for feature extraction. A method to analyse the fluctuations in the solar irradiance is via the solar Clearness Index. Cluster analysis on the Clearness Index will be explored in Chapter 4. The functionality of the clustering results will be compared and examined with the full dataset for the PV system sizing in Chapter 5.

Minimising the LCOE for the PV-AD-EES system

Many optimal sizing algorithms such as HOMER rely on a brute-force approach to determine the optimal component size. This involves performing sensitivity analysis on the system by varying the components' sizes and the system configuration with the least cost chosen; hence, they are computationally expensive to use. Driven by reducing discount rates, the plummeting costs of PV panels and EES, a sizing method is proposed to maximise the PV capacity, i.e., using solar energy to meet the community load. The system will be sized to maximise the PV penetration. However, the costs of PV and EES need to be reduced and the projected costs for EESs are explored in Chapters 2 and 3. In conjunction to the costs, policy incentives, i.e.,

reduced discount rates are required for this objective to be achievable. The LCOE analysis for the sized and operating system will be provided and discussed in Chapter 6.

To fulfil the load requirement of a small community in Kenya's rural area

The system should be able to provide the electrical power to meet the load demand at all times while fulfilling its operational constraints. Such constraints are power balance, EES SOC limits and AD biogas power plant output limits. A scaled-down national load curve in Kenya has been used to represent the small community's energy consumption. The operational costs should be minimised for the system. An operating regime has been devised in Chapter 6 to fulfil this criterion with the projected levelized costs.

Figure 1.10 presents the hybrid system schematic diagram. The key parameters to be considered include fuel consumption for AD biogas power plant, SOC for EES and PV power generation. A bi-directional inverter was used for converting the right DC/AC voltage level of the busbars. A solar charge controller is used for obtaining the correct DC voltage level so that the storage can be connected to the energy system. It is worth mentioning that the actual structure and connections for a MW-size system can be different, which is not considered in the scope of this thesis for the techno-economic analysis. For MW scale energy system analysis, typically a simple schematic of the hybrid system is provided such as in [30]. The research framework is depicted in Figure 1.11 showing the work to be conducted and how the research goal is achieved.

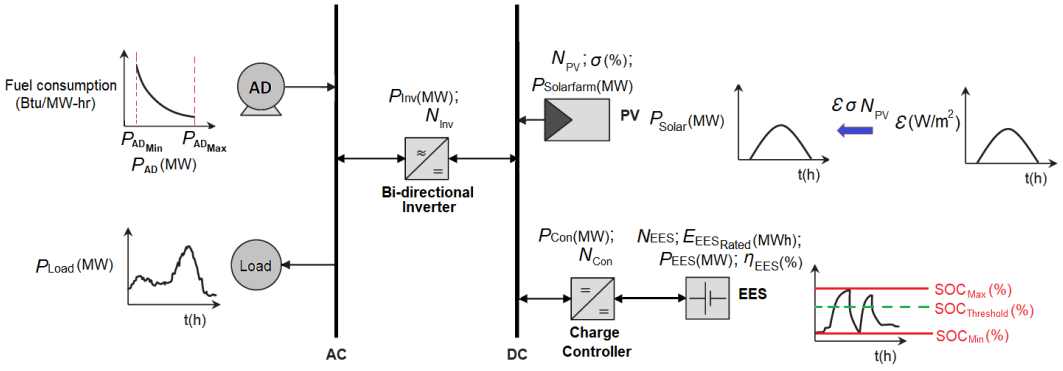


Figure 1.10. Hybrid system schematic and key parameters.

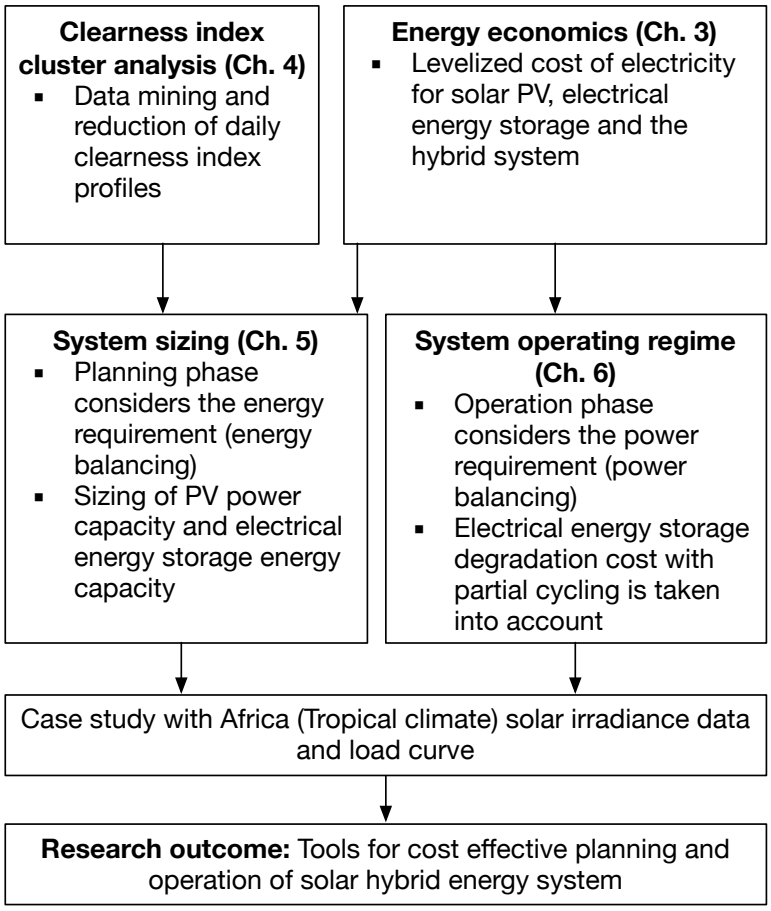


Figure 1.11. Research framework.

The case study employed in this research is based on the Gorge Farm Energy Park. The park is located approximately 76 km away from Nairobi. It is located in a market town of Naivasha and is 1740 acres of land. Presently, the park produces 2.4 MW of heat and electricity to cultivate flowers and vegetables. The surplus power can provide electricity to a maximum of 6000 rural homes. The park is owned by the Vegpro Group, an East African vegetable and rose exporter [31, 32].

In 2016, Biojoule Kenya, the AD power plant operator, signed the agreement to sell surplus electricity to Kenya Power and Lighting Co. (KPLC). At a production cost of 0.1 $/kWh, the biogas-based electricity is significantly cheaper than diesel-generated power which costs 0.38 $/kWh. Gas engines for the power plant were supplied jointly by Tropical Power, a Kenyan solar and biogas developer, and Clarke Energy, a U.K.-based engine service provider [33].

Since AD plant is dispatchable, this research assumes that the biogas digester can produce the biogas to operate the generator at all times. The availability and production of biogas is not within the scope of research.

1.5 Novelty and knowledge contribution

The research presented in this thesis aims to provide knowledge contribution and novel methodologies in sizing, operation and techno-economic analysis for solar PV-EES-AD hybrid systems. This research has five principal contributions which will be briefly described below:

1. Review on PV and EES global development

A review on the global development for solar PV power systems and EES is provided in the literature review. Renewable energy roadmaps and reports from several well-established organisations and governments such as NREL, U.S. Department of Energy and National Development and Reform Commission of the People's Republic of China have been studied. This provides the research motivation to develop the methodology and techniques for solar PV systems. The recent capital and variable costs and technical specification for different EES have been reviewed.

2. LCOE metric for EES and solar PV hybrid system

A metric for the EES LCOE, which considers the variability of solar PV and electrical energy generation costs has been proposed. This will be useful to evaluate the LCOE for EES technologies with different costs and technical specifications. The marginal LCOE has also been provided to study the levelized cost of the system with different types of investment such as increasing the PV capacity and/or adopting EES.

3. System sizing methodology

A method for sizing the PV and EES hybrid system with AD biogas power plant, aimed at maximising the use of solar energy and overcoming the system’s energy deficit, has been proposed. Four years of solar irradiance data were collected and used for sizing purposes.

Compared to the previous sizing methods, the proposed method is efficient and can provide insights into the energy balance of the system. This may be beneficial in determining the security of power supply at differently rated PV farm capacities.

4. Cluster analysis for daily Clearness Index profiles

The classifications of Clearness Index were provided in the literature. However, there is limited information regarding the practicality of classification results in PV systems. Cluster analysis has been performed on Clearness Index with partition-based and distribution-based methods. The aim is to reduce the data set for PV system sizing purposes. The representatives, i.e., cluster centroids, have been used for PV system sizing to verify the effectiveness of various clustering techniques. Potentially, the clustering results can speed up the PV system operational studies such as the load flow analysis for distribution generation PV systems with multiple locations.

5. Operating regime and EES degradation costs analyses

An operating regime is developed for the hybrid system to use the PV energy first. This regime is based on the merit order dispatch method in which the generation asset with the lowest marginal costs is used first. In principle, the system first uses the solar PV power to meet the load demand followed by the power generated from a biogas generator. If both generating assets are not able to deliver power, energy will be discharged from EES to meet the load demand. In this work, the costs incurred for different operating methods, i.e., EES or AD with varying dispatch priority have been studied. The LCOE for the system and system components have been studied by considering the EES degradation costs with a capacity fade model.

To disseminate the research results in this thesis, conference and journal papers have been published and some are currently under revision or preparation. This can be found in Chapter 7 Section 3.

Chapter 2

Literature review

This chapter provides a literature study on the techno-economic analysis, sizing and operating methods for PV, anaerobic digestion biogas power plant and EES renewable hybrid systems. The chapter identifies the research gaps in the areas of energy economics, data analytics for solar irradiance and methodologies in sizing and operating of the hybrid system. The recent EES costs data for conducting the research have been presented. The present and predicted global penetration of PV and EES systems, which directly relates to system's size have been provided. The pros and cons for a range of electrical energy storages for PV system have been reviewed. This will be useful for providing a benchmark for selecting a type of EES for the hybrid system.

Section 2.1 provides the current status and future plans for PV system developments in a global context for U.S.A., China, India, Australia, Germany and Japan. The growth and economic projection of EES for grid systems are provided in Section 2.2. A list of EES for the PV system is provided and discussed in Section 2.3. Section 2.4 identifies the knowledge gaps in the current literature. The chapter will be concluded with a summary in Section 2.5.

2.1 PV system global development

Several countries are aiming to maximise their solar energy portfolios [34]. Greenpeace stated that it is possible to become 100 % renewable by 2050, therefore experiencing a very sharp increase in installations [35]. To provide a glance of the PV capacity significance in a power system, the term PV penetration is used. The PV penetration level is normally used to conduct various sensitivity analyses for a power system with a PV generator. This is the total amount

of PV nameplate capacity divided by the total amount of system generators' nameplate capacities in a power system. The definition of PV penetration level has been discussed in [36, 37] and is calculated using Equation (2.1). It is worth mentioning that other definitions of penetration level for distributed generators have also been defined such as in [38] where the peak load of the system is used as the denominator. It is worth mentioning that PV penetration can also be considered in terms of electricity generation (MWh).

$$\text{PV penetration (\%)} = \frac{\text{Sum of PV generators nameplate capacity (MW)}}{\text{Sum of all system generators nameplate capacity (MW)}} \qquad (2.1)$$

Figure 2.1 presents the trends for global power capacity of solar PV systems from various literatures and case scenarios. Greenpeace has provided a forecast of global PV penetration under two scenarios, namely the "revolution scenario" and the "reference scenario". It is shown that there is a sharp linear growth in solar power capacity with respect to time.

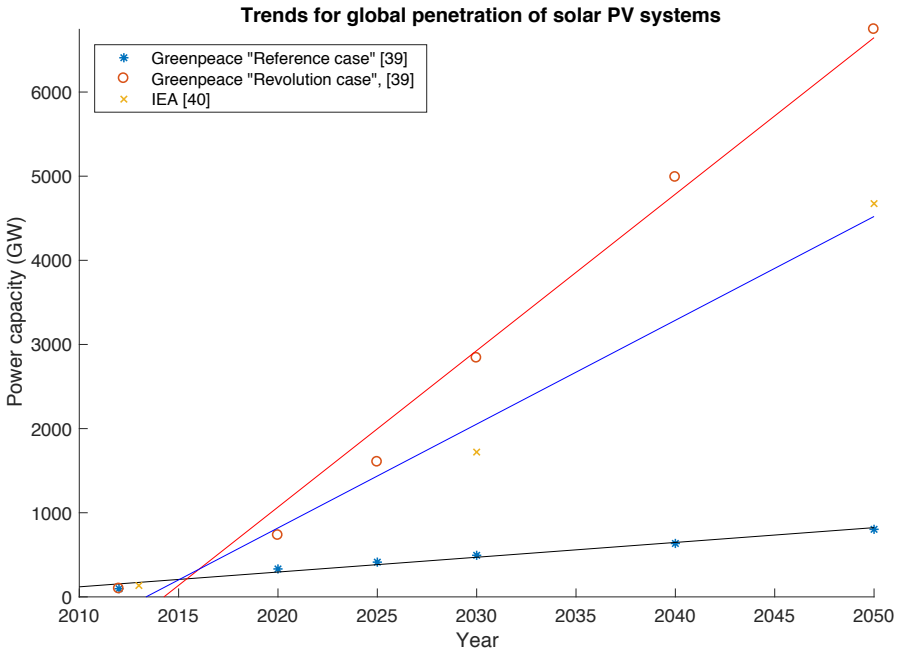


Figure 2.1. Trends for global penetration of solar PV systems [39, 40].

2.1.1 U.S.A.

Solar energy constitutes the largest percentage in the renewable energy mix in the United States with the possibility that solar energy generation can greatly be beyond the total electricity consumption [41].

According to the Solar Grand Plan, the country aims to meet 69 % of the energy demand by 2050 with PV. This will contribute to 60 % CO_2 emission reduction from the 2005 levels. Furthermore, it is expected that 250 GW and 2900 GW of PV capacity will be developed by 2030 and 2050, respectively [42]. Other projects were developed recently to help achieve this goal. The SunShot initiative, launched in 2011, aims to make PV electricity to reach grid parity by 2020 without the use of subsidies. Cost targets were set to 0.09 $/kWh for residential PV, 0.07 $/kWh for commercial PV and 0.06 $/kWh for utility-scale PV systems. It proved to be a success, and five years after the establishment of the initiative, 70 % of the progress for the 2020 goals was achieved [43]. More recently in November 2016, the SunShot 2030 was established to further reduce the cost of PV electricity. The cost targets are 0.05 $/kWh, 0.04 $/kWh and 0.03 $/kWh for residential, commercial and utility-scale PV systems, respectively [44].

2.1.2 China

China has abundant solar energy. Presently, solar energy is largely used at the residential level for solar stoves, solar water heaters and passive solar houses. The country is experiencing a rapid development in solar power generation technologies. According to [45], China has produced around 18 % of the PV products globally as a result of more than 400 Chinese PV companies' production. In 2012, six Chinese PV manufacture companies were listed among the top ten global PV cell manufacturers which are Yingli Solar, Suntech, Trina Solar, Canadian Solar, JA Solar and Jinko Solar [46]. However, the quantity of solar energy generated within the country is relatively little. Due to the overproduction of solar modules and less

installations of PV power plants, the solar PV manufacture industry in China has suffered. The production utilisation rate of solar cells has surpassed the production utilisation rate of polysilicon since 2011, and the import of polysilicon has become necessary. Worsening the situation, many polysilicon manufactures have shut down because of the price drop in polysilicon. The imbalance of polysilicon and solar PV cell production utilisation rate is expected to be more severe in the years to come [47, 48].

The strategic promotion of the PV industry based on comprehensive policy has been studied and discussed in [49]. Investment should be increased in technical research and development to control key techniques and manufacturing requirements. The plan from National Development and Reform Commission (NDRC) in 2007 stated that the country aspires to have an installed PV capacity of 1.8 GW by 2020 [45]. The latest plan, the 13th Five-Year plan [50], mentioned that the country aims to achieve 110 GW of total installed solar capacity by 2020. This growth consists of 60 GW of distributed solar PV and 5 GW of thermal solar power. In 2015, the country had a total installed solar power capacity of 42 GW. By 2050, the renewable energy penetration will be at 85 % and 2.7 TW of solar power will be installed with a total annual output of 9.66 trillion kWh – a contribution of 64 % to the total power generation [51].

2.1.3 India

India also has abundant solar energy. Currently, solar energy is mostly used for water heaters and the PV industry in India has just begun. As reported in [52], the solar industry in India could be globally significant by 2020 given that the government utilises effective project planning and sufficient financing. The Jawaharlal Nehru National Solar Mission has been initiated to stimulate the growth of solar PV energy. It is expected that 20 GW of power will be produced from solar PV by 2022 [53].

2.1.4 Australia

By the end of 2014, close to 1.4 million homes in Australia had PV systems installed [54]. On average, the residential PV system installation cost declined from approximately 12 AU$/W in 2008 to less than 2 AU$/W in 2014. Three elements, namely, the appreciation of the Australian dollar, significant cost reductions of solar panels, and increased competition between PV system installers in the country might have contributed to the cost reduction.

2.1.5 Germany

Germany's installed PV capacity is the highest in the world [55, 56]. The country aims for PV penetration to reach 52 GW by 2020. The high PV installation rate during 2009–2012 has led to significant issues regarding the distribution grids with rated capacities outnumbering the annual peak demand during several occasions. Although the EES market is expanding in the country, there is a lack of standards and methods for comparing the efficiency and performance of EES in a PV system. Germany aims to produce 80 % of its electrical energy with renewable sources by 2050.

2.1.6 Japan

In July 2008, the government underpinned a national target for PV penetration in the country. By 2020 and 2030, the country aims to increase its PV generation to ten times and 40 times from 2008, respectively. This implies that the country should produce 14 GW and 53 GW of solar power by 2020 and 2030, respectively. To help achieve this goal, in April 2009, the government started an economic stimulus measure known as the J-Recovery Plan. This has changed the initial goal for 2020 to a total installed capacity to 28 GW. Following the March 2011 earthquake that triggered the nuclear power plant disaster in Fukushima, Japan started planning an entirely novel energy strategy [57]. On 14th September 2012, the Innovative Energy and Environment Strategy was explored by the Japanese government. The fundamental idea of the strategy is to minimise the generation share of nuclear power. This will lead to an

increased adoption of renewable energy types such as wind and solar. The feed-in tariff program, commenced on 1st July 2012, significantly contributes to the growth of PV system installations. Figure 2.2 presents the future prediction for PV systems penetration of various countries in GW as reported by various organisations. It is anticipated that the PV capacity will grow with time for many developed and developing countries.

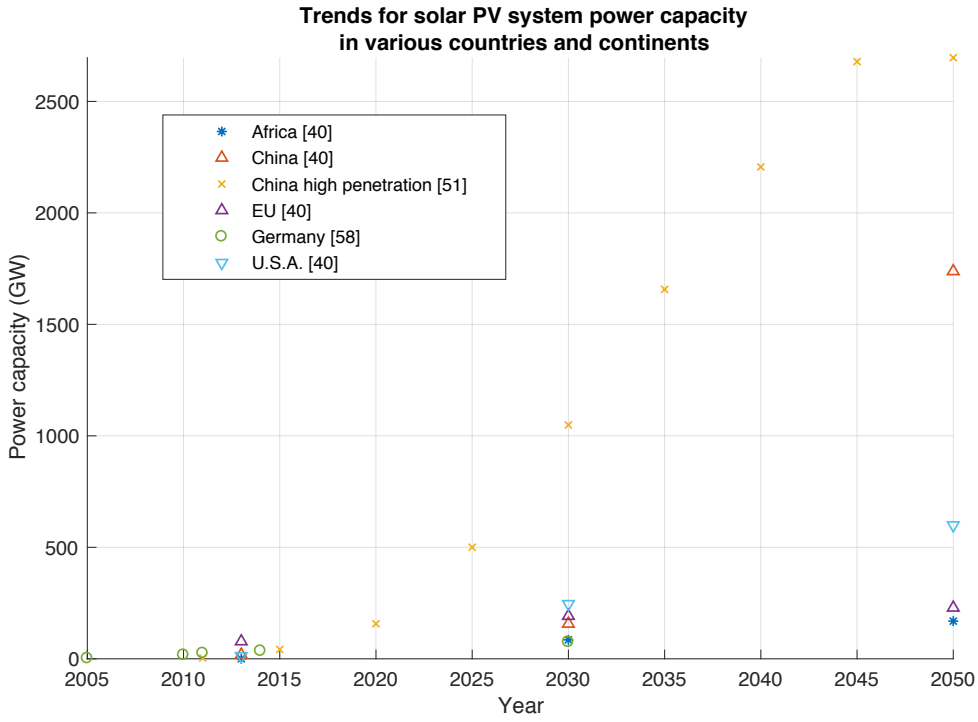


Figure 2.2. Solar PV system power capacity in various countries and continents.[58].

Figure 2.3 depicts the logarithmic scale of Figure 2.2. It shows an increase of solar power installation capacity by 2020 for all countries and continents. For instance, for China, it shows an increase of about 100 times, i.e., 20-decibel difference with respect to the year 2013. The decibel scale is calculated with Equation (2.2):

$$N_{\mathrm{dB}} = 10\log_{10}\left(\frac{W_Y}{W_{\mathrm{Yref}}}\right) \tag{2.2}$$

W_Y (W) and W_{Yref} (W) are the PV capacities in year Y and the reference year, i.e., the first year with recorded PV capacity.

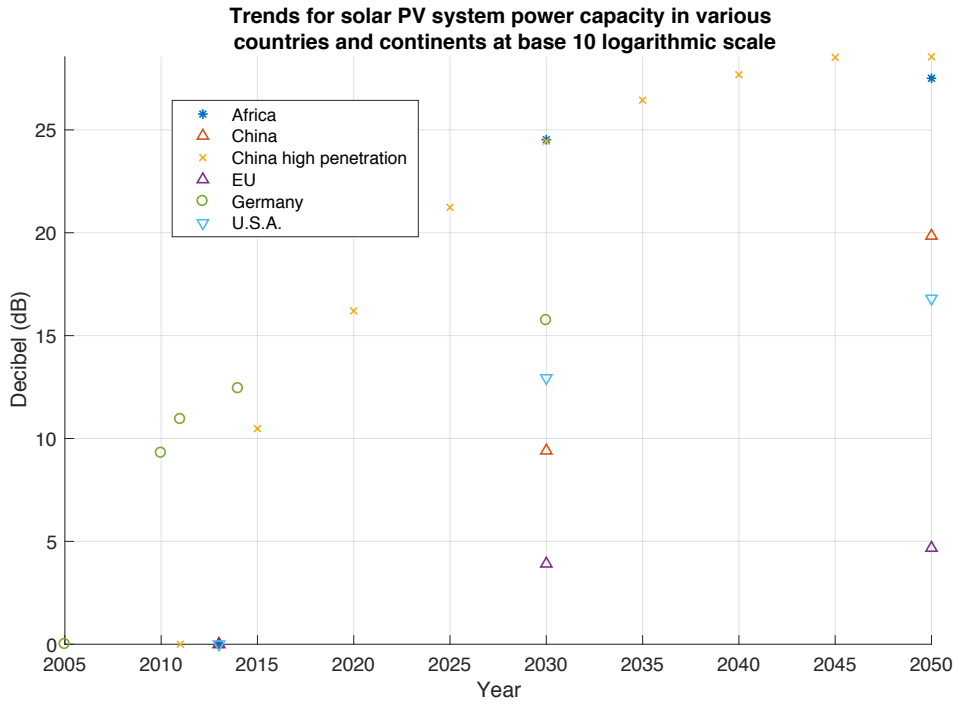


Figure 2.3. Solar PV system power capacity in various countries and continents at base 10 logarithmic scale.

Table 2.1 presents the top 10 largest MW-scale PV farms globally till 2016. The installation capacity of PV plants increased dramatically from 2011 and reached 580 MW by the end of 2015.

Location (State, Country)	Description	Size (MW)	Construction Date
U.S.A., Rosamond, C.A.	Solar Star Projects [59]	579	2013–2015
U.S.A., Riversize County, C.A.	Desert Sunlight Solar Farm [60]	550	2011–2015
U.S.A., San Luis Obispo County, C.A.	Topaz Solar Farm [61]	550	2011–2014
China, Longyangxia Dam, Qinghai Province	Longyangxia Hydro-Solar PV Station [62]	480	2014–2015
India Charanka, Patan District	Charanka Park PV Power Plant [63]	345	2010–2016
France, Cestas, Bordeaux, Gironde	Centrale solaire de Cestas [64]	300	2014–2015
U.S.A., Yuma County, A.Z.	Agua Caliente Solar Project [65]	290	2010–2014
U.S.A., Boulder City, N.V.	Copper Mountain III Solar Facility [66]	250	2013–2015
U.S.A., San Luis Obispo, C.A.	California Valley Solar Ranch [67]	250	2011–2013
U.S.A., Lancaster, C.A.	Antelope Valley Solar [68]	242	2011–2014

Table 2.1. Top 10 largest solar farms across the globe as of 2016.

2.2 Application and selection of EES for PV system

2.2.1 EES costs

The average residential energy storage systems' installation cost will drop from 1600 $/kWh in 2015 to 250 $/kWh by 2040 [69], and 70 % reduction in the price is expected by 2030 [70]. Figure 2.4 presents the projected costs for EES. It shows that the costs of EES could be constant at 350 $/kWh around 2030. This cost is for the battery pack only. As also discussed in [71], for electric vehicle batteries, the cost is not for the entire storage system and does not include the converters. The storage technology will mature by then, and the associated costs will be manufacturing and maintenance costs. Grid scale storage will benefit from the technological advancement in storage for EVs and in the residential scale. Hence, the cost of battery packs in the grid scale is also expected to drop and possibly be similar [72].

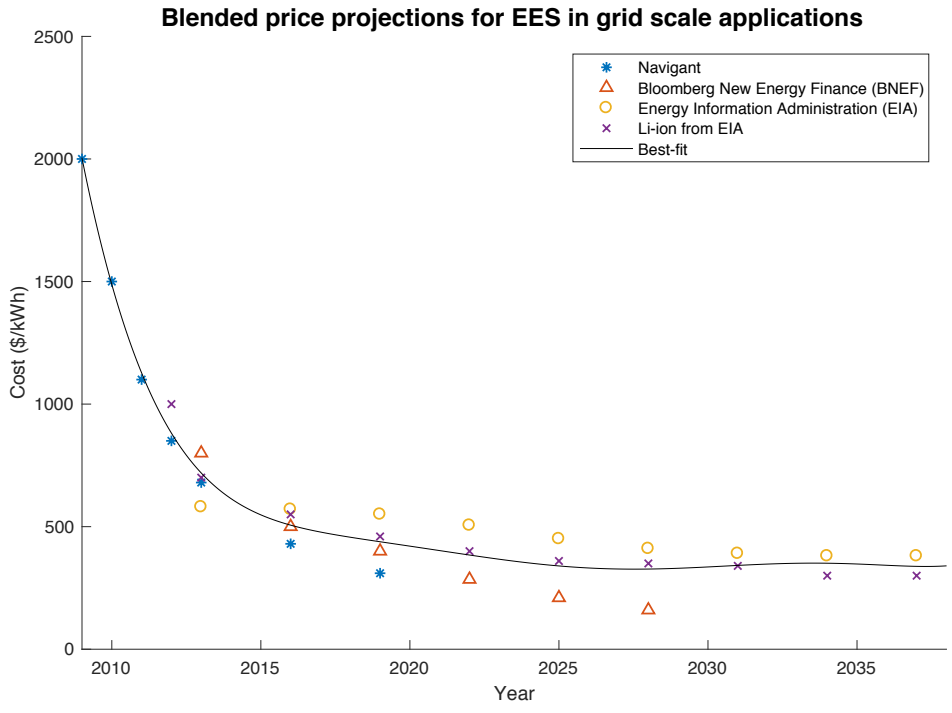


Figure 2.4. Blended price projections for EES in grid scale applications [73, 74].

2.2.2 Grid storage growth

IHS Technology has reported that grid-connected energy storage projects reached 2 GW globally by 2016; this is a 20 % growth from the end of 2015 [75]. The surge is due to the government funding programs, EES cost reductions and utility tenders [26]. Figures 2.5 to 2.8 present the installation energy storage capacity worldwide and for India, U.K., and U.S.A. respectively.

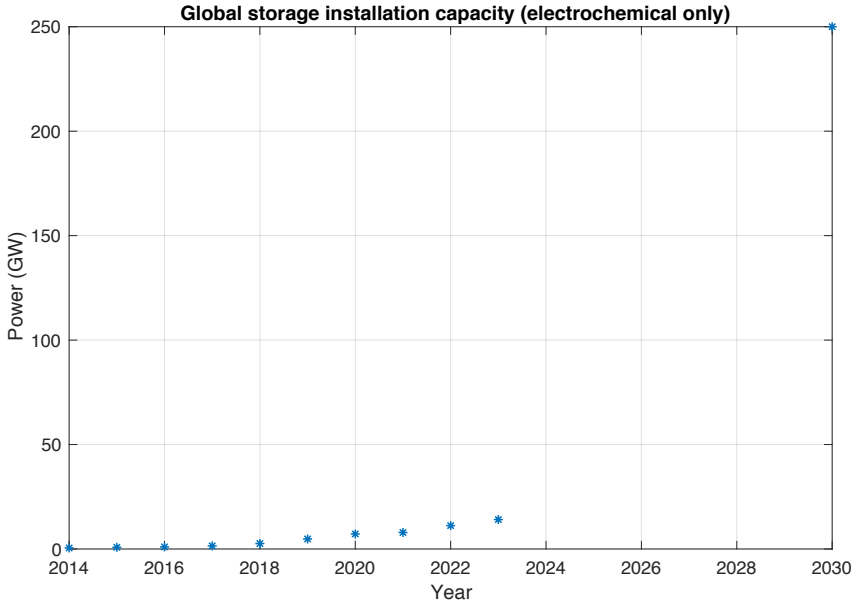


Figure 2.5. Global storage installation capacity (electrochemical only) [74, 76].

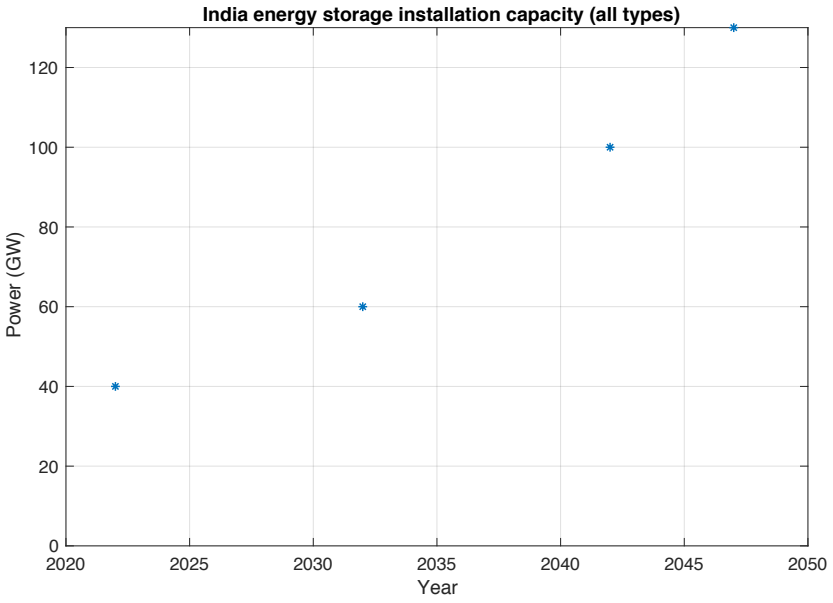


Figure 2.6. India energy storage installation capacity (all types) [77].

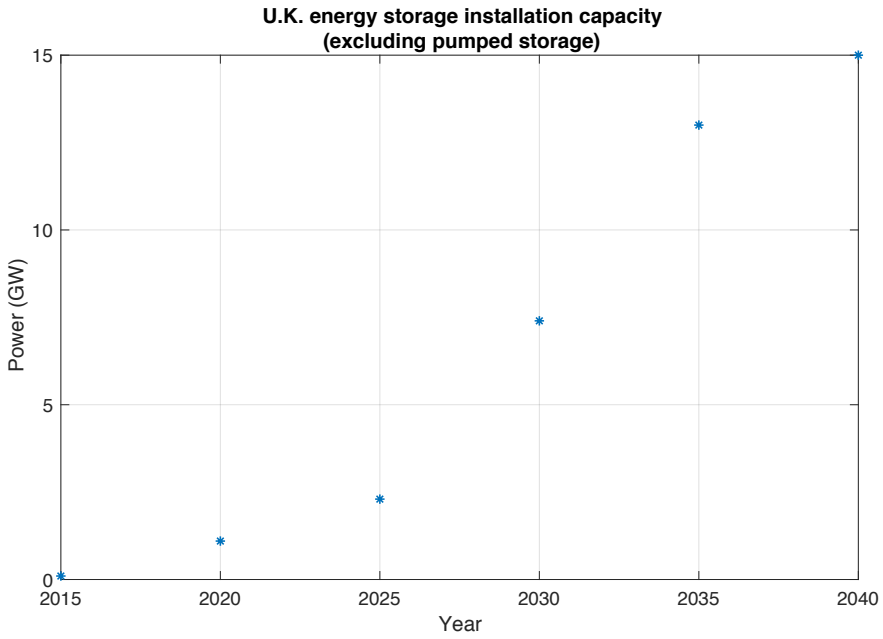


Figure 2.7. U.K. energy storage installation capacity (excluding pumped storage) [78].

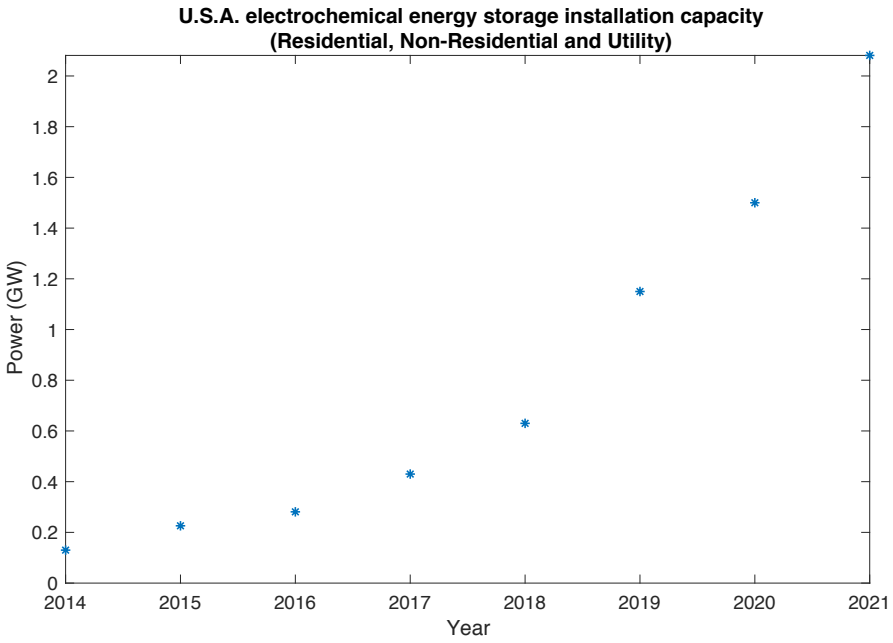


Figure 2.8. U.S.A. electrochemical energy storage installation capacity (Residential, Non-Residential and Utility) [79].

Several countries aim to maximise their EES portfolio to counteract the adverse effect of solar PV systems. Hence, this leads to a sharp increase in the deployment of EES across the globe. In the U.S.A., 111.8 MW of EES was developed by the end of 2015. The EES market in the U.S.A. will exceed 2 GW per year by 2021. This value is higher than the cumulative total of

EES deployment in 2013 and 2014 [80]. India has ambitious targets for adopting renewable PV energy and energy storage technologies, and this can be used to achieve this target [77]. It is expected that 250 GW of EES will be built by 2030 [76]. In China, EES is already being used for smoothing wind turbine output in wind farms. A lithium iron phosphate battery system demonstration project with a rated capacity of 14 MW has been built in Zhangbei, China [81]. The complete project is expected to have 110 MW of energy storage. China aims to deploy additional mature energy storage technologies into their grid in the near future. Table 2.2 presents the top 10 largest EESs by rated power capacity as of 2016.

Name	Location	Technology	Power capacity (MW)	Energy capacity (MWh)	Status	Description
AES Alamitos Energy Storage Array	Long Beach, California, United States	Li-ion	100	400	Contracted	The EES will be placed in a large building named Alamitos Power Center and will be used as replacement of peaking power plant. It will also be used for balancing intermittent renewables.
Solar Energy Corporation of India (SECI) -100MW	Ananthapuramu, Andhra Pradesh, India	Electro-chemical	100	400	Announced	The EES will be built as an addition to the recent commissioned 750 MW solar farm.
Kingfisher Project (Stage 2)	Roxby Downs, South Australia, Australia	Li-ion	100	400	Under construction	The EES will be paired with a 100 MW solar farm.
Kyushu Electric - Buzen Substation - Mitsubishi Electric / NGK Insulators	Buzen, Fukuoka Prefecture, Japan	Sodium-Sulphur	50	300	In operation	Mainly used for stabilising power flow and frequency introduced by renewables. It can also optimise the operation of the system by efficient coordination of EES and dispatchable sources.
Gyeongsan Substation ESS - 48 MW ESS - KEPCO / Woojin / LG Chem	Gyeongsan-si, Gyeongsangbuk-do, South Korea	Li-ion	48	12	In operation	The EES is mainly used for transmission congestion relief, voltage support and frequency regulation.
Nishi-Sendai Substation - Tohoku Electric / Toshiba	Sendai, Miyagi Prefecture, Japan	Li-ion	40	20	In operation	The EES was built to minimise the frequency fluctuation from PV plant.
40 MW - AES / National Grid Corp. of the Philippines (Kabankalan)	Kabankalan, Negros Occidental, Philippines	Li-ion	40	Unknown	In operation	The EES is one of the largest electrochemical storage systems in Asia. It provides voltage support and frequency regulation and aims to improve the ancillary services.
Minami-Soma Substation - Tohoku Electric / Toshiba	Minamisoma, Fukushima Prefecture, Japan	Li-ion	40	40	In operation	The EES aims to provide better energy management and improve renewable energy supply and demand balance.
Notrees battery storage project – Duke Energy	Goldsmith, Texas, United States	Advanced lead-acid	36	24	In operation	The EES was built to relieve the intermittency issues created by a 153 MW wind power farm in western Texas. A grant from U.S. Department of Energy Office of Electricity American Recovery and Reinvestment Act was issued to support the project development.
Non-gong substation EES – 36 MW EES – KEPCO/Kokam	Non-gong substation, South Korea	Lithium nickel manganese cobalt	36	13	Contracted	The EES was built to provide frequency regulation at the Non-gong substation. The project began in June 2016.

Table 2.2. The top 10 largest EES under commission or in operation as of 2016 [82].

2.3 Overview of different EES for PV system

To enhance the system reliability and to utilise the surplus energy, the presence of EES is essential in any hybrid renewable energy system [24]. The EES should have the following characteristics for a PV system [83]:

- The energy and power capacity to encounter the variable grid energy demands;
- Robustness to substantial cycling (charging and discharging);
- Very quick response time (milliseconds to seconds); and
- Ability to withstand irregular full discharging.

The EESs that are suitable for PV systems are Redox flow battery (RFB), Sodium-Sulphur (NaS) battery, Nickel–Cadmium (Ni-Cd) battery, Lead-acid battery and Lithium-ion (Li-ion) battery [84]. The following section provides an overview of these EES technologies. Tables 2.3 and 2.4 summarise the technical specifications and the capital and operating costs for different EES technologies. The information will be useful in evaluating the economic projections of hybrid PV-EES systems [85].

2.3.1 Redox flow battery

The RFB consists an ion-exchange membrane that separates two porous carbon electrodes. Storage tanks are used to store the positive and negative electrolytes including the supporting electrolyte and the active species. The flow of electric current is provided by ion exchange through the membrane during the circulation of liquids in the respective half-cells. To achieve high energy capacity, pumps are used with storage tanks to circulate huge volumes of electrolytes. While the RFB is at operation, oxidation or reduction reaction at both electrodes occur [86, 87].

Various chemical elements can be used for the RFB system such as all-Copper, Zinc-Bromine, all-Iron and Iron-Chromium. Vanadium is highly favoured in the use for RFB this is primarily because both half-cells use the same element which avoids the cross-contamination of both

half-cell electrolytes [88]. The vanadium ions remain in different oxidation states to store or release chemical potential energy.

The cycling performance and the performance enhancement of iron-chromium RFB with interdigitated flow fields were studied in [89] and [90], respectively. As explained, the use of iron-chromium for RFB is promising. This is mainly due to the inexpensive costs of iron and chromium and the active materials used for the RFB which could be at a cost of 17 $/kWh. A new RFB based on Zinc–Iron (Zn–Fe) with triple-electrolyte double-membrane design is predicted to have a system capital cost of under 100 $/kWh [91]. The low cost is achieved by a combination of high cell performance and the use of inexpensive materials (i.e., iron and zinc). The RFB technology shows a promising future, and it is expected that it will be widely deployed in PV systems.

Generally, the advantages of RFB are that the energy and power ratings are independently and highly scalable; this can be defined by the size of the electrolyte storage tank and the number of stacks of electrochemical cells [87, 88, 92]. Moreover, energy storage capacity does not suffer from degradation. The disadvantages are the capital cost and the comparatively expensive balance of system [88, 89]. The energy density is generally lower compared to other EESs.

2.3.2 Lead-acid battery

The history of lead-acid batteries can be traced back to the 19th century, and they are considered to be the oldest and the most popular EESs. This is mainly due to their low cost. They can be found in a range of applications such as off-grid power systems, electric vehicles and uninterruptible power supplies. Standard lead-acid batteries with additional ultra-capacitors are the building blocks of advanced lead-acid battery technology. Lead-acid battery is a mature technology with established recycling infrastructure. However, it faces issues regarding the

partially charged state operation and may result in reduced efficiency after each charge. Short lifespan and low depth of discharge can also be an issue.

2.3.3 Lithium-ion (Li-ion) battery

Transportation and electronics industries have used Li-ion batteries since many decades. Li-ion batteries are replacing lead-acid batteries in many areas and applications. The desirable features of Li-ion are its comparatively low self-discharge, excellent charging efficiency and high energy density. The traditional Li-ion battery uses Lithium cobalt oxide for the positive electrode. There are other variations of batteries based on the Li-ion battery such as the lithium iron phosphate battery which uses the lithium iron phosphate for the positive electrode instead. It shares similar characteristics as Li-ion battery with a longer cycle-life. In general, Li-ion remains relatively more expensive compared to other available storage technologies.

2.3.4 Sodium-Sulphur (NaS) battery

Compared to other EESs, NaS batteries are mostly used in the MW-scale. NGK Insulators Ltd., Japan, has manufactured the most NaS batteries. As of 2017, the global installation capacity is approximately 530 MW [93].

The advantages of this EES technology are its high cycling efficiencies, long lifetime and high energy density. It is also manufactured from inexpensive materials. The main issues with NaS are the need to operate at 300 to 350 °C high temperatures. The thermal management requirement to keep the integrity of ceramic separator and cell seal, which would crack at lower temperature, will be an issue. Sodium polysulfides are highly corrosive and this presents another problem for ceramic insulator protection.

2.3.5 Nickel-Cadmium (Ni-Cd) battery

Ni–Cd batteries are considered one of the oldest EES technologies that received further research improvements from the 1990s. A wide range of applications, from uninterruptable power supply to telecommunications systems uses this EES. Globally speaking, the largest Ni-

Cd battery is in Fairbanks, Alaska, U.S.A. with a rated capacity of 27 MW. It is also largest EES in the U.S. A. and has been running since 2003 [94]. The technology is currently very expensive compared to other EES technologies, and the toxicity of the heavy metals (Cd and Ni) can cause a severe problem with disposal handling.

Tables 2.3 and 2.4 present the technical specifications and the economics for different batteries. This information is required to conduct techno-economic analysis.

Type	Typical size (MW)	Cycles at 80 % DOD (x1000)	Expected useful lifetime (Years)	Maximum DOD (%)	Round-trip efficiency (%)
Vanadium RFB	10	10–13	15–20	100	75–85
Zn-Br RFB	2	5–10	5–15	60–70	72–80
Lead-acid	20-70	2–4.5	5–15	60–80	65–90
Li-ion	10	1.5–4.5	5–15	80–100	85–95
Ni-Cd	40	2–2.5	10–20	80	60–75
NaS	8	2.5–4.5	10–15	80–85	75–90

Table 2.3. Technical specifications for different EES technologies [2, 29, 95-100].

Type	Capital cost $/kWh	Fixed O&M $/kW-yr	Variable O&M $/MWh
Vanadium RFB	460–1600	3.8-19.4	0.22–3.14
Zn-Br RFB	200–595	3.6-7.7	0.34–2.25
Lead-acid	206–950	3.6-14.5	0.17–0.58
Li-ion	500–2500	2.2-15.3	0.45–6.29
Ni-Cd	632–1256	4.5-26.9	unknown
NaS	200–632	2.2-19.4	0.34–6.29

Table 2.4. Current typical capital and operation and maintenance costs for different EES technologies [2, 95, 96, 99, 100].

With a focus on VRB and Li-ion in this research, Table 2.5 provides a comparison of the pros and cons and the maturity of VRB and Li-ion. Along with Li-ion, VRB is currently one of the mature technologies for grid scale storage application and is currently available for commercial use [83, 101].

	VRB	Li-ion
Advantages	• Power and energy ratings are independent and highly scalable • No degradation in energy storage capacity • High cycle-life, up to 10,000 cycles • Capable to achieve very deep cycle, i.e., 100 % depth of discharge	• High energy and power density • Low self-discharge • High round-trip efficiency
Disadvantages	• High balance of system costs • Reduced efficiency due to rapid charge/discharge • Energy density and power density are generally lower compared to other EESs	• High capital cost • Requirement of battery management system for operation, management and against cell degradation • Limited thermal tolerance • Thermal run away due to electrolyte decomposition
Commercial maturity	Demonstration/early commercialised	Demonstration
Technological maturity	Development phase	Development phase
References	[2, 29, 83, 95–105]	[2, 29, 83, 95–100, 105]

Table 2.5. A summary on commercial-socio based information for VRB and Li-ion battery in grid scale application.

2.4 Research gaps

2.4.1 LCOE for solar PV and electrical energy storage

There are many ways to calculate the economic viability of distributed generation and energy efficiency projects. The capital cost of equipment, the operation and maintenance costs and the fuel costs must be combined in certain ways so that a comparison can be made. The generally used economic metrics are return on investment, simple payback period, initial rate of return, net present value, internal rate of return and LCOE [13].

Return on investment: It is a simple ratio on the total net income, i.e., gross profit minus the

expenses with respect to the total investment. The metric is simple to use and can provide a quick comparison of the profitability of renewable projects. However, there are several drawbacks. With no accounting policies such as interest rates and depreciation policy, comparisons can be confusing and incomplete. Equation (2.3) defines the return on investment.

$$\text{ROI} = \frac{\text{Net income (\$)}}{\text{Net expenditure (\$)}} \tag{2.3}$$

Simple payback period: Measured in years to calculate the duration to breakeven, it is a simple ratio of the additional initial cost in $ to the yearly savings in $/yr. For example, a more energy-efficient air humidifier costing an extra 500 $ and which can save 100 $/yr in electricity would have a simple payback of 5 years. With the advantage of being easily understandable, the disadvantages are similar nature to those of return on investment. Equation (2.4) defines the simple payback period.

$$\text{Simple payback period} = \frac{\text{Incremental cost } \Delta C(\$)}{\text{Annual savings } S(\$\text{yr}^{-1})} \tag{2.4}$$

Initial rate of return: This metric is the inverse of the simple payback period. It is the ratio of the yearly savings to the additional initial investment. An example of a 20 % initial rate of return would be a more energy-efficient air humidifier that costs an extra 500 $ but can contribute to a saving of 100 $/yr in electricity. This metric is useful for providing a simple "minimum threshold" indicator. To further explain, if the investment has an initial rate of return under the threshold, the proposed plan in the project can be dropped. The initial rate of return is defined in Equation (2.5) below:

$$\text{Initial rate of return} = \frac{\text{Annual savings } S(\$)}{\text{Incremental cost } \Delta C(\$\text{yr}^{-1})} \tag{2.5}$$

Net Present Value (NPV): The aforementioned three methods are too simple, and the time value of money is neglected. According to the "time value of money" principle, there is a greater economic benefit in receiving the cash and energy now than at a particular time than

later as time progresses due to earning potentials [106]. This metric uses the discount rate to consider this. NPV can indicate the value a project or an investment brings to the firm. If NPV is greater than zero, it indicates that the investment would add value to the firm. The converse happens if NPV is less than zero. Zero NPV indicates that the firm will neither profit nor lose with the investment. This metric is a prerequisite and is the numerator for the levelized cost of electricity. NPV is defined in Equation (2.6) below where CF is the net cash flow ($):

$$\text{NPV} = \sum_{t=0}^{n} \frac{CF_t}{(1+r)^t} \tag{2.6}$$

Internal Rate of Return (IRR): This is the discount rate that makes the NPV of the project equal to zero. As suggested, the advantage of using IRR is that the exact rate of return for each project with different costs of investment can be obtained, therefore allowing the investor to estimate the potential returns before the project commences. However, the method does not consider critical factors such as project duration and future expenditure. The metric only compares the cash flow to the existing costs. The IRR is calculated with Equation (2.7) given below:

$$\sum_{t=0}^{n} \frac{CF_t}{(1+\text{IRR})^t} = \text{NPV} = 0 \tag{2.7}$$

LCOE: All of the above-mentioned metrics focus on the monetary, i.e., the price of dollar for electricity generation. The shortcoming with these approaches is that the energy, i.e., kWh is not presented in the economic analysis. To compare the cost of generation and storage sources, the research scope is limited to the use of LCOE.

LCOE is a measure of costs which attempts to compare different methods of electricity generation on a comparable basis. It is an economic assessment of the average total cost of building and operating a power-generating asset over its lifetime divided by the total energy output of the asset over that lifetime. The LCOE can also be regarded as the minimum cost at

which electricity must be sold in order to achieve breakeven over the project's lifetime. The aim of LCOE is to provide comparison of different technologies, e.g., wind, solar and natural gas of unequal life spans, project sizes, different capital costs, risks, returns and capacities.

The general equation for LCOE [107, 108] is defined in Equation (2.8). It is essentially the lifetime cost of the system divided by the lifetime energy production of the system.

$$\text{LCOE} = \frac{\text{Lifecycle cost (\$)}}{\text{Lifetime energy production (kWh)}} \tag{2.8}$$

Variable renewable generators such as solar PV are unlike conventional generators; they cannot be dispatched (except by curtailing output) and their output varies depending on local weather conditions which are not accurately predictable. Many analyses have considered the lifecycle or levelized cost solely for storage component without considering the cost at a system level and the energy exchange between generation source and storage [95, 98, 109, 110]. LCOE analyses for renewable systems are also already well established and have been presented in numerous articles such as [111]. However, the cost analysis for the PV-EES system and particularly the analysis of levelized cost of storage have not been given sufficient attention and have not been clearly justified.

The cost analysis for various EESs in the grid-connected system is presented in [109]. It calculates the electricity cost added by storing electricity for different storage technologies. It has made comparisons solely for storage technologies, but the paper has not considered renewable energy systems. The economic implications of EES technologies are obscured for the power grid stakeholders [95]. If the cost of charging electricity would be deducted from the LCOE delivered by EES, the net levelized cost of storage (LCOS) would be provided as in Equation (2.8) below [95].

$$\text{LCOS} = \text{LCOE} - \frac{\text{price of charging power}}{\text{overall efficiency}} \tag{2.9}$$

Equation (2.9) states that LCOS will be less than LCOE. The cost of storage should be higher

than that of the system as the storage cost needs to include the cost of electricity generation to be stored in the EES. The storage will have an efficiency factor; hence, the storage output energy will be lower than the electrical energy generated by the source. It is noted that the variable generators, i.e., renewables, are not considered in the calculation of LCOS or LCOE for the system. The energy stored in the storage system is affected by the electrical energy production of renewable sources.

In general, the future perspective is promising for Lithium-ion (Li-ion) batteries in power system applications as the retail price is declining and the technical specifications are reaching new heights with reduced manufacturing costs, extended lifetimes, use of new materials and improved safety parameters. Li-ion and lead-acid batteries are suitable for short duration services whereas NaS and Vanadium Redox flow batteries (VRB) are suitable for long duration services [98].

A study of the LCOE for hydrogen-bromine flow battery is provided in [110]. It mentioned that although the capital cost of storage is of critical importance, the most significant metric is the LCOE and it should be the value to be minimised instead of capital cost. At 0.40 $/kWh, the hydrogen-bromine flow battery system is too expensive for grid-level application due to hydrogen storage and power electronics' equipment costs.

Li-ion batteries are the most common storage technology, and VRB are emerging as another storage option for grid applications [83]. The World Energy Council [96] has proposed a formula, as shown in Equation (2.10), known as the Levelized Cost of Storage. It enables comparisons between different types of storage technologies in terms of average cost per produced and stored kWh.

$$\mathrm{LCOS} = \frac{I_{\mathrm{o}} + \sum_{t=1}^{n} \frac{C_{\mathrm{Storage}_t}}{(1+r)^t}}{\sum_{t=1}^{n} \frac{E_{\mathrm{Storage}_t}}{(1+r)^t}} \tag{2.10}$$

I_{o} is the initial investment cost and C_{Storage_t} and E_{Storage_t} are the total costs and energy output at year t, respectively. r is the discount rate. It is mentioned that the LCOS formula only summarises the general LCOS of each technology, i.e., without implementing the application cases to a specific context such as for a PV system. This suggests that the renewables industry faces two chief challenges when applying the LCOS metric:

1. Arbitrariness: The application case varies widely and depends on the type of service provided;
2. Incompleteness: The cost calculation does not reflect the characteristics of storage. Traditionally, LCOE is reflected upon by the applied discount factor. As it neglects higher potential revenues, from providing flexibility, it is a simplified approach for the actual value of storage.

Policymakers should examine storage through holistic case studies in context instead of only emphasising on generic cost estimations. Lazard [29] modelled ten different use cases for storage including frequency regulation, grid balancing and micro-grid support with the possibility of eight different storage technologies, ranging from compressed-air energy storage to Li-ion batteries. The required energy output for different storage applications were predetermined. Because of the operating and physical conditions, some electrical energy storages would need to be overrated. This oversizing results in less than 100 % DOD over a single cycle.

The LCOS provided by Lazard is an optimistic estimation, and in practice, the storage system will not be utilised till 100 % of its capacity. In the case of PV integration, the energy stored in the storage system depends on the PV system output, and this is highly arbitrary as it depends on the nature of solar irradiance. Therefore, the LCOS will be different in real-life situations and is expected to be higher. The values provided by Lazard can be used to compare different storage technologies and applications but cannot be used for system resource planning and

decision-making. The operational parameters used in Lazard's LCOS study for PV integration are presented in Table 2.5.

Parameters	
Project lifetime (Year)	20
Discount rate (%)	8
Storage power capacity (MW)	2
Storage energy capacity (MWh)	4
Cycles per day (100 % DOD)	1.25
Days of operation per year	350
Annual electrical energy production (MWh)	1750
System's total generated electrical energy (GWh)	35

Table 2.5. Parameters used for LCOS study for PV integration [29].

The report did not provide the method for LCOS calculation. It is assumed that the results are calculated with Equation (2.9). The results of LCOS for PV integration with the lower and upper bound range for different storage technology are provided in Table 2.6. The results from Table 2.6 will be useful to provide a comparison with the results in the case study in this chapter. Table 2.7 presents a comparison on the levelized cost analysis features for the three prominent hybrid renewable energy system software packages. It is observed that LCOS is currently not included.

	LCOS ($/kWh)	
Storage Type	**Lower bound**	**Upper bound**
Zinc	0.245	0.345
VRB	0.373	0.950
Li-ion	0.355	0.686
Lead	0.402	1.068
Sodium	0.379	0.957

Table 2.6. Current LCOS for PV integration [29].

	HOMER Pro	RETScreen Expert	System Advisor Model (SAM)
Developer	HOMER Energy LLC	Natural Resources Canada	National Renewable Energy Laboratory
Availability	Priced	Free	Free
Description	The software can provide hourly interval data analysis, hence better modelling of the intermittency of renewables. It is capable of performing brute-force system optimisation such as for components sizing purposes. The software may generate synthetic hourly solar data from monthly average Clearness Index or daily radiation data if real data is unavailable.	The software evaluates the performance of systems based on statistical monthly average data. One of the major advantages of the software is that it has an abundant amount of geographical data built-in, which is obtained from NASA's climate database.	The software is used for studying grid-connected systems only, and currently does not support stand-alone system analysis. Shading and snow data can be included in the analysis to model the reduced PV output. A database of hourly solar irradiance data is provided from NREL database.
Supported energy storage model	Flywheel, customisable batteries, flow batteries and hydrogen	Thermal storage tank	Lead-acid and Li-ion
Provide LCOE?	Yes	No	Yes
Provide LCOS?	No	No	No
Reference	[112]	[113]	[114, 115]

Table 2.7. Comparison of levelized cost analysis features for the prominent hybrid renewable energy system software packages.

A novel methodology for the calculation of levelized cost of stored energy was proposed in [116]. New terms were proposed such as price increase factor and internal transfer cost to calculate the LCOE of the hybrid system. These two terms are currently not well defined in the industry and no literature has discussed them, hence, these values are not practical for calculations. As stated in [117], the economic estimation on hybrid systems utilising a combination of PV, EES and cogeneration is difficult, and at present, no comprehensive method exists for guiding decision makers. The proposed LCOE for the hybrid system is given

in Equation (2.11) below [117]:

$$\mathrm{LCOE} = \frac{I + \sum_{t=1}^{n} \frac{(Ii + O + F_{\mathrm{CHP}})}{(1+r)^t}}{\sum_{t=1}^{n} E_{\mathrm{tPV}}(1-d_{\mathrm{PV}})^t + \frac{E_{\mathrm{tCHP}}(1-d_{\mathrm{CHP}})^t}{(1+r)^t}} \tag{2.11}$$

I is the total installation cost which includes the cost of PV, battery and the Combined Heat and Power (CHP); i is the interest rate on the hybrid system for 100 % debt financing. O is the total operation and maintenance cost. F_{CHP} is the annual fuel cost of the CHP unit. E_{tPV} and E_{tCHP} are the rated annual electrical energy production from PV and CHP units, respectively. d_{PV} and d_{CHP} are the degradation rates for PV and CHP units, respectively. The electrical energy produced by the PV system is not discounted. It does not reflect the actual value of the PV energy in the future. The equation for the hybrid system LCOE does not discount the energy lost from using the storage system due to round-trip efficiency in which the total energy output from the system is the electrical energy produced by PV and the CHP unit.

Reference [118] has discussed and proposed the LCOE metric for energy storage. The authors claim that large-scale storage is becoming a significant issue for utilities. Therefore, this justifies the development of a levelized cost algorithm which accommodates storage systems. In the LCOE equation for energy storage, the energy output from the energy storage is assumed to be the annual electrical energy production of the system. This may not be the case as not all electrical energy produced by the system will be delivered by the energy storage.

This section of the literature review concludes that the LCOE needs to be modified to consider the stochastic properties of solar energy. Additionally, the LCOS is a recent research topic on quantifying the cost of storage. However, EES does not generate electricity from primary energy sources, and there is a need to include this into the levelized cost analysis.

2.4.2 Clearness Index cluster analysis for PV system sizing

The use of models with CIs for any solar system applications such as solar hydrogen production is appropriate and simple. This is because CI only requires the global solar irradiance data [119]. The knowledge of the statistical behaviour of the short-term variability of solar irradiance will provide a more accurate evaluation of the uncertainty in the long-term annual energy production of solar power plants [120]. CI can be used to train the Markov transition matrix to approximate the daily irradiance value with the Markov model [121]. Irradiance sequences can be generated via this method. Reference [122] uses CI to segregate the forecasting complexity into the prediction of solar geometry and the prediction of cloudiness and aerosol. The quadratic and cubic equations which are based on global solar irradiance data exhibit the highest accuracy in predicting the diffuse fraction as a function of CI [123–125].

CI can be effective in providing information on the fluctuation of irradiance. Wavelet analysis is applied to the daily CI profiles in [126] which is decomposed into components to evaluate the endurance and magnitude of various fluctuations of the solar irradiance.

PV generations are commonly presented by Beta distribution [127]. This assumption has been widely used for the system planning purposes. However, in reality, the underlying distribution may vary widely due to the hemisphere and climate of the location [128]. Reference [129] determined the parameters of the appropriate distribution that provide the optimum fit for CI. The global solar irradiance is thereafter predicted from CI using inverse transformation of the cumulative distribution function. The proposed method effectively predicts the monthly average global solar irradiance.

Pattern recognition and cluster analysis have been applied to other renewable sources such as wind. A statistical approach was proposed for improving short-term wind electric power forecast based on the pattern recognition technique [130]. The predictions on wind speed and direction to identify patterns of the wind behaviour, at the location considered to obtain a

stochastic distribution of the daily wind speed, were studied in [131]. A statistical hybrid wind power forecast technique was proposed in [132] in which weather events were clustered with respect to the most important weather forecast parameters. Additional research effort is required in the area of pattern recognition and cluster analysis for solar irradiance PV systems. Fractal dimension analysis of daily solar irradiance, measured with a time step of 10 minutes at Golden and Boulder located in Colorado, is provided in [133], aiming to classify daily solar irradiance. Fractal dimension is a ratio providing a statistical index of complexity to compare the fractal pattern changes with the geometric scale at which it is quantified. These results lead to three classes, namely clear sky, partially covered sky and overcast sky. Fractal dimension analysis can be used to classify patterns only and, they do not provide information on the similarities between the classified patterns.

The daily distributions of CI were classified by estimating a finite mixture of the Dirichlet distribution in [134]. The results display four distinct classes of distribution corresponding to various types of days. With Bayesian statistics, the advantages are that the true parameters are interpretable by providing the credible interval. As it is a distribution approach, it lays out a convenient setting for various ranges of models in missing data problems. Algorithms such as Markov chain Monte Carlo requires the statistical properties, e.g., probability distribution of the problem for producing samples. However, with this approach, there are issues with estimating the prior (concentration) parameter for generating the prior distribution. The posterior distributions are heavily influenced by the priors. It is generally more computationally intensive than partition-based approach due to the training of the mixture model. Moreover, the CI in different seasons or months has not been studied or provided.

Hierarchical cluster analysis for the classification of typical meteorological days from global irradiance data is provided in [135]. The classification was performed with aggregation Ward's method. It is observed that the recorded days were clustered in three, four or five groups for

monthly time step and three groups were classified for annual time-step. The authors relied on discriminant analyses to evaluate the number of clusters and this was achieved by visual inspection. Hierarchical clustering is a method of cluster analysis by building a hierarchy of clusters. There are two approaches; the more common approach is known as the Agglomerative 'bottom up'. Each pattern starts in its own cluster, and clusters are merged as each pattern moves up the hierarchy. In the Divisive 'top down' approach, all patterns start in one cluster and get divided as one moves down the hierarchy. The advantage of hierarchical clustering is that the number of clusters do not need to be specified. The disadvantage is that it is a greedy algorithm; the most optimal short-term clusters might not necessarily provide the best overall clustering. The algorithm cannot undo the clustering procedure by revisiting the previous hierarchical stage. Given n_{v} patterns, the computational complexity can be very high for both approaches, with divisive clustering being an exhaustive search at $O(2^{n_{\mathrm{v}}})$ which is nearly intractable with large datasets.

Having reviewed the clustering and classification methods for CI, partition-based clustering approaches such as *K*-means and Fuzzy C-means can also be used for this research. The traditional distance metrics such as the Euclidean distance and the Manhattan distance are static. This is also one of the issues dealing with outliers in the dataset. Dynamic distance metrics such as Dynamic Time Warping will be studied for the CI clustering problem.

2.4.3 Efficient method for PV-AD-EES system sizing

Determining the optimal size, i.e., power and energy nameplate capacity, for the generation and storage sources in a stand-alone hybrid renewable energy system is a complicated task because of the high number of variables and the non-linearity characteristics, e.g., fuel consumption of the system components [20].

The objective is to maximise or minimise a cost function in an optimisation problem. The description of the well-known optimisation techniques is given below:

Interior Point method (IP): IP is an algorithm for solving non-linear and linear convex optimisation problems. The Karmarkar's algorithm was developed to overcome the exponential-time computational complexity of the Simplex method. The fundamental idea of the algorithm is that the optimal solutions are approached from the interior of the feasible domain. This results in fewer iterations but require more complicated operations per iteration to find a better moving direction. The direction and step-length are variables that need to be calculated to determine the succeeding interior solution. The line search or trusted region strategy is used to find the local minimum of the objective function. The method uses the optimality condition to determine if the current solution is optimal which essentially implies that the solution is optimal if the feasible direction from the current solution is not in a good direction. The details for the optimisation algorithm can be referred to in [136].

Genetic Algorithm (GA): GA belongs to a class of evolutionary algorithms. It performs mathematical optimisation, adopting ideas from natural selection and biological evolution. The process begins with randomly generating a population of candidate solutions. Chromosome in binary form is used to represent each candidate solution. The term generation is coined for the population at each iteration. The fitness of each candidate solution in the population is evaluated in each generation where the fitness is calculated from the fitness function, a variant of the objective function for the optimisation problem. The population of chromosomes is repeatedly updated at each iteration with crossover and mutation to improve the population. Selection such as tournament selection is performed to determine the parents for the crossover. A crossover is a generic operator that produces a child solution by taking more than one parent solutions. Mutation is a generic operator that changes one or more genes' value in a chromosome, aiming to provide genetic diversity and avoid local minima. At each generation, the process of evaluation, selection, crossover and mutation is performed. The algorithm terminates when the maximum number of generations is reached or when the fitness level has

reached satisfactory. GA can be used for problems that are highly nonlinear, non-differentiable and discontinuous. The details for the optimisation process and algorithm can be found in [137, 138].

Particle Swarm Optimisation (PSO): Similar to GA, the PSO algorithm performs mathematical optimisation with a population of candidate solutions. The algorithm begins by creating a swarm (population) of initial particles (candidate solutions) and assigning them initial velocities. At each iteration, the particle location with the lowest function value is then determined by evaluating the objective function at each location of the particle. The particles update their velocity, based on their current velocity, individual best location and the best location of their neighbours. Subsequently, the particles' locations, velocities and neighbours get updated. The iterative process stops once the stopping criteria such as maximum number of iterations or relative change in the best objective value is reached. The details for the optimisation process and algorithm can be referred to in [138].

Pattern Search (PS): The direct search method does not require the gradient of the objective function to perform mathematical optimisation. This overcomes the challenges for optimisation problems that have objective functions which are not continuous or differentiable. There are numerous types of direct search methods with the most notable one is the Generalized Pattern Search algorithm (GPS). With this algorithm, a sequence of points is generated from the mesh scalar and the pattern vector. At each iteration, the algorithm searches the set of points around the current point known as the mesh vector. The optimal point from the mesh vector is then determined which improves the objective function at the current point. The new point will be the current point for the next algorithm iteration given that the objective function could be improved. The details for the algorithm can be found in [139].

Simulated Annealing (SA): This optimisation method models the material heating physical process. Initially, the material is heated to a high value with the temperature slowly decreasing

to reduce the defects. A new point is randomly generated at each iteration based on the distance from the current point, i.e., the point from the previous iteration. The distance is calculated from a probability distribution and is a function of the temperature. The new point should generally minimise the objective function but also has a probability of raising the value of the objective function. This is done to overcome the issue of the optimal solution being trapped in the local minima, by exploring globally. The temperature for the algorithm can be systematically reduced by the Annealing Schedule. The algorithm will converge to an optimal point as the temperature decreases while reducing the extend of its search. The details for the algorithm can be referred to in [138].

A model aimed to minimise the cost of the PV system according to the minimisation of the PV array area and battery storage is presented in [140]. The method calculates the minimum number of storage days and the minimum PV array area. A comparison between stand-alone and hybrid system sizing is presented. However, the cost is not evaluated for the system. The study uses average solar irradiance to determine the PV module characteristics which does not consider the daily fluctuation of solar irradiance and daily energy storage requirement.

Reference [141] presents a PV-diesel hybrid power system with battery backup for a village with the computer package HOMER. HOMER [142] is an optimisation software package which simulates different renewable energy sources' system layouts and sizes them on the basis of net present cost. It uses sensitivity analysis to consider different generation capacities and battery storage capacities to determine the optimal size of the system. The issue with this program is the high computational requirement due to the large number of cases required to be computed. The study required a total of 448,000 runs based on 28 sensitivities where sensitivities are defined as the sizing control parameters such as the size of PV, diesel generator etc. Additionally, the software is of "Black Box" code utilisation such that there is no

knowledge of its internal operation and optimisation algorithm [143]. In the present study, it aims to use all renewables by replacing diesel with AD which is a controllable renewable.

An optimal sizing method for wind-solar-battery hybrid system with stand-alone and grid-connected modes was proposed in [144]. A brute force technique was used to determine the optimal sizing by searching for the best combinations of the PV-wind-battery while satisfying the proposed constraints. Loss of power supply probability and the fluctuation rate of the total output of renewable sources relative to the average load power were calculated for every probable combination. The optimal combination was chosen with minimum system cost. This method has a very high computational complexity and will scale up if detailed sizing is required. A comparison of the sizing method has been made with HOMER, and the authors claim that the proposed approach has a higher computational cost. Generators were not considered for the sizing purposes.

The techno-economic feasibility studies of utilising PV-diesel-battery hybrid systems to meet the load of a residential building with an annual electrical demand of 35.12 MWh and a commercial building with an annual electrical demand of 620 MWh are presented in [145] and [146], respectively. HOMER was used to carry out these studies. They concluded that the hybrid system offers several benefits: PV penetration is high; load can be fulfilled in the optimal way; diesel maintenance can be minimised, and reliable power supply could be increased. The study uses monthly average daily solar global irradiance as input for sizing purposes. The uncertainty aspect was not included in solar PV generation. The discount rate and financing costs were not considered when performing the economic analysis.

An optimal sizing methodology for a stand-alone and grid-connected PV-biomass hybrid energy system that serves the electricity demand of a typical village is presented in [147]. The results obtained suggest that grid-connected hybrid system may be a cost-effective electrification solution for numerous villages in developing countries. However, in practice, it

is impossible to be grid-connected in numerous locations especially for remote areas. Energy storage systems should be employed to overcome this issue. The technical constraints from the biomass gasifier were not considered in the study. Furthermore, the average global solar irradiance was used for the study.

A study on optimal sizing of a hybrid wind-PV-diesel stand-alone power system is presented in [148]. The consideration focused on the investment cost (installation and unit costs) and fuel cost minimisation with constraints on the reliability requirement and CO_2 emission limit. The output power of diesel generator ranges from 0 kW to the rated capacity, the technical and environmental constraints of diesel generator have been neglected in the study.

An algorithm for the economical design of a utility-scale photovoltaic power plant by compromising between the cost of energy and the availability of the plant was proposed in [149]. The paper introduces the Effective Levelized Cost of Energy (ELCOE) index as the core of the proposed design algorithm. ELCOE is an improved index based on the conventional LCOE that includes the availability of a power plant in economical assessments. However, the ELCOE proposed did not consider the use of storage systems.

This section of the literature review suggests that there is a need for sizing of solar PV power plants to maximise the use of solar energy while considering the AD biogas generator's minimum output constraint. Unlike the 'trial and error' and probabilistic approaches mentioned previously, a deterministic approach for system energy balance can be useful in determining the required size of the PV farm and the sizing of EES based on the system energy deficit.

2.4.4 Operating regime for PV-AD-EES system and EES degradation costs analysis

The operating strategy for a system with an EES and PV generator is relatively simple. Surplus energy is stored in EES and is discharged if the load is greater than generation. Significant questions arise for systems with multiple energy sources. In the case where a dispatchable

source such as AD is included, it is required to determine how the EES is charged and which dispatchable source (AD or EES) is to be used when the load demand is greater than the generation. As mentioned in [20], there are three basic control strategies for a PV-Diesel-EES system. These are known as zero-charge, full cycle-charge and predictive control strategies, respectively. The EES is never charged with the diesel generator in the zero-charge strategy. In the full cycle-charge strategy, diesel generator is used to charge the EES to 100 % SOC when the generator is on. Figure 2.9 presents the simple flowcharts for the zero-charge and full cycle-charge strategies. Predictive control strategy requires the forecast of renewable generation and load demand to charge the EES. The algorithm for such a strategy can be found in [93]. The advantage of this strategy is that energy wastage in surplus energy production from renewables is reduced. An interesting research question to be answered is about determining the optimal point for the SOC between 0 % to 100 % to be charged with diesel in order to provide a minimum operational cost [20]. In other words, the strategy will be less of an extreme and will be between zero-charge and full cycle-charge.

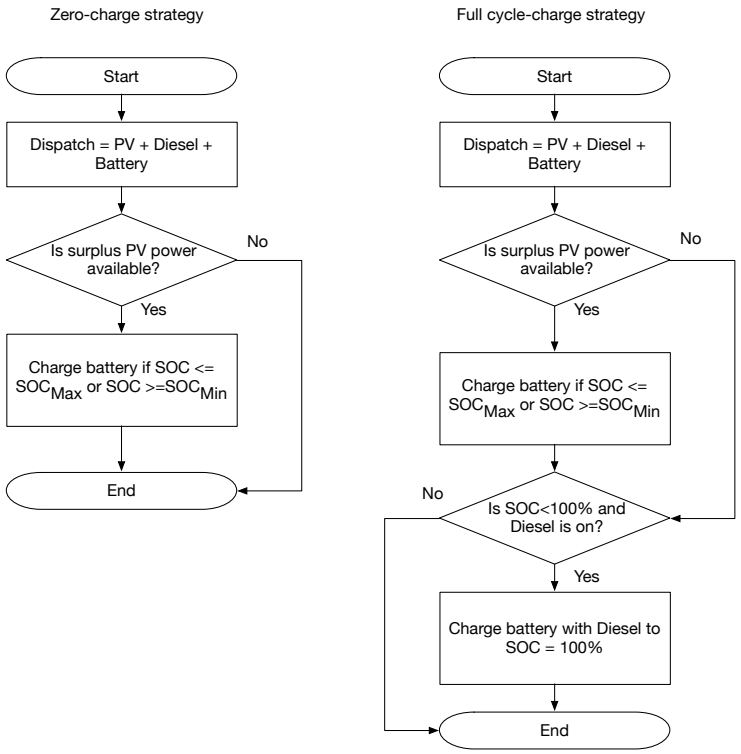


Figure 2.9. Simple flowcharts for zero-charge and full cycle-charge strategies.

Scheduling regimes such as rule-based strategies [150] have the advantage of not needing renewable and load forecasting for optimal operation. Additionally, complexity is further reduced when online optimisation is not required. The work did not mention the degradation and costs of EES and highlighted them as future work.

There are numerous research works on cycle-life studies and the costs due to EES degradation for hybrid renewable energy systems [151–154]. However, most of them do not consider partial charge-discharge cycles and the use of DOD, only accurate for initial SOC at 100 % for EES cycle-life calculations. Electrical energy delivered is also used to consider the DOD in some articles such as [151], and the actual values of the SOCs may be neglected. Theoretically, for instance, the electrical energy output from EES at SOCs of 100 % to 80 % may be the same as a situation for 40 % to 20 %. Recent literature [155, 156] has confirmed that partial charge-discharge cycles at different SOC states have a profound effect on the State of Health, i.e., discharge capacity of the EES, and consequently affects the total rated cycle-life.

Due to irregular load demands and PV power fluctuations induced from stochastic solar irradiance, the hybrid power system is highly susceptible to irregular SOCs and charge and discharge cycles. It is paramount that the degradation costs and replacement costs are accurately assessed for EES in hybrid power system analysis and optimisation [157, 158].

In the recent decade, there has been an upsurge in research related to using EES for power systems such as in charging regimes for electric vehicles [151, 152, 159], profit maximisation with energy tariffs [160, 161] and off-grid system operations [20, 162]. Mostly, this literature has considered the degradation effect of EES to an extent and has made attempts to consider the storage costs. However, the effects of irregular cycling and partial cycles of EES have not been properly addressed. Some works have considered using reference DOD to compute the rated cycle-life for the EES.

Reference [163] presents the grid-tied electrical hubs with distributed generation and energy storage for satisfying the electricity demand in Sri Lanka. The SOC for the EES has been considered for the control of the dispatchable energy source. However, the cost of storage and degradation effect have not been included.

The economic operation for a diesel-PV-EES island micro-grid in rural areas with a two-stage model predictive control strategy is proposed in [164]. The system's economics is assessed with the LCOE metric. Replacement and operational costs, which are functions of DOD and cycle-life, for EES are included in the study. However, it is unclear how the DOD and cycle-life are included and considered.

Levelized Cost of Delivery (LCOD) is proposed in [85] to compute the levelized cost of EES in PV system. The highlight of the work is that it is necessary to include the electrical energy production costs, i.e., generator costs into the storage costs. The work could be improved by also including the cost aspect of EES degradation.

EES degradation is considered with a fixed degradation cost in [165]. The cost competitiveness of the EES with respect to conventional generation is not provided.

Comparisons of several energy storage technologies in a variety of realistic micro-grid settings have been developed in [166]. The Energy System Model aims to provide similar functions to the well-known micro-grid software HOMER but with improvements in battery modelling. It is not known if and how the costs in partial cycles and irregular discharges are considered.

The economic feasibility of EES for electric bill management applications has been provided in [167]. A range of EESs have been included; these are Li-ion, zinc, an advanced lead-acid, a Sodium-Sulphur (NaS) and a flow battery with no degradation consideration. The techno-economic assessment of distributed EES for load shifting application is provided in [168]. Li-ion, NaS and redox batteries were included in the study but again, no degradation was considered.

The work in [158] aims to develop degradation cost functions for optimisation models in off-grid power system. The battery replacement cost has been provided for different ratios for battery degradation costs to diesel cost. LCOE has not been not studied in this work.

An exhaustive study to determine the optimal combination of renewable electricity sources and EES connected to a 72 GW grid system is provided in [169]. It aimed to find the least-cost combination of renewable generation and EES to match the load demand. It concluded that excess renewable production can result in lower costs for the system. The argument is that the electrical load will be met with less storage thus lowering the total system cost. The LCOE has not been studied, and it is unknown how storage degradation costs are considered.

Reference [152] proposes an optimal generation scheduling model for a system with thermal power plant, PV plant, wind farm and EES while considering the degradation cost of ESS. Lead-acid and Nickel Metal Hydride (NiMH) batteries were considered. This work aimed to include the temperature and DOD for the battery degradation cost. The battery degradation cost was modelled and fitted with a piecewise linear function. However, cycle-life effects with irregular cycling were not considered, and the degradation model is only applicable for the cycles with initial SOC at 100 %.

As reported in [160], a feed-in tariff scheme has already been established in Japan to promote the use of PV generators with EES. Many researchers studied the operation of grid-connected PV-EES system. However, attention has seldom been paid to the impact of the EES degradation characteristics. The work in [160] aims to evaluate the energy and cost savings for a grid-connected PV-EES system for a household. Operational optimisation model was constructed for considering the degradation characteristics of EES. The model has two objective functions; the operating costs and the energy savings. The study concluded that a grid-connected PV-EES system was more efficient in energy saving operations. The cycle degradation was defined by

the number of cycles and the cycle degradation rate. DOD degradation was considered to have occurred when the DOD was more than 70 %.

The stochastic problem for micro-grid energy scheduling with distributed generator and controllable loads such as plug-in electric vehicles is presented in [151]. EES degradation costs and cycle-life were calculated with DOD. The DOD in this case is the ratio of the energy delivered from the EES to the rated energy capacity. Partial cycling has not been included or discussed.

HOMER was used for designing a PV-biomass-diesel hybrid system for off-grid and grid-connected scenarios in [170]. The system's configuration was optimised for different load profiles. Surrtte 6CS25P flooded battery was used for the off-grid case. However, details or studies for the EES have not been provided.

Reference [171] proposes a method to simultaneously optimise the rule-based operating strategy and the EES capacity for a grid-connected PV-EES system. Given the present cost of storage, it claimed that using EES with the conventional operating strategy is not profitable but increases the Self-Sufficiency Ratio (SSR). It was reported that the system uses more renewables with a higher SSR.

A micro-grid charging and discharging strategy is given in [153]. A three-parameter function is fitted to estimate the battery cycle-life under different DODs. With this function, the depreciation cost model of Li-ion battery was developed. The authors acknowledged that the battery charge and discharge cycles under working conditions are composed of several micro-cycles with different DODs. To overcome this issue, the rain-flow counting method was employed to decompose the complex cycles to micro cycles of different DODs. Charge/discharge cycles were counted with respect to each range of the DOD for the year. Partial cycling was not included, and this method may not be appropriate if the initial SOC is not at 100 %. A sizing methodology with Loss of Load Probability for an off-grid PV system

with lead-acid battery is presented in [172]. This work also adopts the rain-flow counting method for battery lifetime estimation. It is unclear if the rain-flow counting method can accurately represent the EES degradation, and a comparison with the capacity fade model should be made.

A model for the operation of distribution companies in regulating price or locational marginal price mechanisms is given in [154]. Two types of EES were considered, namely lead-acid and lithium-ion. It could be observed that there were multiple partial charging and discharging, at different SOCs throughout the time interval. It requires to consider the partial cycles for a more accurate optimisation problem formulation.

Reference [150] presents the rule-based strategies for operating an EES connected to a self-consumed PV system to reduce payments to the grid. As stated by the authors, the work does not consider the degradation cost of using the EES.

As suggested in this section of the literature review, at present there is little amount of work in levelized cost calculations for renewable energy system operation with EES energy discharge at different SOC ranges. Adopting the cell degradation model for levelized calculation will be an aspect of this research.

2.5 Summary

In this chapter, it has been established that for the off-grid system to accommodate the anticipated increase of PV power capacity, system sizing and scheduling methods are required to maximise the use of PV energy and to minimise the generation costs, considering the biogas emission constraint and degradation costs of EES. It is evident that the costs of EES is experiencing an exponential decrease with respect to time, which results in a universally adopted EES for various grid applications. The technical and economic aspects of six different types of EES were examined, which will be useful for techno-economic analyses for storage systems. The gap analysis is given in Section 2.4 and has highlighted four different research

areas to be conducted. Chapter 3 begins with proposing the levelized cost metrics for solar PV and electrical energy storage. These will be used for evaluating the economic viability in sizing and operation of the hybrid system.

Chapter 3

Levelized cost of electricity for solar photovoltaic and electrical energy storage

This chapter presents the methods for studying the LCOE for PV system and EES. The research question arises for determining the LCOE for EES when EES is paired with solar PV to utilise surplus electricity. The proposed metrics will be used for calculating the LCOE for EES, solar PV and the hybrid system. Since EES does not produce electrical energy as it is not a generator, a new metric Levelized Cost of Delivery (LCOD) is proposed to calculate the LCOE for the EES. Marginal LCOEs have been studied to understand the levelized cost with different system investments. The proposed cost calculation methods are evaluated with two types of EESs (Vanadium Redox flow battery (VRB) and Lithium-ion (Li-ion) battery). The recent system component costs data presented in Chapter 2 is used for the analysis. The results are compared with Lazard to understand the implication of the proposed methods. The marginal LCOE and LCOD indices can assist policymakers to consider the discount rate, the type of storage technology and sizing of components in a PV-EES hybrid system.

The chapter proceeds as follows: The methods for analysing the LCOE for PV systems are provided in Section 3.1. Section 3.2 presents the derivation for the LCOD and the $\mathrm{LCOE}_{\mathrm{System}}$, i.e., the LCOE for the combined assets PV and EES. Section 3.3 provides the marginal LCOE derivations and the case studies. Chapter summary is provided in Section 3.4.

3.1 Levelized cost of electricity for solar PV

There are two methods commonly used to calculate the LCOE; the "discounting" method and the "annuitizing" method [173]. In the discounting method shown in Equation (3.1), the stream of real future costs and electrical outputs identified as C_t and E_t in year t are discounted back with discount rate r to a present value (PrV). The PrV of costs is then divided by the PrV of lifetime output.

$$\mathrm{LCOE}_{\mathrm{Discount}} = \frac{\mathrm{PrV(Costs)}}{\mathrm{PrV(Output)}} = \frac{\sum_{t=0}^{n} \frac{C_t}{(1+r)^t}}{\sum_{t=0}^{n} \frac{E_t}{(1+r)^t}} \tag{3.1}$$

In the ''annuitizing'' method shown in Equation (3.2), the costs, i.e., the present value of the stream over the device's lifetime is determined and then transformed into an equivalent annual cost using the standard annuity formula. The equivalent annual cost is then divided by the average annual electrical output over the lifetime of the plant where n is the lifetime of the system in years.

$$\mathrm{LCOE}_{\mathrm{Annuitizing}} = \frac{\mathrm{Ann(Costs)}}{\mathrm{Ave(Output)}} = \frac{\left(\sum_{t=0}^{n} \frac{C_t}{(1+r)^t}\right)\left(\frac{r}{1-(1+r)^{-n}}\right)}{(\sum_{t=1}^{n} E_t)/n} \tag{3.2}$$

The LCOE will be the same for the two methods given that the discount rate and energy output in Equation (3.1) are identical for calculating the annuity factor in Equation (3.2). The annual energy output must also be constant over the lifetime of the device for the levelized costs to be the same under both methods. The costs are converted to a constant value over time with the annuity method. This implies that it is only appropriate where the flow of energy output is constant. Many researches commonly assume that the annual energy output is constant for estimating the levelized costs. Due to weather perturbations, the renewable technologies' annual energy output would vary from day-to-day. Therefore, the discounting method will provide more accurate results than the annuitizing method when calculating LCOE for

renewable sources.

One of the misconceptions while calculating LCOE is that the summation does not start from $t = 0$ to include the project cost at the beginning of the first year [174]. The first year of the cost should not be discounted to reflect the present value, and there is no system energy output to be degraded. Reference [174] also provides a review on the methodology of properly calculating the LCOE for solar PV. The equation for calculating the LCOE for a PV system is given in Equation (3.3) below:

$$\text{LCOE} = \frac{\sum_{t=0}^{n}(I_t + O_t + M_t + F_t)/(1+r)^t}{\sum_{t=0}^{n} E_t/(1+r)^t} = \frac{\sum_{t=0}^{n}(I_t + O_t + M_t + F_t)/(1+r)^t}{\sum_{t=0}^{n} S_t(1-d_{\text{PV}})^t/(1+r)^t} \quad (3.3)$$

It is worth noting that the initial investment I_t should be one-off payment. It should not be discounted and excluded from the summation. The LCOE for PV systems provided by the authors in [174] also considers the degradation factor of PV modules. The electrical energy generated in a given year E_t is the rated energy output per year S_t multiplied by the degradation factor $1 - d_{\text{PV}}$ which decreases the energy output with time. The maintenance costs, operation costs and interest expenditures for time year *t* are denoted as M_t, O_t and F_t, respectively.

3.2 Cost calculation methodology

LCOE work that considers the cost of storage and renewable energy systems as a whole rather than separately has been discussed in Chapter 2. Moreover, it has been observed that the daily average global solar irradiance or capacity factor is commonly used to calculate the total electrical energy generation of the hybrid system. This will provide a less accurate study due to the absence of the consideration of variability of renewable sources. This section aims to provide the methodology to better represent the LCOE for a PV-EES hybrid system.

It is common to store excess electrical energy generated by PV in storage systems to be used later on. The PV energy at an available time instance should be used directly to support the load and to avoid the losses due to round-trip efficiency, η_{EES}. The total energy is split into two

types, the surplus and the direct energy as shown in Figure 3.1. Surplus energy, E_{Surplus}, is the extra electrical energy generated by a PV system and not consumed by the load. Direct energy, E_{Direct}, is the electrical energy that is consumed by the load directly. C_{Surplus} and C_{Direct} are the costs to generate surplus and direct electrical energies, respectively.

Equation (3.4) gives the LCOE for a PV system which has both the direct and the surplus energy components. The surplus energy can be stored in EES. To fully utilise the PV energy, as the surplus energy cannot be used when load demand is less than the generation output, there is a need to store the energy. Moreover, the energy delivered by EES will be reduced due to the round-trip efficiency. LCOE_{PV} will be reduced when storage is included in the system by utilising the surplus energy.

Energy storage is not an electrical energy source, and the definition of LCOE only considers electrical energy generation [175]. As a result, the definition of LCOE for PV system with EES needs further consideration in order to provide a more accurate representation of the LCOE. Equation (3.4) shows LCOE with two partitions, namely, direct and surplus energy from the conventional LCOE in Equation (3.5).

$$\text{LCOE}_{\text{PV}} = \frac{\sum_{t=0}^{n} \frac{C_{\text{Surplus}_t}}{(1+r)^t}}{\sum_{t=0}^{n} \frac{(E_{\text{Surplus}} + E_{\text{Direct}})_t}{(1+r)^t}} + \frac{\sum_{t=0}^{n} \frac{C_{\text{Direct}_t}}{(1+r)^t}}{\sum_{t=0}^{n} \frac{(E_{\text{Surplus}} + E_{\text{Direct}})_t}{(1+r)^t}} \tag{3.4}$$

$$\text{LCOE}_{\text{PV}} = \frac{\sum_{t=0}^{n} \frac{(C_{\text{Surplus}} + C_{\text{Direct}})_t}{(1+r)^t}}{\sum_{t=0}^{n} \frac{(E_{\text{Surplus}} + E_{\text{Direct}})_t}{(1+r)^t}} \tag{3.5}$$

Figure 3.1 shows the energy flow diagram of the renewable energy system and storage. The PV array in the system is separated into two sets. The net energy output of the EES needs to consider η_{EES}. The EES experiences the electrical energy flowing in and out.

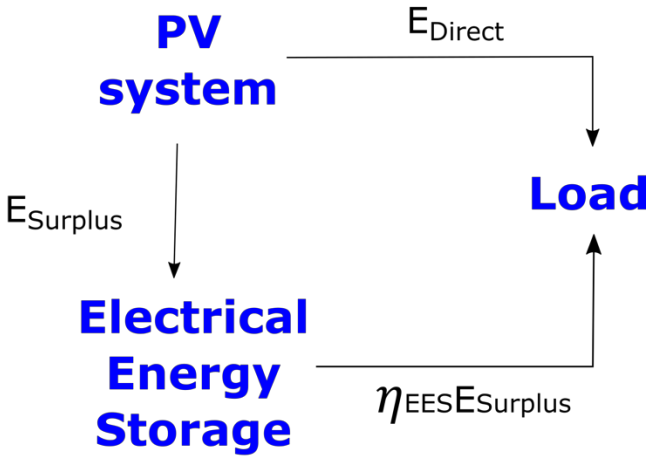


Figure 3.1. Energy flow diagram of the PV system and electrical energy storage.

To simplify the derivation process, Equations (3.6) to (3.10) will be used for the LCOE calculations in the upcoming derivations.

$$C_{\mathrm{EES}} = C_{\mathrm{Cap_{EES}}} + \sum_{t=0}^{n} \frac{C_{\mathrm{O\&M_{EES}}_t}}{(1+r)^t} \tag{3.6}$$

$$E_{\mathrm{EES}} = \eta_{\mathrm{EES}} \sum_{t=0}^{n} \frac{E_{\mathrm{Surplus}_t}(1-d_{\mathrm{EES}})^t}{(1+r)^t} \tag{3.7}$$

$$C_{\mathrm{PVsurplus}} = \left(C_{\mathrm{Cap_{PV}}} + C_{\mathrm{Inst_{PV}}}\right) N_{\mathrm{Surplus_ave}} + \sum_{t=0}^{n} \frac{\sum_h^m C_{\mathrm{O\&M_{PV}}} N_{\mathrm{Surplus}_h}}{(1+r)^t} \tag{3.8}$$

$$C_{\mathrm{PVdirect}} = \left(C_{\mathrm{Cap_{PV}}} + C_{\mathrm{Inst_{PV}}}\right) N_{\mathrm{Direct_ave}} + \sum_{t=0}^{n} \frac{\sum_h^m C_{\mathrm{O\&M_{PV}}} N_{\mathrm{Direct}_h}}{(1+r)^t} \tag{3.9}$$

$$E_{\mathrm{PV_{Directtotal}}} = \sum_{t=0}^{n} \frac{E_{\mathrm{Direct}_t}(1-d_{\mathrm{PV}})^t}{(1+r)^t} \tag{3.10}$$

d_{EES} and d_{PV} are the annual performance degradation rates for storage and the PV array, respectively. $N_{\mathrm{Direct_ave}}$ and $N_{\mathrm{Surplus_ave}}$ are the fraction of the PV array for generating direct energy and surplus energy for storage, respectively. N_{Direct_h} and N_{Surplus_h} are the fraction of PV array at hour h for generating direct energy and surplus energy for storage, respectively. E_{Direct} is the electrical energy generated from PV and directly supplied to the load without

going through storage. $C_{\mathrm{PVsurplus}}$ and C_{PVdirect} are the total lifetime costs of PV generation that produce the surplus and direct consumption of energy for the system, respectively.

3.2.1 Electrical energy storage

The derivation of the LCOE for the EES is given in Equations (3.11) to (3.14). The LCOE of the energy in the storage is given in Equation (3.11).

$$\mathrm{LCOE}(\mathrm{E_{In}}) = \frac{\sum_{t=0}^{n} \frac{C_{\mathrm{In}_t}}{(1+r)^t}}{\sum_{t=0}^{n} \frac{E_{\mathrm{In}_t}}{(1+r)^t}} \tag{3.11}$$

C_{In_t} is the total cost ($) for delivering the PV energy (kWh) into EES in year *t*. E_{In_t} is the input energy for the EES in year *t*. The LCOE for EES in a renewable energy system is more complicated to comprehend. It is necessary to consider the cost of the solar array, generating the surplus energy to be stored into the EES. This is because the electrical energy stored in the EES is produced by the solar array. The LCOE of the energy delivered by the EES is given in Equations (3.12) and (3.14):

$$\mathrm{LCOE}(\mathrm{E_{Out}}) = \frac{\sum_{t=0}^{n} \frac{C_{\mathrm{In}_t}}{(1+r)^t} + \sum_{t=0}^{n} \frac{C_{\mathrm{Storage}_t}}{(1+r)^t}}{\eta_{\mathrm{EES}} \sum_{t=0}^{n} \frac{E_{\mathrm{In}_t}}{(1+r)^t}} \tag{3.12}$$

$$\mathrm{LCOE}(\mathrm{E_{Out}}) = \frac{\sum_{t=0}^{n} \frac{C_{\mathrm{In}_t}}{(1+r)^t}}{\eta_{\mathrm{EES}} \sum_{t=0}^{n} \frac{E_{\mathrm{In}_t}}{(1+r)^t}} + \frac{\sum_{t=0}^{n} \frac{C_{\mathrm{Storage}_t}}{(1+r)^t}}{\eta_{\mathrm{EES}} \sum_{t=0}^{n} \frac{E_{\mathrm{In}_t}}{(1+r)^t}} \tag{3.13}$$

$$\mathrm{LCOE}(\mathrm{E_{Out}}) = \frac{C_{\mathrm{PVsurplus}}}{E_{\mathrm{EES}}} + \frac{C_{\mathrm{EES}}}{E_{\mathrm{EES}}} \tag{3.14}$$

After splitting Equation (3.12) into two individual components, the final form of the LCOE for the EES is given in Equation (3.15).

$$\mathrm{LCOE}(\mathrm{E_{Out}}) = \mathrm{LCOD} = \frac{1}{\eta_{\mathrm{EES}}} \mathrm{LCOE}\left(E_{\mathrm{Surplus}}\right) + \mathrm{LCOS} \tag{3.15}$$

In practice, E_{In} will be the surplus energy, and E_{Surplus} will flow into the storage as a

dispatchable source of power later. Therefore, C_{In} will be $C_{\text{PVsurplus}}$, the fraction of PV array that produced the surplus energy for the system. The electrical surplus energy may be generated in certain hours of the day by the same panels producing directly-used energy in certain other hours. Therefore, a panel can produce both excess and direct electricity, depending on time of the day and/or seasonal conditions. As proposed in Equation (3.12), the cost of the electricity delivered by storage needs to consider the fraction of solar array for producing the surplus electrical energy. To calculate the fixed costs (capital and installation costs) for the PV system, the fraction of PV arrays generates the surplus and direct energy needs to be fulfilled. The operation and maintenance costs vary throughout the lifetime of the system. Equations (3.16) and (3.17) present the average of fraction for direct and surplus energy respectively for the PV array. The fraction of array for direct and surplus energy at a particular time instance *h* is presented in Equations (3.18) and (3.19), respectively. The fraction of the array should constitute the PV array for the system, N_{Total}, in the PV system as given in Equations (3.20) and (3.21).

$$\widehat{N}_{\text{Direct}} = \frac{\sum_{h=0}^{m} P_{\text{Direct}}(h)}{\sigma \sum_{h=0}^{m} \varepsilon(h)} \tag{3.16}$$

$$\widehat{N}_{\text{Surplus}} = \frac{\sum_{h=0}^{m} P_{\text{Surplus}}(h)}{\sigma \sum_{h=0}^{m} \varepsilon(h)} \tag{3.17}$$

$$N_{\text{Direct}_h} = \frac{P_{\text{Direct}}(h)}{\sigma \varepsilon(h)} \tag{3.18}$$

$$N_{\text{Surplus}_h} = \frac{P_{\text{Surplus}}(h)}{\sigma \varepsilon(h)} \tag{3.19}$$

$$N_{\text{Total}} = \widehat{N}_{\text{Direct}} + \widehat{N}_{\text{Surplus}} \tag{3.20}$$

$$N_{\text{Total}} = N_{\text{Direct}_h} + N_{\text{Surplus}_h} \tag{3.21}$$

σ is the PV array efficiency (%), ε is the solar irradiance (Wm^{-2}) and *h* is the time interval of the system operation. When solar irradiance is zero, there will be zero power output therefore

P_{Surplus} will also be zero. The situation will be 0/0, that is, mathematically, it is an undefined solution. In real-life situation, these cases should not be considered; however, the situation when there is a PV output should be considered. Therefore, the study is limited to cases in which P_{Surplus} or P_{Direct} is not zero. There will be situations when there is a P_{Direct} but no P_{Surplus} as the generated power is supplied to the load fully.

3.2.2 Solar PV and storage system

For the PV and EES storage system, the following LCOE relationship will hold:

$$\text{LCOE}_{\text{System}} = \frac{\sum_{t=0}^{n} \frac{C_{\text{System}_t}}{(1+r)^t}}{\sum_{t=0}^{n} \frac{E_{\text{System}_t}}{(1+r)^t}} \tag{3.22}$$

C_{System_t} and E_{System_t} are the total cost and total electrical energy production from the system at time t, respectively. The total cost of the renewable system is the sum of PV generation and storage costs. The total electrical energy produced by the system is the energy output of EES and the energy directly delivered to the load by PV. In this chapter, the term $\text{LCOE}_{\text{System}}$ is used to denote the LCOE for the PV and EES system. It does not consider the context of stand-alone or on-grid systems. The purpose of $\text{LCOE}_{\text{System}}$ is to provide the understanding of the cost implications to the renewable and storage assets. Therefore, the LCOE for the system is given in Equation (3.23).

$$\text{LCOE}_{\text{system}} = \frac{C_{\text{PVsurplus}} + C_{\text{EES}} + C_{\text{PVdirect}}}{E_{\text{EES}} + E_{\text{PV}_{\text{Directtotal}}}} \tag{3.23}$$

3.3 Case studies

3.3.1 Data acquisition

Solar irradiance and load data were obtained for the studies in this chapter. The SKS 1110 pyranometer device manufactured by Skye Instruments [176] was used to collect the irradiance

data. Four years of complete solar irradiance data in 2009–2012 were collected in Johannesburg. The sampling rate is one sample/30min. Due to the restricted space to present the hourly annual solar irradiance, Figure 3.2 shows solar irradiance collected for the first six days in 2009–2012.

The representative daily national load curve for Johannesburg and Kenya is presented in Figure 3.3. The load curve is of annual average. As explained in [177], the national load starts rising at 18:30 and reaches its peak at 20:30. The variation of the national load curve depends on the energy consumption of residents and industries. According to the governmental report for Kenya [178], the load consumption is consistent throughout the year. One of the reasons can be the consistent upper and lower temperature throughout the year with very few Celsius degree differences for the highest and lowest temperature for the 12 months [179].

According to the governmental report in [178], the urban to rural consumption ratio is approximately 4:1 as of 2010 and is expected to decrease over time. Total consumption in rural areas is of the same trend as that of the urban areas. Rural areas' annual consumption increased from 165 GWh in 2006 to 290 GWh in 2010.

According to the works in [180, 181] and the governmental report in [178], a single load curve can be used to represent the daily consumption for the country as there is little to negligible variation in the load pattern throughout the week and the month. The shape of the national load profile for South Africa, e.g., Johannesburg and Kenya is very similar [182, 183]. It is therefore logical to assume that the load curve for Johannesburg is similar to that for Kenya.

PV projects are currently favourable in Kenya. Kenya has an abundant source of solar irradiance and it is capable of generating several times more electricity from PV than the total annual consumption delivered by the national grid. The economic value of PV has already exceeded the potential project costs in 2012 [181], and grid-connected PV systems may already be more economical than the most expensive conventional power plants such as gas turbines

and medium-speed diesel generators. PV is currently the largest share of power generation mix in Kenya [184].

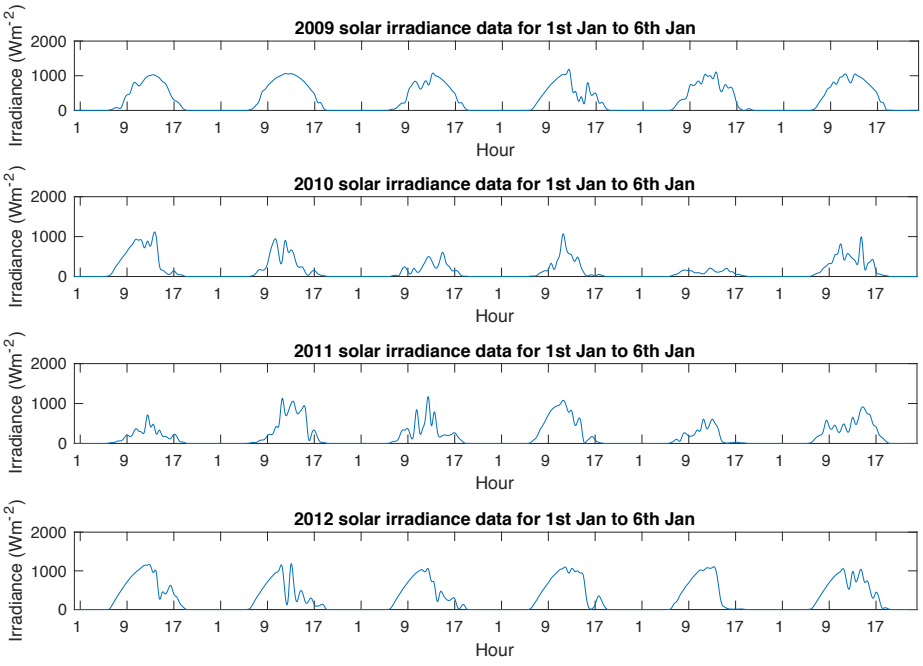


Figure 3.2. Solar irradiance between 1st Jan. to 6th Jan. in 2009–2012 at Johannesburg.

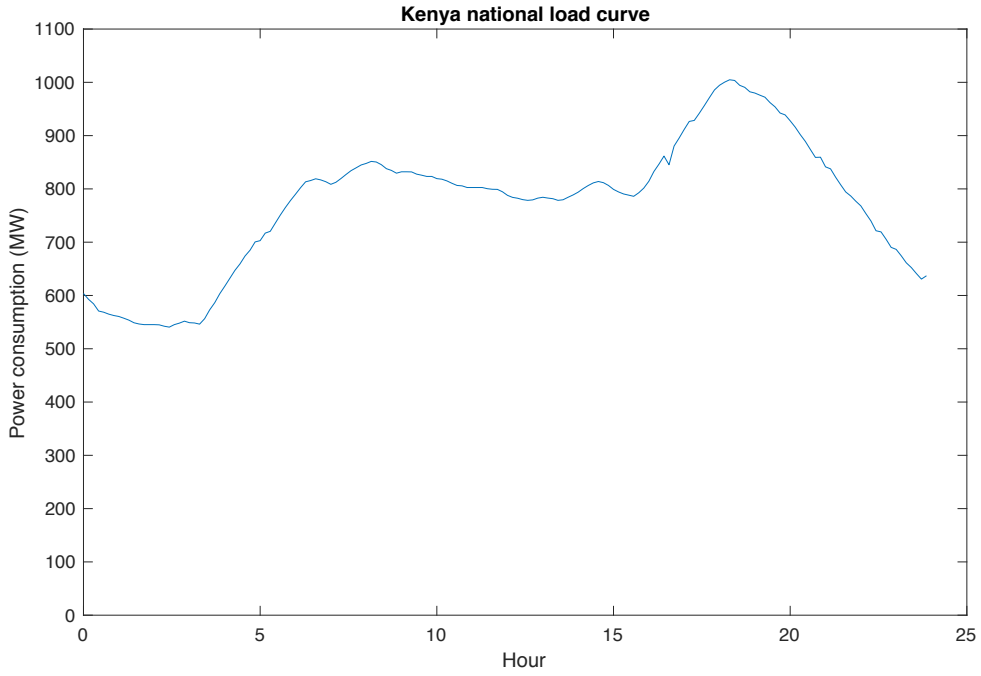


Figure 3.3. A representative daily national load curve for Kenya and Johannesburg.

3.3.2 Cost and asset specification

The cost and asset specifications are presented in Table 3.1. The Li-ion reaches the end-of-life when the charging capacity is between 70–80 % of the rated capacity [185, 186]. The solar panel to be used for the system is the Sharp ND-250QCS.

		EES	
	PV	**VRB**	**Li-ion battery**
Capital cost (C_{Cap})	120 ($/unit) [187, 188]	760–1600 ($/kWh) [29, 99]	715–1640 ($/kWh) [29, 99]
Installation cost (C_{Inst})	108 ($/unit) [187]	N/A	N/A
O&M cost ($C_{O\&M}$)	6 ($/unit-year) [187]	100–140 ($/MWh) [99]	80–95 ($/MWh) [99]
System lifetime (*n*)	N/A	20 years [29, 99]	15 years [29, 99]
Round-trip efficiency (η_{EES})	N/A	70 % [29, 99]	90 % [29, 98, 99]
Degradation rate	0.5 %/year [149, 189]	0.1 %/year [116]	2 %/year [116]

Table 3.1. Cost and technical specification of the system components for the case study.

The solar cell has an efficiency of 15.3 % and has a rated power of 250 W [187]. The lifetime of PV panels can be up to 25 years [190], which exceeds the lifetime of EES. In the case studies, the lifetime of PV panels is assumed to be the same as the storage system and the project lifetime.

3.3.3 Marginal levelized cost of electricity

The concept of marginal LCOE is proposed in this chapter. By definition, marginal cost is the cost of producing one more unit of output. In this chapter, marginal LCOE is proposed to examine the long-term investment by incorporating additional PV capacity and storage into the system. This will be useful to understand the cost implication with respect to the system investment. In this chapter, three different cases of the marginal LCOE are studied with the following assumptions.

Case 1: The peak of solar power meets the load demand with little surplus energy available;

Case 2: Extra PV capacity is added to the system and additional solar power will be generated. However, the surplus energy will be discarded because no storage is available;

Case 3: Storage will be used to store the surplus energy. The size of PV capacity is the same as that in Case 2.

To provide the visual illustration for the concepts of marginal LCOE, a constant linear load curve and clear sky irradiance are used as shown in Figure 3.4. The total cost and energy to calculate the LCOE for the system in the case studies are given in Equations (3.24) and (3.25), with $\mathrm{C}_{\mathrm{Case}(k)}$ as the annual cost for the PV array and $\mathrm{E}_{\mathrm{PV}(k)}$ as the annual electricity production from the PV array in Case k.

$$C_{\mathrm{Total}_{\mathrm{case}(k)}} = \sum_{t=0}^{n} \frac{C_{\mathrm{Case}(k)_t}}{(1+r)^t} \tag{3.24}$$

$$E_{\mathrm{Total}_{\mathrm{case}(k)}} = \sum_{t=0}^{n} \frac{E_{\mathrm{Case}(k)_t}}{(1+r)^t} \tag{3.25}$$

In Case 1, the load uses all the produced solar energy. LCOE is then calculated. The load power is assumed to be at the maximum point of the solar power curve for the default case. The LCOE for the default case is:

$$\mathrm{LCOE}_{\mathrm{Basecase}} = \frac{C_{\mathrm{Total}_{\mathrm{case1}}}}{E_{\mathrm{Total}_{\mathrm{case1}}}} = \frac{C_{\mathrm{Pvdirect}}}{E_{\mathrm{Pvdirect}}} \tag{3.26}$$

In Case 2, additional PV capacity is invested into the system. However, there is no storage device. Therefore, the surplus energy will be wasted. The solid black area is the extra solar energy produced in the system that is consumed by the load compared to Case 1. Figure 3.4 visually represents the three cases. $E_{\mathrm{Total_case2}}$ is obtained by taking away E_{Surplus} from the total electrical energy production from PV, E_{PV2} is due to no energy storage present in the

system. The marginal LCOE from Case 1 to Case 2 is:

$$\mathrm{LCOE}_{\mathrm{Marginal}(1-2)} = \frac{\Delta \mathrm{C}}{\Delta \mathrm{E}} = \frac{C_{\mathrm{Total}_{\mathrm{case2}}} - C_{\mathrm{Total}_{\mathrm{case1}}}}{E_{\mathrm{Total}_{\mathrm{case2}}} - E_{\mathrm{Total}_{\mathrm{case1}}}} \tag{3.27}$$

$$\text{where } E_{\mathrm{Total}_{\mathrm{case2}}} = E_{\mathrm{Case2}} - E_{\mathrm{Surplus}} \tag{3.28}$$

In Case 3, further investment is put into the system compared to Case 2 by including EES. The surplus energy will be stored in the EES and consumed by the load. The marginal LCOE from Case 2 to Case 3 is:

$$\mathrm{LCOE}_{\mathrm{Marginal}(2-3)} = \frac{\Delta \mathrm{C}}{\Delta \mathrm{E}} = \frac{C_{\mathrm{Total}_{\mathrm{case3}}} - C_{\mathrm{Total}_{\mathrm{case2}}}}{E_{\mathrm{Total}_{\mathrm{case3}}} - E_{\mathrm{Total}_{\mathrm{case2}}}}$$

$$= \frac{(C_{\mathrm{EES}} + C_{\mathrm{Total}_{\mathrm{case2}}}) - C_{\mathrm{Total}_{\mathrm{case2}}}}{E_{\mathrm{Total}_{\mathrm{case3}}} - E_{\mathrm{Total}_{\mathrm{case2}}}} = \frac{C_{\mathrm{EES}}}{E_{\mathrm{EES}}} = \mathrm{LCOS} \tag{3.29}$$

The marginal LCOE from Case 2 to 3 can be converted into LCOS as given in Equation (2.9). A single combination investment of additional PV capacity and storage can be applied to Case 1. The marginal LCOE from Case 1 to Case 3 is provided in Equation (3.30).

$$\mathrm{LCOE}_{\mathrm{Marginal}(1-3)} = \frac{\Delta \mathrm{C}}{\Delta \mathrm{E}} = \frac{(C_{\mathrm{Total}_{\mathrm{case2}}} - C_{\mathrm{Total}_{\mathrm{case1}}}) + C_{\mathrm{EES}}}{(E_{\mathrm{Total}_{\mathrm{case2}}} - E_{\mathrm{Total}_{\mathrm{case1}}}) + E_{\mathrm{EES}}} \tag{3.30}$$

A sensitivity analysis was conducted by varying the PV rated capacity. As depicted in Figure 3.5, Case 1 consists of a solar farm with rated capacity of 2.5 MW, an arbitrary size used for the initial rated capacity of the solar farm. The calculated peak output power from the PV farm is 1.9 MW. As no surplus energy is available for Case 1, the load curve will have a peak of 1.9 MW. This real-life load profile will be fixed throughout the sensitivity analysis for the study. The storage system used is VRB with storage capacity of 3 MWh. The storage capacity is calculated by the average surplus electricity produced per day in a year at the maximum PV rated capacity, i.e., 5 MW. This is $1081\ \mathrm{MWh}/365 = 2.96\ \mathrm{MWh}$ for the system. For the sensitivity analysis, the solar and load power for the 5 MW case is shown in Figure 3.6. It can be observed that there are days where surplus electricity exists compared to the base case in Figure 3.5. As reported in [191], the current discount rate for PV is 6–9 %. The discount rate

could be as much as 2–3 % lower over the next decade and could fall by a further 1–2 % by 2040. A discount rate at 5 % is used to align with the best discount rate for PV systems in Kenya [184].

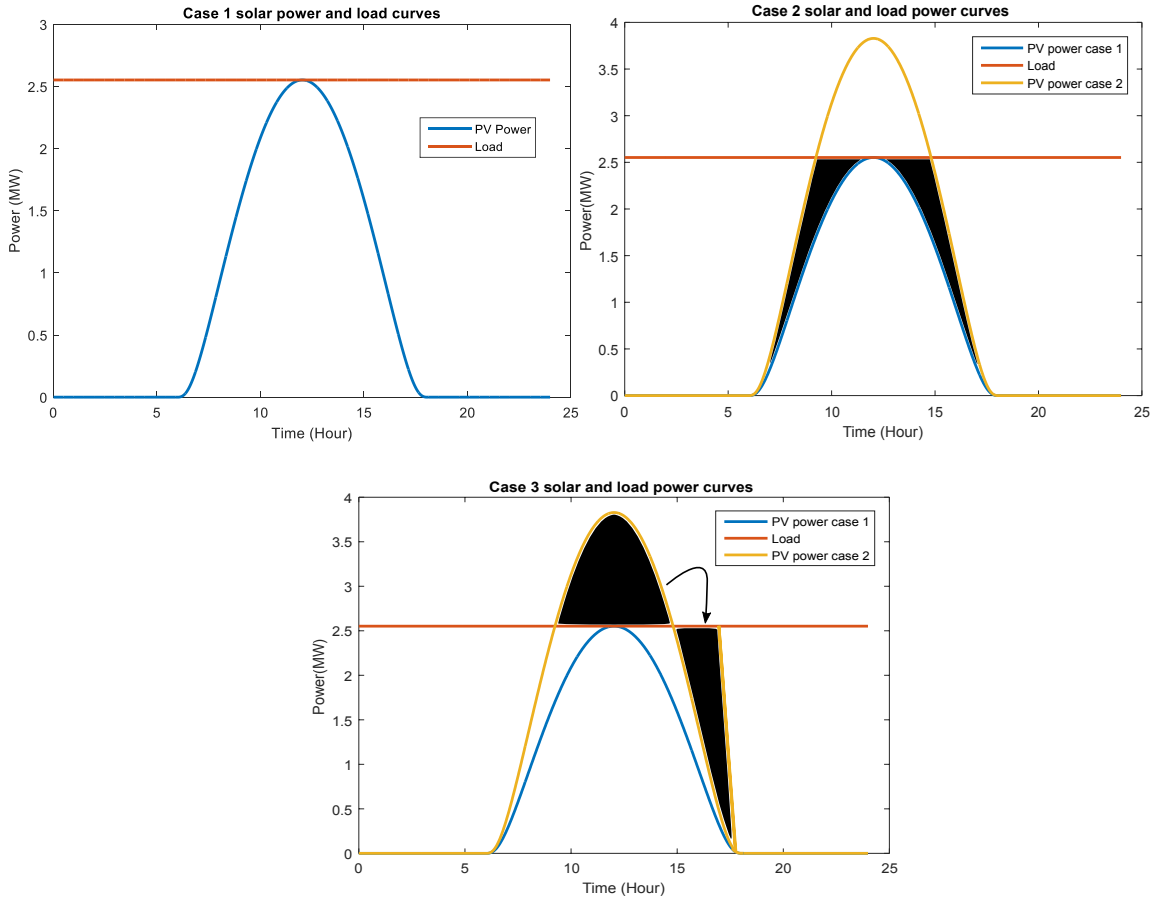


Figure 3.4. Solar and load curve for Cases 1, 2, and 3.

The resultant $\mathrm{LCOE}_{\mathrm{Basecase}}$ for the system is 0.093 $/kWh. The results from the sensitivity analysis on marginal LCOE, $\mathrm{LCOE}_{\mathrm{System}}$, and LCOD are presented in Figure 3.7.

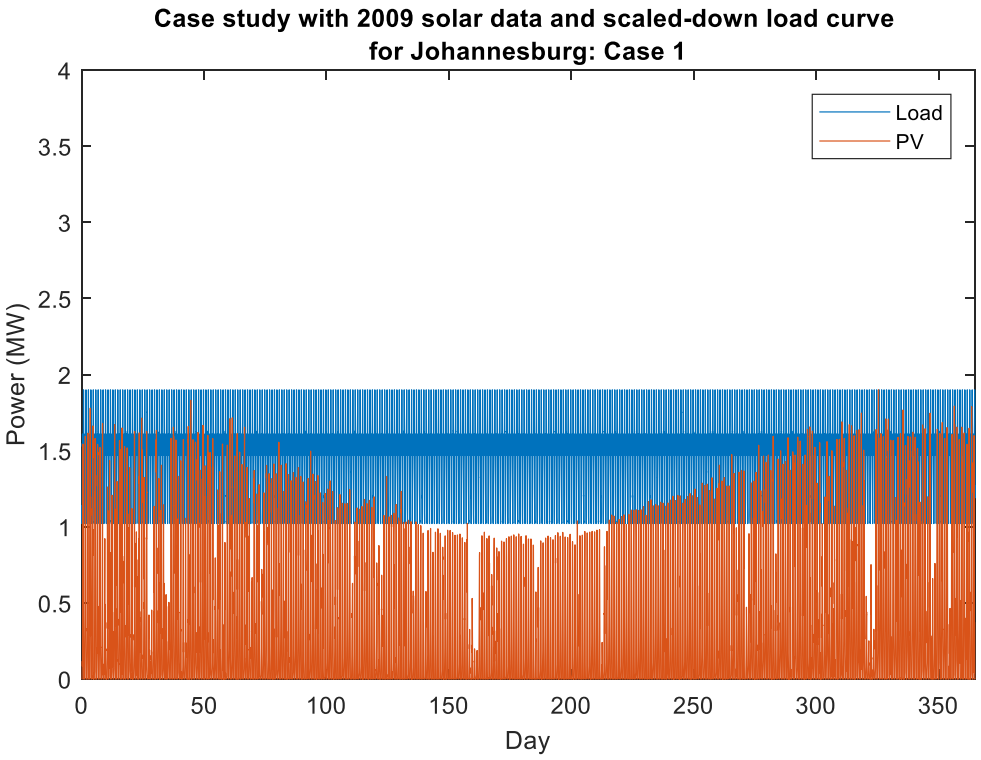


Figure 3.5. Solar and load power curves for Case 1 in sensitivity analysis.

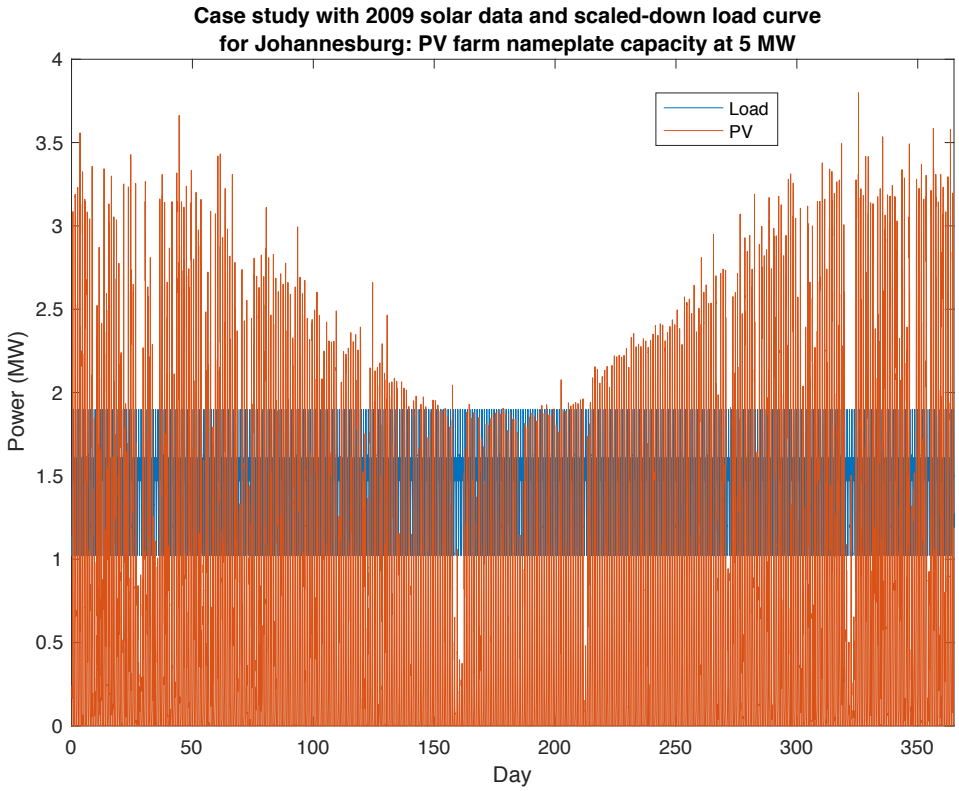


Figure 3.6. Solar and load power curves for a 5 MW nameplate PV farm.

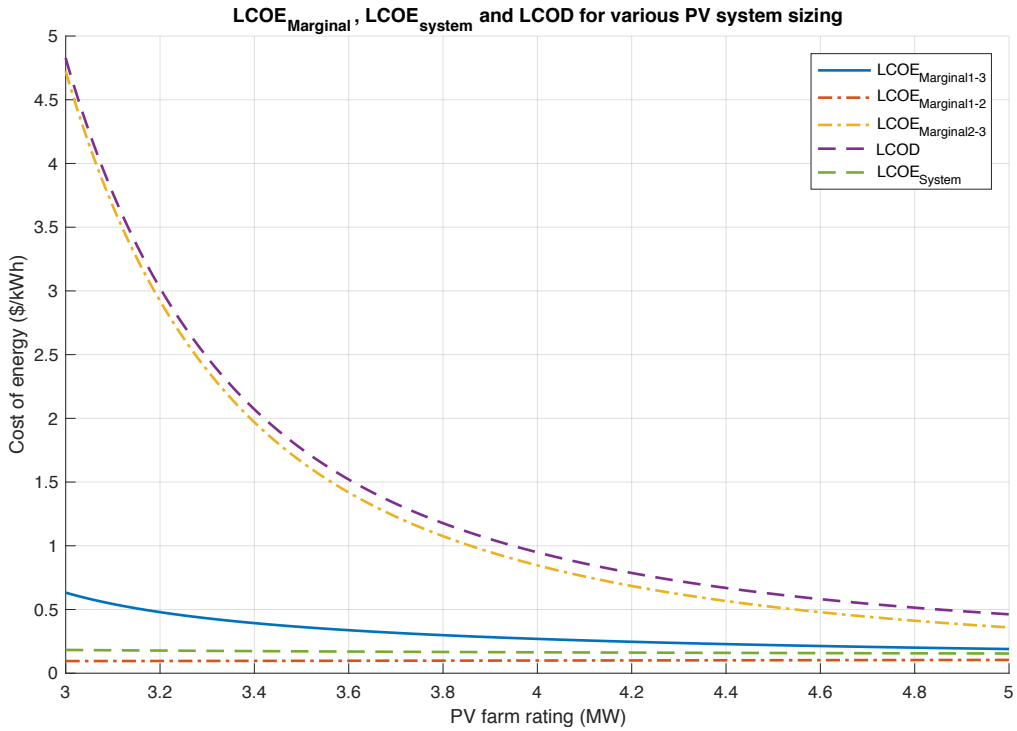


Figure 3.7. Marginal LCOE, LCOD and $\mathrm{LCOE}_{\mathrm{system}}$ with respect to PV capacity.

As evident, the value of $\mathrm{LCOE}_{\mathrm{System}}$ is different from the total of $\mathrm{LCOE}_{\mathrm{Basecase}}$ and $\mathrm{LCOE}_{\mathrm{Marginal}(1-3)}$ as the summation of Equations (3.26) and (3.30) does not equal to Equation (3.23). The LCOD and $\mathrm{LCOE}_{\mathrm{Marginal}(2-3)}$ increase exponentially when the PV capacity is reduced. By increasing the PV rated capacity by one MW, i.e., from 3 to 4 MW, the LCOE for storage and delivery can be reduced by a factor of four. This is because the EES discharges more electricity when the PV produces surplus electricity. The non-linear functions for LCOD and LCOS as showed in Equations (3.15) and (3.29) affect the LCOE. This phenomenon is consistent with the LCOS for pumped storage provided in [28] such that it will experience an exponential decrease with an increase in energy discharge from the storage system. This is because the storage will store less energy with less surplus PV power. Evidently, the $\mathrm{LCOE}_{\mathrm{Marginal}(2-3)}$ is less than LCOD as LCOD includes the cost for the fraction of solar array used to provide energy for the EES. $\mathrm{LCOE}_{\mathrm{Marginal}(1-2)}$ experiences an increase as the PV capacity increases; this is due to the energy wastage from not utilising the surplus energy.

$LCOE_{System}$ will decrease with an increase in PV capacity as the energy is stored and utilised. $LCOE_{Marginal(1-3)}$ is less than $LCOE_{Marginal(2-3)}$ and LCOD due to the inclusion of the additional PV capacity and surplus energy in system from Case 1 for non-storage. The $LCOE_{Marginal(2-3)}$ is of higher value than the Lazard's result of LCOS in Table 2.6. As explained previously, Lazard assumed that the storage system is used at full capacity at all times. In a PV hybrid system, the storage system will seldom be used to the maximum, and the energy depends on surplus power. The following phenomena can be observed.

1. System without storage attracts a small LCOE but naturally at lower security of supply and the marginal LCOE will increase with the increase of PV capacity. This signifies that the cost of system will increase with additional PV capacity.
2. LCOD and $LCOE_{Marginal(2-3)}$ can experience a decrease with the increase of PV capacity. The EES will deliver more energy as the surplus energy increases.
3. From the investment point of view, it can be seen that it is important to add a battery as a component of the system rather than adding it at a later stage. The costs for separating the system can be high compared to the overall cost of the system.

3.3.4 LCOD and $LCOE_{System}$ for VRB and Li-ion battery

A scenario has been developed with the load and generation data from Kenya and Johannesburg, respectively. As discussed in Section 3.3.1, the daily electricity consumptions of Kenya and Johannesburg are very similar [182, 183]. The national load curve has been down-sized with the peak load at 2 MW to represent a load demand for a typical rural community in Africa. The rated capacity of the PV farm is 5 MW. The calculated capacity factors for the PV system are 12.02 %, 11.67 %, 12.26 % and 12.61 % for years 2009, 2010, 2011 and 2012, respectively. The purpose of this study is to calculate the $LCOE_{System}$ and LCOD for a real-life renewable energy system with storage. $LCOE_{System}$ is the LCOE for the combined assets, PV and EES. Two types of dominant EES technologies, Li-ion and VRB have

been studied. In this study, three ranges of cost values have been used to determine the cost of electricity for LCOD and $\mathrm{LCOE_{System}}$. These are lower bound, upper bound and medium bound costs. The cost calculation was performed for each year of the four years of data. Sensitivity analysis was conducted for a range of discount rates. One of the vital input parameters for LCOE calculations is the value of the discount rate. The discount rate essentially considers the time value of money, through monetary depreciation, as well as the investments risks. PV systems are considered much higher risks when compared with traditional power plants, and therefore, they will be at higher discount rates.

The results are summarised as box plots in Figures 3.8 and 3.9. According to Figure 3.8, LCOD is higher with Li-ion than VRB for both the median and minimum values when the discount rate is less than 8 %. The discount rate needs to be 10 % or more when LCOD for VRB is higher than that for Li-ion. It can be assumed that adding EES to the system can increase the $\mathrm{LCOE_{System}}$ at a high discount rate with wider cost variation. This is due to the capital and installation cost of the system being more dominant. At a low discount rate, the value of energy will have less depreciation with respect to time. The results of LCOD and $\mathrm{LCOE_{System}}$ are provided in a range of values due to uncertainty in the annual electrical energy production from the PV system and the range of EES costs.

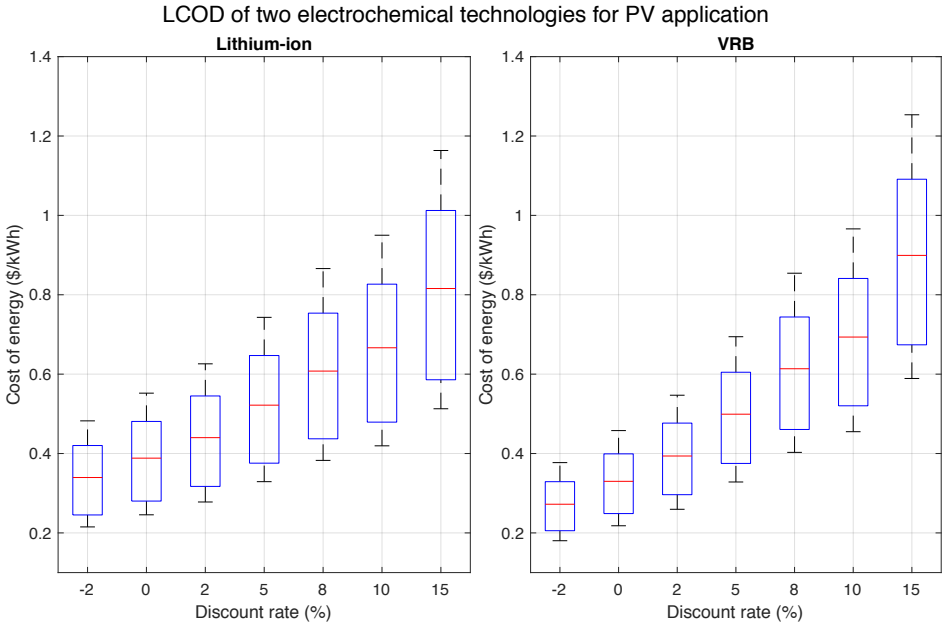


Figure 3.8. LCOD for Li-ion and VRB at various discount rates.

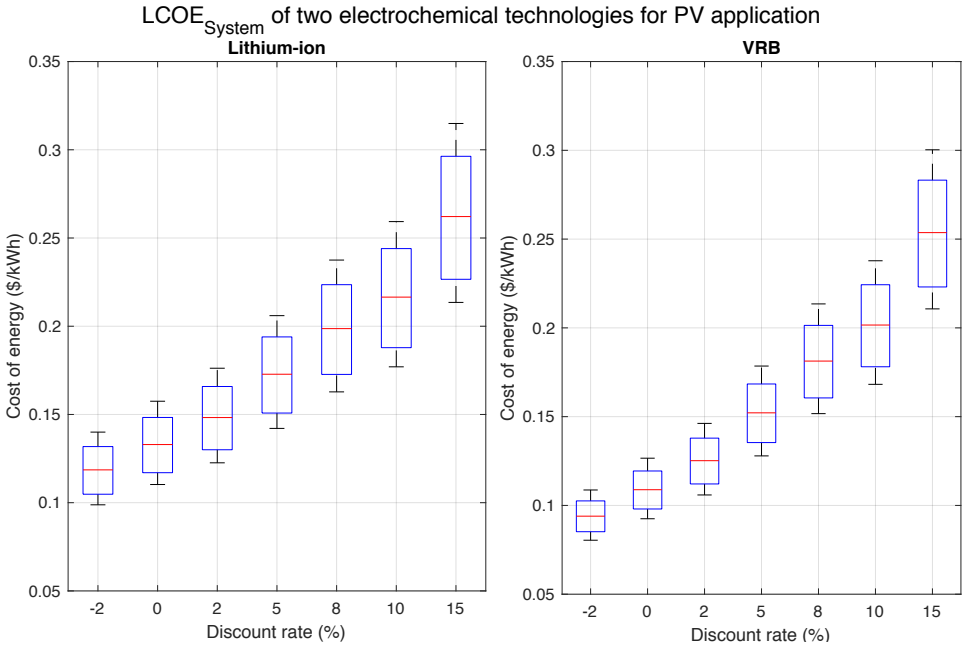


Figure 3.9. $\mathrm{LCOE}_{\mathrm{System}}$ for Li-ion and VRB at various discount rates.

The results for $\mathrm{LCOE}_{\mathrm{System}}$ at various discount rates for the two EES technologies are presented in Figure 3.9. It shows that the LCOE is lower for VRB in all the studied discount rates and price range considerations. Although Li-ion battery has a higher round-trip efficiency than VRB, the lifetime of the system is considerably shorter, and this significantly affects the

$\mathrm{LCOE}_{\mathrm{System}}$.

The proposed methods could also be used to assess various EES technologies although in this chapter, only VRB and Li-ion battery cases were provided as examples. This method provides decision makers a practical approach to consider the competitiveness of each technology for a given application with renewables in particular. Parameters such as round-trip efficiency, EES lifetime and discount rate have all been included in the studies, and the functionality of the method has been shown with real-life data. LCOS and LCOD will be higher than $\mathrm{LCOE}_{\mathrm{System}}$. Although the analyses show that the LCOD is cheaper for Li-ion than that for VRB at present, the $\mathrm{LCOE}_{\mathrm{System}}$ as a system could be lower for VRB compared to Li-ion. As energy storage has numerous applications for power systems such as grid balancing and frequency regulation, the LCOS and LCOD will be significantly different due to the operating conditions of the EES. With additional irradiance data, it will be possible to obtain a better determination of the cost of deployment of renewables' systems with integration of energy storage system.

3.4 Summary

This chapter provided the LCOE calculation methods for PV and EES. By considering the electrical energy generation costs, the LCOD and the LCOE for PV systems with storage have been proposed. The LCOD for VRB and Li-ion battery were studied. The long-term economic impacts for storage and PV system were provided and discussed with respect to marginal LCOE. It was shown that including an EES can minimise the lifetime cost of the system if PV generation is included. The LCOD decreases with an increase in PV generation capacity. The findings reveal that with the present costs and technical specifications, VRB has a lower LCOD compared to Li-ion at a low discount rate for PV energy storage application. The work in this chapter forms the foundation for evaluating the levelized costs for the sizing and operation regime tasks in the upcoming chapters.

Chapter 4

Daily Clearness Index profiles cluster analysis

This chapter aims to discover patterns in the CI and to construct centroids for the daily CI profiles via cluster analysis. The objective is to reduce the size of the dataset for the hybrid system sizing while providing satisfactory PV and EES capacities. Due to the monitoring costs, limited number of studies on PV systems operation in remote areas exist. To reduce the costs, clustering results are required for analysing the performance and sizing of PV systems. Generally, the centroids will be useful to provide a standardised methodology for PV system design and analysis. Due to various weather perturbation effects, the stochastic nature of real-life solar irradiance has been a major issue for solar photovoltaic (PV) system planning and performance evaluation. The variation in CI could be significant in different seasons. In this chapter, cluster analysis with Gaussian Mixture Models, *K*-Means with Euclidean distance, *K*-Means with Manhattan distance, Fuzzy C-Means with Euclidean distance and Fuzzy C-Means with Dynamic Time Warping (FCM DTW) have been performed for the four seasons. Real-life weather condition data collected from Weatherunderground.com has been used to correlate the weather conditions with the clustered profiles. This will be beneficial in estimating the CI profile for a typical day provided with respect to the weather conditions.

This chapter provides the grouping of daily CI profiles to construct centroids with cluster analysis. Section 4.1 presents the clear-sky solar model and the real-life solar data for CI calculation. The research problem and the preliminary understanding will also be discussed. The clustering algorithms and distance metrics used for clustering daily CI profiles are provided in Section 4.2. Section 4.3 presents the clustering results for the four seasons with the

five clustering techniques. The clustering results are further evaluated with the weather condition data, with the results and discussion presented in Section 4.4. The section concludes with a summary in Section 4.5.

4.1 Clearness Index development

4.1.1 Clear-sky solar irradiance model

Under perfect atmospheric conditions, the earth will absorb the solar irradiance which is equal to the solar constant minus the amount absorbed by the atmosphere of the earth. The solar constant has a value of 1367 Wm^{-2}. The global solar irradiance on a horizontal surface has two main components, namely the direct beam component and the diffuse sky irradiance.

The other factor in the attenuation of the atmosphere is a function of the concentrations of the various elements in the atmosphere [192]. Their impacts can be assessed by comparing the actual observed optical depth with the theoretical optical depth of a perfectly clean dry scattering Rayleigh atmosphere. The ratio of the two optical depths is known as the air mass 2 Linke turbidity factor, T_{LK}. The clear-sky beam irradiance normal to the horizontal surface I_{Model} is calculated as mentioned in references [193, 194].

$$I_{\mathrm{Model}} = I_{\mathrm{Solar}}\varepsilon_{\mathrm{c}} \exp\left(-0.8662 T_{\mathrm{LK}} m_{\mathrm{Optic}} \delta_{\mathrm{r}}\left(m_{\mathrm{Optic}}\right)\right) \sin\gamma_{\mathrm{s}} \tag{4.1}$$

$$\varepsilon_{\mathrm{c}} = 1 + 0.0334\cos(j' - 2.80^{o}) \tag{4.2}$$

$$j' = \frac{J_{\mathrm{Julian}} * 360}{365.25} \tag{4.3}$$

$$m_{\mathrm{Optic}} = (p/p_{\mathrm{o}})/\{\sin\gamma_{\mathrm{s}} + 0.50572(\gamma_{\mathrm{s}} + 6.07995)^{-1.6364}\} \tag{4.4}$$

I_{Solar} is the solar constant, ε_{c} is the correction factor to mean solar distance, m_{Optic} is the optical air mass corrected for station height, γ_{s} is the solar altitude angle in degrees and δ_{r} is the Rayleigh optical depth, J_{Julian} is the Julian day and j' is the Julian day angle. p/p_{o} is the pressure correction for station height and is calculated with Equation (4.5) given below:

$$\frac{p}{p_{\mathrm{o}}} = \exp\left(-\frac{z}{H_{\mathrm{R}}}\right) \tag{4.5}$$

z is the site elevation above sea level in metre and H_{R} is a constant at 8400 metres. δ_{r} is calculated as follows [195]:

$$\frac{1}{\delta_{\mathrm{r}}(m_{\mathrm{Optic}})} = 6.6296 + 1.7513m_{\mathrm{Optic}} - 0.1202{m_{\mathrm{Optic}}}^2 + 0.0065{m_{\mathrm{Optic}}}^3$$

$$- 0.00013{m_{\mathrm{Optic}}}^4 \qquad if\ m_{\mathrm{Optic}} < 20 \tag{4.6}$$

$$\frac{1}{\delta_{\mathrm{r}}(m_{\mathrm{Optic}})} = 10.4 + 0.718m_{\mathrm{Optic}} \qquad if\ m_{\mathrm{Optic}} >= 20 \tag{4.7}$$

The solar altitude angle is calculated as a function of time of day with Equation (4.8) [193].

$$\gamma_{\mathrm{s}} = \sin^{-1}(\sin\phi\sin\delta + \cos\phi\cos\delta\cos\omega) \tag{4.8}$$

$$\omega = 15(h - 12) \tag{4.9}$$

ϕ, δ and ω are the latitude of location, solar declination angle and solar hour angle, respectively; all are in degrees. h is the instantaneous time of the day in hour with values between 0 and 23.

4.1.2 Clearness Index

CI at instantaneous time h is expressed as a ratio between 0 and 1 in which 1 signifies that there is no loss in irradiance, i.e., all the insolation is of direct beam irradiance, and 0 implies that there is no irradiance due to complete cloud cover. It is worth mentioning that CI can be undefined when no irradiance is available such as before sunrise and after sunset. These conditions are not considered in this work as they are not applicable for the study. CI is calculated with Equation (4.10) below:

$$\mathrm{CI}(h) = \frac{I_{\mathrm{Pyranomter}}(h)}{I_{\mathrm{Model}}(h)} \tag{4.10}$$

$I_{\mathrm{Pyranomter}}$ is the real-life solar irradiance and I_{Model} is the clear-sky solar irradiance from the solar model. To calculate the solar model irradiance for CI, the T_{LK} is set to 1 to remove the

effect due to the clear-sky solar irradiance atmospheric absorption and scattering. These phenomena can be reflected in the CI as it considers the total irradiance reduction from the clear-sky irradiance. Figure 4.1 presents the clear-sky and real-life solar irradiance for a typical day in January at Johannesburg.

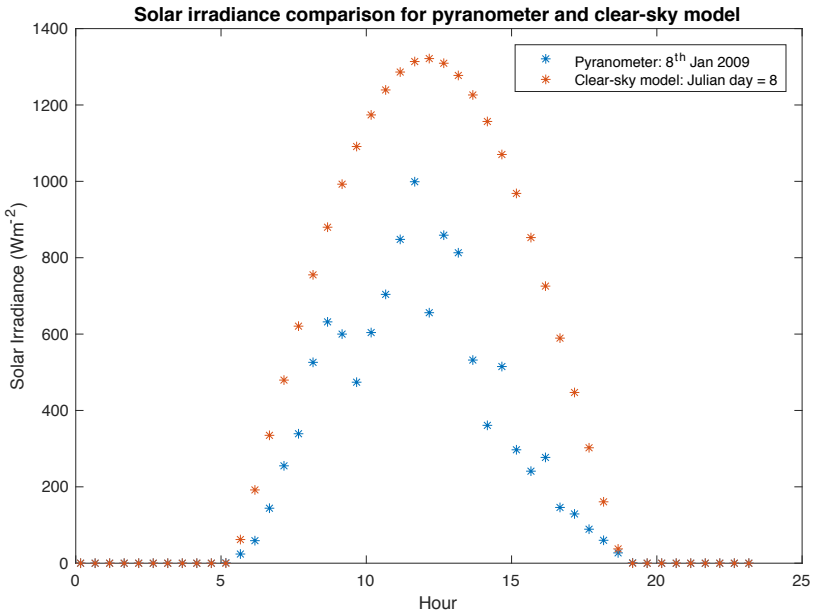


Figure 4.1. Solar irradiance for clear-sky model and real-life (pyranometer) data in Johannesburg.

In addition to the solar irradiance dataset for Johannesburg introduced in Chapter 3, a solar irradiance dataset from Kenya has also been included for the CI cluster analysis. It is four years of solar irradiance data (2011–2014) obtained from Solargis company. The location chosen for collecting irradiance data is Gitaru dam, Kenya with coordinates (0.789°S,37.73°E) and elevation at 969 metres. The sampling rate is 1 sample/15 min.

CI for four different seasons between 2009–2012 in Johannesburg is shown in Figure 4.2. The CI for four different seasons between 2011–2014 in Kenya is presented in Figure 4.3. Each colour represents a CI profile for a day. 20 profiles were plotted for each season.

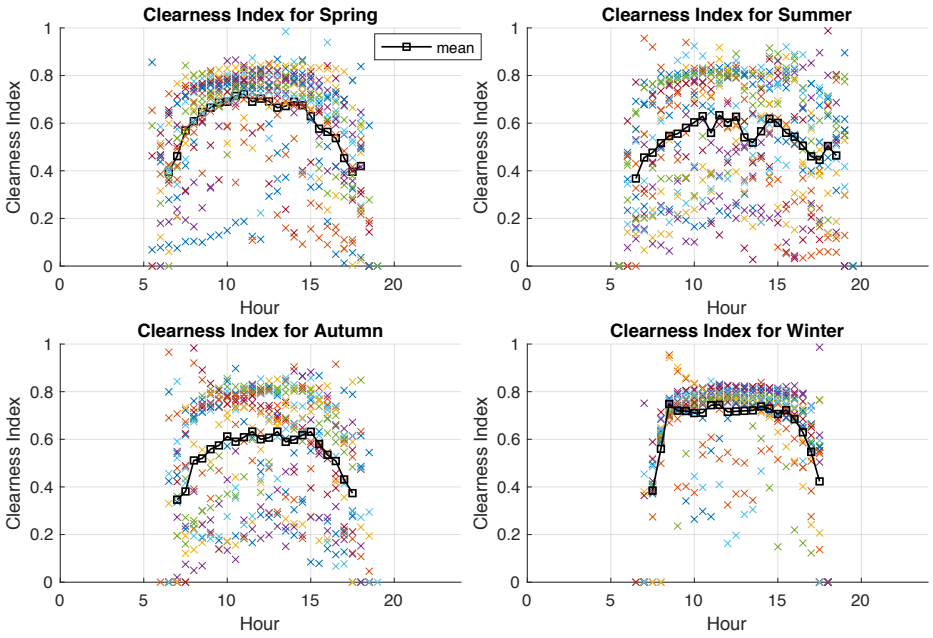


Figure 4.2. Clearness Index for the four seasons in Johannesburg.

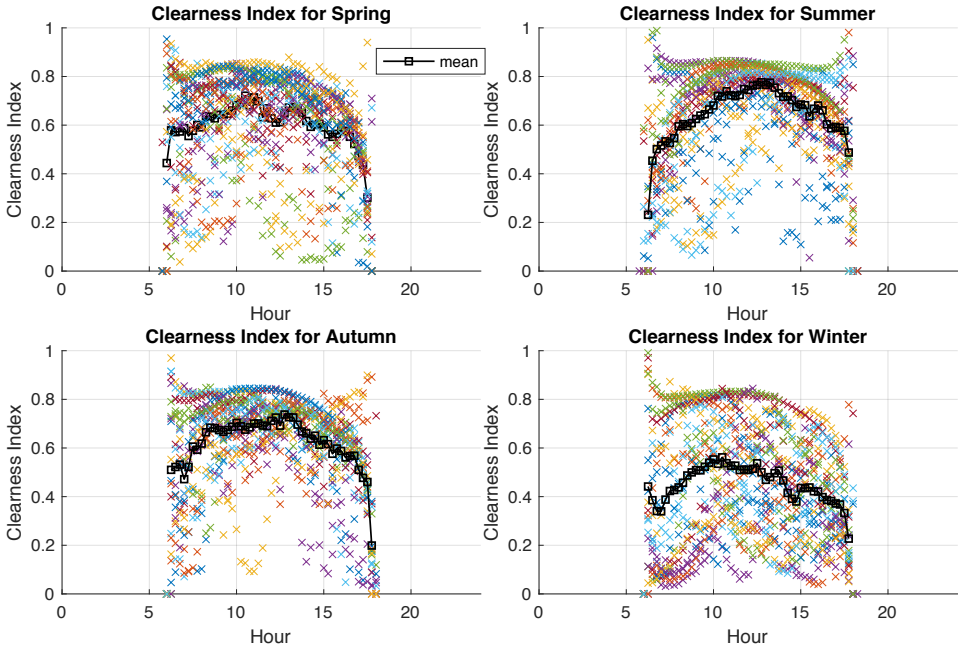


Figure 4.3. Clearness Index for the four seasons in Kenya.

For Johannesburg, it can be seen that in winter there are significantly more clear days, i.e., higher CI. In contrast, CIs in summer are mostly below 0.3. CI also displays the nature of uncertainty and the daily fluctuation. Kenya has clear days during summer, autumn and spring.

The solar insolation during winter is greatly reduced in Kenya. The reasons for variation in CI are essentially due to cloud movement and weather conditions.

4.2 Clustering methods

4.2.1 Distribution-based clustering

In distribution-based clustering, clusters can be defined as objects belonging most likely to the same distribution. A Gaussian Mixture Model (GMM) is a weighted sum of m_{c} components, i.e., the number of clusters. The Gaussian mixture densities for vector x is given in Equation (4.11) [196] below:

$$g_{x;w,\theta}(x;w,\theta) = \sum_{i=1}^{m_{\mathrm{c}}} w_i g_{x;\theta_i}(x;\theta_i) \tag{4.11}$$

w is the mixture weight with the constraints $w_i > 0$ and $\sum_{i=1}^{m_{\mathrm{c}}} w_i = 1$. $g_{x;w_i,\theta_i}(x;w_i,\theta_i)$ is known as the Gaussian component densities. The parameter θ contains the component weights w_i, mean vectors, μ_i and the covariance matrices Σ_i. This is expressed in Equation (4.12) [196] below:

$$\theta = \{w_1, w_2, \dots, w_{m_{\mathrm{c}}}, \mu_1, \mu_2, \dots, \mu_{m_{\mathrm{c}}}, \Sigma_1, \Sigma_2, \dots, \Sigma_{m_{\mathrm{c}}}\} \tag{4.12}$$

For $h_{n_{\mathrm{v}}}$ to be the number of elements in the vector $x_{n_{\mathrm{v}}}$, the log likelihood function is given in Equation (4.13) [196] below:

$$L(\theta) = \sum_{n_{\mathrm{v}}=1}^{h_{n_{\mathrm{v}}}} \ln \sum_{i=1}^{m_{\mathrm{c}}} w_i g_{x;\theta_i}\left(x_{n_{\mathrm{v}}};\theta_i\right) \tag{4.13}$$

The Expectation-Maximisation (EM) algorithm aims to calculate the maximum likelihood estimation of the marginal likelihood in an iterative process. The process consists of two stages; the expectation step and maximisation step.

1. Expectation step: Calculates the expected value of the log likelihood function under the current estimate of the parameters $\theta^{(t_{\mathrm{it}})}$ at t_{it} iteration [196, 197].

$$B\left(\theta;\theta^{(t_{\mathrm{it}})}\right)=E_{X,\theta^{(t_{\mathrm{it}})}}[L(\theta)] \tag{4.14}$$

2. Maximisation step: Finds the parameter that maximises the following quantity [196, 197]:

$$\theta^{(t_{it}+1)}=\underset{\theta}{\operatorname{argmax}}\,B\left(\theta;\theta^{(t_{it})}\right) \tag{4.15}$$

4.2.2 Partition-based clustering

K-Means clustering aims to classify the objects into the clusters with the nearest mean. It is an iterative algorithm and begins with choosing *K* initial cluster centres. The distances of all observations to each centroid are computed. The object is assigned to the cluster with the closest centroid. The new centroid locations are determined by calculating the average of the objects in each cluster. Given data with n_{v} vectors of equal lengths, $X=\left\{x_1,x_2,\dots,x_{n_{\mathrm{v}}}\right\}$, *K*-Means determines cluster centres for *K* clusters of vectors with equal lengths $V=\{v_1,v_2,\dots,v_K\}$, by minimising the objective function as given in Equation (4.16) [198] below:

$$\min_{V}\sum_{i=1}^{K}\sum_{j=1}^{n_{\mathrm{v}}}D^2\left(x_j,v_i\right) \tag{4.16}$$

where *D* is the distance function, such as Euclidean distance (ED), Manhattan distance (MD) and Dynamic Time Warping (DTW) etc.

The Fuzzy C-Means (FCM) algorithm is an extended version of the *K*-Means algorithm including the fuzzy-partition matrix. Each object can belong to more than one cluster. The iterative process is similar to *K*-Means. The objective function is given in Equation (4.17) [198] below:

$$\min_{V}\sum_{i=1}^{K}\sum_{j=1}^{n_{\mathrm{v}}}(w_{ij})^{m_{\mathrm{fuzz}}}D^2(x_j,v_i) \tag{4.17}$$

The fuzzifier m_{fuzz} determines the level of cluster fuzziness, where $1 \leq m_{\text{fuzz}} \leq \infty$. A high m_{fuzz} results in smaller membership values. The centroid for FCM is calculated with Equation (4.18) [198].

$$v_i = \frac{\sum_{j=1}^{n_v} (w_{ij})^{m_{\text{fuzz}}} x_j}{\sum_{j=1}^{n_v} (w_{ij})^{m_{\text{fuzz}}}}, i = 1, \dots, K. \tag{4.18}$$

The fuzzy-partition matrix is given in Equation (4.19) [198].

$$w_{ij} = \frac{1}{\sum_{h=1}^{K} \left(\frac{D(x_j, v_i)}{D(x_j, v_h)} \right)^{\frac{2}{m_{\text{fuzz}}-1}}} \tag{4.19}$$

One of the crucial elements in partition-based cluster analysis is the function used to measure the similarity between time series. The distance metric can have a profound effect on the clustering of times series and on their respective clusters.

ED and MD are the most frequently used distance measures for data mining. Although both have been deployed in many time series application fields, the metric has many pitfalls for time series analysis. They can only be used for time series of equal length and are prone to noise and outliers which are common in real-life temporal sequences especially when noise and uncertainty exist in the data source [199]. Another major issue with ED is that the metric is based on the comparison between data points at the same time interval. Time series regularly suffer transformations in the time axis although the series are in a similar shape, which is due to the perturbation of the solar irradiance, and in the context of CI, there will be time discrepancies for sunrise and sunset in the clear-sky solar model and real-life solar irradiance data. Let x_i and v_j each be a *d*-dimensional vector, and the ED and MD between the two vectors are presented in Equations (4.20) [198] and (4.21) [200], respectively.

$$\text{ED} = \sqrt{\sum_{f=1}^{d} (x_{if} - v_{jf})^2} \tag{4.20}$$

$$\mathrm{MD} = \sum_{f=1}^{d} |x_{if} - v_{jf}| \tag{4.21}$$

Dynamic Time Warping (DTW) has many features that may overcome the drawbacks of ED and MD. Essentially, the objective of DTW is to find the optimal alignment between the two series by searching for the minimal path in a distance matrix that defines a mapping between them while satisfying the moving restrictions during the searching process, i.e., only vertical, horizontal and diagonal moves are allowed. This results in stretching and compressing of time series. The mapping for each pair of points in the series can be determined by distance metrics such as ED, Manhattan, etc. The distance metric used for FCM DTW is ED. The outputs of DTW are the cost matrix that denotes the cost values, i.e., the DTW distance between the two indexes and the warping path. The chief weakness of DTW is the computational complexity. The algorithm for calculating the DTW for two time series is given in [201]. To demonstrate the effects on the CI profiles with DTW, Figures 4.4 and 4.5 depict the comparison between the original and the warped CI profiles for Clusters 1 and 4 respectively for winter, Kenya.

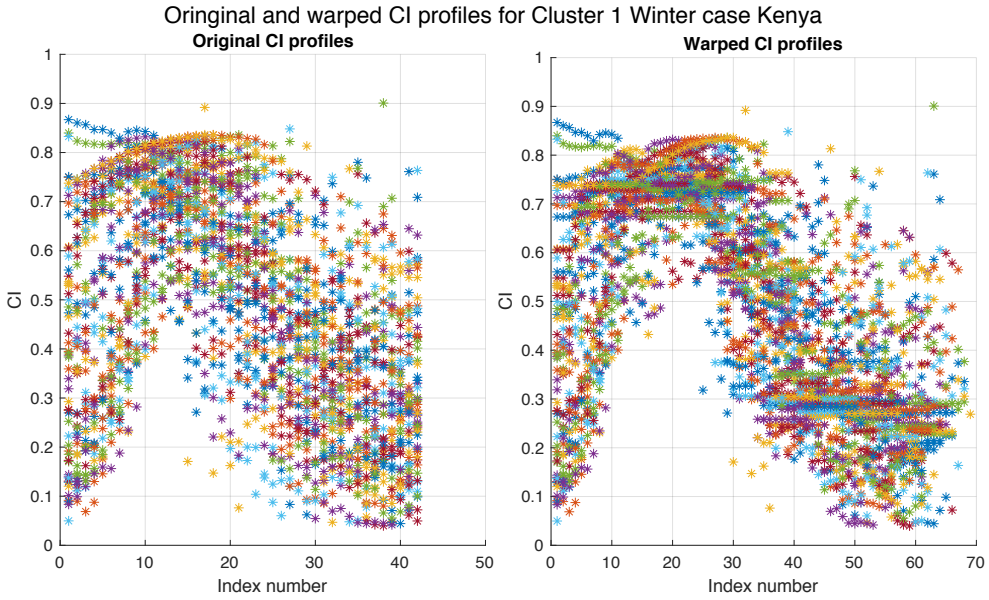


Figure 4.4. Original and warped CI profiles for Cluster 1 for winter, Kenya.

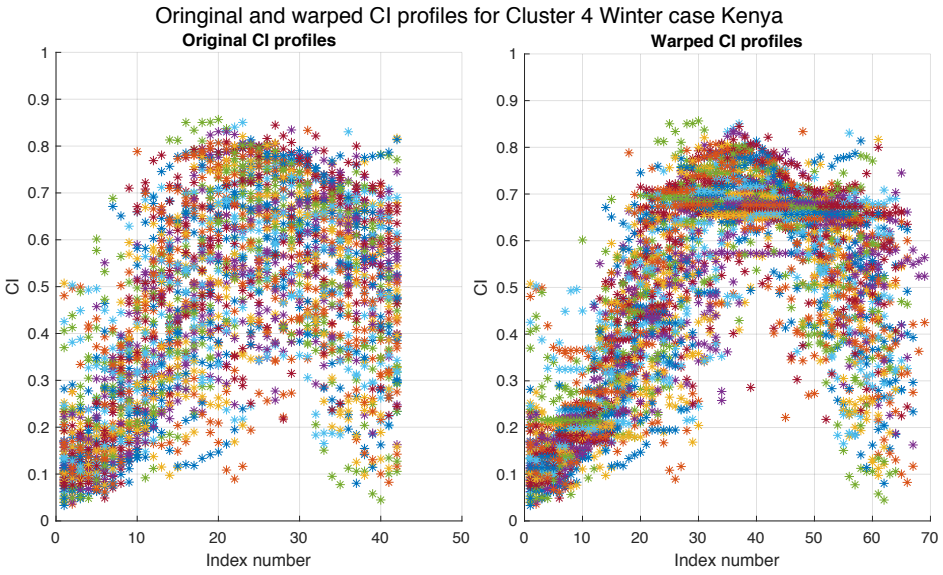


Figure 4.5. Original and warped CI profiles for Cluster 4 for winter, Kenya.

The reference CI profile for DTW is the centroid of the cluster. The clustering results were obtained from FCM DTW clustering which will be presented in Section 4.3.3. The clusters for winter, Kenya can be found in Figure 4.21 in Section 4.3.3. The warped CI profile can be significantly different from the original CI profile to minimise the ED between the two vectors. This is the dynamic property of DTW and is useful for shape-based similarity measure.

The principal challenge in applying DTW distance to partition-based clustering techniques is calculating the average of a set of time series. To overcome this issue, DTW Barycenter Averaging (DBA) is used for DTW averaging. Unlike the traditional centroid calculation method where the mean is directly determined, the aim of DBA is to minimise the sum of squared DTW distances between the centroid sequence and the set of sequences to be clustered. This is essentially achieved by performing two iterative procedures. The first stage involves performing DTW on the sequence to be clustered and the centroid to be refined. The associations between them are retained to be stored in the association table. The second stage involves updating each index of the centroid with the Barycentre of the indexes associated with it from the association table by calculating the mean. The standard deviation of the centroid

can also be calculated with the association table. The algorithm for DBA can be found in [202]. Figure 4.6 shows the CI in the association table during the averaging process for the six clusters for winter, Kenya. It is worth mentioning that the number of CI at each index number might be different as opposed to one CI per interval. This is because an index of a sequence might contribute to the update position of multiple indexes of the average vector, i.e., centroid.

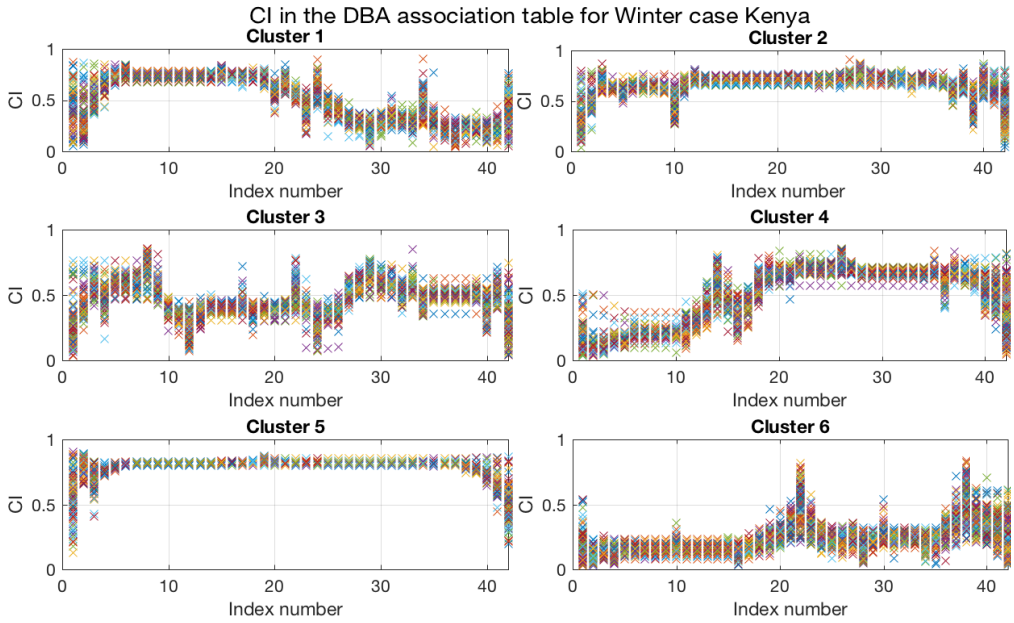


Figure 4.6. Association table in DBA for winter, Kenya.

As explained previously, the cluster centres cannot be calculated with the traditional method in Equation (4.18) when considering DTW as the distance function in Equation (4.17). The cluster centres are calculated with DBA instead. To initialise the cluster centres in each cluster, the time series are assigned to the cluster having the maximum membership degree. The cluster centres will be refined in the iterative FCM optimisation process. The partition matrix is calculated with Equation (4.19) where D stands for the DTW distance.

4.2.3 Comparison of computational complexities

Let n_{v}, t_{it} and d be the number of profiles, number of iterations and number of profile's dimension, respectively. The K-Means Computational Complexity (CC) for ED or MD is approximated as $\mathrm{O}(n_{\mathrm{v}}Kdt_{\mathrm{it}})$ [203]. For FCM with ED, the CC is approximated as $\mathrm{O}(n_{\mathrm{v}}K^2dt_{\mathrm{it}})$.

The FCM suffers higher computation costs compared to *K*-Means. This is due to the need to update the fuzzy-partition matrix in each iteration [204].

For GMM clustering, the CC is mainly associated with the EM algorithm. This is approximated as $O(t_{it} n_v K(1+d^2)+K)$ [197] which is higher than the partition-based clustering methods for high dimensional data [205, 206]. The covariance and mean matrix grow in the size of Kd^2 and Kd, respectively.

For FCM DTW, the differences in CC per iteration with respect to the standard FCM algorithm are the distance and centroid calculations. The CC of DTW is quadratic, d^2, unlike the linear computation costs for ED and MD [202]. Therefore, the total complexity for distance calculation is $O(n_v d^2)$. The centroids are calculated with the DBA method and have a computation cost of $O(t_{it} nv d^2)$ [202]. The resulting FCM DTW computation cost is therefore $O[n_v d^2 I(K^2 n_v d^2)]$ which simplifies to $O(t_{it} n_v^2 K^2 d^4)$. FCM DTW has the highest CC compared to other clustering methods, and future research should look for more efficient methods in using DTW for FCM clustering.

4.3 Cluster analysis and discussions

4.3.1 Clustering of daily Clearness Index profiles

Cluster analysis aims to determine the smallest number of clusters for the daily CI profiles, while minimising the intra-cluster distance. To achieve this, it is required to minimise the total distance between each clustered profile with respect to their centroids. Five clustering methods described previously have been studied and compared. These are FCM with Euclidean distance (FCM ED), FCM with Dynamic Time Warping (FCM DTW), *K*-Means with Euclidean distance (*K*-Means ED), *K*-Means with Manhattan distance (*K*-Means MD) and GMM. The cluster number to be evaluated is from 2 to 15. The total intra-cluster distance is calculated with Equation (4.22) and is used as an indicator of merit.

$$D_{\text{Total}} = \sum_{i=2}^{K} \sum_{j=1}^{n_v} D^2(x_j, v_i) \tag{4.22}$$

As the clustering algorithms contain random variables, 50 repeated tests were conducted and the minimum results are kept. The total intra-cluster distance with respect to different number of clusters for the four seasons is provided in Figure 4.3. Compared to different clustering methods, there is a huge difference in the total intra-cluster distance for winter and summer cases. This can be explained by the level of uncertainty associated with the season. There is significantly more fluctuation in the summer season, hence, the total intra-cluster distance will be increased. It is observed that FCM DTW has significantly smaller total intra-cluster distance for all cases. FCM ED performs marginally better than *K*-Means ED in most cases given the fact that it performs in analysing uncertainty, i.e., clusters with various sizes and shapes arising from the fuzzifier used for calculation where the profiles may belong to more than one cluster. It is worth mentioning that the intra-cluster distance for *K*-Means MD should not be compared with other intra-cluster distances as ED and MD are different metrics.

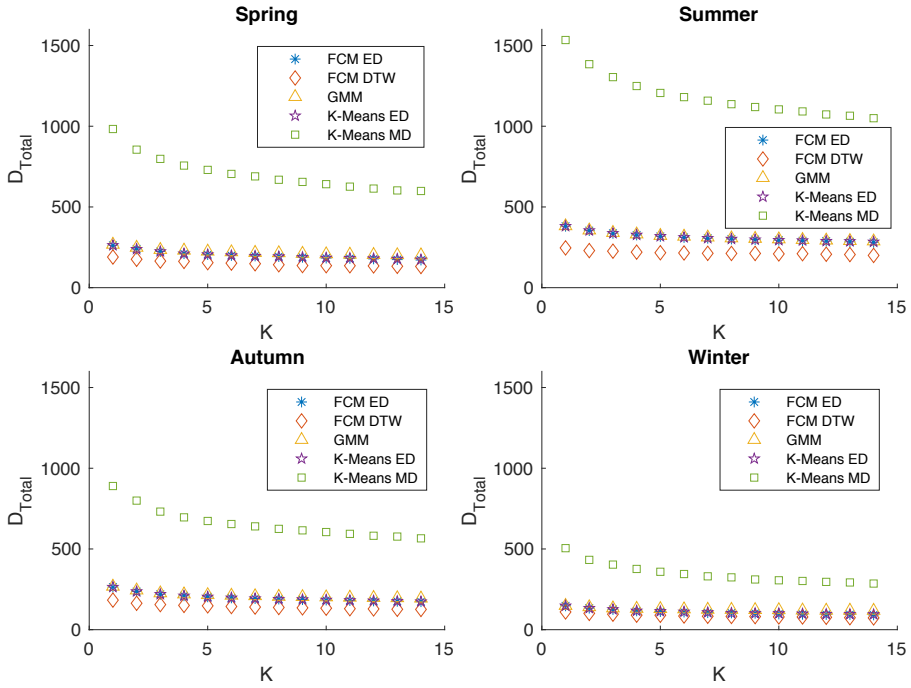


Figure 4.7. Total intra-cluster distance for different number of clusters for Johannesburg.

ED is used to compute the intra-cluster distance for GMM. It is evident that the total intra-cluster distance for GMM is marginally higher than *K*-Means methods. *K*-Means aims to minimise the intra-cluster distance with ED while GMM aims to maximise the maximum-likelihood via the EM algorithm which does not consider minimising the distance.

4.3.2 Fuzzy decision making

One of the major challenges in using cluster analysis is to determine the optimal number of clusters. Traditionally, this is achieved by using criteria such as Silhouette index, Dunn's index and Calinski-Harabasz index. Essentially, these indices aim to determine some form of relationship between the within cluster cohesion and the cluster separation to evaluate the clusters' validity. The details of these indices and the distance suitability are provided in [200]. It is observed that the criteria are deemed ineffective for dataset with significant amount of noise or uncertainty [200]. Moreover, the optimal number of clusters is problem dependent, and the mentioned criteria rarely provide the same results. A technique for determining the optimal number of clusters, by first evaluating the number of clusters that provides the best trade-off for minimising the total intra-cluster distance, is proposed here. Consequently, if the resultant centroids have similar characteristics, i.e., mean and standard deviation, the similar clusters will be grouped together with the new centroid calculated. Without prior knowledge of the selection of candidate partitions in the Pareto set, an unweighted fuzzy logic decision-making strategy [207] is employed to yield the best trade-off solution.

In this chapter, it is assumed that the preferences of minimising the number of clusters and total intra-cluster distance are unbiased. Fuzzy logic decision-making is formulated as follows: m_{Nondom} is equal to 15 and represents the number of non-dominated solutions, and n_{obj} is the number of objective functions. In this case, n_{Obj} is equal to 2 because the objective is to minimise the number of centroids and the total intra-cluster distance. The fuzzy membership is defined below:

$$\mu_{\text{fuzz}_i}(j) = \frac{f_i - f_i^{\min}}{f_i^{\max} - f_i^{\min}}, i = 1,2 \tag{4.23}$$

f_i stands for the solutions in the i^{th} objective function. The normalised membership for each solution is expressed as:

$$\mu_{\text{fuzz}}(j) = \frac{\sum_{i=1}^{n_{\text{Obj}}} \mu_{\text{fuzz}_i}(j)}{\sum_{j=2}^{m_{\text{Nondom}}} \sum_{i=1}^{n_{\text{Obj}}} \mu_{\text{fuzz}_i}(j)} \tag{4.24}$$

The most satisfactory solution in this case is selected with the minimum fuzzy membership value [207]. The normalised fuzzy memberships for the four seasons, calculated with the intra-cluster distances given in Figure 4.7 are presented in Figure 4.8. The clustering methods exhibit similar trends for the normalised fuzzy membership with respect to cluster number. This explains that the optimal number of clusters is similar for the different clustering techniques.

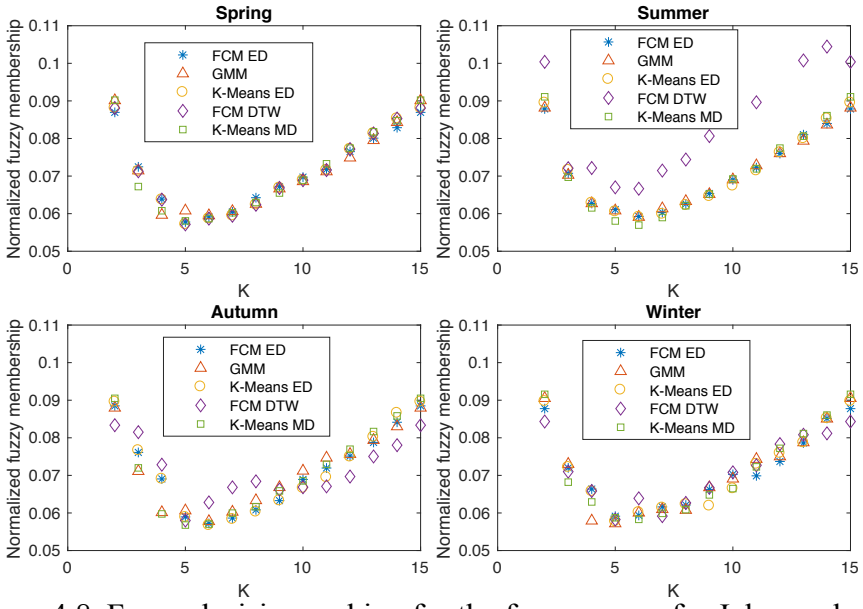


Figure 4.8. Fuzzy decision making for the four seasons for Johannesburg.

Figure 4.9 shows the centroids for winter, Johannesburg with different clustering techniques for Johannesburg. The centroids for FCM ED and *K*-Means ED in winter case show a similar shape. Recalling the results in Figure 4.7, the total distance for the two approaches are very similar. The number of representations for clear days are different. It is one centroid for GMM, two centroids for FCM ED and *K*-Means ED and three centroids for *K*-Means MD and FCM

DTW. A method is required to minimise the number of centroids with similar shapes and magnitude to reduce redundancy.

According to Figure 4.10, the centroids for summer, Johannesburg suggest that the clustering performance of FCM ED, *K*-Means ED, *K*-Means MD and GMM are similar. It is worth noting that the clustering problem for the summer case is significantly more challenging than the winter case. This is due to the fact that CI fluctuates more in summer.

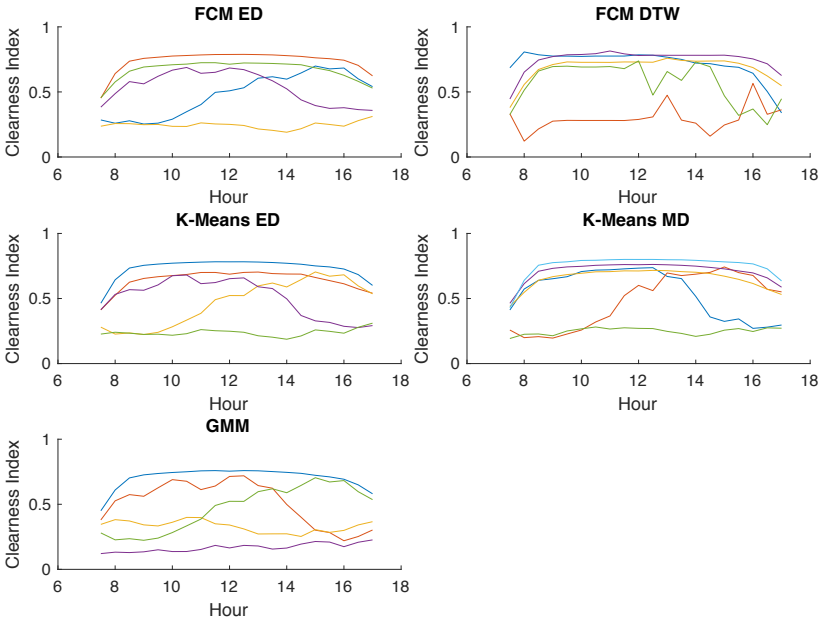


Figure 4.9. Centroids for different clustering techniques for winter, Johannesburg.

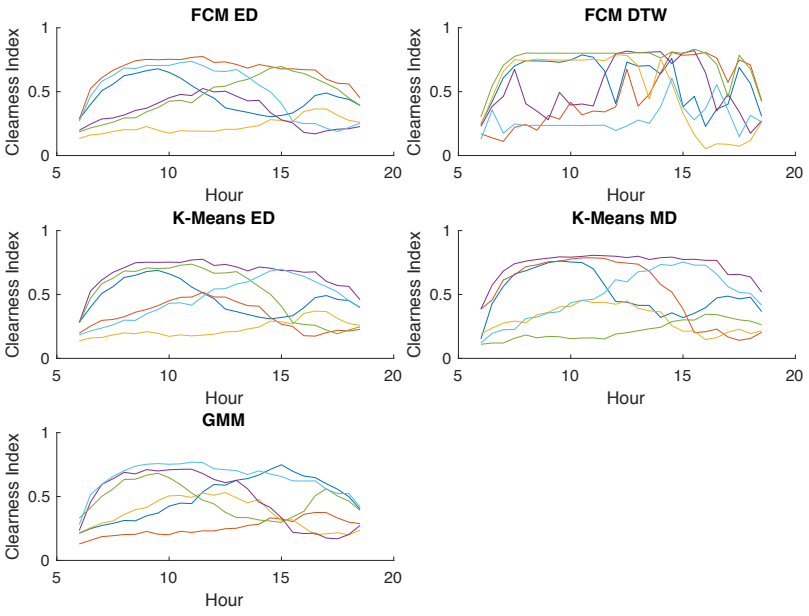


Figure 4.10. Centroids for different clustering techniques for summer, Johannesburg.

The centroids for autumn and spring, Johannesburg obtained from the various clustering methods are depicted in Figures 4.11 and 4.12, respectively. It can be observed that centroids with the ED and MD distances are generally smooth. This may introduce issues with capturing the irradiance fluctuations.

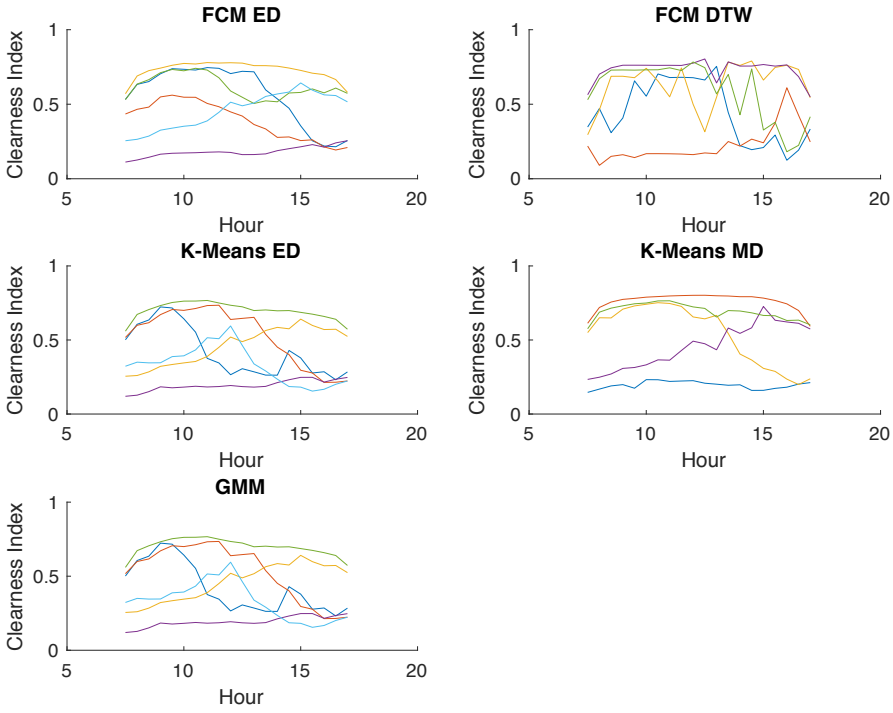


Figure 4.11. Centroids for different clustering techniques for autumn, Johannesburg.

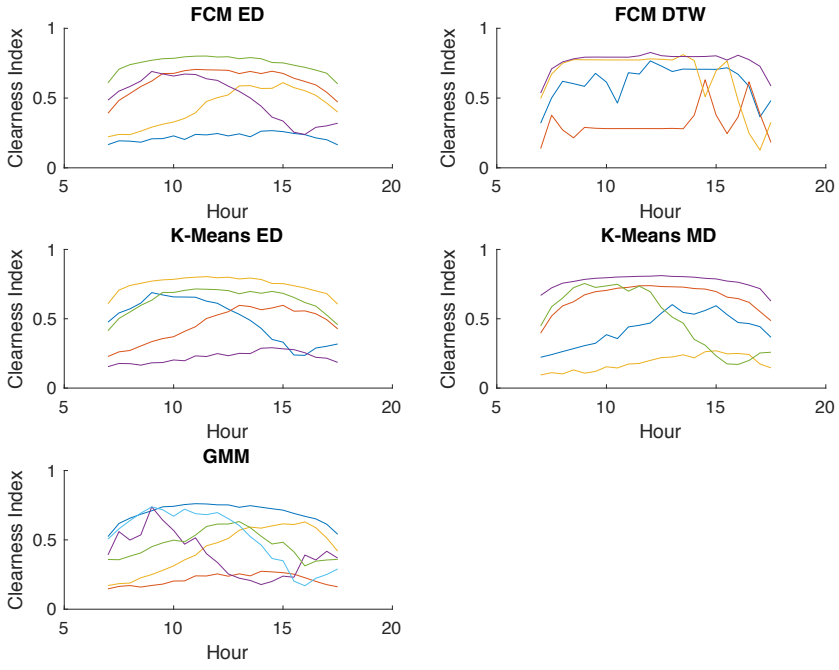


Figure 4.12. Centroids for different clustering techniques for spring, Johannesburg.

The centroids' comparison for the five clustering methods for Kenya are provided in Figures 4.13 to 4.16. It can be observed that there are redundant centroids for spring, summer and autumn cases. These centroids will be grouped together to form a cluster.

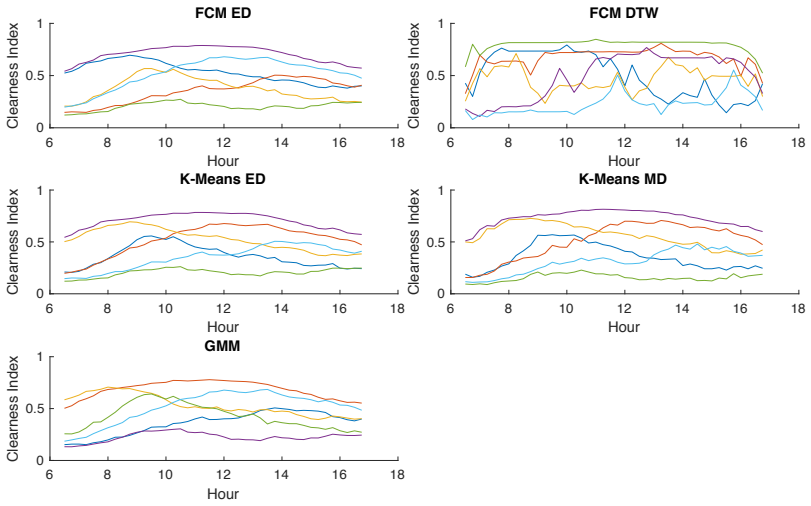


Figure 4.13. Centroids for different clustering techniques for winter, Kenya.

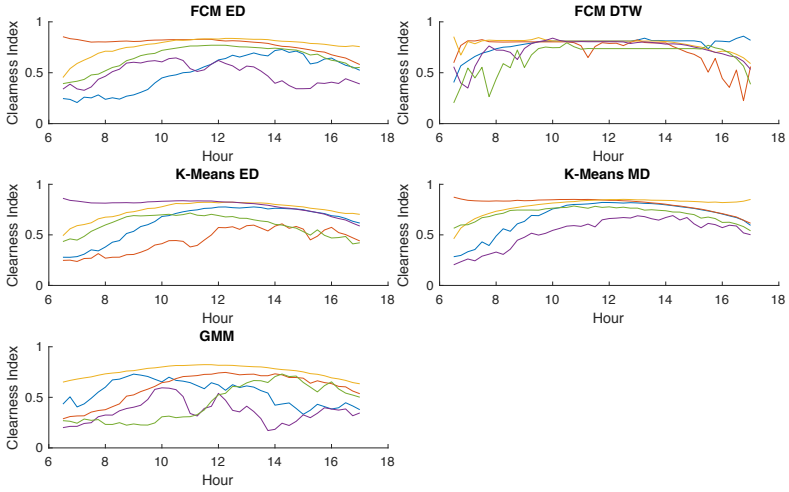


Figure 4.14. Centroids for different clustering techniques for summer, Kenya.

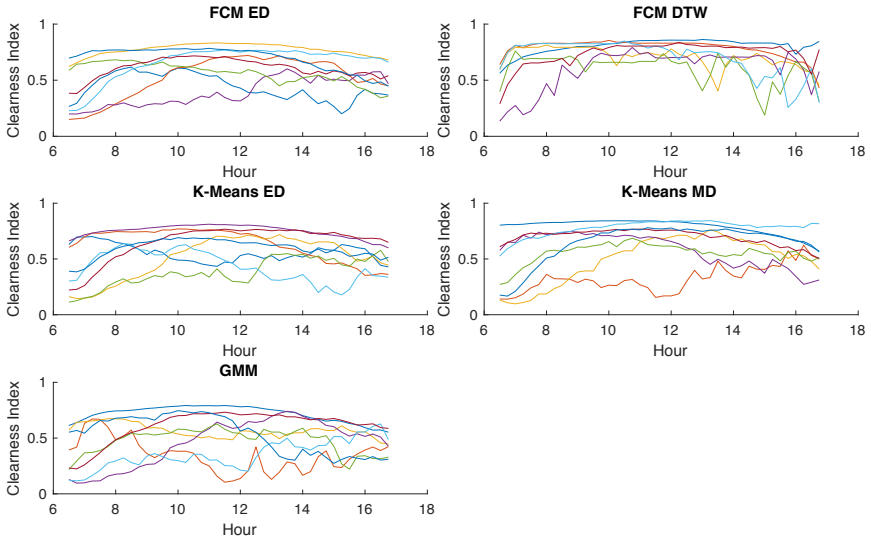


Figure 4.15. Centroids for different clustering techniques for autumn, Kenya.

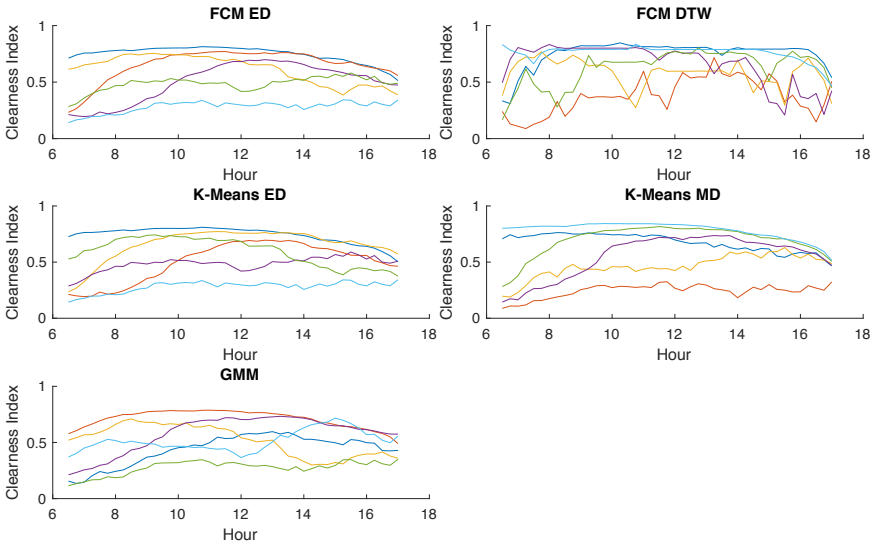


Figure 4.16. Centroids for different clustering techniques for spring, Kenya.

4.3.3 Reduction of clusters with centroid evaluation

The *K*-Means-related clustering techniques consider solely the intra-cluster compactness, i.e., the distances between the objects and the centroids [208]. The inter-cluster separation, i.e., the distances between the centroids themselves are not well considered during the clustering process. Redundant or similar clusters and centroids can be eliminated by evaluating the centroid's standard deviation and mean. In the first step, a mean similarity matrix and standard deviation similarity matrix, both with size *K* by *K,* are constructed to determine if the clusters

are similar. If the element in the matrix falls below a predefined threshold, in this case 0.1 for both variables, then the element will be set to 1. This signifies that the two clusters have similar characteristics. The corresponding elements in the two matrices with binary numbers will be multiplied together to provide the similarity matrix, *M*. Once the similar clusters are grouped together, the new centroid is calculated by calculating the average of the centroids by considering the weights with the number of profiles in the original cluster. The procedure is presented in Table 4.1.

Input: $C = \{c_1, c_2, ..., c_k\}$: the set of all centroids
card: the cardinality of each cluster
Output: C' : the reduced set of centroids
1. Calculate the similarity matrix *M*
2. $s = \{1, 2, ..., k\}$
3. Find the all-zero rows of *M*
   $s' \leftarrow$ the indices of all-zero rows
   $C' = \{c_i \mid i \in s'\}$
4. $s = s - s'$
5. **while** *s* is non-empty
   $s' = \{s_i \mid i = 1 \; or \; M_{s_1,i} = 1\}$
   $C_new = \frac{\sum_{i \in s'} c_i \cdot card_i}{\sum_{i \in s'} card_i}$
   $C' = C' \cup C_new$
   $s = s - s'$
   End

Table 4.1. Algorithm for reduction of redundant centroids.

Figure 4.17 shows that the centroids for FCM DTW for winter, Johannesburg can be reduced from the original five centroids, as shown in Figure 4.9, to three centroids. It also presents the daily CI profiles with their respective centroids. The percentage day covered for clear days in Cluster 3 is 78 % which is the highest compared to other seasons at Johannesburg. The black, blue and red lines from Figure 4.17 to Figure 4.24 give the centroids, the centroids with plus

one and those with minus one standard deviation, respectively, calculated with the association table in DBA.

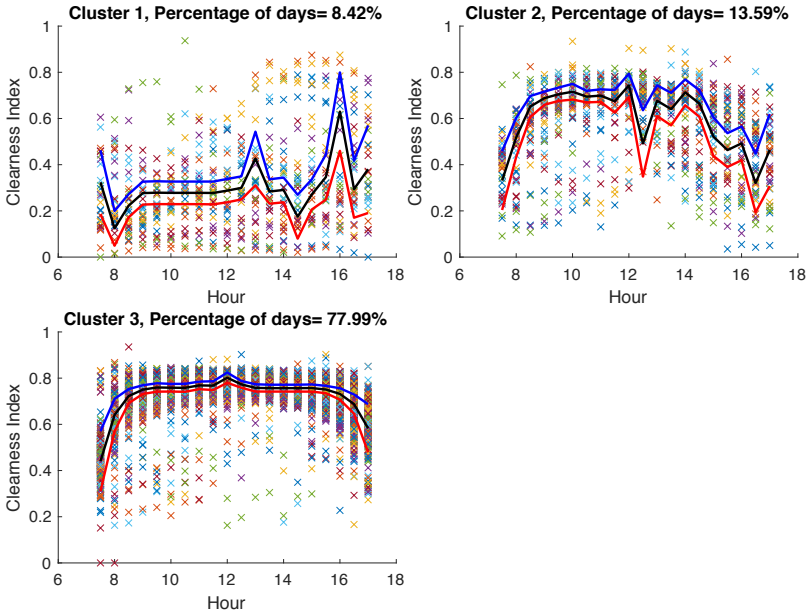


Figure 4.17. CI profiles in respective centroids for FCM DTW for winter, Johannesburg.

Figure 4.18 presents the daily CI profiles with respect to their centroids for FCM DTW for summer, Johannesburg.

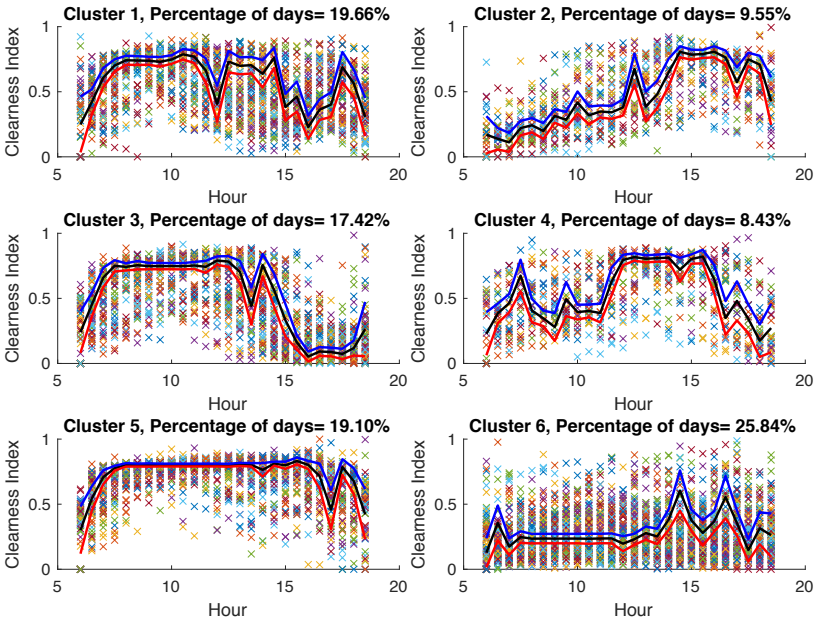


Figure 4.18. CI profiles in respective centroids for FCM DTW for summer, Johannesburg.

The clear days are presented in Cluster 5 which approximately constitutes 19.10 % of the days of the season. Cluster 3 shows that the perturbation takes place during late afternoon. Cluster 6 presents the CI profile where the CI is generally low for the whole day. The clustering results display an interesting pattern and could be understood and quantified. The optimal number of clusters for the four seasons with the five clustering techniques for Johannesburg are provided in Table 4.2. Figure 4.19 depicts the clustering results for the autumn case.

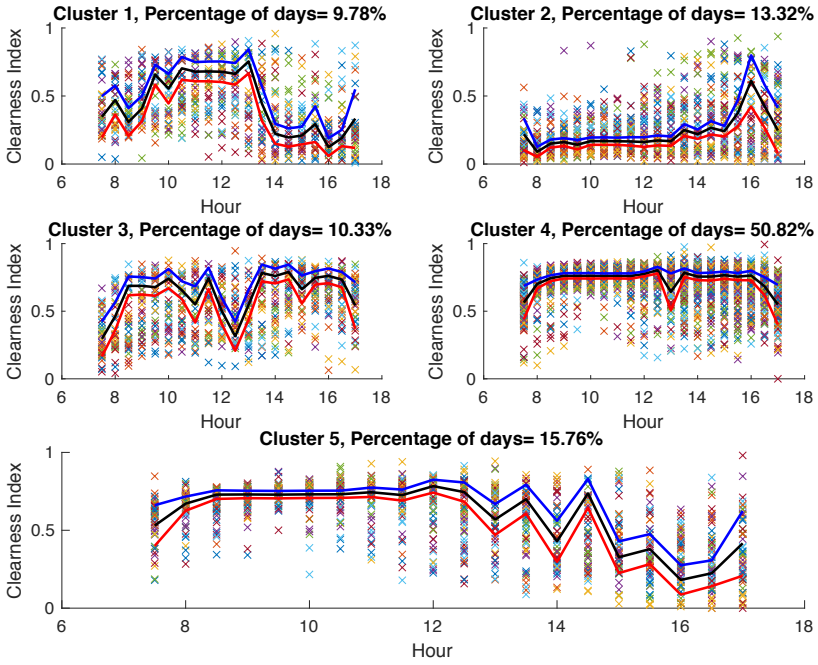


Figure 4.19. CI profiles in respective centroids for FCM DTW for autumn, Johannesburg.

The clustering results for spring, Johannesburg with FCM DTW are presented in Figure 4.20. Cluster 4 provides the grouping of the clear days.

	Spring	Summer	Autumn	Winter
FCM ED	5	6	6	4
FCM DTW	4	6	5	3
GMM	6	6	6	5
K-Means ED	5	6	6	4
K-Means MD	5	6	5	4

Table 4.2. Optimal number of clusters for Johannesburg.

For Kenya, the daily CI profiles are constructed for the four seasons with FCM DTW and the results are presented from Figures 4.21 to 4.24. The number of clusters obtained from fuzzy

decision results with cluster reductions are presented in Table 4.3. As depicted in Figure 4.21, the ‘clear days’ for spring in Kenya belongs to Cluster 1. The cluster has high CI values with little fluctuations. The CIs with lowest values are situated in Cluster 2.

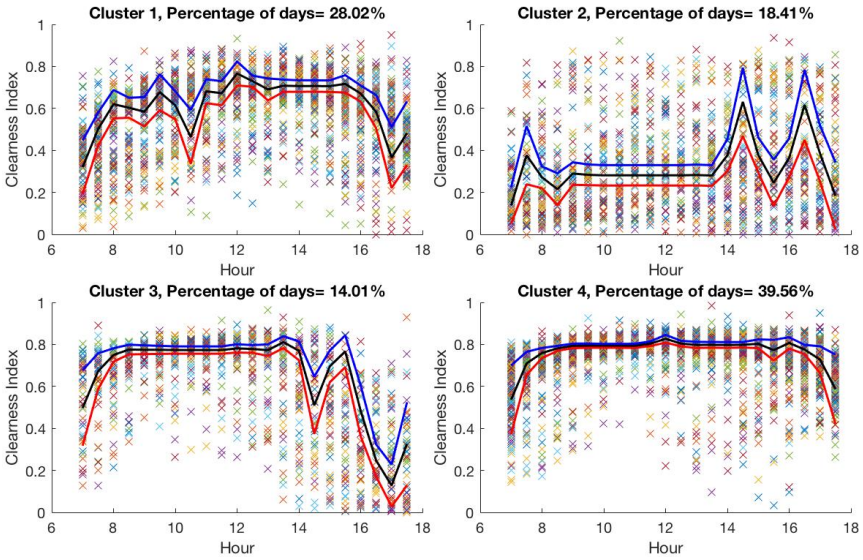


Figure 4.20. CI profiles in respective centroids for FCM DTW for spring, Johannesburg.

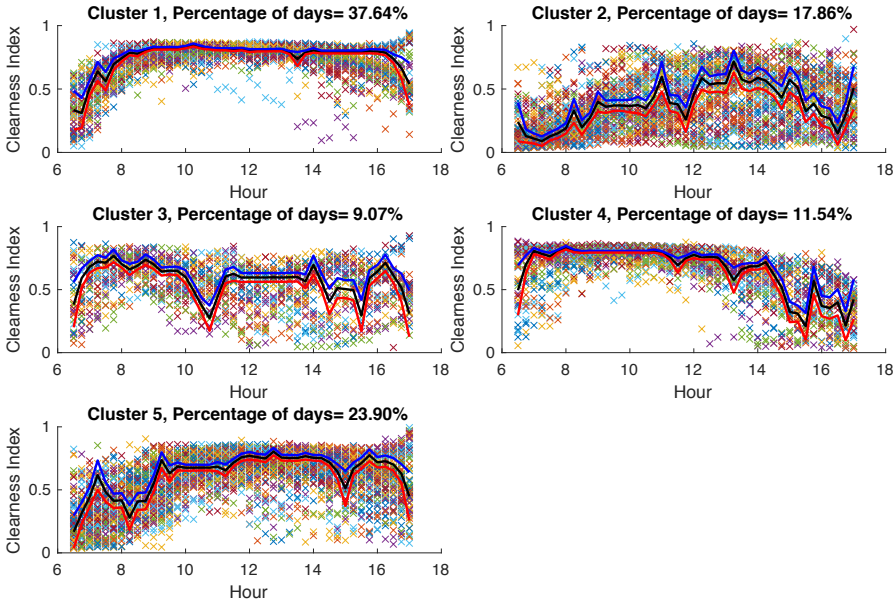


Figure 4.21. CI profiles in respective centroids for FCM DTW for spring, Kenya.

The ‘clear day’ for summer in Kenya, shown in Figure 4.22, belongs to Cluster 1. Although the other centroids are generally of high mean value, there are some sort of perturbations such as the centroid in Cluster 3 which reaches a value of 0.3 at 7 am.

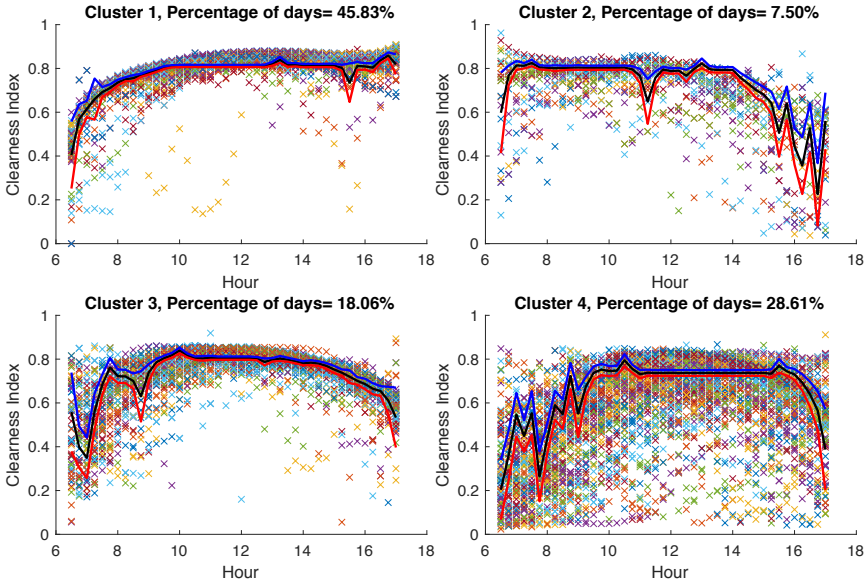


Figure 4.22. CI profiles in respective centroids for FCM DTW for summer, Kenya.

As presented in Figure 4.23, the ‘clear days’ for autumn in Kenya belong to Clusters 1 and 6. Although Clusters 2 and 4 show some high CI values, the CI suffers from cloud covering. The ‘clear days’ for winter in Kenya belong to Cluster 5 as shown in Figure 4.24.

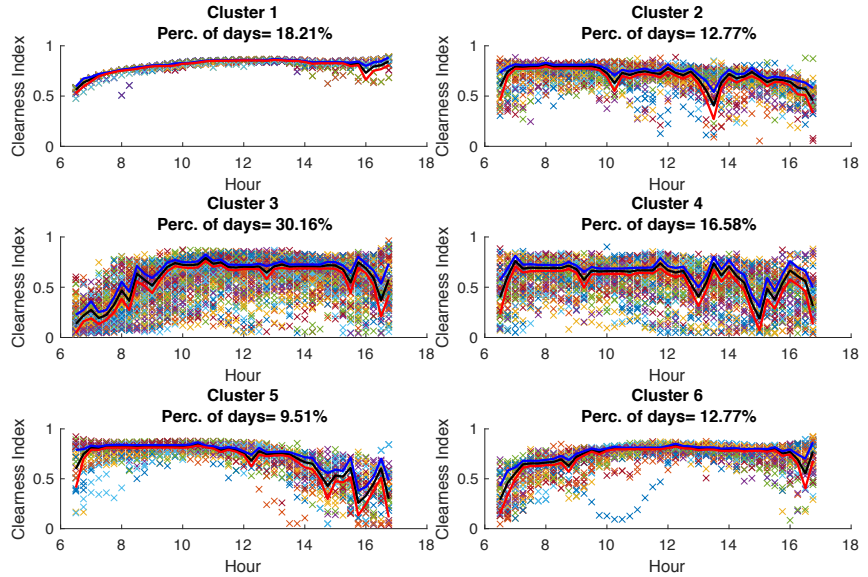


Figure 4.23. CI profiles in respective centroids for FCM DTW for autumn, Kenya.

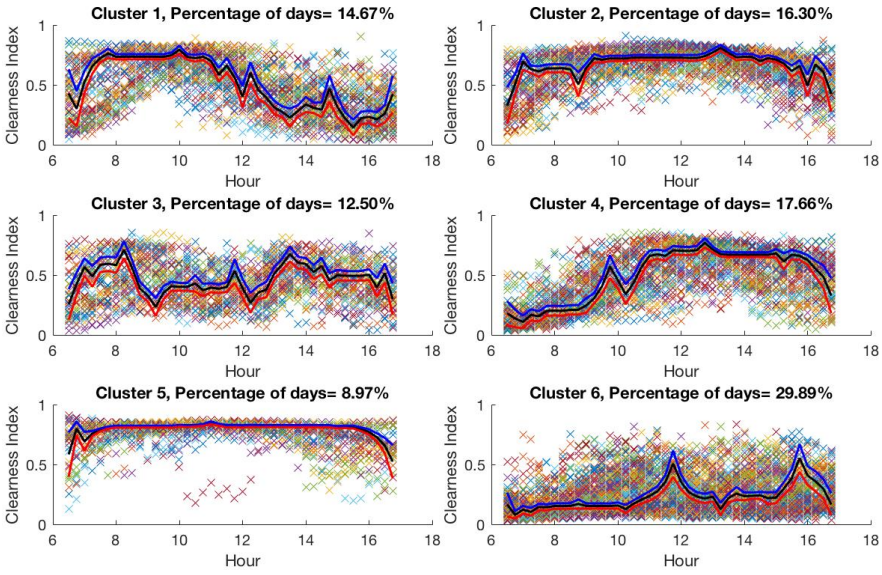


Figure 4.24. CI profiles in respective centroids for FCM DTW for winter, Kenya.

	Spring	Summer	Autumn	Winter
FCM ED	6	5	8	6
FCM DTW	5	4	6	6
GMM	6	5	8	6
K-Means ED	6	5	8	6
K-Means MD	6	5	8	6

Table 4.3. Optimal numbers of clusters for Kenya.

4.3.4 Centroids comparison with real-life CI profiles

The Mean Squared Error (MSE) metric is used to examine the similarities of the cluster centroids with the real CI profiles. The error should be as minimal as possible, ideally zero, to have a competent representation of the CI profile. The MSE between the centroid and the CI profile is given in Equation (4.25) below:

$$\text{MSE} = \frac{1}{d}\sum_{f=1}^{d}(x_{if} - v_{jf})^2 \tag{4.25}$$

The comparison of centroids with the CI profiles for the five clustering methods are presented in Figures 4.25 to 4.29. For each cluster, the CI profiles with the minimum MSE are obtained. It is shown that FCM DTW cluster analysis can achieve a lower MSE when comparing the

minimum MSE with other clustering methods with the largest minimum MSE at Cluster 3 being 0.0032.

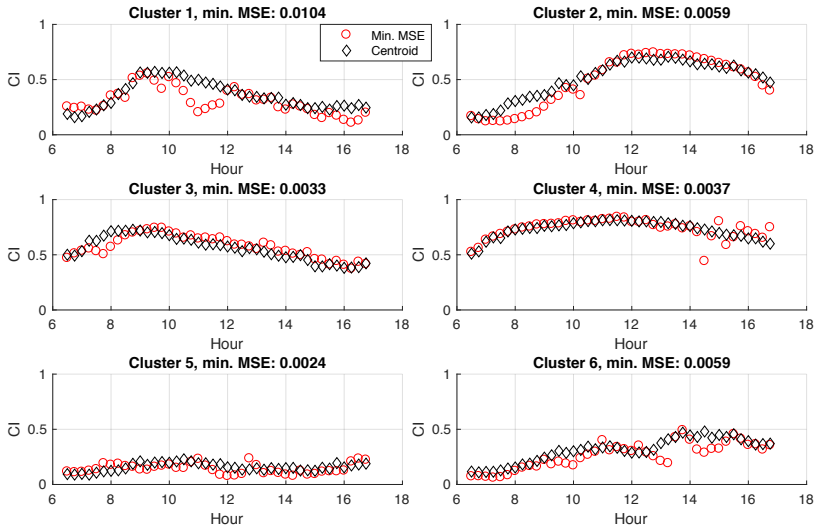


Figure 4.25. MSE between centroids and real profiles with *K*-Means MD for winter, Kenya.

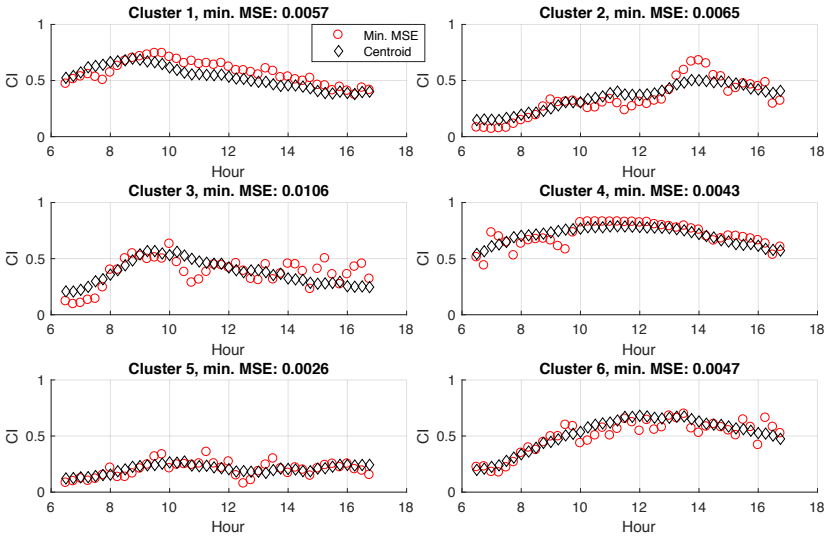


Figure 4.26. MSE between centroids and real profiles with FCM for winter, Kenya.

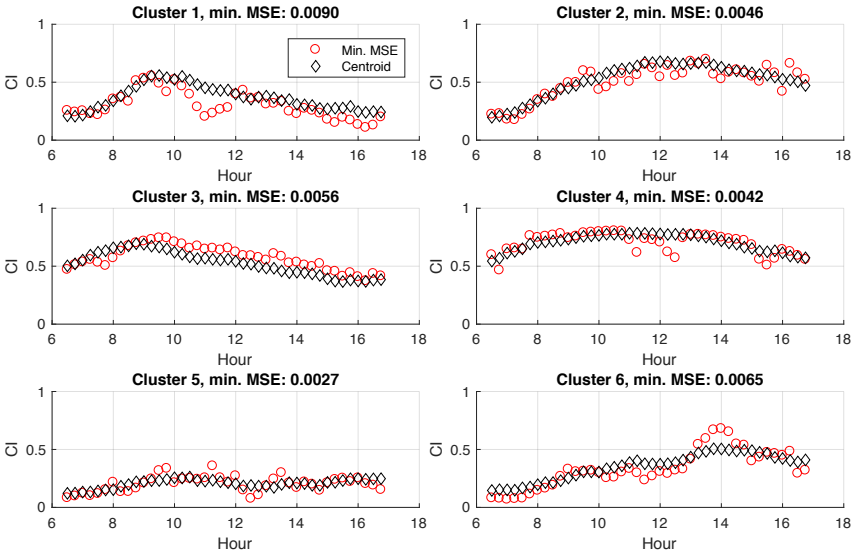


Figure 4.27. MSE between centroids and real profiles with *K*-Means ED for winter, Kenya.

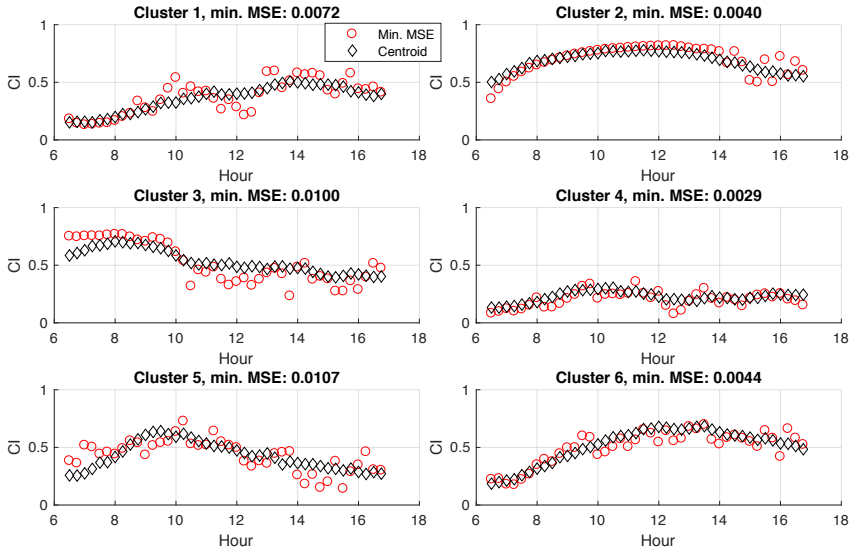


Figure 4.28. MSE between centroids and real profiles with GMM for winter, Kenya.

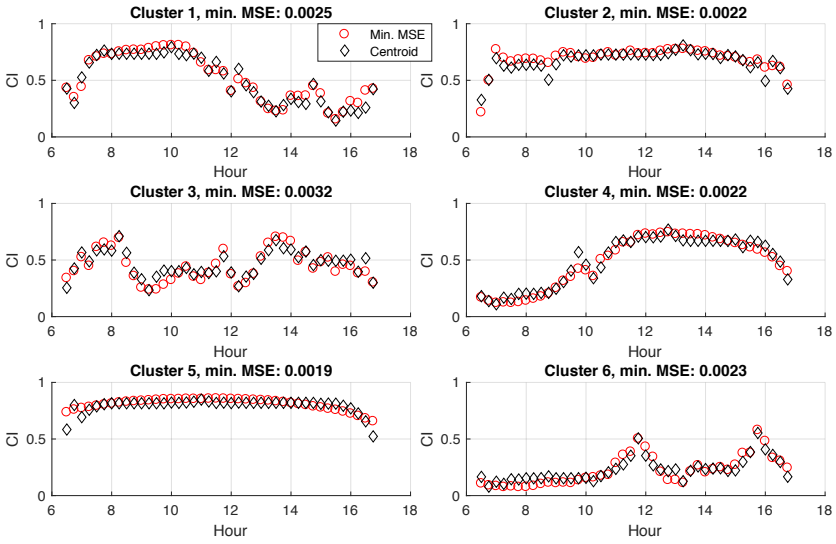


Figure 4.29. MSE between centroids and real profiles with FCM DTW for winter, Kenya.

4.4 Clearness Index and weather conditions analysis

The FCM DTW clustering results are further studied with the weather conditions data. The corresponding weather conditions for the solar irradiance dataset for Kenya, were obtained for Nairobi Jomo, Kenya, from Weather Underground [209]. The weather conditions for dataset with Johannesburg were also collected from the database of the same website.

The dataset with weather conditions to be analysed is shown in Table 4.4. Columns 1, 2, 3 and 4 represent the time in year, month, day and hour in the MATLAB format, respectively. The solar irradiance is provided in column 5. The weather condition and the CI are provided in columns 6 and 7, respectively. The CI can be 'NaN' in cases where solar irradiance is not available, i.e., 0/0. These data are excluded in the study as they are not relevant.

This section aims to study how well the proposed clustering method correlates with the weather forecasting information, i.e., weather conditions. This will confirm the dependency of the CI and the weather conditions and additionally, the accuracy of the clustering results. The results will also suggest that the clustering procedure can be applied to other locations for PV system evaluations such as sizing and distribution system load flow analysis.

Year	Month	Day	Hour/Minute (MATLAB)	Irradiance (Wm^{-2})	Weather condition	Clearness Index
2011	9	1	0.004166667	0	'Scattered Clouds'	NaN
2011	9	1	0.014583333	0	'Scattered Clouds'	NaN
2011	9	1	0.025	0	'Scattered Clouds'	NaN
2011	9	1	0.035416667	0	'Scattered Clouds'	NaN
2011	9	1	0.045833333	0	'Clear'	NaN
2011	9	1	0.05625	0	'Clear'	NaN
2011	9	1	0.066666667	0	'Clear'	NaN
2011	9	1	0.077083333	0	'Clear'	NaN
2011	9	1	0.0875	0	'Scattered Clouds'	NaN
2011	9	1	0.097916667	0	'Scattered Clouds'	NaN
2011	9	1	0.108333333	0	'Scattered Clouds'	NaN
2011	9	1	0.11875	0	'Scattered Clouds'	NaN
2011	9	1	0.129166667	0	'Partly Cloudy'	NaN
2011	9	1	0.139583333	0	'Partly Cloudy'	0
2011	9	1	0.15	4	'Partly Cloudy'	0.077318929
2011	9	1	0.160416667	20	'Partly Cloudy'	0.166207348
2011	9	1	0.170833333	43	'Mostly Cloudy'	0.219380228
2011	9	1	0.18125	66	'Mostly Cloudy'	0.240601593
2011	9	1	0.191666667	211	'Mostly Cloudy'	0.59744908
2011	9	1	0.202083333	223	'Mostly Cloudy'	0.51692384
2011	9	1	0.2125	313	'Mostly Cloudy'	0.61587608
2011	9	1	0.222916667	390	'Mostly Cloudy'	0.668906293
2011	9	1	0.233333333	472	'Mostly Cloudy'	0.720190264
2011	9	1	0.24375	541	'Mostly Cloudy'	0.746385476
2011	9	1	0.254166667	599	'Scattered Clouds'	0.757265334
2011	9	1	0.264583333	655	'Scattered Clouds'	0.767355712
2011	9	1	0.275	701	'Scattered Clouds'	0.768428757
2011	9	1	0.285416667	731	'Scattered Clouds'	0.7561521
2011	9	1	0.295833333	765	'Mostly Cloudy'	0.752372712
2011	9	1	0.30625	825	'Mostly Cloudy'	0.776718747
2011	9	1	0.316666667	884	'Mostly Cloudy'	0.801696435
2011	9	1	0.327083333	908	'Mostly Cloudy'	0.797818216

Table 4.4. Data structure for time, irradiance, weather conditions and CI.

One of the major issues that needs to be addressed is the question of "How is a 'clear day' defined?". For instance, can a day with strong cloud cover in the noon for two hours and no cloud for the rest of the day be classified as a 'clear day'? This question will be explored and addressed in the following section. As shown in Table 4.4, the weather condition for each time interval can be different, hence, there will be a degree of ambiguity in defining 'clear day'. In practice and in real-life situations, there are very few instances of '100 %' clear days. According to the weather glossary from timeanddate.com [210], the 'clear' weather condition is defined as a sky condition of less than 1/10 cloud coverage. The 'partly cloudy' condition is defined as the sky condition when between $7/10^{th}$ and $3/10^{th}$ of the sky is covered and is used more frequently for night. The 'scattered clouds' condition is defined as a cloud layer that covers between $3/8^{th}$ and ½ of the sky.

According to Weatherunderground [209], there are 42 other terms such as, 'rain', 'thunderstorm', 'drizzle', 'snow', 'haze', etc. that may be used to represent the weather

condition for a particular time instance. In this context, a 'clear day' can be defined as having a high CI value and in general, associated with the weather conditions of 'clear', 'partly cloudy' and 'scattered clouds'. Table 4.5 presents the algorithm to calculate the percentage of 'clear days' for the season with the dataset provided in Table 4.4.

Input: $R = \{R_1, R_2, \ldots, R_h\}$: object with the set of daily time and weather for h time intervals
threshold: percentage of cloud cover to define if a day is 'clear day'
start: element number in the array for sunrise
end: element number in the array for sunset
Output: R'': the percentage of 'clear' condition for the season

```
for i1 = 1:length(R)
  for i2 = start:end
    if (R{1, i1}(i2, 6) == 'clear' or 'scattered clouds' or 'partly cloudy') is true
    S(i1, i2) = 1;
    elseif R{1, i1}(i2, 6) == empty is true
    S(i1,i2) = NaN;
    else
    S(i1,i2) = 0;
    end
  end
end
perc_clear = sum(S, 2)/length(S, 2);
for i3 = 1:length(R)
  if (perc_clear(i3) > threshold) is true
   R'(i3) = 1;
  else
   R'(i3) = 0;
  end
end
R'' = sum(R') / length(R');
```

Table 4.5. Algorithm for calculating the total percentage of 'clear days' with weather data.

As presented in Table 4.5, the algorithm aims to calculate the percentage of 'clear days' by assigning binary values to the time instances, and there is no need to use CI values. It should be worth noting that there are missing weather data in the dataset. These are then converted to 'NaN' and are neglected during the summation process of the algorithm.

The threshold can be seen as a sensitivity value and a key parameter in the algorithm. If sensitivity value is above the threshold, it is expected that the CI produced for the day will be

of high value with little perturbation. It should be recognised that due to different locations and climates, it the threshold might possibly be different. The threshold aims to provide the percentage of 'clear days' from the weather analysis that represents the closest percentage of the total number of 'clear day' clusters. The comparison of results for the cluster and weather analyses are presented in Tables 4.6 and 4.7 for the Kenya and Johannesburg studies.

		Spring	Summer	Autumn	Winter
Cluster analysis	**Cluster number**	1	1	1 and 6	5
	Total percentage (%)	37.64	45.83	30.98	8.97
Weather analysis		36.47	47.23	31.01	7.72
Threshold (%)		45	50	35	10
Absolute difference (%)		1.17	1.4	0.04	1.25

Table 4.6. Percentage of 'clear days' with cluster analysis and weather analysis for Kenya.

		Spring	Summer	Autumn	Winter
Cluster analysis	**Cluster number**	4	5	3 and 4	3
	Total percentage (%)	39.56	19.10	50.82	77.99
Weather analysis		39.78	17.18	51.38	79.67
Threshold (%)		95	95	85	80
Absolute difference (%)		0.22	1.92	0.56	1.68

Table 4.7. Percentage of 'clear days' with cluster analysis and weather analysis for Johannesburg.

As depicted in Tables 4.6 and 4.7, the total percentage of 'clear days' suggests that there are more 'clear days' in Johannesburg than Kenya for spring, autumn and winter. However, such a comparison is invalid as the threshold value is different for both studies. The amplitude of centroids is generally higher for Kenya than for Johannesburg for all clusters and seasons. It can be concluded that the threshold value can influence the percentage of 'clear days' for a particular season. The threshold for Kenya is lower than Johannesburg; this indicates that it requires less appearances of 'clear sky'/ 'scattered clouds'/'partly cloudy' conditions for the

day to be classified as a ‘clear day’. The threshold is the percentage that represents the ‘clear day’ duration. For instance, with a threshold of 25 % and an average daily sunshine hour in Kenya of 12 hours effectively implies that the day will be classified as a ‘clear day’ if it contains three hours of ‘clear sky’/ ‘scattered clouds’/‘partly cloudy’. The percentage difference is larger for summer than for other seasons in Johannesburg. This may be due to the increased fluctuations of the CIs for the season as shown in Figure 4.2, and it has proved to be more difficult with respect to providing high quality clusters.

This section evaluates the clustering results with the forecast weather conditions. The results show that the weather condition can affect the CI and subsequently the percentage of ‘clear days’. It is possible to estimate the shapes and magnitude of daily CI profiles with given limited weather condition data.

4.5 Summary

This chapter presents the feature extraction of daily CI profiles with five different cluster analysis techniques. Regarding partition-based clustering, it is observed that the fluctuations in the daily CI profiles are better captured with DTW distance. This is due to its dynamic properties. It is worth mentioning that centroids can be efficient for other planning and operation purposes for PV systems such as optimal placement of phasor measure unit and load flow analysis. The solar irradiance scenario reduction with the clustering method proposed here can reduce the computational time by avoiding computing placement and load flow cases with similar irradiance conditions. The next chapter will study the hybrid system sizing problem with the clusters and validate its practicality for PV system planning.

Chapter 5

Hybrid system sizing

This chapter presents a deterministic approach for sizing a solar PV and EES with AD to satisfy a proportional scaled-down demand of the national load in Kenya, Africa. The aim is to achieve a minimal LCOE for the system with maximum PV penetration in accordance with the PV system future growth and capital cost reduction. The energy imbalance between generation and demand due to AD generator constraint and solar resource is the primary focus for the sizing regime.

The economic feasibility of building a hybrid system will first be studied by comparing the levelized costs of a system solely powered by AD. This requires the use of the levelized cost metrics derived in Chapter 3. The centroids for the daily CI profiles obtained in Chapter 4 will be used for the system sizing. Four years of solar data collected from Kenya and Johannesburg will be used for system sizing. Seven types of optimisation techniques will be compared for studying the optimisation problem.

Section 5.1 defines the sizing context and the optimisation problem. Section 5.2 introduces the optimisation methods, and comparisons will be made to obtain the optimal solution to the sizing problem. The method for daily optimal sizing and the system sizing with complete dataset is provided in Section 5.3. Section 5.4 presents the results for system sizing with the reduced data set obtained from the clusters in Chapter 4. The LCOE analysis for the comparison of AD-only system and a hybrid system is presented in Section 5.5. The chapter will be concluded with a summary in Section 5.6.

5.1 Optimal sizing problem

Optimal sizing is defined as the sizing to achieve the minimal LCOE. For the stand-alone hybrid renewable power system, this is achieved by determining the balance of energy supply and demand. When the system is oversized (surplus energy is more than the deficit energy), energy wastage will occur and LCOE will increase. An undersized system will cause energy imbalance and lead to reduced energy security.

Energy security is defined as "consistent availability of sufficient energy in various forms at affordable prices" [211]. International Energy Agency (IEA) defines energy security as "the uninterrupted availability of energy sources at an affordable price" [212]. Hence, the energy security considered here is the availability. The risk with undersized or reduced availability will be the increasing trigger of power outage and unintentional drop in voltage for the hybrid system.

The objective function is:

$$\min_{\text{area}} \left| E_{\text{Storage}} - E_{\text{Deficit}} \right| \tag{5.1}$$

where,

$$E_{\text{Storage}} = E_{\text{Surplus}} \cdot \eta_{\text{EES}} \tag{5.2}$$

E_{Storage} is the energy produced from the PV system to be stored to meet E_{Deficit} with round-trip efficiency η_{EES} considered.

$$E_{\text{Surplus}} = \int_{h=0}^{24} P_{\text{Surplus}}(h)dh \tag{5.3}$$

E_{Surplus} is the additional energy produced from the PV system. P_{Surplus} is the instantaneous PV power subtracted by the instantaneous load demand when load demand is less than the PV power.

$$E_{\text{Deficit}} = \int_{h=0}^{24} P_{\text{Deficit}}(h)dh \tag{5.4}$$

E_{Deficit} is the energy required from storage to meet the load that cannot be met by PV and AD during hour h. P_{Deficit} is the deficit power when no solar or AD power is available to support load demand. The constraints for the AD system are given in Equations (5.5) to (5.7):

$$P_{\text{AD}_{\text{Min}}} \leq P_{\text{AD}}(h) \leq P_{\text{AD}_{\text{Max}}} \tag{5.5}$$

$$\text{P}_{\text{AD}_{\text{Min}}} = \text{P}_{\text{AD}_{\text{Max}}} * 0.4 \tag{5.6}$$

$$P_{\text{AD}}(h) = P_{\text{Load}}(h) - P_{\text{Solar}}(h) \tag{5.7}$$

It is assumed that AD will not produce power when the power output drops below 40 % of the rated capacity as shown in Equation (5.6). Equation (5.7) suggests that the output power from AD plant P_{AD} will be used to support the load demand after P_{Solar} has reached the output capacity during time *t*. Ramp rates are not considered as reciprocating gas engines are flexible generation technologies, i.e., load following power plants [148, 213]. Reasonable assumptions have been made for case studies and the rated capacity of AD; $P_{\text{AD}_{\text{Max}}}$ is at 2.4 MW [214] with η_{EES} at 70 % [29, 99]. The output power of solar panel, P_{Solar} is given by Equation (5.8). According to references [215, 216], an operating spinning reserve at 20 % of the maximum demand, i.e., 2 MW is reasonable for a power system.

$$P_{\text{Solar}} = \text{Irradiance } (\text{Wm}^{-2}) * \text{ Area } (\text{m}^2) * \text{Efficiency } (\%) \tag{5.8}$$

5.2 Comparison of optimisation methods

To obtain a better intuition of the optimisation problem, Figure 5.1 depicts a plot of the objective function and the variable to be minimised for a case on 27th Dec 2012 in Johannesburg. Initially, not shown in the figure, the objective function is minimum because the system's energy balance is achieved due to sufficient deployment of AD power to support the load demand. As the penetration of solar energy increases, AD will switch off due to the constraint given in Equations (5.5) to (5.7).

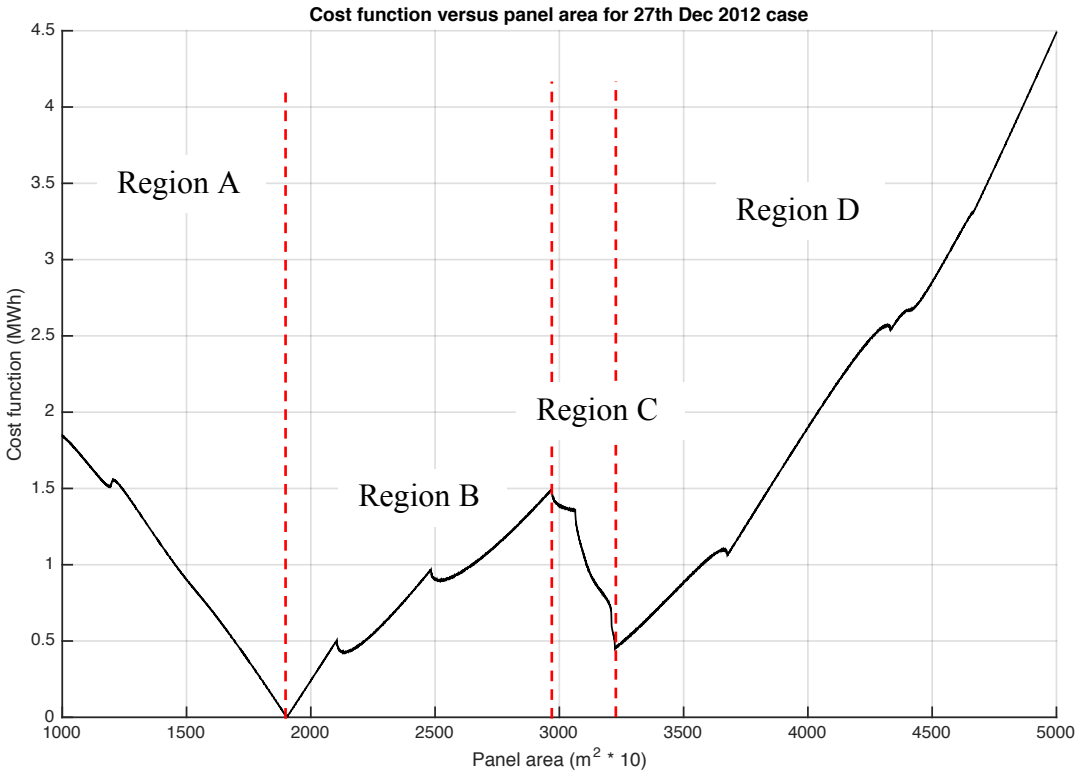


Figure 5.1. Objective function with solar panel area variation for 27th Dec. 2012 lower bound (LB) case, Johannesburg.

The solar power curves used for the case studies are from the practical irradiance data and not from the clear sky model, hence, it contains perturbations. This will influence the switching of AD in an unsystematic manner. The energy imbalance reduces in Region A due to additional PV capacity that provides enough surplus energy to meet deficit energy. In Region B, the energy imbalance increases due to abundant solar surplus energy. In Region C, the energy balance decreases because the AD constraint is triggered and deficit energy in the system increases. In Region D, the cost function will become positive infinite as the panel area approaches infinity; this implies that there will be excessive surplus energy. The optimisation function is highly non-linear with multiple local minima.

Seven different types of optimisation techniques have been studied for the optimal sizing problem. These are Interior Point method (IP), Pattern Search (PS), Genetic Algorithm (GA), Genetic Algorithm with Interior Point method (GAIP), Particle Swarm Optimisation (PSO),

Particle Swarm Optimisation with Interior Point method (PSOIP) and Simulated Annealing (SA). These optimisation methods are described in Section 2.4.3.

For this optimisation problem, two different search boundaries have been used to study the optimisation problem. The Lower Bound (LB) case is from 10000 to 50000 m^2 and the Upper Bound (UB) case is from 50000 to 200000 m^2. LB is kept 10000 m^2 to make sure that the hybrid system has a reasonable penetration of solar PV energy. For IP, SA and PS, the initial points need to be predefined. For this study, initial points are 30000 and 120000 for LB and UB cases, respectively.

The results for the 17th, 21st and 22nd days in Figure 5.2 are erroneous as the cost function values are high and the resulting panel area is at the search boundary, i.e., 10000 or 50000 m^2. The x-axis represents the day for the daily case sizing and the y-axis is the cost function to be minimised. The optimal solution is not in the search boundary; hence, the required panel area is significantly larger. This is due to the poor weather conditions of the day and the lack of solar irradiance. More solar panels are required to provide enough solar energy.

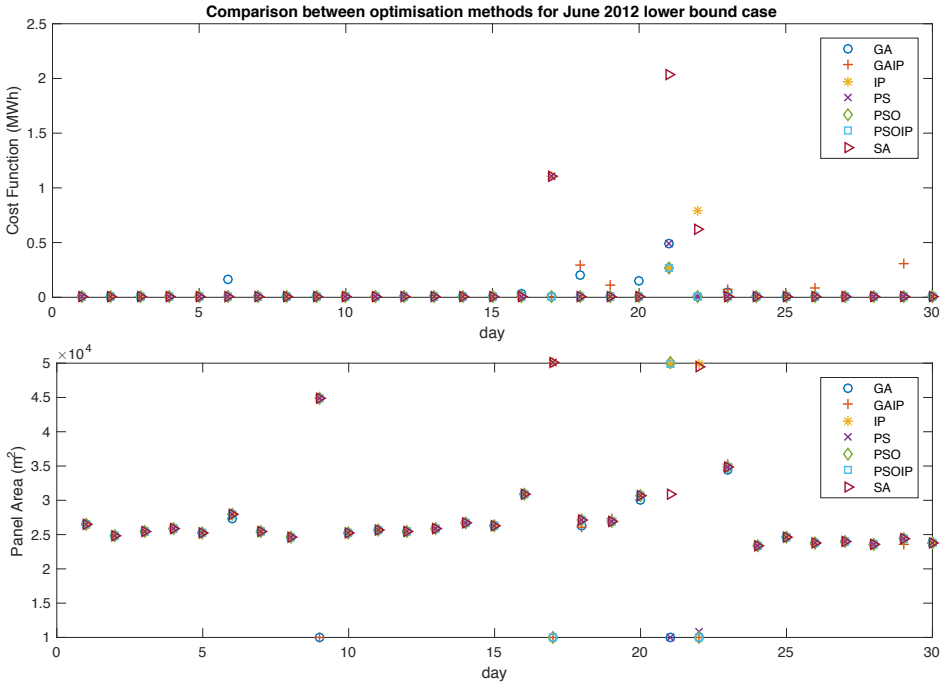


Figure 5.2. PV system sizing for June 2012 LB case, Johannesburg.

Most of the results are similar with few cases where there are high discrepancies. For 22nd June 2012 LB, the cost function values for IP and SA are high compared to other optimisation methods as shown in Figure 5.3. This represents the two optimisation methods which are inferior for this optimisation problem.

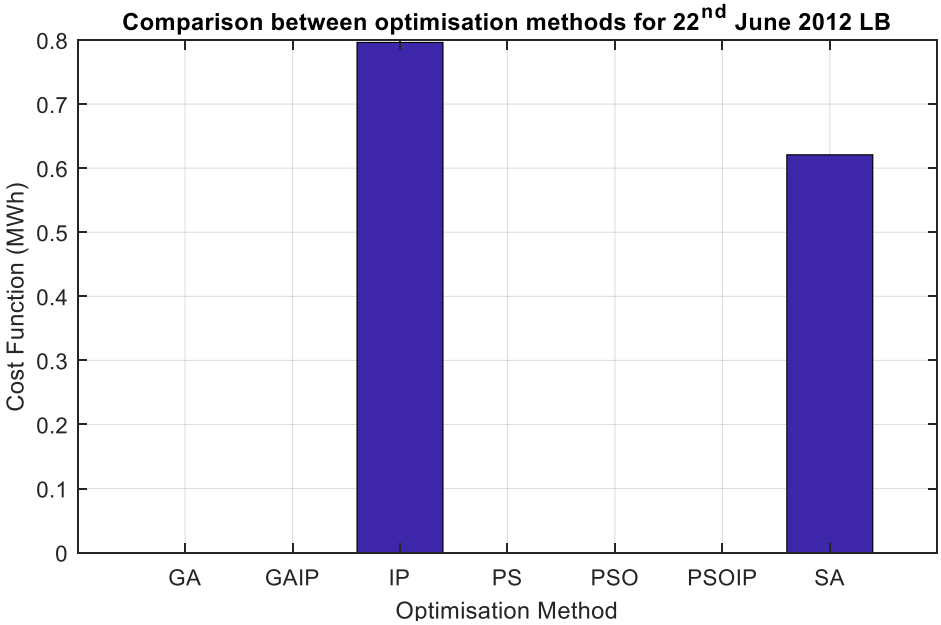


Figure 5.3. Optimisation method comparison for 22nd June 2012 LB, Johannesburg.

A UB case is used to size the solar panels for extreme weather conditions. Figure 5.4 shows the results for the June 2012 case. Converse to Figure 5.2, the cost function values are high for all days except for the 17th, 21st and 22nd. This signifies that feasible solutions exist for these days, and the cost function can be minimised. The optimisation results for 22nd June 2012 UB are shown in Figure 5.5. The panel areas for the optimisation methods are given in Table 5.1.

	Panel area ($10^4 m^2$)						
	GA	GAIP	IP	PS	PSO	PSOIP	SA
22nd June 2012 UB	8.117	8.004	8.032	7.632	8.033	8.033	8.033
22nd June 2012 LB	1.000	1.000	4.993	1.080	1.000	1.000	4.940

Table 5.1. Panel area for the LB and UB optimisation cases for 22nd June 2012.

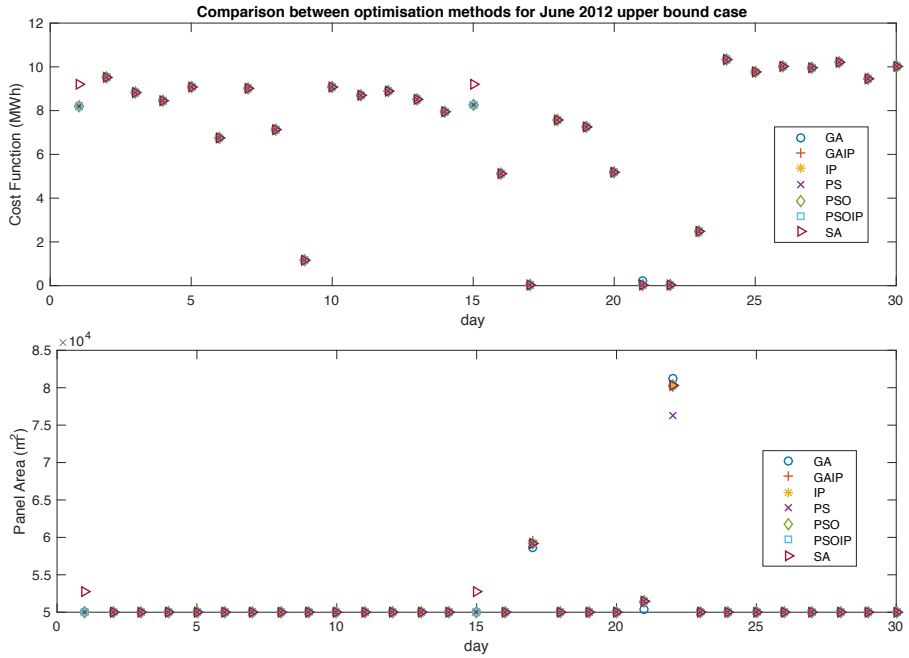


Figure 5.4. PV system sizing for June 2012 UB case, Johannesburg.

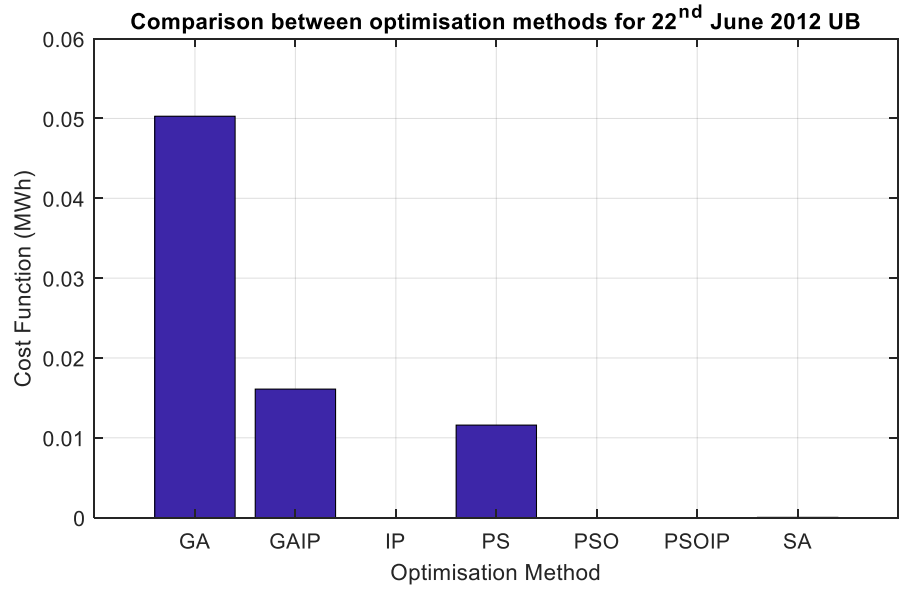


Figure 5.5. Optimisation method comparison for 22nd June 2012 UB, Johannesburg.

Considering the factors of minimal cost function value and the ability to reach the global optimal, it can be concluded that PSOIP is the best candidate for this optimisation problem. However, it should be noted that the choice of optimisation algorithm is problem dependent as explained in [143].

5.3 Hybrid system sizing with the complete solar irradiance dataset

The optimisation process begins with data treatment. Four years of solar irradiance are segmented into individual days to determine the required panel area for each day. LB and UB cases are computed for each day. If there is a feasible solution in the UB, this result will be replaced in the LB result as this signifies that the required panel area is much higher. The four years of daily case optimisation results are shown in Figures 5.6 and 5.7 for Johannesburg and Kenya, respectively. The red crosses in the box plot are the 'outliers' of the sizing results and have a high contrast with the mean. The explanation of the outliers is due to the low solar irradiance of the day and the requirement of a large panel area to produce sufficient surplus energy. A comparison between the results for the two locations suggests that Kenya has a higher solar insolation than Johannesburg since the required panel area is less. There are generally less outliers for Kenya such as for Jan., Feb., and March. This signifies that the solar irradiance fluctuation is less severe.

The search boundary needs to be divided into two known cases, namely, the LB case and UB case. As shown previously, this is because the search boundary is too large for the optimisation algorithms to converge and to determine the correct optimal point. As a common procedure with applying PSO to an engineering problem, PSO parameters such as the inertia range and minimum fraction neighbours were tuned to provide optimal results. The inertia range determines the contribution rate of a particle's previous velocity to that at the current time step. The proper selection of the neighbourhood size affects PSO's trade-off between exploration and exploitation, and unfortunately, there is no formal procedure to determine the optimal size. Table 5.2 gives the parameters and values for the PSO algorithm for the daily case sizing.

Max iteration	500
Inertia range	[0.1 1.0]
Self-adjustment weight	1.49
Social-adjustment weight	1.49
Function tolerance	1e-6
Minimum fraction neighbours	0.5

Table 5.2. Parameters for PSOIP for daily case optimisation.

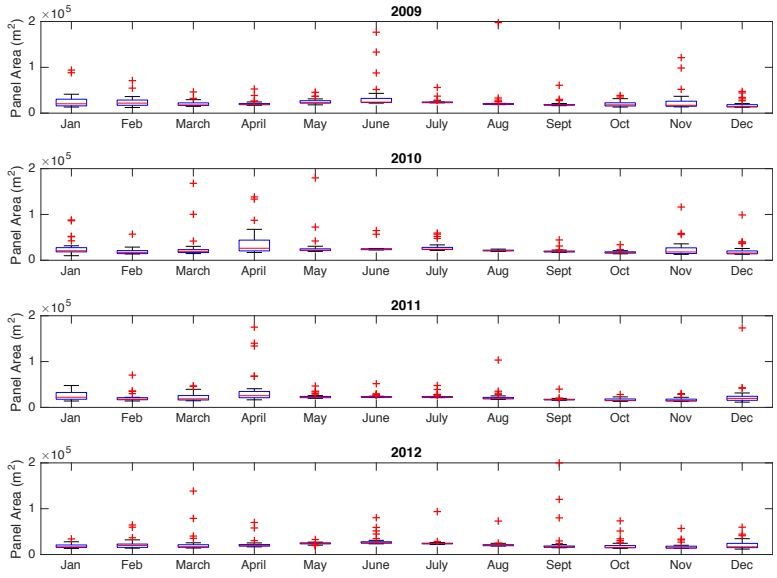


Figure 5.6. Optimisation results for the daily case PV system sizing, Johannesburg.

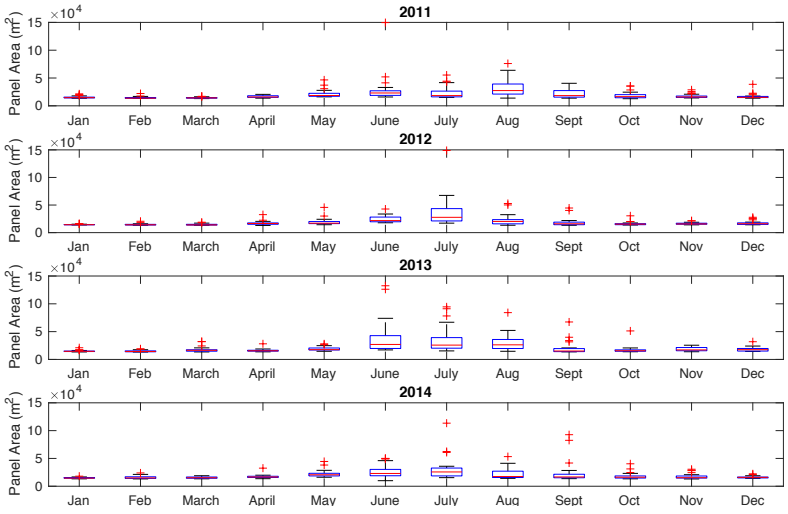


Figure 5.7. Optimisation results for the daily case PV system sizing, Kenya.

5.3.1 Sizing of solar panels

The solar panel to be used for the hybrid system is the Sharp ND-R250A5. It has an efficiency of 15 %, i.e., 150 Wm^{-2} at Standard Test Conditions [187].

Annual sizing case study: The daily solar irradiance profiles are connected as one annual profile for the annual sizing case study. The daily load curve is repeated according to the number of days in the annual case. The optimisation is performed with PSOIP. Tables 5.3 and 5.4 show the number of panels for the four years of data for Johannesburg and Kenya, respectively. For Johannesburg, it is safe to assume that the area of panels required is 20000 m^2 and the system capacity is equivalent to 3 MW. For Kenya, the rated capacity of PV farm can be rounded to 2.5 MW. The case for Kenya in 2012 is special and requires a capacity of 2.86 MW.

This may be explained by the increase in the solar insolation during the year. When compared to the daily sizing case, it can be seen that the annual sizing case gives a "smoothing effect" since it averages the load and solar data first before the optimisation performs. The implication of the energy balance is less well understood with this sizing approach.

Year	Panel area (m^2)	Rated capacity of PV farm at 15 % solar cell efficiency (MW)
2009	19770	2.97
2010	19851	2.98
2011	19468	2.93
2012	19051	2.86

Table 5.3. Annual case sizing results, Johannesburg.

Daily Sizing Case Study: Due to the stochastic effect and inconsistent solar irradiance level in different seasons, it is impossible to determine the exact rated capacity of the solar farm to provide enough supply to the grid. It is impractical to install a PV system that can provide a solution to all events always; either the events would have to be very modest or the EES very large. It is difficult to draw conclusion and insights from the box plot in Figure 5.6. A method has been proposed to determine the solar farm capacity by creating a histogram and considering

the rated capacity of each day for the four years of data. The solar farm power rating for an individual day is calculated using Equation (5.9).

$$P_{\mathrm{SolarFarm}_{Day}} = P_{\mathrm{Panel_rated}} * N_{\mathrm{PV}_{Day}} \quad (5.9)$$

$N_{\mathrm{PV}_{Day}}$ is the panel area for the given day and $\mathrm{P}_{\mathrm{Panel_rated}}$ is the rated capacity of the PV panel.

Year	Panel area (m^2)	Rated capacity of PV farm at 15 % solar cell efficiency (MW)
2011	15980	2.40
2012	15454	2.32
2013	16136	2.43
2014	16262	2.44

Table 5.4. Annual case sizing results, Kenya.

Figure 5.8 shows the solar farm power rating for four years of daily case in a histogram plot for Johannesburg calculated with Equation (5.9). The histogram plot for Kenya is depicted in Figure 5.9. This effectively displays the probability distribution function values for the required sizing of the solar panels. The calculated value is then rounded up to the nearest positive infinity. As shown in the figure, most of the required capacity is in the range of 2 to 6 MW with a few cases above 10 MW. This can be explained due to the poor weather and low irradiance. It will be uneconomical to size the PV system to provide solar energy to these extreme cases. The AD generator could be utilised to meet the energy requirements in this case. The histograms indicate that at a lower PV power capacity, i.e., 1 to 3 MW, the energy deficit will occur less for Kenya than Johannesburg. At 3 MW, the count values for Johannesburg and Kenya are 670 and 1030, respectively.

Since the marginal cost for PV is close to zero, AD has a higher operating cost, i.e., fuel cost and hence, it is less affordable and reduces the security of supply. Therefore, it is ideal to maximise the use of PV to meet deficit energy. A security of supply index is defined here, presenting the percentage of days for which the deficit energy will be met. Ideally, this index should be maximised. This is defined in Equation (5.10) as follows:

$$\text{Security of supply } = \frac{\text{Number of days for } E_{\text{Surplus}} \geq E_{\text{Deficit}}}{\text{Total number of days}} * 100 \qquad (5.10)$$

It is impossible to reach 100 % secure energy supply due to resource inadequacy and unexpected high electricity consumption. Therefore, decision must be made to accept the security that is financially and technically viable. It is a decision-making process to select a rational measure to accept the security level [217]. Tables 5.5 and 5.6 provide the security of supply at various solar power ratings for Johannesburg and Kenya, respectively. At 2 MW in Johannesburg, only 1.30 % of days in 4 years have enough solar energy supply and up to 90 % of days are covered when the sizing is at 5 MW. The capital cost increases significantly by increasing the solar farm by 1 MW. The sizing for the solar farm at Johannesburg is chosen at 5 MW as the increase in the total percentage cover is very small when the sizing is above this value.

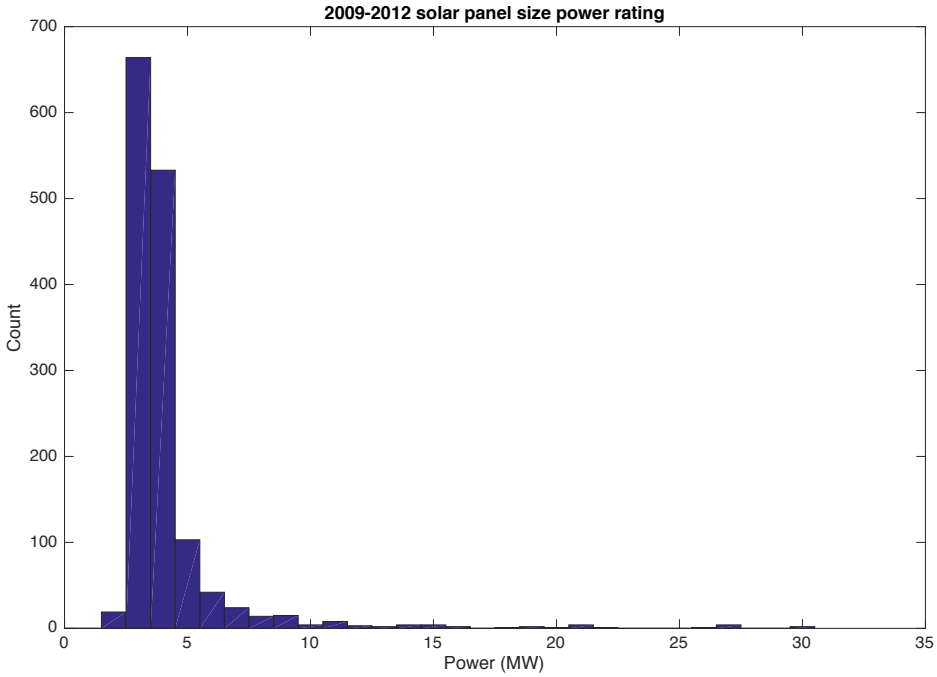


Figure 5.8. Count for daily case solar panel sizing, Johannesburg.

For Kenya, 86.72 % of days are secure when the sizing of the PV farm is at 4 MW. The security will increase slightly at higher nameplate ratings. In the case of deficit energy, the energy requirements could be met by temporarily running AD at minimum output.

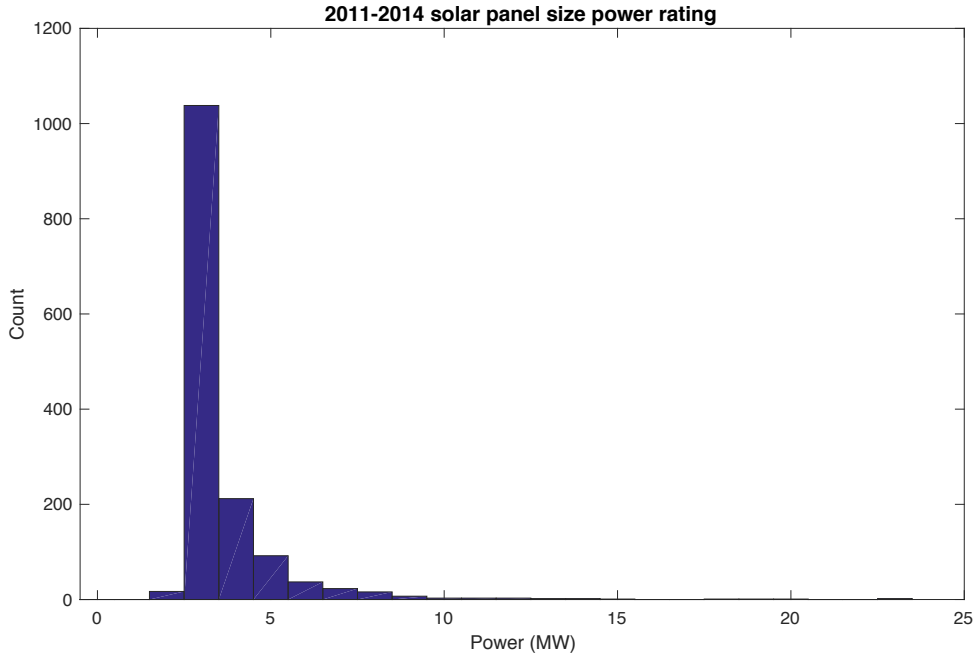


Figure 5.9. Count for daily case solar panel sizing, Kenya.

Power rating (MW)	Percentage for 4 years (%)	Security of supply (%)
2	1.30	1.30
3	45.5	46.8
4	36.5	83.4
5	7.06	90.5
6	2.88	93.4
7	1.64	95.0
7+	4.94	

Table 5.5. Percentage day covered at different power ratings, Johannesburg.

Power rating (MW)	Percentage for 4 years (%)	Security of supply (%)
2	1.16	1.16
3	71.05	72.21
4	14.51	86.72
5	6.30	93.02
6	2.53	95.55
7	1.57	97.13
7+	2.87	

Table 5.6. Percentage day covered at different power ratings, Kenya.

5.3.2 Sizing of storage

After the PV farm's size has been determined, E_{Deficit} is calculated for each day to determine the energy required to be stored in the system. Table 5.7 shows the results for E_{Deficit} with the maximum value for the corresponding year at Johannesburg. It shows that the deficit energy in 2011 is significantly lower and 2009 has the highest deficit. Figure 5.10 shows the solar irradiance curves with the Julian day number for the maximum E_{Deficit} during the daily sizing case in Johannesburg. The irradiance curve for 2011 shows less fluctuation compared to the other three years. This could reduce the number of switching of the AD system, and deficit energy could be reduced, resulting in a lower energy storage requirement.

Year	E_{Deficit} (MWh)	E_{PV} (MWh)
2009	4.96	2.32
2010	4.82	2.15
2011	3.98	2.62
2012	4.71	2.01

Table 5.7. Maximum E_{Deficit} for 2009–2012, Johannesburg.

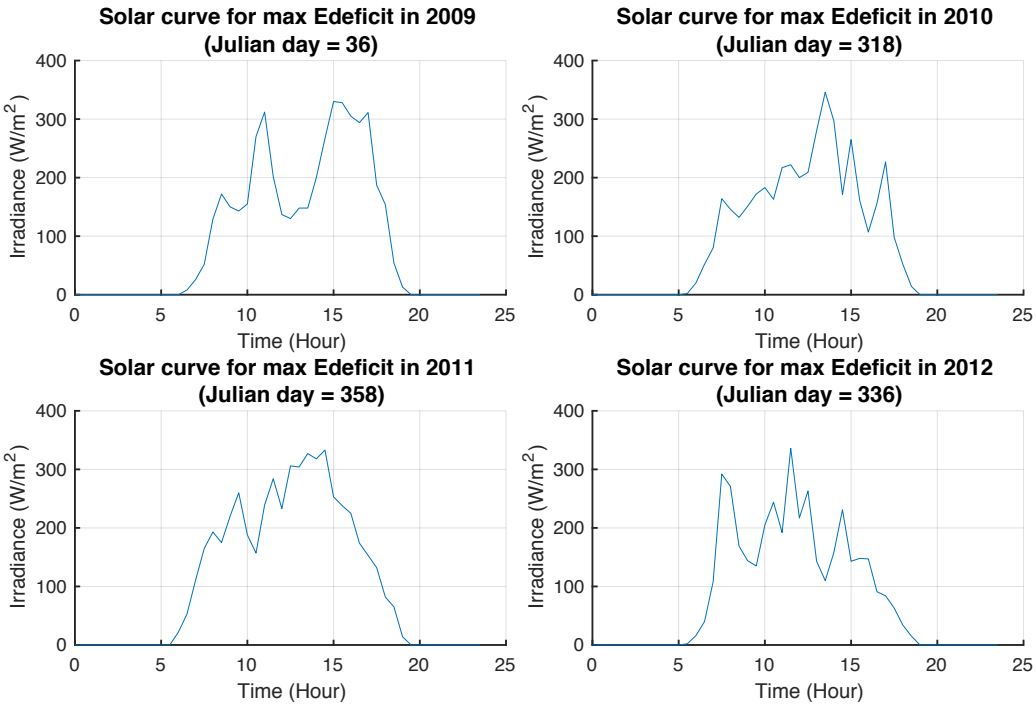


Figure 5.10. Solar irradiance curves for 2009–2012 at maximum E_{Deficit}, Johannesburg.

Table 5.8 provides the maximum values of E_{Deficit} for Kenya with the solar irradiance curve for the day where the maximum E_{Deficit} occurred during the year depicted in Figure 5.11. The irradiance curves indicate that there are severe fluctuations and low magnitudes of irradiance, i.e., maximum at 470 W/m^2 in 2013. The deficit energy is generally less for Kenya than for Johannesburg.

Year	E_{Deficit} (MWh)	E_{PV} (MWh)
2011	4.34	2.65
2012	3.77	1.73
2013	3.87	2.21
2014	3.69	1.76

Table 5.8. Maximum E_{Deficit} for 2011–2014, Kenya.

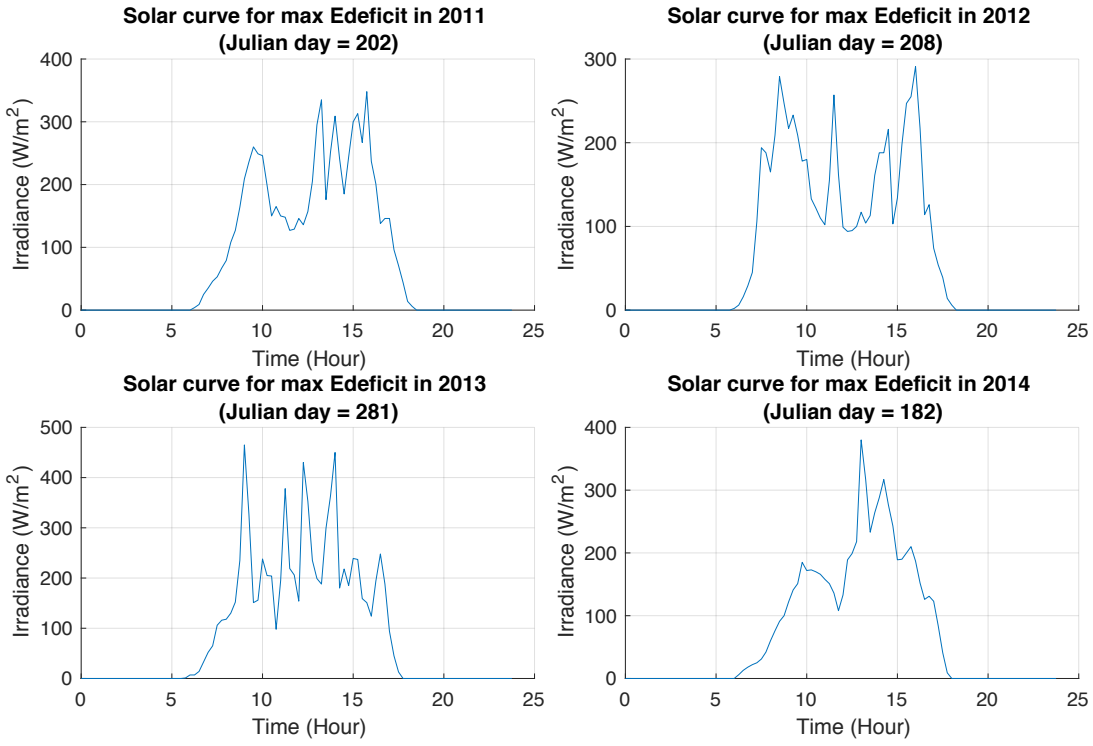


Figure 5.11. Solar irradiance curves for 2011–2014 at maximum E_{Deficit}, Kenya.

For Johannesburg, the storage is to be sized at 5 MWh considering that E_{Deficit} is under 5 MWh for the four years. For Kenya, the maximum E_{Deficit} is at 4.34 MWh. The storage can be sized to 4.5 MWh.

5.3.3 Sizing of inverter and solar charge controller

The following constraints in Equations (5.11) to (5.12) need to be fulfilled for the proposed hybrid system. The total power output of inverters and solar charge controllers need to be larger than the rated capacity of solar PV.

$$P_{\mathrm{Inv}} N_{\mathrm{Inv}} \geq P_{\mathrm{Solarfarm}} \tag{5.11}$$

$$P_{\mathrm{Con}} N_{\mathrm{Con}} \geq P_{\mathrm{Solarfarm}} \tag{5.12}$$

P_{Inv} and P_{Con} are the rated power of the inverter and solar charge controller, respectively. N_{Inv} and N_{Con} are denoted for the number of inverters and solar charge controllers. $P_{\mathrm{Solarfarm}}$ is the rated capacity of the solar farm, which is at 5 MW for Johannesburg. The optimal sizing result for each component of the hybrid system is presented in Table 5.9.

System component	Optimal size	
	Kenya	**Johannesburg**
PV	4 MW	5 MW
Vanadium Redox flow battery (VRB)	4.5 MWh	5 MWh
Inverter (Schneider Electric XW4024) (4 kW/unit)	1000 units	1250 units
Solar Charge Controller (Outback FM 80) (2 kW/unit)	2000 units	2500 units

Table 5.9. Summary of optimal size for the hybrid system.

MW solar PV systems usually consist of many units of components at kW scale [218]. Solar PV farms can be built using string inverters that connect a string of solar modules ranging 1–5kW [219, 220]. By regulating the battery voltage level, solar charge controllers control the amount of charge flowing in and out of the battery [221]. Each solar charge controller can be connected to up to four strings of solar modules to reduce power loss [222]. Each charge controller is assumed to be connected to a low voltage 48 V DC busbar. Due to the complexity with sizing and techno-economic analysis, the problem is simplified by neglecting the DC-DC or DC-AC power conversion between different voltage levels. By including these conversion costs, it is expected that the LCOE will increase due to reduced electricity output (conversion losses) and cost of equipment.

5.4 Hybrid system sizing with the cluster dataset

Contrary to using the complete dataset for system sizing in Section 5.3, the daily solar irradiance profiles are constructed from the CI cluster centroids from Chapter 4. The daily clear-sky solar irradiance profile for autumn, spring, winter and summer are calculated with the equinoxes (20th March and 23rd Sept.), the winter solstice (21st June) and the summer solstice (21st Dec.), respectively. Equation (5.13) presents the calculation of the constructed solar irradiance:

$$I_{\text{Construct}}(h) = \text{CI}(h) * I_{\text{Model}}(h) \tag{5.13}$$

The constructed solar irradiance profiles with FCM DTW for winter, summer, autumn and spring cases in Johannesburg are presented in Figures 5.12 to 5.15, respectively. To consider the dispersion of the clustered data, the plus one and minus one standard deviations of the centroids are included for sizing purposes. The shape of the irradiance for each cluster is distinctive and will be useful for the sizing application.

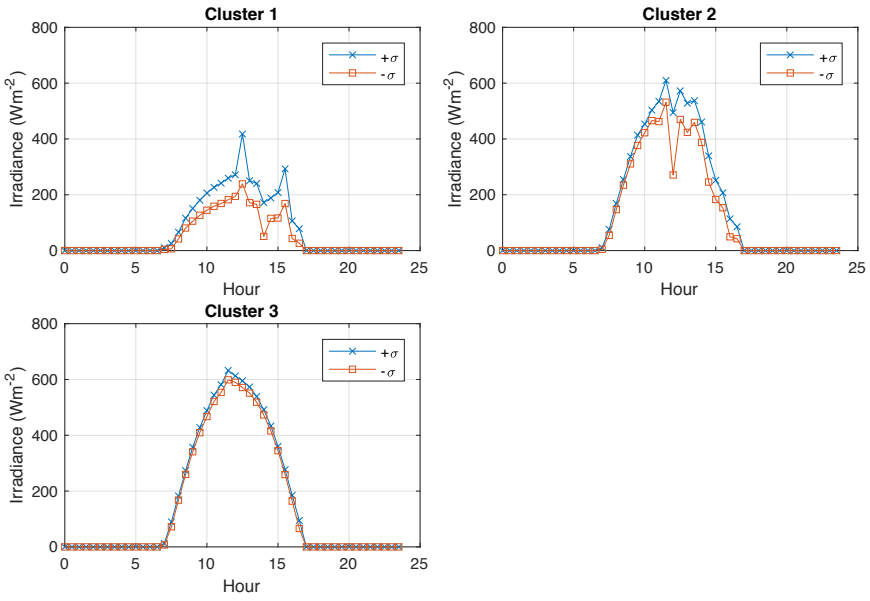


Figure 5.12. Constructed irradiance from centroids in FCM DTW for winter, Johannesburg.

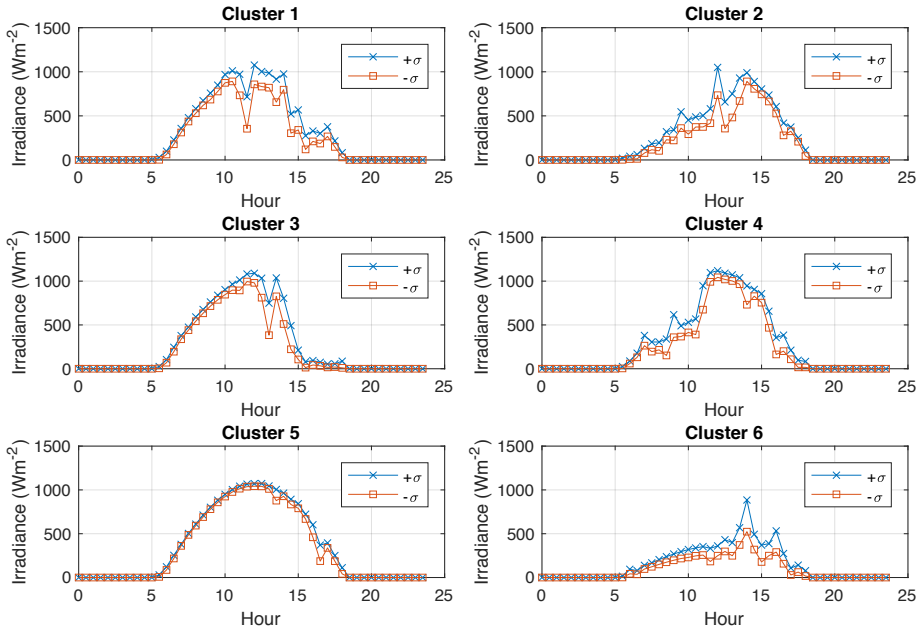


Figure 5.13. Constructed irradiance from centroids in FCM DTW for summer, Johannesburg.

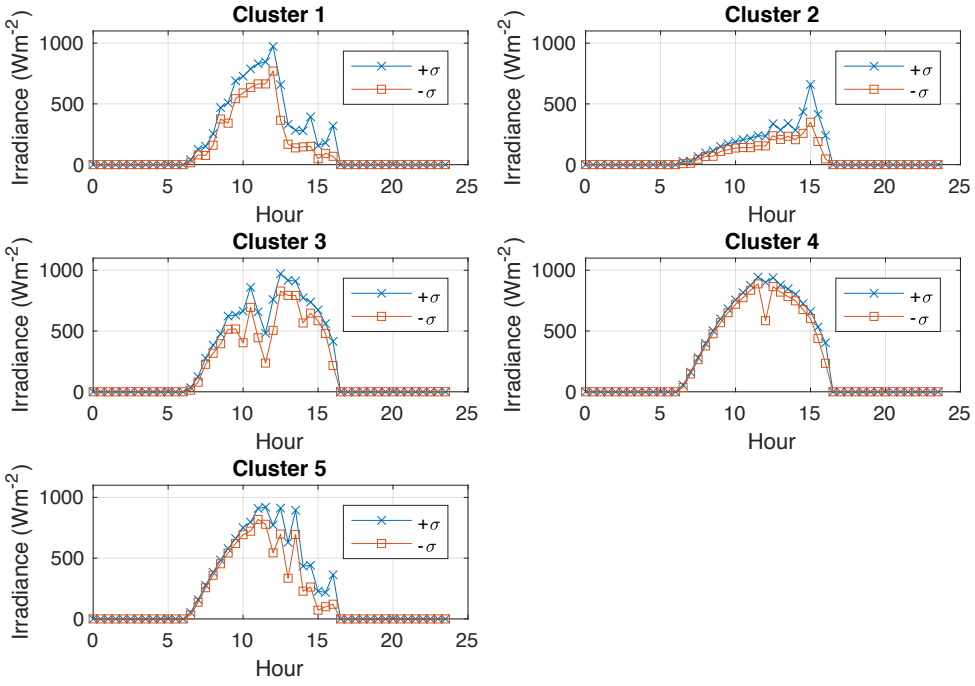


Figure 5.14. Constructed irradiance from centroids in FCM DTW for autumn, Johannesburg.

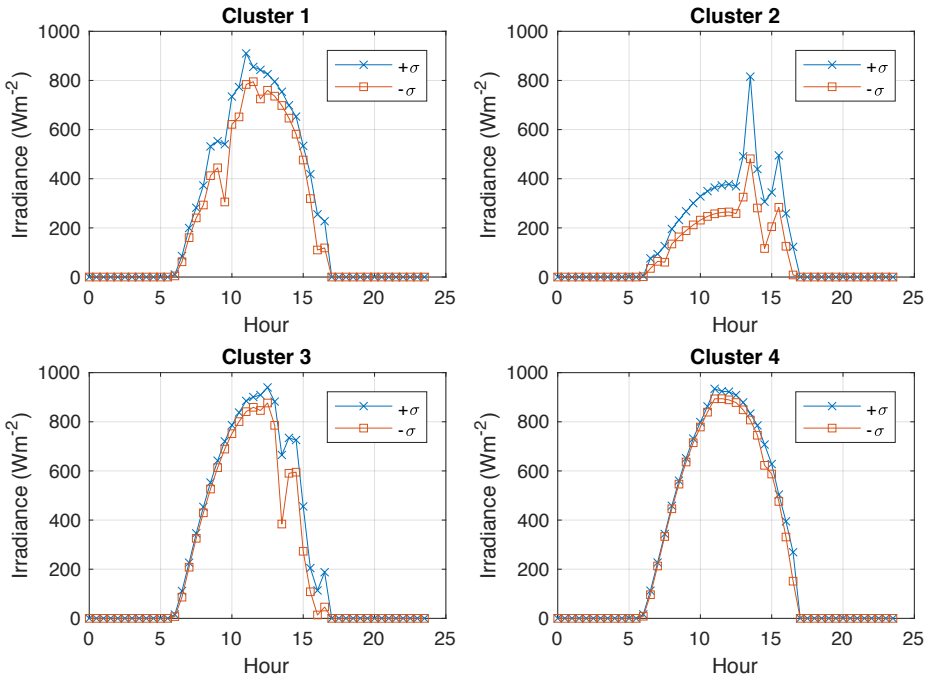


Figure 5.15. Constructed irradiance from centroids in FCM DTW for spring, Johannesburg.

The constructed solar irradiance profiles with FCM DTW for winter, summer, autumn, and spring for Kenya are presented in Figures 5.16 to 5.19, respectively. The fluctuation is minimal for summer and resembles the case with clear-sky irradiance.

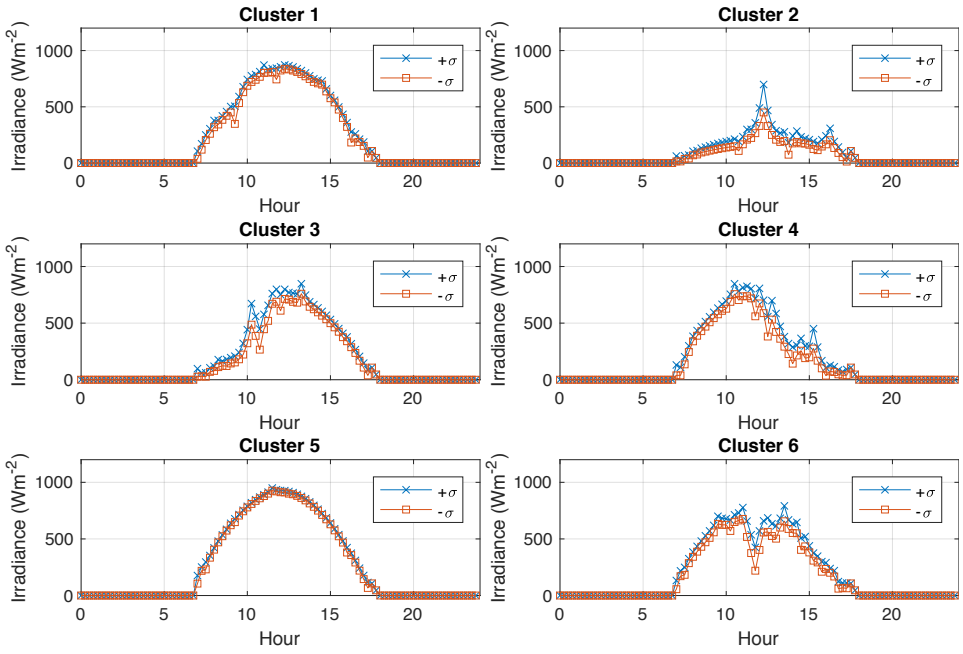


Figure 5.16. Constructed irradiance from centroids in FCM DTW for winter, Kenya.

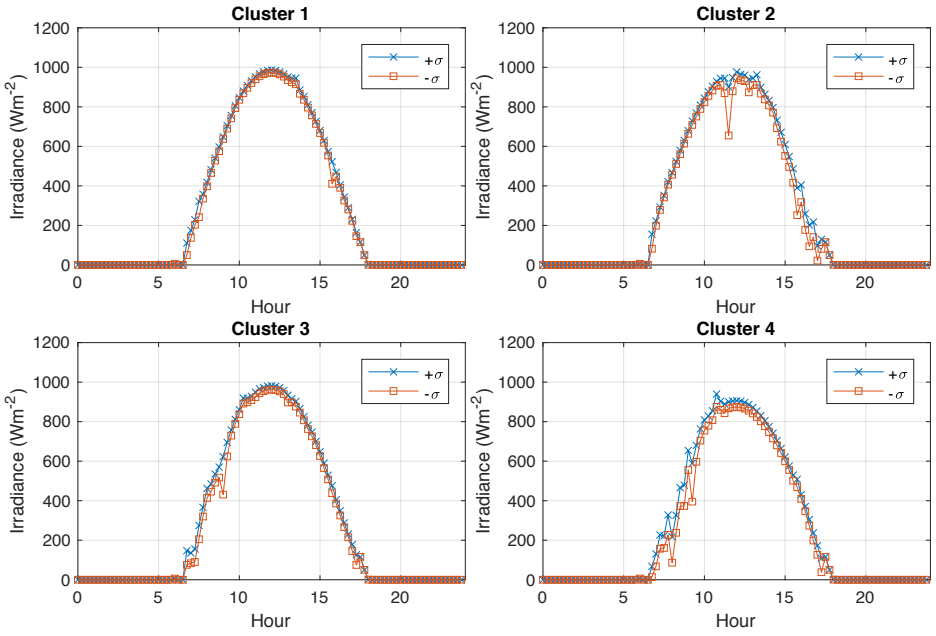


Figure 5.17. Constructed irradiance from centroids in FCM DTW for summer, Kenya.

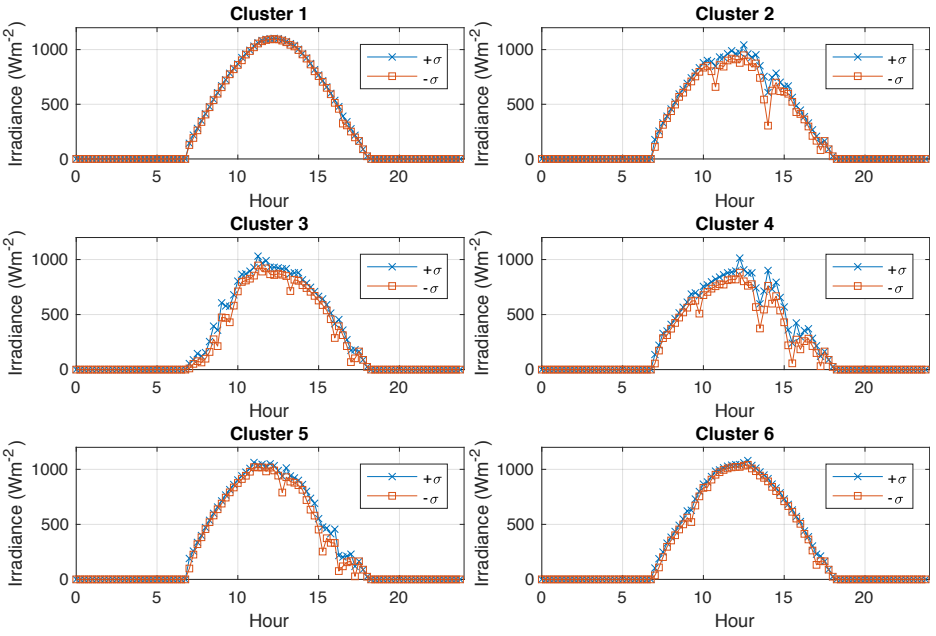


Figure 5.18. Constructed irradiance from centroids in FCM DTW for autumn, Kenya.

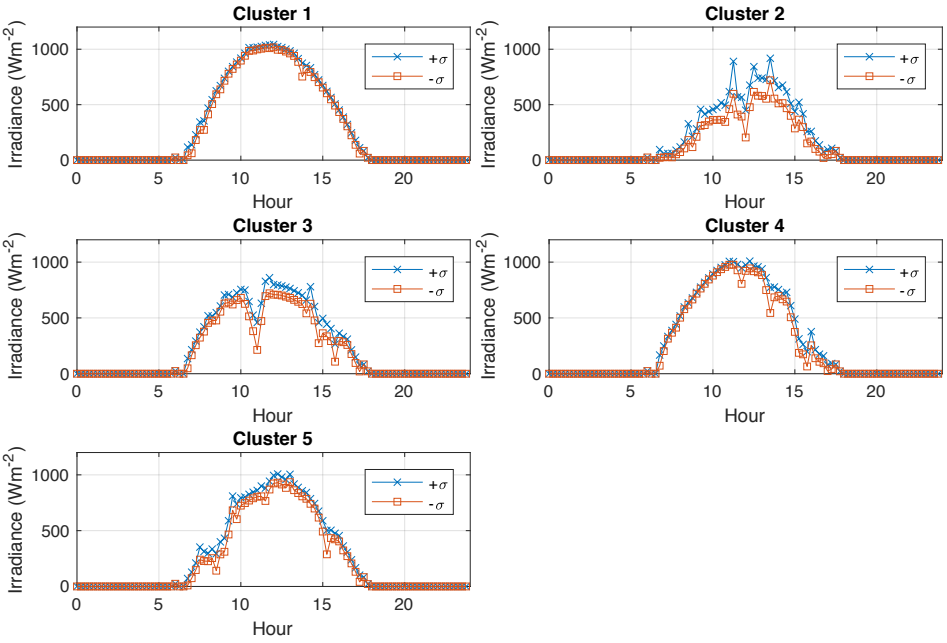


Figure 5.19. Constructed irradiance from centroids in FCM DTW for spring, Kenya.

Having obtained the irradiance profiles from the clustering results, the PV and EES systems can be sized according to the procedure in Section 5.3.

5.4.1 Sizing of solar panels

The PV solar panel areas required to meet the energy deficit of the solar PV hybrid energy system with the clustering results are determined with Particle Swarm Optimisation and Interior Point method. For Johannesburg, Figure 5.20 presents the panel area results with the irradiance profiles developed for each season from five different clustering techniques. The PV farm power capacities derived from the box plot in Figure 5.20 are shown in Figure 5.21. The 'daily sizing case study' method in Section 5.3.1 can be referred for the derivation of PV capacity from panel area. Figure 5.21 reveals that FCM DTW and GMM need a PV capacity of 7 MW whereas FCM ED, *K*-Means ED and *K*-Means MD need 5 MW instead. The energy balance of generation and demand are significantly related to the shape of the solar irradiance profile. These are better captured by GMM and FCM DTW clustering methods which are reflected by the outliers in the PV panel sizing results shown in Figure 5.20 and the centroids in Figures 4.9 to 4.12. The number of count appearances for the PV power capacity above 6

MW is negligible for FCM DTW and GMM. The PV sizing results for Johannesburg with the reduced dataset show consistency with the full data set in Section 5.3.1.

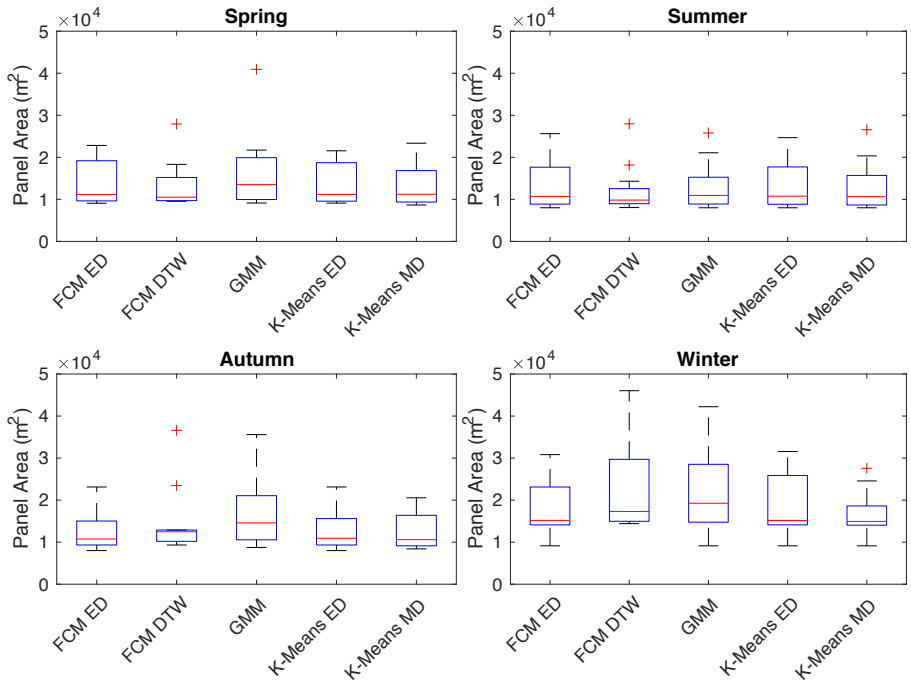


Figure 5.20. Optimisation results for PV panel sizing, Johannesburg.

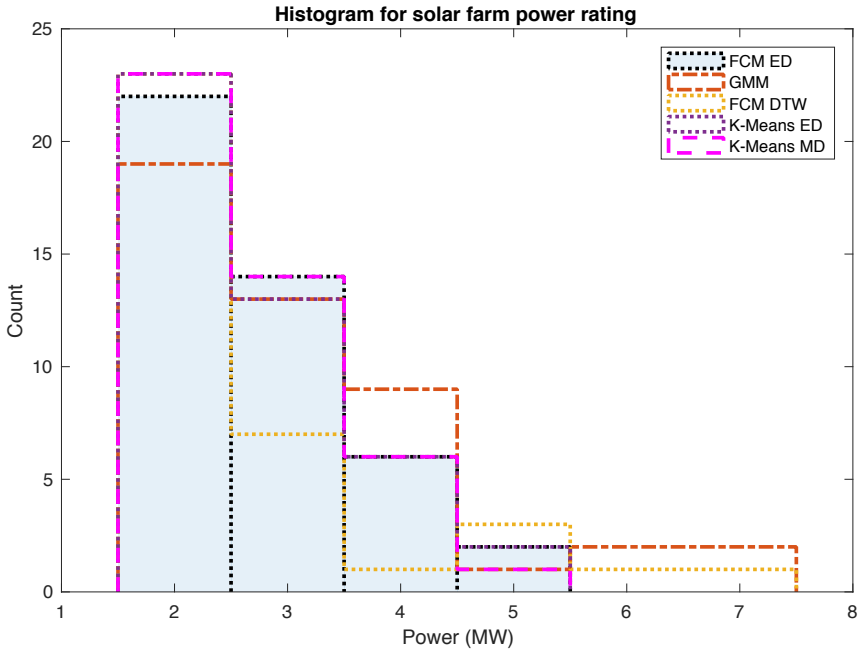


Figure 5.21. PV farm rated capacity (15 % solar cell efficiency) with different clustering techniques, Johannesburg.

Figure 5.22 presents the panel area results with the constructed irradiance profiles for Kenya. Compared to Figure 2.20 for Johannesburg, the panel area is increased due to the increase in the outliers' number. The histogram for the box plot results shown in Figure 5.22 is presented in Figure 5.23.

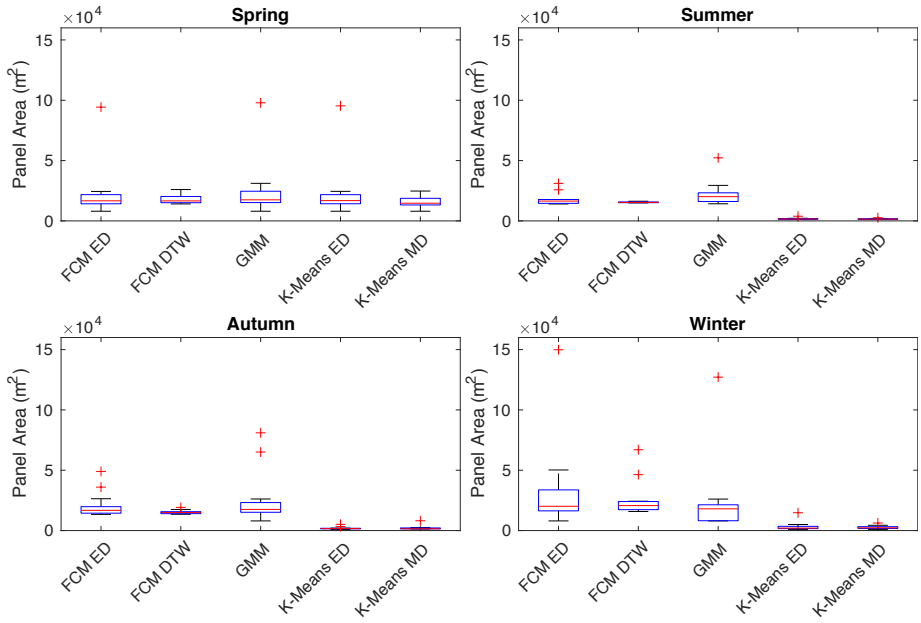


Figure 5.22. Optimisation results for PV panel sizing, Kenya.

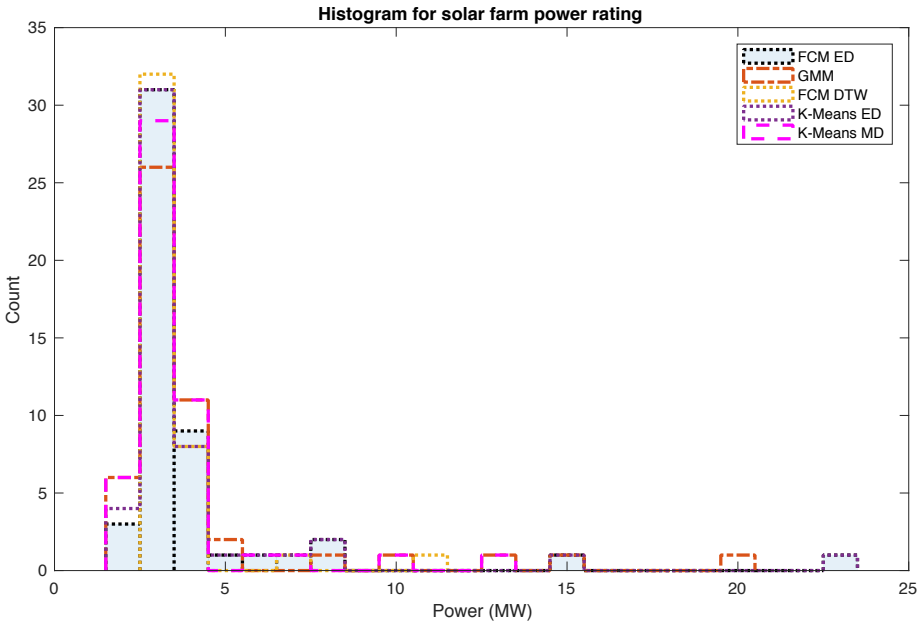


Figure 5.23. PV farm rated capacity (15 % solar cell efficiency) with different clustering techniques, Kenya.

As depicted in Figure 5.23, the count appearance for solar farm power rating at 5 MW and above are arbitrary and insignificant. The solar farm for Kenya should be sized to 4 MW. The result is consistent those provided in Section 5.3.1 for a study with the full dataset. This signifies that the cluster dataset can be used for PV farm sizing.

5.4.2 Sizing of storage

Similar to Section 5.3.2, the aim is to determine the maximum energy deficit of the system with the centroid profiles of the four seasons. The maximum values of E_{Deficit} for Johannesburg and Kenya with five clustering methods are presented in Table 5.10.

Clustering technique	**Maximum E_{Deficit} (MWh)**	
	Johannesburg	**Kenya**
GMM	4.14	3.89
FCM	4.17	3.72
FCM DTW	3.49	3.41
K-Means MD	3.18	3.52
K-Means ED	4.01	3.79

Table 5.10. E_{Deficit} with Johannesburg and Kenya clustered irradiance data.

To elaborate the implications of the energy deficit results from the constructed solar irradiance profiles depicted in Table 5.10, Figure 5.24 depicts the energy deficit for Johannesburg computed using four years of real-life solar irradiance data. For Johannesburg, the real-life solar irradiance profile study shows that the energy deficit can reach 5 MWh. The total number of daily sizing cases, i.e., the total count is 1457. Considering this, the number of additional cases where 4.14 MWh meets the energy demand in contrast to 3.49 MWh is 16. At 3.49 MWh, 1436 cases of energy deficit are covered. The difference in energy storage capacity between FCM DTW and GMM is (4.14-3.49)/3.49 = 18.62 %. By increasing the storage capacity from 3.49 MWh to 4.14 MWh, the additional cases of energy deficit covered is 16/1436 = 1.11 %. This concludes that the system can meet an additional 1.11 % cases of energy deficit with an additional 0.65 MWh storage capacity. This may not be an economical solution, and the issue with energy deficit can be overcome by optimal scheduling as proposed in the next chapter.

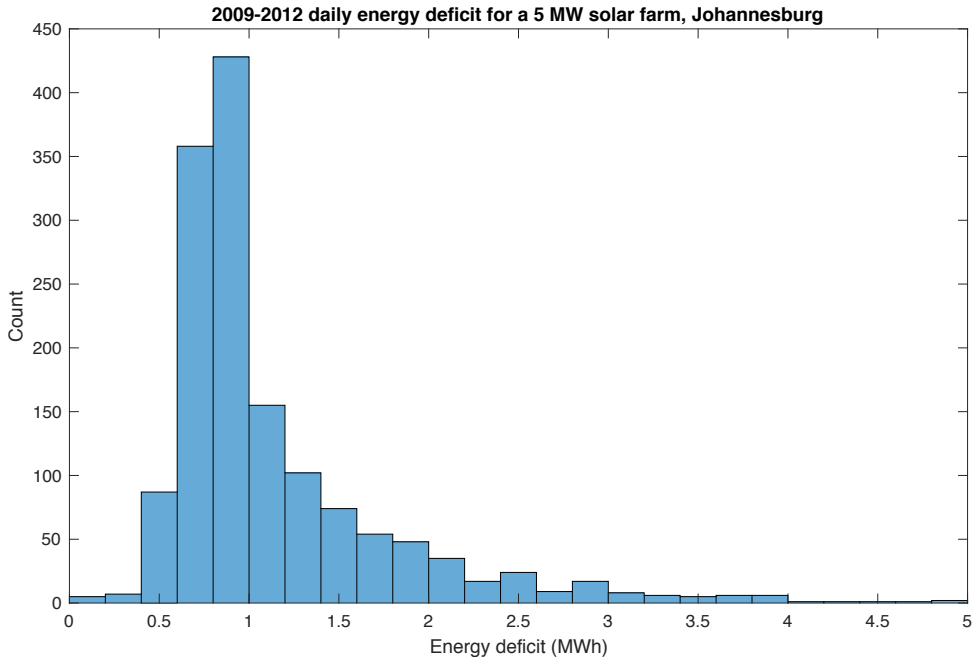


Figure 5.24. Histogram for system energy deficit for four years of daily case study, Johannesburg.

The energy deficit in Kenya, shown in Figure 5.25, can reach 4 MWh as the real-life solar irradiance profile study indicates. The number of count appearances after 3 MWh is negligible. The values of E_{Deficit} for Kenya with different clustering methods shown in Table 5.10 are greater than 3.41 MWh. To yield a conservative design, the size of ESS to meet the energy deficit is rounded up to the nearest integer, i.e., 4 MWh.

The inverter and solar charge controller ratings are calculated with the same methods in Section 5.3.3. It can be concluded that the sizing results obtained with the cluster dataset matches the full dataset.

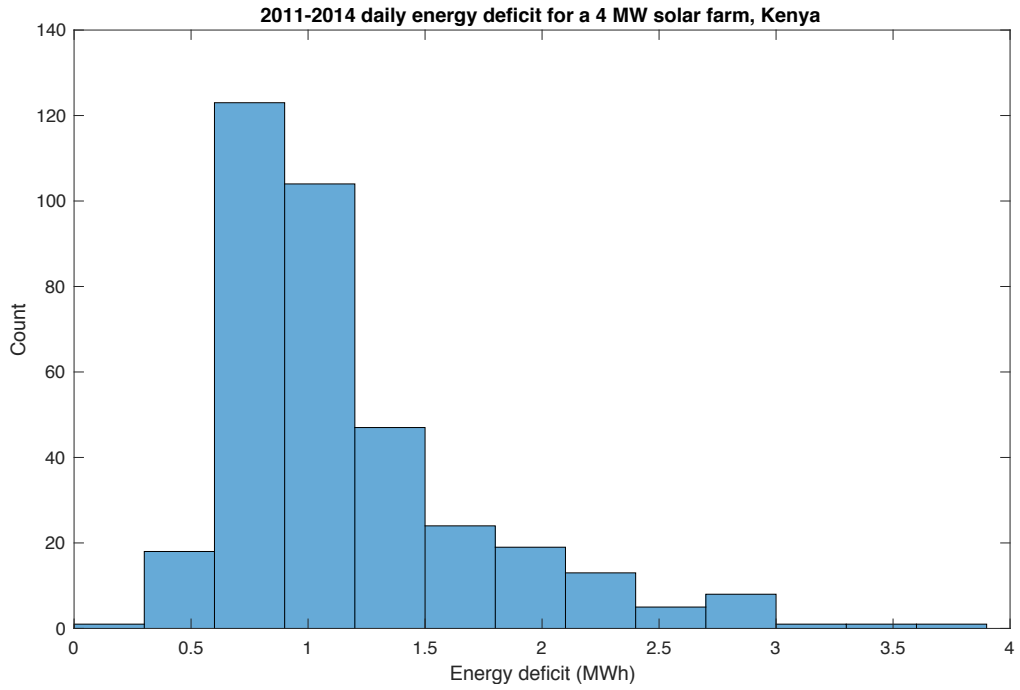


Figure 5.25. Histogram for system energy deficit for four years of daily case study, Kenya.

5.5 Levelized cost of electricity

This section presents the cost calculation of the system. Two different systems, namely the PV-AD-EES hybrid system and the AD biogas only system, will be compared. Table 5.11 presents the cost specification and values of the components.

	PV (Sharp ND-250QCS)	**Vanadium Redox flow battery (VRB)**	**AD**	**Inverter (Schneider Electric XW4024)**	**Solar Charge Controller (Outback FM 80)**
Capital cost ($C_{Cap_{Asset}}$)	120 ($/unit) [187, 188]	760–1600 ($/kWh) [29, 99]	$7.5M [214, 223]	812 ($/unit) [187]	335 ($/unit) [187]
Installation cost ($C_{Inst_{Asset}}$)	108 ($/unit) [187]	N/A	N/A	24.3 ($/unit) [187]	6.7 ($/unit) [187]
O&M cost ($C_{O\&M_{Asset}}$)	6 ($/unit-yr) [187]	100–140 ($/MWh) [29]	350 ($/MW) [224]	2.44 ($/unit-yr) [187]	1.01 ($/unit-yr) [187]

Table 5.11. System component cost specification and values.

5.5.1 Levelized cost of electricity for system

For a hybrid renewable and EES power system, the LCOE can be obtained from Equation (3.22). The total cost of the hybrid renewable system is the sum of PV, AD generation, power conversion and storage costs. The total energy produced by the system is the energy output of EES, the energy directly delivered to the load by PV and the energy produced by AD to overcome the deficit energy. Therefore, the LCOE for the system is given by Equation (5.14).

$$\mathrm{LCOE}_{\mathrm{System}} = \frac{C_{\mathrm{PVsurplus}} + C_{\mathrm{EES}} + C_{\mathrm{PVdirect}} + C_{\mathrm{AD}} + C_{\mathrm{Inv}} + C_{\mathrm{Con}}}{E_{\mathrm{EES}} + E_{\mathrm{PV_{Directtotal}}} + E_{\mathrm{AD_{Total}}}} \tag{5.14}$$

Refer to Equations (3.6) to (3.10) for C_{EES}, E_{EES}, $C_{\mathrm{PVsurplus}}$, C_{PVdirect} and $E_{\mathrm{PV_{Directtotal}}}$ respectively in Section 3.2. The cost and energy calculations for the AD biogas generator is given in Equations (5.15) and (5.16), respectively. The costs for the inverter and solar charge controller are given in Equations (5.17) and (5.18), respectively.

$$C_{\mathrm{AD}} = C_{\mathrm{Cap_{AD}}} + \sum_{t=0}^{n} \frac{C_{\mathrm{O\&M_{AD}}\,t}}{(1+r)^t} \tag{5.15}$$

$$E_{\mathrm{AD_{Total}}} = \sum_{t=0}^{n} \frac{E_{\mathrm{AD}\,t}}{(1+r)^t} \tag{5.16}$$

$$C_{\mathrm{Inv}} = \left(C_{\mathrm{Cap_{Inv}}} + C_{\mathrm{Inst_{Inv}}} + \sum_{t=0}^{n} \frac{C_{\mathrm{O\&M_{Inv}}\,t}}{(1+r)^t} \right) N_{\mathrm{Inv}} \tag{5.17}$$

$$C_{\mathrm{Con}} = \left(C_{\mathrm{Cap_{Con}}} + C_{\mathrm{Inst_{Con}}} + \sum_{t=0}^{n} \frac{C_{\mathrm{O\&M_{Con}}\,t}}{(1+r)^t} \right) N_{\mathrm{Con}} \tag{5.18}$$

In this study, the lifetime of the hybrid system is assumed to be 20 years with Redox flow battery degradation rate d_{EES} at 0.1 %/yr [116] and PV panel degradation rate d_{PV} at 0.05 % [149, 189]. There is an inverter lifetime extension for at least 20 years of full operation by 2013 and 30 years by 2020 [225]. The solar charge controllers and inverters are assumed to be replaced once during the lifetime of the system, and the replacement cost is the same as the

capital cost [187]. N_{Inv} and N_{Con} are the number of units of inverters and solar charge controllers, respectively. $E_{\mathrm{AD_{Total}}}$ is the total lifetime energy output from AD.

5.5.2 Cost analysis for PV hybrid and AD-only systems

The LCOE at discount rates 2, 8, 10 and 15 % are examined for three case studies. The first case study, the AD-only system, is a micro-grid system that generates energy solely using AD with no PV, EES, inverter and solar charge controller installed. The results for the first case study are presented in Table 5.12. The second and third case studies are the hybrid system case studies with VRB's capital, operation and maintenance costs at lower and upper bounds, respectively. The levelized cost analyses for Johannesburg with lower and upper bound storage costs are given in Tables 5.13 and 5.14, respectively. Tables 5.15 and 5.16 present the levelized cost analyses for Kenya. The system's LCOE and LCOD should be decoupled. A low LCOD does not necessary indicate that the system's LCOE will be high. According to Equations (3.15) and (5.13), these relationships are non-linear. The costs are due to the capital, operation and maintenance costs of the generating assets. Additionally, the electrical energy generated or delivered by the asset can affect the levelized cost.

As storage is an expensive component and the energy stored in general is of a smaller proportion compared to generated energy, the ratio of battery cost to the amount of stored energy will be bigger compared to that of the $\mathrm{LCOE_{System}}$. Hence, the system's LCOD is significantly higher than its LCOE. The cross-over point for the system's LCOE can be determined Using sensitivity analysis. The results suggest that by considering the Redox storage at lower bound cost, the hybrid system could be cheaper than running an AD-only system when the discount rate is below 8 %. At a higher bound cost, the discount rate needs to be below 2 %.

r (%)	$\mathbf{LCOE_{System}}$ (\$/kWh)
2	0.383
8	0.403
10	0.409
15	0.427

Table 5.12. AD only case.

r (%)	LCOD (\$/kWh)				$\mathbf{LCOE_{System}}$ (\$/kWh)			
	2009	2010	2011	2012	2009	2010	2011	2012
2	0.83	0.89	0.80	0.74	0.34	0.35	0.34	0.34
8	1.16	1.24	1.11	1.03	0.39	0.40	0.39	0.39
10	1.28	1.36	1.23	1.13	0.41	0.42	0.41	0.41
15	1.58	1.69	1.52	1.41	0.46	0.46	0.42	0.45

Table 5.13. Hybrid system with VRB at lower bound cost, Johannesburg.

r (%)	LCOD (\$/kWh)				$\mathbf{LCOE_{System}}$ (\$/kWh)			
	2009	2010	2011	2012	2009	2010	2011	2012
2	1.21	1.30	1.17	1.07	0.36	0.37	0.36	0.36
8	1.76	1.88	1.68	1.55	0.42	0.43	0.42	0.42
10	1.95	2.08	1.87	1.73	0.44	0.45	0.44	0.44
15	2.46	2.63	2.36	2.18	0.50	0.51	0.50	0.49

Table 5.14. Hybrid system with VRB at upper bound cost, Johannesburg.

r (%)	LCOD (\$/kWh)				$\mathbf{LCOE_{System}}$ (\$/kWh)			
	2011	2012	2013	2014	2011	2012	2013	2014
2	0.97	0.89	1.01	1.01	0.34	0.34	0.34	0.34
8	1.34	1.23	1.40	1.41	0.39	0.38	0.39	0.39
10	1.47	1.35	1.55	1.55	0.40	0.40	0.41	0.40
15	1.82	1.67	1.91	1.91	0.45	0.44	0.45	0.45

Table 5.15. Hybrid system with VRB at lower bound cost, Kenya.

r (%)	LCOD (\$/kWh)				$\mathbf{LCOE_{System}}$ (\$/kWh)			
	2011	2012	2013	2014	2011	2012	2013	2014
2	1.38	1.27	1.45	1.46	0.36	0.35	0.36	0.36
8	2.00	1.83	2.09	2.10	0.41	0.41	0.41	0.41
10	2.22	2.03	2.32	2.33	0.43	0.43	0.43	0.43
15	2.79	2.56	2.92	2.93	0.48	0.48	0.48	0.48

Table 5.16. Hybrid system with VRB at upper bound cost, Kenya.

Table 2.6 indicates that the LCOS for Redox storage system in renewable energy system integration is between 0.373 to 0.950 \$/kWh with a discount rate of 8 %. As the cost is fixed while both variable cost and energy are affected equally by the discount rate, LCOS increases

as discount rate increases. The LCOD of the system is much higher than LCOS when the cost of storing the energy is included. As reported in [191], the current discount rate for solar PV and AD is 6–9 % and 7–10 %, respectively. The discount rate for technologies that are supported by a policy could be as much as 2–3 % lower over the next decade and could fall by a further 1–2 % by 2040. The LCOE for the hybrid system has been given the assumption that the capital cost of PV will be reduced by 50 % compared to that for PV system in [187] due to Swanson's law [188]. At high discount rates, capital intensive generation sources such as PV will be at a disadvantage because the value of energy would be lower in future.

Generally, AD-only system can have a smaller LCOE but it might be different for a smaller discount rate. This is likely to be the future trend. If there are incentives, for example for equipment cost, there could be a reduction in capital cost and thus it could be better to have a hybrid system as this leads to a lower LCOE.

5.6 Summary

This chapter proposes a deterministic approach for sizing a stand-alone high penetration PV system with support from EES and AD biogas power plant. Two datasets were used to perform the hybrid system's component sizing. These are known as the full dataset and the cluster dataset. The sizing results showed that the cluster dataset can accurately perform the component sizing as the results are consistent with the full dataset. The sizing results also conclude that FCM DTW and GMM can better capture the fluctuation of the CI values. This observation is significant for the case with Johannesburg.

It was found that the optimal sizing ratios for the generation sources, AD and PV at Johannesburg and Kenya are 2.4:5 and 2.4:4, respectively. The levelized costs were evaluated for the two systems, namely the hybrid system and the AD biogas power plant system. This revealed that the hybrid energy system is more economical than using AD biogas power plant alone when the discount rate drops below 8 % with the current technology costs.

Chapter 6

Operating regime and EES degradation cost analyses

This chapter presents the operating regime for the hybrid system that provides the optimal dispatch of PV, AD and EES. The LCOE will be calculated for the system to demonstrate that the sizing regime presented in Chapter 5 provides near optimal solutions given the condition that PV penetration should be maximised. The SOC for each partial discharge cycle is considered for the EES degradation costs. The expected number of EES replacements are provided for the system's lifetime. Section 6.1 presents the context of the operation problem, the operating regime and the case studies. The operational cost model for biogas power plant and the study on EES degradation costs are provided in Section 6.2. The LCOE equations for the system and components are presented in Section 6.3. The LCOE analyses can be found in Section 6.4. Additionally, the system's LCOE with future discount rates and capital costs are analysed for different PV and EES capacities. The chapter will be concluded with a summary in Section 6.5.

6.1 Problem context and operating regime

6.1.1 Problem context

The aim of the system is to provide the required electrical power with PV, AD and EES to meet the load demand at all times in the most cost-effective manner. This implies that the generation and load power must be balanced. The equality constraints for power balance are given in Equations (6.1) and (6.2).

$$P_{\text{Generation}}(h) = P_{\text{Load}}(h) \tag{6.1}$$

$$P_{\text{Generation}}(h) = P_{\text{PV}_{\text{Direct}}}(h) + P_{\text{AD}_{\text{Direct}}}(h) + \eta_{\text{EES}}[P_{\text{EES}_{\text{S1}}}(h) + P_{\text{EES}_{\text{S2}}}(h)] \quad (6.2)$$

$P_{\text{PV}_{\text{Direct}}}$ and $P_{\text{AD}_{\text{Direct}}}$ are the PV and AD power is used to meet the load directly. $P_{\text{EES}_{\text{S1}}}$ and $P_{\text{EES}_{\text{S2}}}$ are the stage 1 and stage 2 power outputs from EES. Stage 1 is when the EES outputs power to meet the demand when the energy stored in it is above an SOC threshold. Stage 2 is when the EES outputs power to meet the energy deficit in the system. η_{EES} is the round-trip efficiency for the storage system. This will further be elaborated with the introduction of the operating regime in Section 6.1.2.

The SOC limits to prevent EES over charging/discharging are defined in Equation (6.3). The power output of biogas generator should not exceed its rated capacity as shown in Equation (6.4). Due to its minimum loading constraint the biogas power plant is required to turn off when the power output is below 40 % of its rated power output [226] as given in Equation (5.6).

$$\text{SOC}_{\text{Min}} \leq \text{SOC}(h) \leq \text{SOC}_{\text{Max}} \quad (6.3)$$

$$P_{\text{AD}_{\text{Min}}} \leq P_{\text{AD}_{\text{Direct}}}(h) + P_{\text{AD}_{\text{Store}}}(h) \leq P_{\text{AD}_{\text{Max}}} \quad (6.4)$$

$P_{\text{AD}_{\text{Store}}}$ is the power output from AD that is to be stored in EES. $P_{\text{AD}_{\text{Min}}}$ and $P_{\text{AD}_{\text{Max}}}$ are the maximum and minimum power outputs from AD, respectively. SOC_{Min} and SOC_{Max} are the maximum and minimum SOCs, respectively. The instantaneous power output of the PV plant is calculated with Equation (5.8) as a function of the panel area N_{Total}, panel efficiency σ and irradiance ε. The cost and size of components are given in Table 6.1.

	PV (Sharp ND-250QCS)	AD (Caterpillar G3512E Genset)	EES (graphite/ $LiCoO_2$)	Solar Charge Controller (Outback FM 80)	Inverter (Schneider Electric XW6048)
Size	250 W	1.2 MW [227]	2 MW, 5 MWh	2 kW [226]	6 kW [187]
Unit	20000 [226]	2 [226]	1 [226]	2500	834
$\boldsymbol{C_{\mathrm{Cap_{Asset}}}}$	120 ($/unit) [226]	$7.5M [226]	1500 ($/kWh) [85]	335 ($/unit) [226]	1518 ($/unit) [187]
$\boldsymbol{C_{\mathrm{Inst_{Asset}}}}$	108 ($/unit) [226]	N/A	N/A	6.7 ($/unit) [226]	30.38 ($/unit) [187]
$\boldsymbol{C_{\mathrm{Asset_{O\&M_{Var}}}}}$	N/A	$C_{\mathrm{AD_{Fuel}}} + C_{\mathrm{AD_{Labour}}}$	0.42 ($/MWh) [85] + $C_{\mathrm{EES_{DegkWh}}}$	N/A	N/A
$\boldsymbol{C_{\mathrm{Asset_{O\&M_{Fixed}}}}}$	6 ($/unit-yr) [226]	300 ($/kW-yr) [224]	2.12 ($/kW-yr) [85]	1.005 ($/unit-yr) [226]	4.6 ($/unit-yr) [187]

Table 6.1. Component costs and sizes.

6.1.2 Operating regime

The off-grid system will operate in the most cost-effective manner with the proposed regime. Essentially, the operating regime will operate with the following characteristics:

- Since the fuel cost for PV is zero, PV will be given priority and be used first to meet the load demand before the deployment of AD or EES power;
- Surplus PV energy will be stored in EES while fulfilling the SOC constraints;
- AD will be used to meet the load demand when PV power is unavailable;
- EES will be used to meet the deficit energy, i.e., the situation when no PV power is available, and AD is switched off.
- When there is insufficient PV power, AD will be switched off, and EES will have insufficient stored energy to meet the load demand; AD will then operate at minimum

power output to meet the load demand. Any surplus energy generated from AD will be stored in EES.

An interesting research question to be addressed is "how will the EES dispatch method influence the cost of the system and its components?". To answer this, a SOC threshold is defined known as $\mathrm{SOC}_{\mathrm{Threshold}}$ to bias the dispatch priority for EES and AD. The operating regime can be divided into three phases, shown in Figure 6.1, as explained below:

Phase 1 (Blue): In the first phase, the SOC at hour h will be compared with the predefined $\mathrm{SOC}_{\mathrm{Threshold}}$. If the SOC is greater than or equal to the threshold, EES will be discharged first to meet the demand given that the load is greater than the PV output. The power to be discharged is $P_{\mathrm{EES}_{\mathrm{S1}}}$. It is expected that a lower $\mathrm{SOC}_{\mathrm{Threshold}}$ will reduce energy spillage and surplus energy from PV will be better utilised. Less biogas will be used. However, more EES cycles will occur throughout the system's lifetime due to excessive discharging.

Phase 2 (Orange): The regime will determine if there is deficit power for the instance. If so, EES will be discharged to meet the load while satisfying the constraint. The power to be discharged is $P_{\mathrm{EES}_{\mathrm{S2}}}$. AD will be turned on to minimum output to meet the load if EES does not have enough stored energy. During this time, any surplus power from AD will be stored in EES.

Phase 3 (Red): This phase will calculate the energy to be stored from the surplus power from AD and PV.

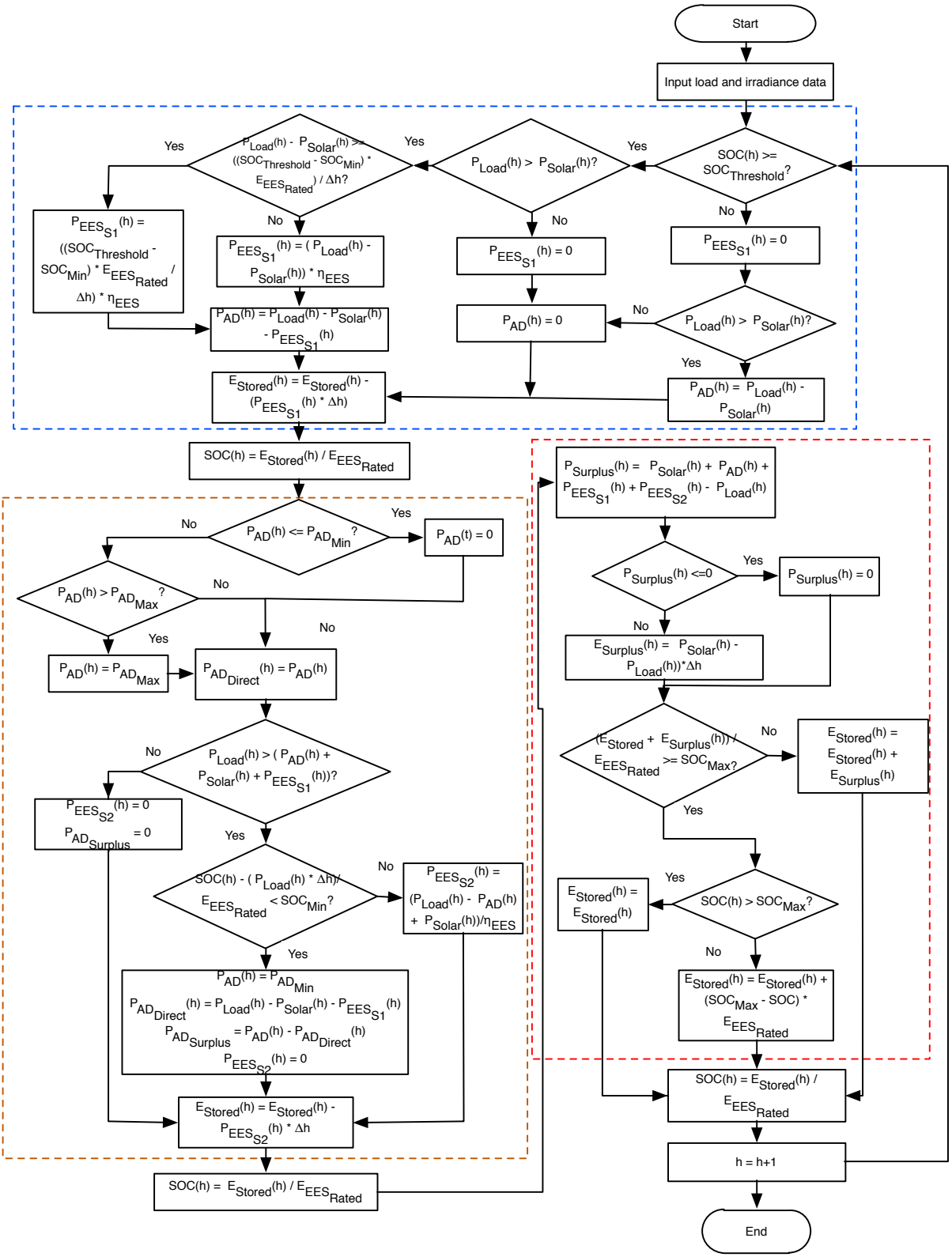


Figure 6.1. Proposed hybrid system operating regime.

6.1.3 Case study

Case studies were conducted with MATLAB to verify the dispatch methods and operating regime. The studies were for $SOC_{Threshold}$ at 100 %, i.e., the EES did not have the priority to discharge over AD. Figure 6.2 presents the results for five days of system operation in January. Power curtailment was applied to PV, and the discarded surplus energy produced by PV is shown in green. At this point, the EES is fully charged. The EES is discharged to meet the power deficit when PV output is increasing during sunrise and decreasing during sunset. The AD part loading constraint is triggered at these instances.

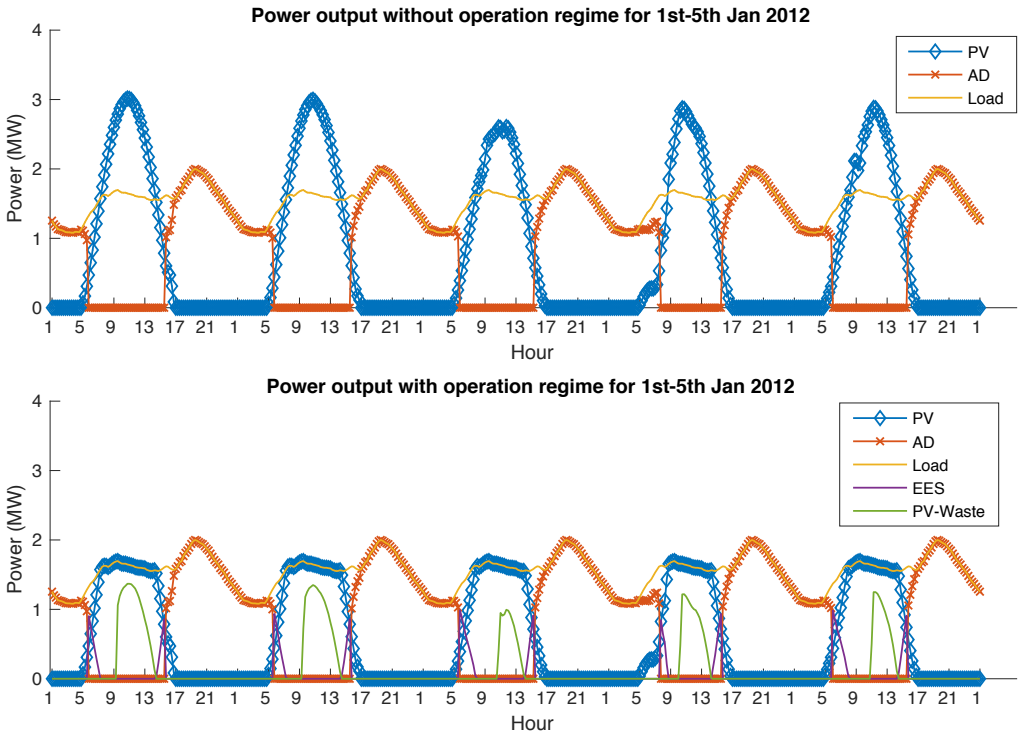


Figure 6.2. System's power output for winter.

Figure 6.3 shows the simulation results for five days of system operation in November. As stated previously, November is the month with most repeated rains in the year. This introduces severe fluctuations to the PV power output. All PV power is used during this period either to meet the demand directly or store in EES. Due to the power deficit, there are instances where

both AD and EES are used to meet the demand. It can be confirmed that the workable operation of the hybrid system is achieved with the proposed regime.

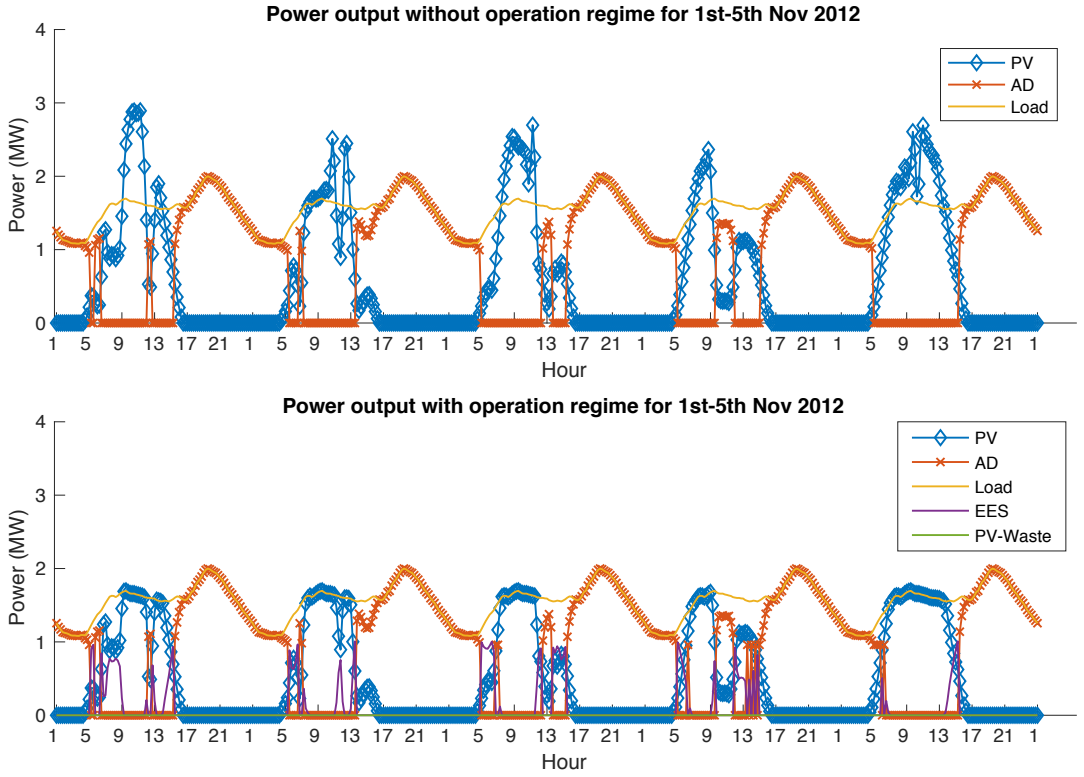


Figure 6.3. System's power output for autumn.

The SOC for the system with $SOC_{Threshold}$ at two extremes is presented in Figure 6.4. It can be observed that deep discharges occur in January when $SOC_{Threshold}$ is set at 0 %. The solar power is better utilised, i.e., less energy spillage occurs because the storage is fully used at the beginning of the regime. Unlike when $SOC_{Threshold}$ is set at 100 % as shown in the adjacent figure, the EES is rarely discharged and is kept at high SOC. Surplus power will be wasted, i.e., surplus energy will not be stored as EES will be full most of the time.

For November, surplus power is not an issue as the EES is never fully charged. When $SOC_{Threshold}$ is set at 0 %, the SOC is mostly at a minimum of 0 %. This can be explained by the fact that the EES is used at a priority similar to the case in January with $SOC_{Threshold}$ at 0 %. The EES is less susceptible to a full discharge when $SOC_{Threshold}$ is 100 %. In general, the

EES of a practical hybrid system will experience numerous partial cycles with different SOC ranges to fulfil the system energy requirement.

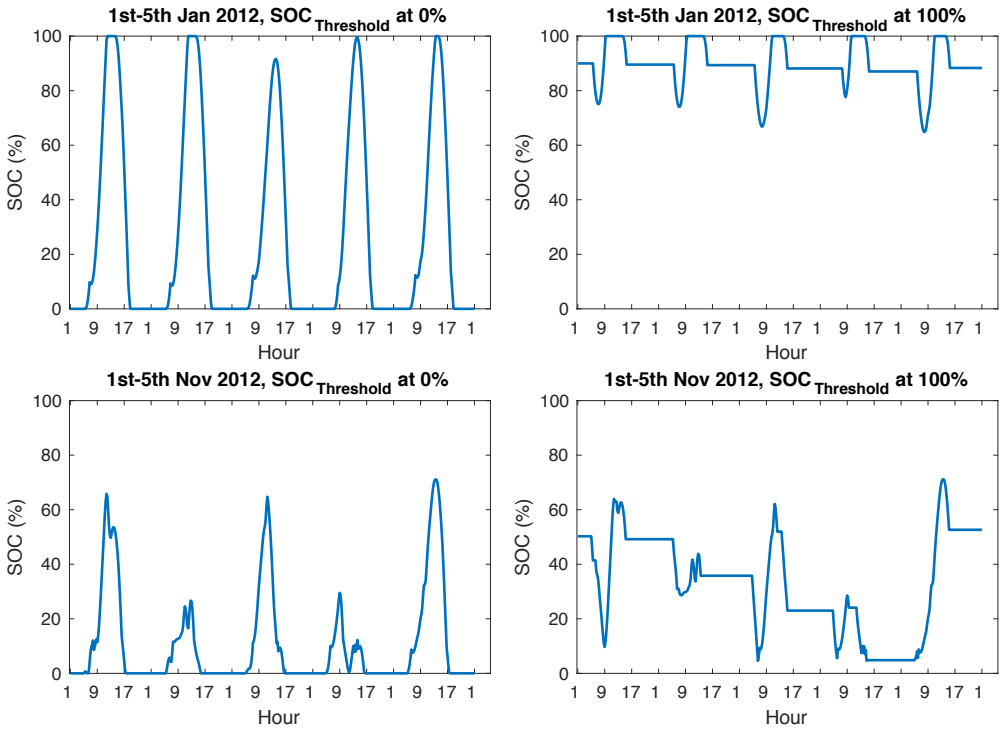


Figure 6.4. EES SOC for 0 % and 100 % $SOC_{Threshold}$ in summer and spring.

A sensitivity analysis for $SOC_{Threshold}$ with steps at 0.01, from 0 to 1 is carried out for the system's lifetime operation. The power output and SOC are stored for cost analysis and will be presented in Section 6.3.

6.2 Operational cost models for AD and EES

Apart from capital costs, there are operational costs associated with EES and AD. These can be classified into fixed and variable costs. For AD, fixed operational costs include labour and routine generator maintenance. Fuel cost to produce electrical power is the variable operational cost for AD. The fixed operational costs for EES are the operation and maintenance costs such as routine battery services. As stated in [228], identifying the operating cost for EES is challenging as it does not consume fuel unlike the AD source. The energy cost can be assigned to the EES to represent the cost for charging and can act as the 'fuel' cost. Furthermore, another

variable operational cost should be included to model the degradation of EES due to charging and discharging. This is known as degradation cost and can be divided into two types; the degradation cost per kWh and degradation cost per cycle. Degradation cost per kWh is defined as the cost ($) for the energy discharged from the battery. The battery will need to be replaced when its total energy throughput is equal to its rated lifetime energy throughput. Degradation cost per cycle is calculated with the cost per cycle ($) for each DOD as a fraction of the battery capital cost ($) and the remaining cycles to failure [158]. Calendar aging is not considered here.

6.2.1 AD operational cost model

The Caterpillar G3512E Genset [227] is adopted to model the biogas power plant, with a rated capacity of 1.2 MW. The cost for AD power generation is given in Equation (6.5).

$$C_{\mathrm{AD_{Fuel}}}(t) = C_{\mathrm{Gas}}.\frac{P_{\mathrm{AD}}(t).\left[a.{P_{\mathrm{AD}}}^{2}(t) + b.P_{\mathrm{AD}}(t) + c\right]}{\mathrm{LHV}} \tag{6.5}$$

C_{Gas} is the AD gas cost at 6.97 $/mcf [229], LHV is the Lower Heating Value at 905 btu/ft^3 [227]. The fuel consumption is a quadratic function with constants a, b and c at 0.0016, -3.935 and 1064,1 respectively.

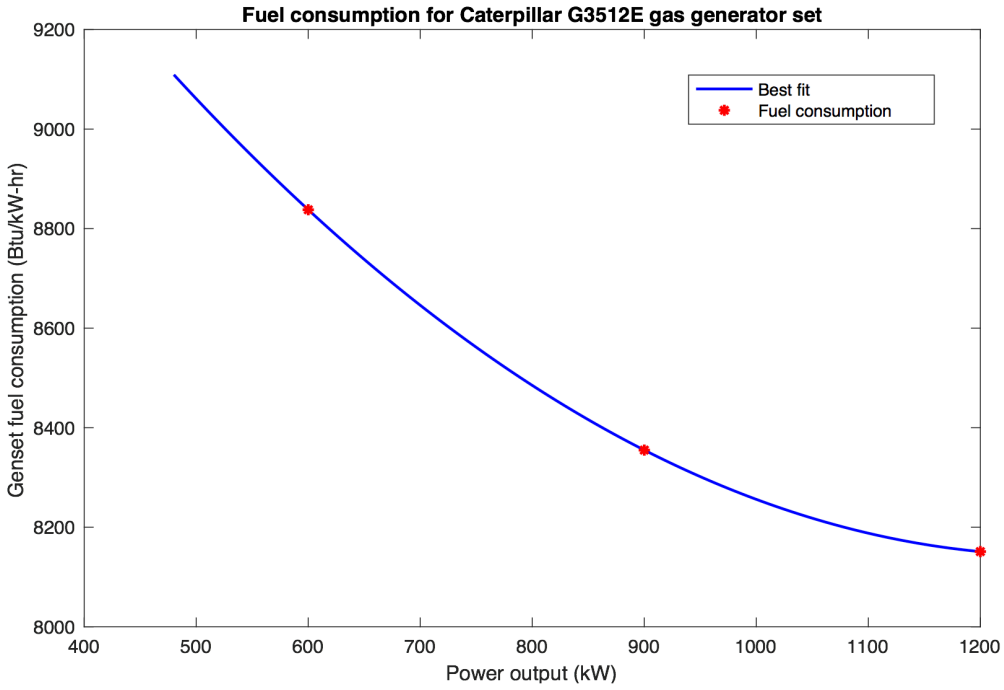


Figure 6.5. Fuel consumption curve for AD [227].

The fuel consumption curve is displayed in Figure 6.5 which shows a significant relationship. The fuel consumption is at the lowest when the power output is maximum. This is because the generator achieves the highest operation efficiency at rated capacity. The generator set should avoid meeting partial load demand, hence, the constraint.

6.2.2 $LiCoO_2$ degradation cost model and number of replacements

Contrary to many researches which use DOD or energy discharge content in kWh to calculate the EES degradation, this work uses a capacity fade model to quantify the degradation costs. In recent years, there have been published materials studying Li-ion capacity fading. The factors that are studied are mainly on DOD, discharge C-rate and operating temperature. In [230], the cycle-life of a graphite/$LiFePO_4$ battery was researched and subsequently, the cycle-life models were built. Three parameters were studied, with six temperatures from -30 °C to 60 °C, five DODs from 10–90 % and four C-rates ranging from C/2 to 10 C. A power law relationship was established between the capacity fade and the charge throughput, representing the amount of charge delivered by EES during cycling. The highlight is that the capacity loss was mainly affected by temperature and time while the effect of DOD was less of a concern with a C-rate of C/2.

The capacity loss rates of a Li-ion cell with nickel cobalt aluminium cathode under a restricted range (30–90 % SOC) and full discharge (0–100 % SOC) for two temperatures (25 °C and 60 °C) were studied in [231]. It was found that capacity fading can be reduced with a reduced SOC range.

Further analysis in cycle-life study with restricted range for Li-ion cell was conducted in [156] with graphite/$LiCoO_2$ cells. It was found that the capacity loss can be affected by change in SOC (ΔSOC), mean SOC and C-rate. A power law model was developed for capacity fading of graphite/$LiCoO_2$ cells under various SOC ranges. Authors claim that the ΔSOC and mean SOC during operation should be minimised to decrease the long-term capacity fade rate,

resulting in higher number of equivalent cycles or increased cumulative discharge capacity throughout the EES lifetime. Also reported in [155], increased cycle-life can be a result in cycling in lower charged states for Li-ion cells.

The degree of EES degradation is a function of number of cycles, change of SOC and amount of energy that flows through it [158]. The normalised discharge capacity model in [156] was adopted to study the degradation cost for EES. However, this model has several limitations. First, it is unable to capture the unexpected capacity loss behaviour for low SOC ranges such as 0–60 % in the presented case study. However, the results indicate that the proposed model yields negative results for low SOC ranges. The experiment results for normalised discharge capacity with respect to the equivalent full cycle are above the fitted curve. It is expected that there will be more cycles than the computed result from the model therefore the degradation should be less for low SOC ranges.

The second limitation is that in the study for complete discharge range, i.e., 0–100 % SOC, there is a sudden increase in capacity loss rate after 500 equivalent full cycles. This suggests that a new degradation mechanism is triggered, and it is in the form of linear capacity fade model. To overcome this issue in the study, a function was fitted with the data points obtained from the normalised discharge capacity model with the number of equivalent full cycles for 100 % DOD between 0–100 % SOC. On inspection, this number was found to be approximately 850 full cycles [156]. The fitted function is shown in Figure 6.6, and the data points generated from normalised discharge capacity model after 30 % DOD have been neglected as they prevent the best fit from the 100 % DOD. Moreover, after 45 % DOD, an unreasonable increase in cycle-life occurs.

During a discharge cycle, the mean SOC is calculated with Equation (6.6):

$$\mathrm{SOC}_{\mathrm{Mean}} = \frac{\mathrm{SOC}_{\mathrm{Upper}} + \mathrm{SOC}_{\mathrm{Lower}}}{2} = \frac{\mathrm{SOC}_{h_1} + \mathrm{SOC}_{h_2}}{2} \tag{6.6}$$

$\mathrm{SOC_{Upper}}$ is the SOC when discharge begins and $\mathrm{SOC_{Lower}}$ is the SOC when charging begins for each partial cycle. The time h_1 is used to locate the time when the SOC is at the maximum of a previous cycle. The change in SOC is given in Equation (6.7):

$$\Delta\mathrm{SOC} = \mathrm{SOC_{Upper}} - \mathrm{SOC_{Lower}} \tag{6.7}$$

The rated cycle-life and a_{ees} are calculated with Equations (6.8) and (6.9) [156], respectively.

$$Ratedcycle_{\mathrm{SOC_{Upper}},\mathrm{SOC_{Lower}}} = e^{\frac{\ln\left(\frac{100^{0.453}.(100-\mathrm{NDC})}{a_{\mathrm{ees}}}\right)}{0.453}} \quad \text{when } \mathrm{SOC_{Upper}} \neq 1 \tag{6.8}$$

$$a_{\mathrm{ees}} = 3.25 * \mathrm{SOC_{Mean}}.(1 + 3.25 * \Delta\mathrm{SOC} - 2.25 * \Delta\mathrm{SOC}^2) \tag{6.9}$$

where NDC is the Normalized Discharge Capacity at 80 %. The three-parameter equation in Equation (6.10) [153, 171] is used to fit the rated cycle for deep discharge situations and $\mathrm{SOC_{Upper}}$ at 100 % during a discharge cycle.

$$Ratedcycle_{100\%,\mathrm{SOC_{Lower}}} = \frac{d_{\mathrm{ees}}}{(\mathrm{DOD} - e_{\mathrm{ees}})^{f_{\mathrm{ees}}}} \quad \text{if } \mathrm{SOC_{Upper}} = 1 \ \& \ \mathrm{SOC_{Lower}} < 0.55 \tag{6.10}$$

where d_{ees}, e_{ees} and f_{ees} are constants with values 1278, -0.36 and 1.265, respectively.

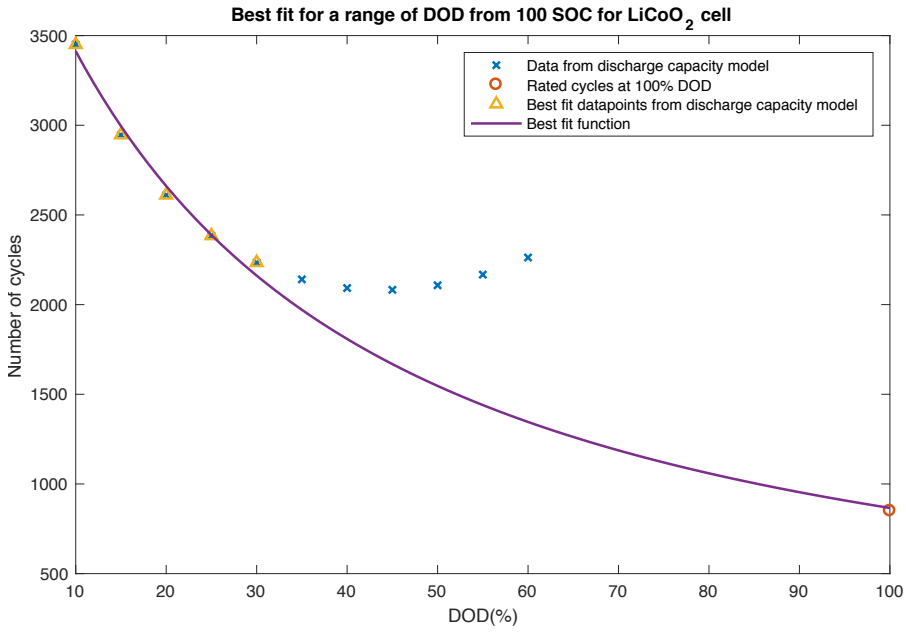


Figure 6.6. $LiCoO_2$ cycle-life function for discharge from 100 % SOC.

The purpose to calculate the degradation cost per cycle is to determine the number of EES lifetime replacements. The value for the whole EES is calculated and then the cost of every discharge cycle is recorded. The EES will need to be replaced once the maximum capital cost is reached [158]. The replacement cost per discharge cycle for year t and cycle T is calculated with Equation (6.11) and the number of lifetime replacements is calculated with Equation (6.12).

$$C_{\mathrm{EES_{Replacement}}}(t,T) = \frac{C_{\mathrm{Cap_{EES}}}.E_{\mathrm{EES_{Rated}}}}{Ratedcycle_{\mathrm{SOC_{Upper}},\mathrm{SOC_{Lower}}}(t,T)} \tag{6.11}$$

$$N_{\mathrm{EES}} = \frac{\sum_t^n \sum_T^m C_{\mathrm{EES_{Replacement}}}(t,T)}{C_{\mathrm{Cap_{EES}}}.E_{\mathrm{EES_{Rated}}}} \tag{6.12}$$

$C_{\mathrm{Cap_{EES}}}$ and $E_{\mathrm{EES_{Rated}}}$ are the capital cost and rated energy capacity of EES. $Ratedcycle_{\mathrm{SOC_{Upper}},\mathrm{SOC_{Lower}}}$ is the rated cycle-life for the EES given a discharge cycle from $\mathrm{SOC_{Upper}}$ to $\mathrm{SOC_{Lower}}$. Figure 6.7 shows a comparison of Li-ion cells with different cycle-life under a range of DOD from 100 % SOC. $LiCoO_2$ cells have a shorter life span compared to other chemistries, and $LiFePO_4$ can double the rated cycle-life at low DODs [232]. A lower degradation per cycle and degradation per kWh can be achieved with a higher rated cycle-life.

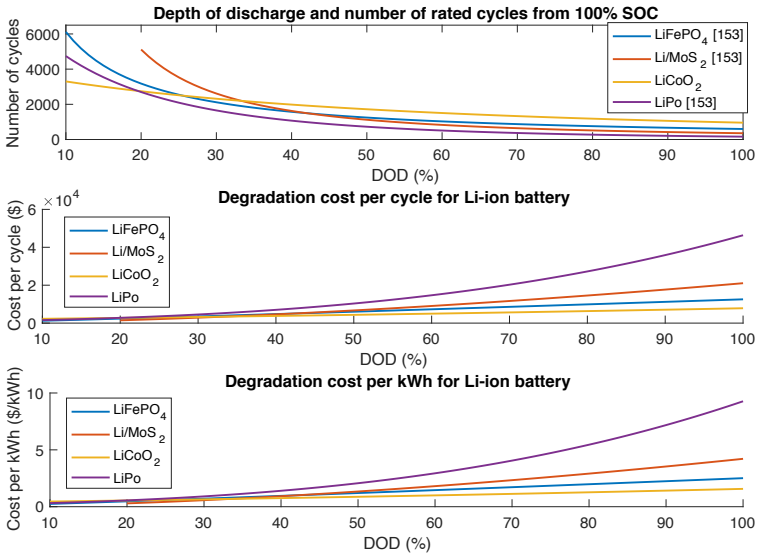


Figure 6.7. Comparison of Li-ion EES degradation costs and cycle-life for discharge from 100 % SOC.

A sensitivity analysis with a range of $SOC_{Threshold}$ was conducted on the system to study the required number of EES lifetime replacements. Figure 6.8 displays the simulation results. Since the number of EES cannot be a fraction, the obtained result is rounded up to the nearest integer. The number of replacements increases as the $SOC_{Threshold}$ is reduced. To explain these phenomena, Figure 6.9 provides the histogram for changes in SOC and SOC occurrences for the lifetime operation with $SOC_{Threshold}$ at 0 % and 100 %. With $SOC_{Threshold}$ at 100 %, the SOCs are mostly situated in the higher region and the results in a higher SOC_{Mean}. However, the total number of discharges given by the integral of the number of occurrences for ΔSOC is less for the case when $SOC_{Threshold}$ is at 0. There are more deep discharges for the case with $SOC_{Threshold}$ at 0 % as represented by ΔSOC. In summary, a $SOC_{Threshold}$ at 0 % will generally on average result in a lower SOC_{Mean}, but the increase in total number of discharges and the deep discharge cycles have a larger impact on the EES degradation and result in an increased number of EES replacements.

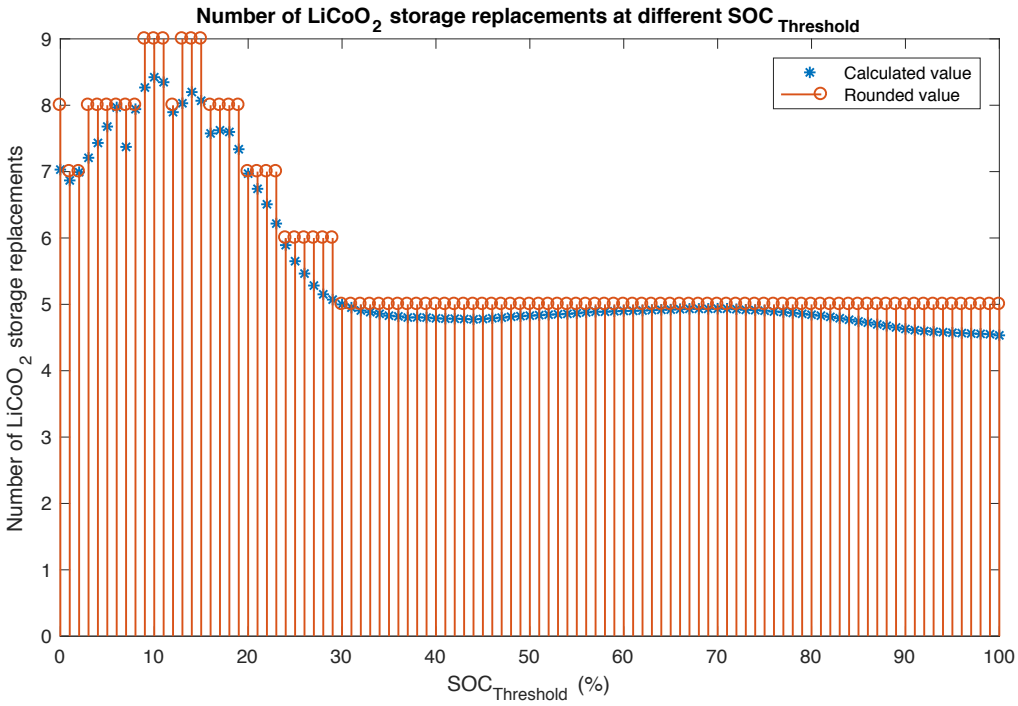


Figure 6.8. Number of lifetime EES replacements for different $SOC_{Threshold}$.

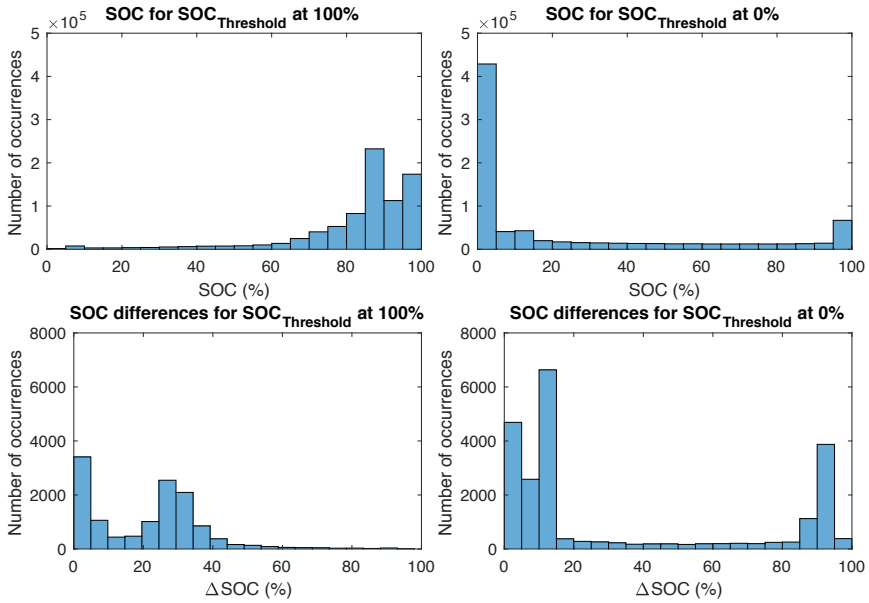


Figure 6.9. System's lifetime SOCs and SOC differences for $\mathrm{SOC_{Threshold}}$ at 0 % and 100 %.

6.3 Levelized cost of electricity

The LCOE for individual components and for the system are studied with the established operation cost models for AD and EES. It is of crucial importance to understand the cost implications of how generation assets and EES will react to the operating regime. The cost is largely affected by the asset lifetime electricity production as well as the operational costs or degradation costs for the case with EES. The system has a lifetime of 22 years with discount rate at 8 % [85, 184].

6.3.1 LCOE for PV

The LCOE for PV can be calculated with Equations (6.13), (6.14) and (6.15) below:

$$\mathrm{LCOE_{PV}} = \frac{C_{\mathrm{PV}}}{E_{\mathrm{PV}}} \tag{6.13}$$

$$C_{\mathrm{PV}} = N_{\mathrm{Total}}.\left(C_{\mathrm{Cap_{PV}}} + C_{\mathrm{Inst_{PV}}}\right) + \sum_{t=0}^{n} \frac{N_{\mathrm{Total}}.\, C_{\mathrm{PV_{O\&M_{Fixed}}}}}{(1+r)^t} \tag{6.14}$$

$$E_{\mathrm{PV}} = \sum_{t=0}^{n} \frac{(1-d_{\mathrm{EES}})^t.\sum_{j=1}^{h} P_{\mathrm{PV_{Direct}}}(t,j) + P_{\mathrm{PV_{Store}}}(t,j)}{(1+r)^t} \tag{6.15}$$

$C_{\mathrm{Cap_{PV}}}$, $C_{\mathrm{Inst_{PV}}}$, and $C_{\mathrm{PV_{O\&M_{Fixed}}}}$ are the capital, installation and operation and maintenance costs respectively for PV. d_{EES} is the annual degradation constant for the PV panel at 0.5 % [85]. $P_{\mathrm{PV_{Direct}}}$ and $P_{\mathrm{PV_{Store}}}$ are the power outputs from PV that are used to meet the demand and to be stored in EES, respectively. Since the system is off-grid, the wasted energy from the PV generator not used directly to meet the demand or get stored in EES is not included in the lifetime energy production as the generated electricity will not be sold and the cost cannot be recovered, resulting in a higher levelized cost.

6.3.2 LCOE for AD

The LCOE for AD can be calculated with Equation (6.16) below:

$$\mathrm{LCOE_{AD}} = \frac{C_{\mathrm{AD}}}{E_{\mathrm{AD_{Total}}}} \tag{6.16}$$

$$C_{\mathrm{AD}} = C_{\mathrm{Cap_{AD}}} + \sum_{t=0}^{n} \frac{C_{\mathrm{AD_{O\&M_{Fixed}}}} . P_{\mathrm{AD_{Max}}} + \sum_{j=1}^{h} C_{\mathrm{AD_{O\&M_{Var}}}}(t,j)}{(1+r)^t} \tag{6.17}$$

$C_{\mathrm{Cap_{AD}}}$ and $C_{\mathrm{AD_{O\&M_{Fixed}}}}$ are the capital and fixed annual O&M costs for AD. The variable operation and maintenance cost for AD, $C_{\mathrm{AD_{O\&M_{Var}}}}$, is calculated with Equation (6.18) below:

$$C_{\mathrm{AD_{O\&M_{Var}}}}(t,j) = C_{\mathrm{AD_{Fuel}}}(t,j) + (C_{\mathrm{AD_{Labour}}}/2).P_{\mathrm{AD}}\Delta h(t,j) \tag{6.18}$$

$C_{\mathrm{AD_{Labour}}}$ is the labour cost for operating the AD at \$0.05/kWh [224]. The AD lifetime energy production is calculated with Equation (6.19) below:

$$E_{\mathrm{AD_{Total}}} = \sum_{t=0}^{n} \frac{\sum_{j=1}^{h} P_{\mathrm{AD_{Direct}}}(t,j) + P_{\mathrm{AD_{Store}}}(t,j)}{(1+r)^t} \tag{6.19}$$

$P_{\mathrm{AD_{Direct}}}$ is the AD power output that is used to meet the demand directly and $P_{\mathrm{AD_{Store}}}$ is the surplus power from AD that is produced while meeting the deficit demand.

6.3.3 LCOS

The equation for LCOS is given in Equation (2.9). The lifetime cost delivered by storage is given in Equation (6.20) below:

$$C_{\mathrm{EES}} = C_{\mathrm{Cap_{EES}}}.E_{\mathrm{EES_{Rated}}} + \sum_{t=0}^{n} \frac{C_{\mathrm{EES_{O\&M_{Total}}}}}{(1+r)^t} \tag{6.20}$$

$$C_{\mathrm{EES_{O\&M_{Total}}}} = C_{\mathrm{EES_{O\&M_{Fixed}}}}.E_{\mathrm{EES_{Rated}}} + \sum_{T=1}^{m} C_{\mathrm{EES_{DegkWh}}}(t,T) + \sum_{j=1}^{h} C_{\mathrm{EES_{kWh}}}(t,j) \tag{6.21}$$

$C_{\mathrm{EES_{O\&M_{Fixed}}}}$ is the fixed annual EES O&M cost. The variable operational costs for EES include the degradation per kWh cost and energy cost are calculated with Equations (6.22) and (6.23) respectively. m is the number of discharge cycles per year.

$$C_{\mathrm{EES_{DegkWh}}}(t,T) = \frac{C_{\mathrm{Cap_{EES}}}}{Ratedcycle_{\mathrm{SOC_{Upper}},\mathrm{SOC_{Lower}}}(t,T)}.\left[SOC_{\mathrm{Upper}}(t,T) - SOC_{\mathrm{Lower}}(t,T)\right].E_{\mathrm{EES_{Rated}}} \tag{6.22}$$

$$C_{\mathrm{EES_{kWh}}}(t,j) = C_{\mathrm{EES_{O\&M_{Var}}}}.E_{\mathrm{EES_{Store}}}(t,j) \tag{6.23}$$

$C_{\mathrm{EES_{O\&M_{Var}}}}$ is the variable O&M cost for the energy $E_{\mathrm{EES_{Store}}}$ to be stored in EES. The lifetime energy delivered by EES is given in (6.24) below:

$$E_{\mathrm{EES}} = \eta_{\mathrm{EES}} \sum_{t=0}^{n} \frac{\sum_{j=1}^{h}[E_{\mathrm{EES_{S1}}}(t,j) + E_{\mathrm{EES_{S2}}}(t,j)]}{(1+r)^t} \tag{6.24}$$

η_{EES} is the round-trip efficiency of EES, and it is 90 % for Li-ion.

6.3.4 LCOD

LCOD has been proposed in Chapter 3. Equation (6.25) gives the LCOD for the hybrid system.

$$\mathrm{LCOD} = \frac{C_{\mathrm{EES}} + C_{\mathrm{PV_{Storetotal}}} + C_{\mathrm{Con}} + C_{\mathrm{AD_{Storetotal}}}}{E_{\mathrm{EES}}} \tag{6.25}$$

The solar charge controller cost can be obtained from Equation (5.16). Similar to Chapter 5, the number for inverter and solar charge controller replacements during the system's lifetime

is assumed to be two. The cost for producing the electricity from AD to be stored in EES is given in Equation (6.26) below:

$$C_{\mathrm{AD_{Storetotal}}} = C_{\mathrm{Cap_{AD}}} + \sum_{t=0}^{n} \frac{C_{\mathrm{AD_{O\&M_{Fixed}}}} . P_{\mathrm{AD_{Max}}} + \sum_{j=1}^{h} C_{\mathrm{AD_{O\&M_{Store}}}}(t,j)}{(1+r)^t} \quad (6.26)$$

$$C_{\mathrm{AD_{O\&M_{Store}}}}(t,j) = C_{\mathrm{AD_{Fuel}}}(t,j) + C_{\mathrm{AD_{Labour}}} . P_{\mathrm{AD_{Store}}}(t,j) \quad (6.27)$$

$P_{\mathrm{AD_{Store}}}$ is the power generated from AD to be stored in EES, the cost for generating the electricity from PV to be stored in EES is given in Equation (6.28) below:

$$C_{\mathrm{PV_{Storetotal}}} = N_{\mathrm{PV}} . (C_{\mathrm{Cap_{PV}}} + C_{\mathrm{Inst_{PV}}}) + \sum_{t=0}^{n} \frac{C_{\mathrm{O\&M_{PVpro}}} . \sum_{j=1}^{h} N_{\mathrm{Store}}(t,j)}{(1+r)^t} \quad (6.28)$$

Similar to Equation (3.19), the PV panel area used to produce the surplus electricity for storage is calculated with Equation (6.29).

$$N_{\mathrm{Store}}(t,j) = \frac{P_{\mathrm{PV_{Store}}}(t,j)}{\gamma(t,j).\eta_{\mathrm{PV}}} \quad (6.29)$$

The maintenance cost per hour for PV is calculated in Equation (6.30) below:

$$C_{\mathrm{O\&M_{PVpro}}} = \frac{C_{\mathrm{O\&M_{PV}}}}{365 * 24} \quad (6.30)$$

6.3.5 LCOE for system

The system's LCOE is derived in Equation (6.31). It takes the total costs for operating the system and the energy output into account to meet the load demand.

$$\mathrm{LCOE_{system}} = \frac{C_{\mathrm{PV}} + C_{\mathrm{EES}} + C_{\mathrm{Con}} + C_{\mathrm{Inv}} + C_{\mathrm{AD}}}{E_{\mathrm{EES}} + E_{\mathrm{PV_{Directtotal}}} + E_{\mathrm{AD_{Directtotal}}}} \quad (6.31)$$

The inverter cost, C_{Inv}, is calculated with Equation (5.16). The total energy produced by PV and AD during the operation of the system that is used to meet the load demand directly are given in Equations (6.32) and (6.33) respectively as shown below:

$$E_{\mathrm{PV_{Directtotal}}} = \sum_{t=0}^{n} \frac{(1-d_{\mathrm{PV}})^t . \sum_{j=1}^{h} P_{\mathrm{PV_{Direct}}}(t,j)}{(1+r)^t} \quad (6.32)$$

$$E_{\mathrm{AD_{Directtotal}}} = \sum_{t=0}^{n} \frac{\sum_{j=1}^{h} P_{\mathrm{AD_{Direct}}}(t,j)}{(1+r)^t} \tag{6.33}$$

$P_{\mathrm{PV_{Direct}}}$ and $P_{\mathrm{AD_{Direct}}}$ are the power generated from PV and AD respectively for direct consumption.

6.4 LCOE analyses and discussion

6.4.1 Levelized cost for system components

The LCOE results for AD, PV, and EES with $\mathrm{SOC_{Threshold}}$ at different values are displayed in Figure 6.10. The cost for AD is lower when $\mathrm{SOC_{Threshold}}$ is at a higher value. as AD has a higher dispatch priority than EES and more electricity is generated from AD. The cost for EES will increase because of a decreased energy output. LCOD has a curve similar to LCOS but with a larger cost. As explained previously, LCOD considers the energy conversion costs from primary source to electricity for storage. The capital costs for AD and PV have significantly contribute to the actual energy storage costs. The cost for PV increases as $\mathrm{SOC_{Threshold}}$ increases; this is due to less energy delivered by EES.

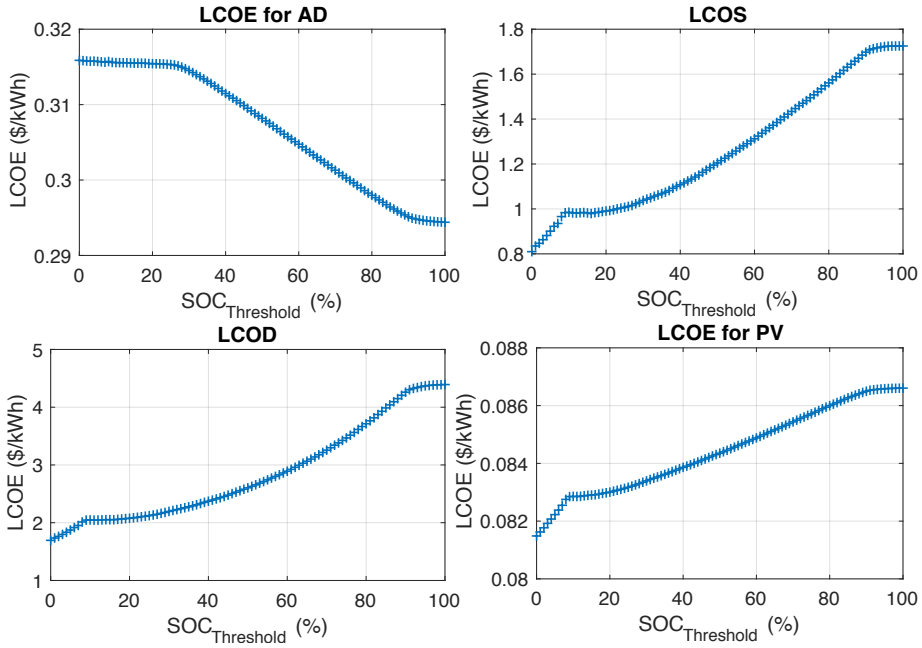


Figure 6.10. LCOE for AD, EES and system at different $\mathrm{SOC_{Threshold}}$ values.

Figure 6.11 shows the system LCOE with all the costs and electricity generation considered. When degradation cost is not considered, $C_{\mathrm{EES}_{\mathrm{DegkWh}}}$ is not included in the LCOE. The diamond and circle symbols denote the maximum and minimum LCOE, respectively. Without the degradation cost, it is identified that the least LCOE is achieved when storage is regularly discharged, i.e., $\mathrm{SOC}_{\mathrm{Threshold}}$ at 25 % and the highest LCOE happens when storage is at minimal use. With degradation cost, the least LCOE is achieved when storage is at minimal use, i.e., $\mathrm{SOC}_{\mathrm{Threshold}}$ at 100 %, and the highest LCOE occurs when storage is used as much as possible. This can be explained stating that degradation cost considers the cycle-life degradation. The cost for each cycle can contribute to the loss in capital value and life expectancy of storage. When degradation is not considered, the frequent use of storage is ideal as it maximises the use of asset and the "fuel cost" for storage is minimal, since the marginal cost for PV is approximately zero. When the degradation cost is not considered, the nonlinear mathematical relationship between cycle-life degradation (cycles) and cost ($) is excluded in the techno-economic analysis.

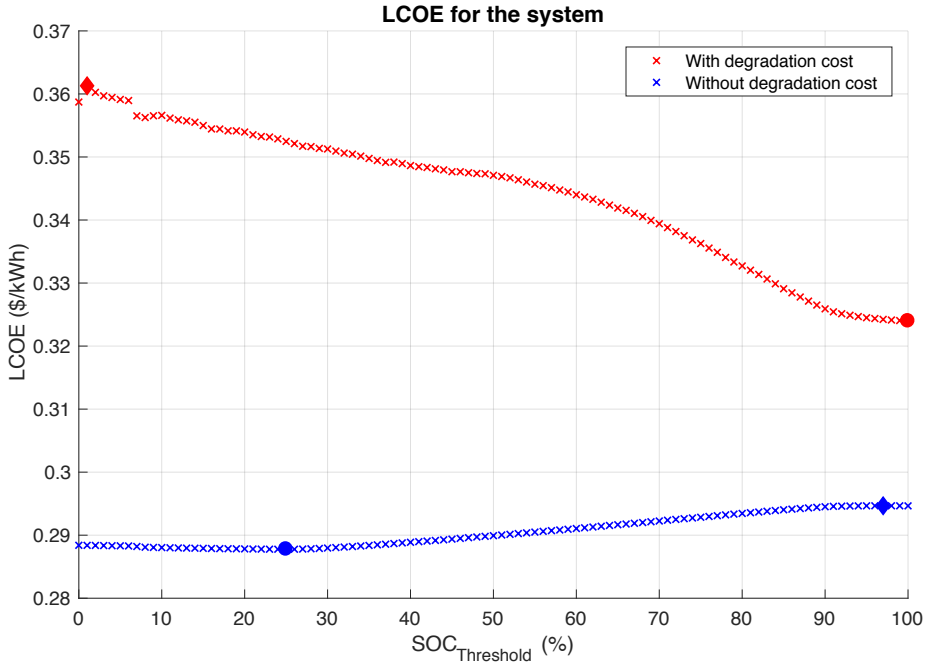


Figure 6.11. System LCOE with and without storage degradation cost.

6.4.2 EES capital costs sensitivity analysis

The capital costs such as manufacturing and the cost of cobalt in cathodes are major factors that prevent the wide-scale adoption of Li-ion at present. As discussed in [71], it is possible for Li-ion batteries to have a capital cost of 200 $/kWh by 2020. Figure 6.12 presents the results for the system LCOE with a sensitivity analysis on the EES capital cost.

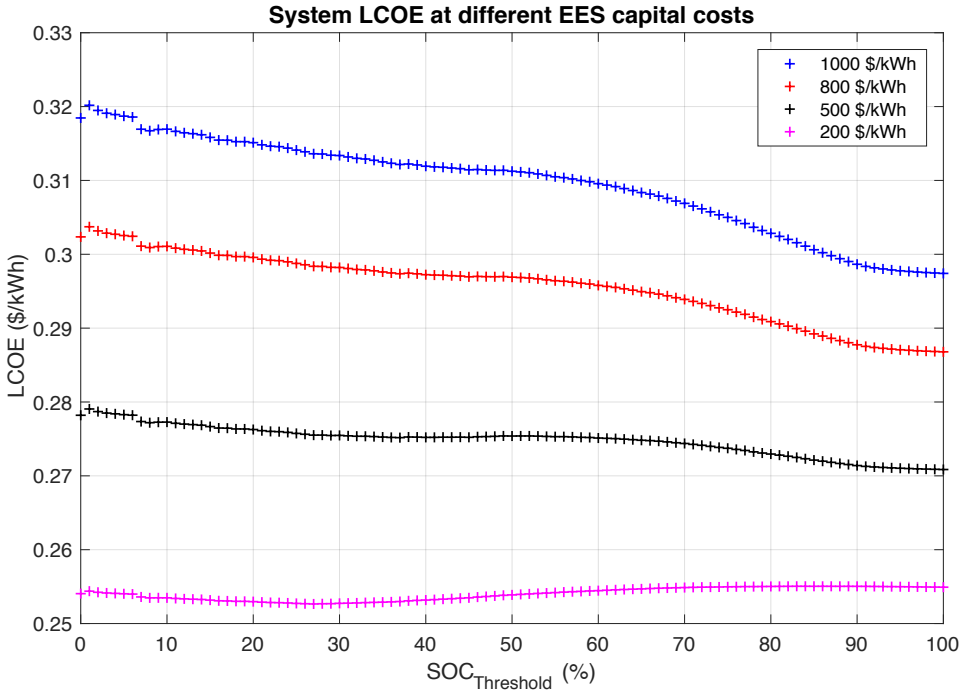


Figure 6.12. System LCOE with different EES capital costs.

At 1000 $/kWh, the system cost is reduced compared to the original study at 1500 $/kWh. As capital cost decreases, the differences in LCOE are minimised with $SOC_{Threshold}$ variation. This signifies that the cost of EES degradation has less influence on the system's cost. At 200 $/kWh, the largest difference in the system's levelized cost is 0.0023 $/kWh. The lowest LCOE for the system is achieved with an $SOC_{Threshold}$ between 25 %–30 %. It is more cost effective to cycle the EES more often and utilise the surplus PV energy than meeting the load demand with biogas. It is worth mentioning that the carbon emission cost might be included in the cost generation for the analysis. Although biogas is seen as a renewable energy source, it still generates a small amount of carbon emission due to the combustion process.

6.4.3 LCOE with PV and EES capacity variation

A sensitivity analysis is conducted with different energy storage capacities (MWh) and PV rated capacities (MW) to examine the LCOE for the system. A $SOC_{Threshold}$ at 30 % is used to frequently cycle the storage system and to use the surplus electricity generated from PV. Figure 6.13 presents the results. The minimal LCOE is achieved when no storage is installed and has a 1.5 MW–2.5 MW of PV rated capacity. Based on the analysis of the operating regime, the current capital cost and negligible marginal cost for PV can offset the biogas fuel cost. Storing the surplus energy produced by PV for later use is not the most economical option. This might be due to the current high capital cost, 1500 $/kWh, for EES.

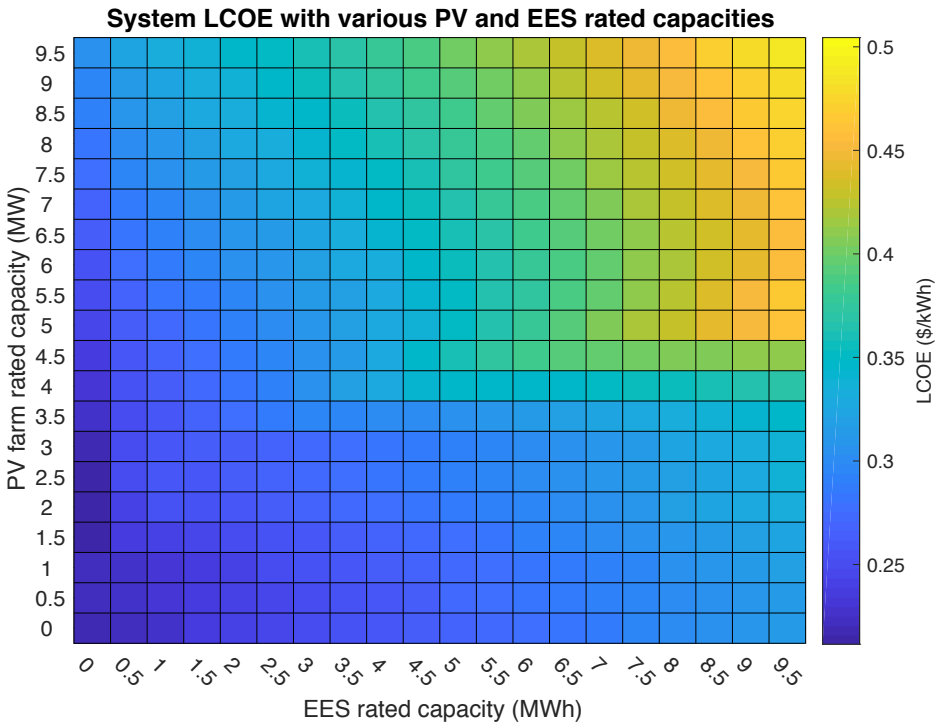


Figure 6.13. System LCOE with different EES and PV rated capacities.

When the PV capacity is below 3.5 MW, the change in LCOE is insignificant as the battery cycling is reduced. This can be explained by the insignificant presence of PV power. The LCOE escalates when EES rated capacity is larger than 4.5 MWh and PV rated capacity above 4.5

MW. This is the contribution from significant storage degradation. The maximum LCOE is located when PV is at 9.5 MW and EES is at 9.5 MWh.

6.5 Summary

An optimal operating regime for the PV-AD-EES system has been proposed in this chapter. One of the contributions in this chapter is that the accuracy of degradation costs for EES, i.e., graphite/$LiCoO_2$ is enhanced by utilising a capacity fade model. The cycle-life with partial SOC range cycles can be identified. The economic implications in this study can be summarised as follows:

- With the current technology costs and a discount rate of 8 %, it is shown that the capital cost for $LiCoO_2$ needs to be reduced to 200 $/kWh to be economically competitive with a dispatchable source such as AD biogas power plant;
- It is not economical to have high penetration of EES and PV with the current capital costs for EES, PV and the current discount rate;
- The insurance cost and financing for AD is not included in the study. This may increase the AD cost and it may be advisable to use a smaller AD plant. There are several issues with the financing of AD plant due to waste treatment difficulties and likelihood of explosion due to the presence of methane.
- According to the operating regime, the increase in system LCOE is insignificant when the PV and energy storage rated capacity is approximately below 4.5 MW and 4.5 MWh, respectively. This might be considered the optimal sizing when the energy storage is sized optimally to use the surplus PV electricity. The optimal sizing results resemble the results provided in Chapter 5.
- Storage degradation cost affects the system LCOE. By including degradation cost, the minimal LCOE is achieved if storage is cycled less frequently. The converse occurs when the degradation cost is excluded.

Chapter 7

Conclusions and future work

This thesis aims to develop methodologies for sizing and operating the Photovoltaic (PV), Anaerobic Digestion biogas power plant (AD) and Electrical Energy Storage (EES) renewable hybrid energy system. Energy economics via Levelized Cost of Electricity (LCOE) is an important indicator to identify the project viability for solar PV projects, particularly in the presence of EES and has been emphasised in this research. Due to the stochastic nature of solar irradiance and the potential amount of large irradiance datasets, data analytics via cluster analysis were examined for the Clearness Index (CI) in Chapter 4. The representatives obtained from the clustering results were used to verify its effectiveness for the PV farm and EES sizing as studied in Chapter 5. With the present discount rate and components costs, it is has been observed that it is more economical to build a hybrid system rather than use AD alone.

In the operational stage of the hybrid system, power balance is of critical importance. The optimal operating regime was devised and presented in Chapter 6. The degradation costs for EES were considered by a cell capacity fade model. The levelized costs were studied with the operating regime at various storage and PV capacities. As identified, the optimal sizing method proposed in Chapter 5 is effective given the future discount rates and components costs.

7.1 Research novelty

Novel methodologies were developed for the hybridisation of PV-AD-EES renewable hybrid systems. These powerful methodologies are generalised and hence, are applicable for system hybridisation at various locations. The novelty of the work in this thesis can be summarised in the following four points:

- The first novel aspect of this work is the development of a levelized cost metric for EES systems. As the EES deployment will increase in the future grid, it is necessary to propose a metric to quantify the levelized cost for storage. As EES does not generate electrical energy but acts as an electrical generator, levelized cost of delivery has been proposed to consider the electrical generated energy to be stored in EES. A case study of the EES coupled with a PV system has been used to understand the proposed metric.
- The second novel aspect of this work is a comprehensive study of CI with cluster analysis. For the first time, Fuzzy C-Means with Dynamic Time Warping (DTW) distance has been applied to the CI. Due to DTW's dynamic properties, the averaging and clustering results of CI were enhanced. Two solar irradiance datasets, Kenya and Johannesburg, were used for the case study.
- The third novel aspect of this work is the sizing methodology for the PV-AD-EES renewable hybrid system. A sizing algorithm has been proposed, offering significant insights on the energy balance and economics. The power constraints from biogas generator have also been included.
- The final novel aspect of this work is the operating regime for the renewable hybrid system. The regime is autonomous and does not require the forecasting of weather and load demand as input. The optimal power outputs for PV, AD, and EES are allocated at each time interval. The levelized costs consider the EES degradation modelled by the capacity fade model.

7.2 Future research areas

To further develop the proposed methodologies for the hybridisation of solar PV hybrid system, four future research areas have been identified and listed as follows:

The first extension to this thesis is related to the levelized cost of delivery metric. For various types of EES, the SOC will have a different impact on energy storage as the potential in using

the battery fully will be different for each case. Therefore, the energy delivered and stored could affect the entire system's performance, that is, the overall LCOD will be changed. SOC may be included in the LCOD.

Due to a range of different parameters that may affect the LCOD, additional sensitivity analyses are required to consider different lifetimes and round-trip efficiencies to provide a more accurate representation of the levelized costs for the different types of EESs, e.g., Lead-acid, Sodium-ion etc.

The second extension of this thesis is regarding the cluster analysis of the CI with FCM DTW. It is possible to include an extra temporal constraint in DTW by limiting the number of vertical or horizontal steps that the path can take consecutively. This adjustment avoids the matching of points that are very far from each other in time and, additionally, reduces the computation cost. The fuzzifier parameter for FCM can be further explored. It is worth mentioning that the optimal number of clusters is problem dependent and may vary depending on the application. The complexity for FCM DTW needs to be substantially reduced to increase the number of clusters for clustering. A possible way to achieve this is to use Segmentation Aggregate Approximation to reduce the number of CI profile's dimension. The cluster results are compared with the weather conditions data and the threshold of 'clear' days is determined. A systematic method to define the threshold, possibly through optimisation approach, will be beneficial. The meaning and indication of threshold need to be further studied with additional irradiance data from other locations and not only for tropical climates as examined in this research. The relationships between the weather conditions and CIs will need to be further analysed via statistical techniques such as probability density estimation.

The third extension of this work is regarding the proposed hybrid system sizing methodology. Currently, the load curve is assumed to be the same for all days in the year due to the small variation reported in the government report and journal articles. Future studies could consider

when the load is irregular or less than the minimum AD output power. This requires additional data. The conventional approach to sizing the power system is to use the cost of energy as the objective function. This approach could also be studied, and comparisons could be made in future work. As the VRB has negligible capacity loss and is capable of providing deep discharge cycles, SOC has not been included in the sizing methodology. However, the SOC, DOD and State of Health of EES need to be considered if other EES technologies are used.

The final extension of this work is regarding the proposed operating regime for the hybrid system. Currently, most EES degradation effects focus on the discharging phase, i.e., depth of discharge and energy delivered by EES. The degradation effect due to the charging phase should also be provided. Temperature and C-rate should be included in the capacity fade model to provide a more realistic analysis. It should be highlighted that the variable to control the dispatch priority of EES and AD, $SOC_{Threshold}$, can be made dynamic to minimise the system's lifetime cost. However, this might require generation and load forecasting.

7.3 Publications

Several journal and conference papers were published and listed as follows:

1. C. S. Lai, Y. Jia, L. L. Lai, Z. Xu, M. D. McCulloch, and K. P. Wong, "A comprehensive review on large-scale photovoltaic system with applications of electrical energy storage," *Renewable and Sustainable Energy Reviews,* vol. 78, pp. 439-451, 2017. Partially reproduced in Chapter 2.
2. C. S. Lai and M. D. McCulloch, "Levelized cost of electricity for solar photovoltaic and electrical energy storage," *Applied Energy,* vol. 190, pp. 191-203, 2017. Partially reproduced in Chapter 3.
3. C. S. Lai, Y. Jia, M. D. McCulloch and Z. Xu, "Daily clearness index profiles cluster analysis for photovoltaic system," *IEEE Transactions on Industrial Informatics,* vol. 13, pp. 2322-2332, 2017. Partially reproduced in Chapter 4.

4. C. S. Lai, X. Li, L. L. Lai and M. D. McCulloch, “Daily clearness index profiles and weather conditions studies for photovoltaic systems,” *Energy Procedia,* vol. 142, pp. 77-82, 2017. Partially reproduced in Chapter 4.
5. C. S. Lai and M. D. McCulloch, "Sizing of stand-alone solar PV and storage system with anaerobic digestion biogas power plants," *IEEE Transactions on Industrial Electronics,* vol. 64, pp. 2112-2121, 2017. Partially reproduced in Chapter 5.
6. C. S. Lai, Y. Jia, Z. Xu, L. L. Lai, X. Li, J. Cao and M. D. McCulloch, “Levelized cost of electricity for photovoltaic/biogas power plant hybrid system with electrical energy storage degradation costs,” *Energy Conversion and Management,* vol. 153, pp. 34-47, 2017. Partially reproduced in Chapter 6.
7. Y. Jia, C. S. Lai, Z. Xu, S. Chai, and K. P. Wong, “Adaptive partitioning approach to self-sustained smart grid,” *IET Generation, Transmission & Distribution,* vol. 11, pp. 485-494, 2017.
8. Y. Jia, C. S. Lai, and Z. Xu, “A spectral approach to efficient identification of uncontrolled separation of power transmission network,” *Electric Power Components and Systems,* vol. 45, pp. 2050-2061, 2017.
9. C. S. Lai and L. L. Lai, "Application of big data in smart grid," Proceedings of the 2015 IEEE International Conference on Systems, Man, and Cybernetics, 2015, pp. 665-670.

References

[1] R. F. Fard, K. Naddafi, M. Yunesian, R. N. Nodehi, M. H. Dehghani, and M. S. Hassanvand, "The assessment of health impacts and external costs of natural gas-fired power plant of Qom," *Environmental Science and Pollution Research,* vol. 23, no. 20, pp. 20922-20936, 2016.

[2] F. Díaz-González, A. Sumper, and O. Gomis-Bellmunt, *Energy Storage in Power Systems*. John Wiley & Sons, 2016.

[3] R. B. Jackson, J. G. Canadell, C. Le Quéré, R. M. Andrew, J. I. Korsbakken, G. P. Peters, et al., "Reaching peak emissions," N*ature Climate Change*, vol. 6, pp. 7-10, 2016.

[4] "EU legislation to control F-gases," European Commission, [Online]. Available: https://ec.europa.eu/clima/policies/f-gas/legislation_en [Accessed: 03.08.2017].

[5] R. O. Yusuf, Z. Z. Noor, A. H. Abba, M. A. A. Hassan, and M. F. M. Din, "Methane emission by sectors: a comprehensive review of emission sources and mitigation methods," *Renewable and Sustainable Energy Reviews,* vol. 16, no. 7, pp. 5059-5070, 2012.

[6] J. G. J. Olivier, G. Janssens-Maenhout, M. Muntean, and J. A. H. W. Peters, "Trends in global CO_2 emissions 2015 report background studies," PBL Netherlands Environmental Assessment Agency, European Commission Joint Research Centre, 2015. [Online]. Available: http://edgar.jrc.ec.europa.eu/news_docs/jrc-2015-trends-in-global-co2-emissions-2015-report-98184.pdf [Accessed: 03.08.2017].

[7] Renewable Energy Policy Network for the 21st century, "Renewables 2016 global status report," [Online]. Available: http://www.ren21.net/wp-content/uploads/2016/06/GSR_2016_Full_Report.pdf [Accessed: 02.08.2017].

[8] D. Hall and P. A. Moss, "Biomass for energy in developing countries," *GeoJournal,* vol. 7, no. 1, pp. 5-14, 1983.

[9] "World energy resources bioenergy 2016," World Energy Council, [Online]. Available: https://www.worldenergy.org/wp-content/uploads/2017/03/WEResources_Bioenergy_2016.pdf [Accessed: 01.03.2017].

[10] J. Goldemberg, *World Energy Assessment: Energy and the challenge of sustainability*. United Nations Pubns, 2000. [Online]. Available: http://www.undp.org/content/undp/en/home/librarypage/environment-energy/sustainable_energy/world_energy_assessmentenergyandthechallengeofsustainability.html [Accessed: 01.08.2017].

[11] "2014 Key world energy statistics,", International Energy Agency, 2014. [Online]. Available: http://www.oecd-ilibrary.org/docserver/download/6414011e.pdf?expires=1474442002&id=id&accname=ocid195129&checksum=AB7D95264B36739092213B90C4ECC805 [Accessed: 03.08.2017].

[12] M. Hosenuzzaman, N. Rahim, J. Selvaraj, M. Hasanuzzaman, A. Malek, and A. Nahar, "Global prospects, progress, policies, and environmental impact of solar photovoltaic power generation," *Renewable and Sustainable Energy Reviews,* vol. 41, pp. 284-297, 2015.

[13] G. M. Masters, *Renewable and efficient electric power systems*. John Wiley & Sons, 2013.

[14] W. G. Adams and R. Day, "The action of light on selenium," *Proceedings of the Royal Society of London,* vol. 25, no. 171-178, pp. 113-117, 1876.

[15] "SOLARGIS," [Online]. Available: http://solargis.info/doc/free-solar-radiation-maps-GHI [Accessed: 03.08.2017].

[16] A. Q. Huang, M. L. Crow, G. T. Heydt, J. P. Zheng, and S. J. Dale, "The future renewable electric energy delivery and management (FREEDM) system: the energy internet," *Proceedings of the IEEE,* vol. 99, no. 1, pp. 133-148, 2011.

[17] L. L. Lai, "Global Energy Internet and interconnection," IEEE Smart Grid Newsletter, 2015. [Online]. Available: http://smartgrid.ieee.org/newsletters/october-2015/global-energy-internet-and-interconnection [Accessed: 03.08.2017].

[18] "World Energy Outlook," International Energy Agency, 2012. [Online]. Available: http://www.worldenergyoutlook.org/media/weowebsite/energydevelopment/2012updates/measuringprogresstowardsenergyforall_weo2012.pdf [Accessed: 02.08.2017].

[19] T. Tezer, R. Yaman, and G. Yaman, "Evaluation of approaches used for optimization of stand-alone hybrid renewable energy systems," *Renewable and Sustainable Energy Reviews,* vol. 73, pp. 840-853, 2017.

[20] J. L. Bernal-Agustín and R. Dufo-López, "Simulation and optimization of stand-alone hybrid renewable energy systems," *Renewable and Sustainable Energy Reviews,* vol. 13, no. 8, pp. 2111-2118, 2009.

[21] "Combustion Engine vs. Gas Turbine: Part Load Efficiency and Flexibility," Wartsila. [Online]. Available: http://www.wartsila.com/energy/learning-center/technical-comparisons/combustion-engine-vs-gas-turbine-part-load-efficiency-and-flexibility. [Accessed: 02.08.2017].

[22] H. J. Lange, A. Banck, and M. Krueger, U.S. Patent No. US 9322302 B2, "Operating internal combustion engines," 26 April 2016.

[23] R. Stone, *Introduction to internal combustion engines: 4th edition*, pp. 206, Palgrave Macmillan, 2012.

[24] A. Mahesh and K. S. Sandhu, "Hybrid wind/photovoltaic energy system developments: Critical review and findings," *Renewable and Sustainable Energy Reviews,* vol. 52, pp. 1135-1147, 2015.

[25] M. Marwali, M. Haili, S. Shahidehpour, and K. Abdul-Rahman, "Short term generation scheduling in photovoltaic-utility grid with battery storage," *IEEE Transactions on Power Systems,* vol. 13, no. 3, pp. 1057-1062, 1998.

[26] J. Runyon, "Energy storage industry off and running in January 2016," Renewable Energy World, Jan. 2016. [Online]. Available: http://www.renewableenergyworld.com/articles/2016/01/energy-storage-set-for-record-year-in-2016.html [Accessed: 01.08.2016].

[27] B. Dunn, H. Kamath, and J.-M. Tarascon, "Electrical energy storage for the grid: a battery of choices," *Science,* vol. 334, no. 6058, pp. 928-935, 2011.

[28] V. Jülch, "Comparison of electricity storage options using levelized cost of storage (LCOS) method," *Applied Energy,* vol. 183, pp. 1594-1606, 2016.

[29] Lazard, "Lazard's Levelized Cost of Storage analysis V1.0," 2015. [Online]. Available: https://www.lazard.com/media/2391/lazards-levelized-cost-of-storage-analysis-10.pdf [Accessed: 07.08.2017].

[30] S. Sarkar and V. Ajjarapu, "MW resource assessment model for a hybrid energy conversion system with wind and solar resources," *IEEE Transactions on Sustainable Energy,* vol. 2, no. 4, pp. 383-391, 2011.

[31] A. Kiganda, "Africa's first grid connected biogas farm in Kenya powers up," Construction Review Online, 2017. [Online]. Available: https://constructionreviewonline.com/2017/01/africas-first-grid-connected-biogas-farm-in-kenya-powers-up/ [Accessed: 07.03.2017].

[32] "Tropical power launches Gorge Farm Energy Park," climatecare. [Online]. Available: https://climatecare.org/tropical-power-launches-gorge-farm-energy-park/ [Accessed: 07.03.2017].

[33] "First African grid-connected biogas-powered electricity plant comes online in Kenya," UK Construction Week. [Online]. Available: https://www.ukconstructionweek.com/news/construction-buzz/992-first-african-grid-connected-biogas-powered-electricity-plant-comes-online-in-kenya-construction-buzz-98 [Accessed: 07.03.2017].

[34] H. Zou, H. Du, J. Ren, B. K. Sovacool, Y. Zhang, and G. Mao, "Market dynamics, innovation, and transition in China's solar photovoltaic (PV) industry: A critical review," *Renewable and Sustainable Energy Reviews,* vol. 69, pp. 197-206, 2017.

[35] S. Chung, "100% renewable energy by 2050? Why wait?," Greenpeace.org, Sept. 2015. [Online]. Available: http://www.greenpeace.org/international/en/news/Blogs/makingwaves/renewable-energy-revolution-2050-Shell/blog/54248/ [Accessed: 02.08.2017].

[36] S. Eftekharnejad, V. Vittal, G. T. Heydt, B. Keel, and J. Loehr, "Impact of increased penetration of photovoltaic generation on power systems," *IEEE Transactions on Power Systems,* vol. 28, no. 2, pp. 893-901, 2013.

[37] S. Eftekharnejad, V. Vittal, G. T. Heydt, B. Keel, and J. Loehr, "Small signal stability assessment of power systems with increased penetration of photovoltaic generation: A case study," *IEEE Transactions on Sustainable Energy,* vol. 4, no. 4, pp. 960-967, 2013.

[38] B. Kroposki, "Reliable, low cost distributed generator/utility system interconnect: 2001 annual report, NREL/SR-560-34634," National Renewable Energy Laboratory, Aug. 2003. [Online]. Available: http://www.nrel.gov/docs/fy03osti/34634.pdf [Accessed: 01.08.2017].

[39] "energy [r]evolution: A sustainable world energy outlook 2015," Greenpeace, 2015. [Online]. Available: http://www.greenpeace.org/international/Global/international/publications/climate/2015/Energy-Revolution-2015-Full.pdf [Accessed: 02.08.2017].

[40] "Techonology roadmap: Solar photovoltaic energy 2014 edition," International Energy Agency, 2014. [Online]. Available: https://www.iea.org/publications/freepublications/publication/TechnologyRoadmapSolarPhotovoltaicEnergy_2014edition.pdf [Accessed: 01.08.2017].

[41] P. Denholm, R. Margolis, T. Mai, G. Brinkman, E. Drury, M. Hand*, et al.*, "Bright future: solar power as a major contributor to the US grid," *IEEE Power and Energy Magazine,* vol. 11, no. 2, pp. 22-32, 2013.

[42] V. Fthenakis, "Considering the total cost of electricity from sunlight and the alternatives [point of view]," *Proceedings of the IEEE,* vol. 103, no. 3, pp. 283-286, 2015.

[43] "About the Sunshot initiative," Office of Energy Efficiency & Renewable Energy, Energy.gov, [Online]. Available: https://energy.gov/eere/sunshot/about-sunshot-initiative [Accessed: 03.08.2017].

[44] "Sunshot 2030," Office of Energy Efficiency & Renewable Energy, Energy.gov, [Online]. Available: https://energy.gov/eere/sunshot/sunshot-2030 [Accessed: 02.08.2017].

[45] X. Yang, Y. Song, G. Wang, and W. Wang, "A comprehensive review on the development of sustainable energy strategy and implementation in China," *IEEE Transactions on Sustainable Energy,* vol. 1, no. 2, pp. 57-65, 2010.

[46] H. Sun, Q. Zhi, Y. Wang, Q. Yao, and J. Su, "China's solar photovoltaic industry development: The status quo, problems and approaches," *Applied Energy,* vol. 118, pp. 221-230, 2014.

[47] X.-g. Zhao, G. Wan, and Y. Yang, "The turning point of solar photovoltaic industry in China: Will it come?," *Renewable and Sustainable Energy Reviews,* vol. 41, pp. 178-188, 2015.

[48] Z. Ming, O. Shaojie, S. Hui, and G. Yujian, "Is the “Sun” still hot in China? The study of the present situation, problems and trends of the photovoltaic industry in China," *Renewable and Sustainable Energy Reviews,* vol. 43, pp. 1224-1237, 2015.

[49] D. Song, H. Jiao, and C. Te Fan, "Overview of the photovoltaic technology status and perspective in China," *Renewable and Sustainable Energy Reviews,* vol. 48, pp. 848-856, 2015.

[50] "Power development 13th Five-Year Plan (In Chinese)," National Development and Reform Commission of the People’s Republic of China, 2016. [Online]. Available: http://www.ndrc.gov.cn/zcfb/zcfbghwb/201612/P020161222570036010274.pdf [Accessed: 02.08.2017].

[51] "China 2050 high renewable energy penetration scenario and roadmap study," Energy Research Institute National Development and Reform Commission, 2015. [Online]. Available: http://www.efchina.org/Attachments/Report/report-20150420/China-2050-High-Renewable-Energy-Penetration-Scenario-and-Roadmap-Study-Executive-Summary.pdf. [Accessed 01.08.2017].

[52] S. Manju and N. Sagar, "Progressing towards the development of sustainable energy: A critical review on the current status, applications, developmental barriers and prospects of solar photovoltaic systems in India," *Renewable and Sustainable Energy Reviews,* vol. 70, pp. 298-313, 2017.

[53] "JNN solar mission: scheme/documents," Ministry of New and Renewable Energy, Government of India. [Online]. Available: http://www.mnre.gov.in/solar-mission/jnnsm/introduction-2/ [Accessed 05.08.2017].

[54] B. Mountain and P. Szuster, "Solar, solar everywhere: Opportunities and challenges for Australia's rooftop PV systems," *IEEE Power and Energy Magazine,* vol. 13, no. 4, pp. 53-60, 2015.

[55] T. Stetz, J. von Appen, F. Niedermeyer, G. Scheibner, R. Sikora, and M. Braun, "Twilight of the grids: The impact of distributed solar on Germany's energy transition," *IEEE Power and Energy Magazine,* vol. 13, no. 2, pp. 50-61, 2015.

[56] J. von Appen, M. Braun, T. Stetz, K. Diwold, and D. Geibel, "Time in the sun: the challenge of high PV penetration in the German electric grid," *IEEE Power and Energy Magazine,* vol. 11, no. 2, pp. 55-64, 2013.

[57] K. Ogimoto, I. Kaizuka, Y. Ueda, and T. Oozeki, "A good fit: Japan's solar power program and prospects for the new power system," *IEEE Power and Energy Magazine,* vol. 11, no. 2, pp. 65-74, 2013.

[58] "REmap 2030 renewable energy prospect: Germany," IRENA, 2015. [Online]. Available: http://www.irena.org/DocumentDownloads/Publications/IRENA_REmap_Germany_report_2015.pdf [Accessed: 04.08.2017].

[59] "Fact sheet: The solar star projects," SunPower Corporation, 2016. [Online]. Available: https://us.sunpower.com/sites/sunpower/files/media-library/fact-sheets/fs-solar-star-projects-factsheet.pdf [Accessed: 02.08.2017].

[60] "Desert Sunlight solar farm," First Solar, [Online]. Available: http://www.firstsolar.com/en/About-Us/Projects/Desert-Sunlight-Solar-Farm [Accessed: 02.08.2017].

[61] "Topaz solar farm," First Solar, [Online]. Available: http://www.firstsolar.com/en/About-Us/Projects/Topaz-Solar-Farm [Accessed: 02.08.2017].

[62] "Case study: solar PV-hydro hybrid system at Longyangxia, China," International Hydro Association, 2015. [Online]. Available: http://www.hydropower.org/blog/case-study-solar-pv-hydro-hybrid-system-at-longyangxia-china [Accessed: 02.08.2017].

[63] "Realtime generation of solar plants in Gujarat," Gujarat Energy Transmission Corporation Limited, 2016. [Online]. Available: https://www.sldcguj.com/RealTimeData/GujSolar.asp [Acessed: 02.08.2017].

[64] "Neoen breaks ground on 300 MW French solar plant," PV magazine, 2014. [Online]. Available: http://www.pv-magazine.com/news/details/beitrag/neoen-breaks-ground-on-300-mw-french-solar-plant_100017099/ - axzz4BLrsOucx [Accessed: 02.08.2017].

[65] "Agua Caliente solar project," First Solar, [Online]. Available: http://www.firstsolar.com/en/About-Us/Projects/Agua-Caliente-Solar-Project [Accessed: 02.08.2017].

[66] "Copper Mountain Solar 3," Cupertino Electric Inc. [Online]. Available: http://www.cei.com/our-work/copper-mountain-solar-3 [Accessed: 02.08.2017].

[67] "Califonia Valley Solar Ranch," Energy.gov. [Online]. Available: http://energy.gov/lpo/california-valley-solar-ranch [Accessed: 03.08.2017].

[68] "Antelope Valley Solar Ranch," Energy.gov. [Online]. Available: http://www.energy.gov/lpo/antelope-valley-solar-ranch [Accessed: 06.08.2017].

[69] Tom Kenning, "Residential storage costs will fall 84% globally by 2040 – BNEF," Energy Storage News, Jun. 2015. [Online]. Available: http://www.energy-storage.news/news/residential-storage-system-costs-to-fall-by-84-globally-by-2040-bnef [Accessed: 06.08.2017].

[70] K. Zipp, "Energy storage prices expected to drop 70% by 2030," Solar Power World, Jan. 2016. [Online]. Available: http://www.solarpowerworldonline.com/2016/01/ideal-

power-partners-with-austin-energy-on-us-doe-funded-projects-to-integrate-solar-pv-and-storage-for-commercial-sites/ [Accessed: 02.08.2017].

[71] B. Nykvist and M. Nilsson, "Rapidly falling costs of battery packs for electric vehicles," *Nature Climate Change,* vol. 5, no. 4, pp. 329-332, 2015.

[72] "Electricity storage and renewables: Cost and markets to 2030," International Renewable Energy Agency, 2017. [Online]. Available: http://www.irena.org/-/media/Files/IRENA/Agency/Publication/2017/Oct/IRENA_Electricity_Storage_Costs_2017.pdf [Accessed: 02.03.2017].

[73] "Industry solar: Crossing the chasm," Deutsche Bank Markets Research, 2015. [Online]. Available: https://www.db.com/cr/en/docs/solar_report_full_length.pdf [Accessed: 02.08.2017].

[74] "Battery storage for renewables: Market status and technology outlook," IRENA, 2015. [Online]. Available: http://www.irena.org/documentdownloads/publications/irena_battery_storage_report_2015.pdf [Accessed: 02.08.2017].

[75] M. Boust, "Grid-connected energy-storage projects in Pipeline to hit 2GW, led by US, China and South Korea," IHS Markit, July 2016. [Online]. Available: https://technology.ihs.com/581101/grid-connected-energy-storage-projects-in-pipeline-to-hit-2gw-led-by-us-china-and-south-korea. [Accessed 02.08.2017].

[76] "Renewables and electricity storage: A technology roadmap for Remap 2030," IRENA, 2015. [Online]. Available: https://www.irena.org/DocumentDownloads/Publications/IRENA_REmap_Electricity_Storage_2015.pdf [Accessed: 06.08.2017].

[77] "User guide for India's 2047 energy calculator, electrical energy storage (EES)," National Instituition for Transforming India. [Online]. Available:

http://www.indiaenergy.gov.in/iess/docs/Storage%20Documentation.pdf [Accessed: 06.08.2017].

[78] "Future energy scenarios: GB gas and electricity transmission," National Grid, 2016. [Online]. Available: http://fes.nationalgrid.com/fes-document/ [Accessed: 06.08.2017].

[79] R. Manghani and B. Simon, "U.S energy storage monitor: Q2 2016," Energy Storage Association and GTM Research, June 2016. [Online]. Available: http://energystorage.org/system/files/resources/gtm_research_-_esa_q2_2016_presentation_2016_06_14_final.pdf [Accessed: 06.08.2017].

[80] M. Munsell, "US energy storage market grew 243% in 2015, largest year on record," Greentech Media, Mar. 2016. [Online]. Available: http://www.greentechmedia.com/articles/read/us-energy-storage-market-grew-243-in-2015-largest-year-on-record [Accessed: 06.08.2017].

[81] "Technology roadmap: energy storage," International Energy Agency, 2014. [Online]. Available: https://www.iea.org/publications/freepublications/publication/TechnologyRoadmapEnergystorage.pdf [Accessed: 06.08.2017].

[82] "Department of Energy global energy storage database," Office of Electricity Delivery & Energy Reliability, Sandia National Laboratories, [Online]. Available: http://www.energystorageexchange.org/ [Accessed: 06.08.2017].

[83] K. Zipp, "What is the best type of battery for solar storage?," Solar Power World, 2015. [Online]. Available: http://www.solarpowerworldonline.com/2015/08/what-is-the-best-type-of-battery-for-solar-storage/ [Accessed: 06.08.2017].

[84] S. Shivashankar, S. Mekhilef, H. Mokhlis, and M. Karimi, "Mitigating methods of power fluctuation of photovoltaic (PV) sources–A review," *Renewable and Sustainable Energy Reviews,* vol. 59, pp. 1170-1184, 2016.

[85] C. S. Lai and M. D. McCulloch, "Levelized cost of electricity for solar photovoltaic and electrical energy storage," *Applied Energy,* vol. 190, pp. 191-203, 3/15/ 2017.

[86] X. Zhou, T. Zhao, L. An, Y. Zeng, and L. Wei, "Critical transport issues for improving the performance of aqueous redox flow batteries," *Journal of Power Sources,* vol. 339, pp. 1-12, 2017.

[87] X. Zhou, T. Zhao, L. An, Y. Zeng, and L. Wei, "Modeling of ion transport through a porous separator in vanadium redox flow batteries," *Journal of Power Sources,* vol. 327, pp. 67-76, 2016.

[88] X. Zhou, Y. Zeng, X. Zhu, L. Wei, and T. Zhao, "A high-performance dual-scale porous electrode for vanadium redox flow batteries," *Journal of Power Sources,* vol. 325, pp. 329-336, 2016.

[89] Y. Zeng, T. Zhao, X. Zhou, L. Zeng, and L. Wei, "The effects of design parameters on the charge-discharge performance of iron-chromium redox flow batteries," *Applied Energy,* vol. 182, pp. 204-209, 2016.

[90] Y. Zeng, X. Zhou, L. Zeng, X. Yan, and T. Zhao, "Performance enhancement of iron-chromium redox flow batteries by employing interdigitated flow fields," *Journal of Power Sources,* vol. 327, pp. 258-264, 2016.

[91] K. Gong, X. Ma, K. M. Conforti, K. J. Kuttler, J. B. Grunewald, K. L. Yeager*, et al.*, "A zinc–iron redox-flow battery under $100 per kWh of system capital cost," *Energy & Environmental Science,* vol. 8, no. 10, pp. 2941-2945, 2015.

[92] X. Zhou, T. Zhao, Y. Zeng, L. An, and L. Wei, "A highly permeable and enhanced surface area carbon-cloth electrode for vanadium redox flow batteries," *Journal of Power Sources,* vol. 329, pp. 247-254, 2016.

[93] Y. X. Wang *et al.*, "Room-temperature Sodium-Sulfur batteries: A comprehensive review on research progress and cell chemistry," *Advanced Energy Materials,* vol. 7, no. 24, 1602829, 2017.

[94] A. Poullikkas, "A comparative overview of large-scale battery systems for electricity storage," *Renewable and Sustainable Energy Reviews,* vol. 27, pp. 778-788, 2013.

[95] B. Zakeri and S. Syri, "Electrical energy storage systems: A comparative life cycle cost analysis," *Renewable and Sustainable Energy Reviews,* vol. 42, pp. 569-596, 2015.

[96] "E-storage: Shifting from cost to value wind and solar applications," World Energy Council, 2016. [Online]. Available: https://www.worldenergy.org/wp-content/uploads/2016/03/Resources-E-storage-report-2016.02.04.pdf [Accessed: 07.08.2017].

[97] G. Locatelli, E. Palerma, and M. Mancini, "Assessing the economics of large Energy Storage Plants with an optimisation methodology," *Energy,* vol. 83, pp. 15-28, 2015.

[98] J. Leadbetter and L. G. Swan, "Selection of battery technology to support grid-integrated renewable electricity," *Journal of Power Sources,* vol. 216, pp. 376-386, 2012.

[99] X. Luo, J. Wang, M. Dooner, and J. Clarke, "Overview of current development in electrical energy storage technologies and the application potential in power system operation," *Applied Energy,* vol. 137, pp. 511-536, 2015.

[100] "Energy storage: Tracking the technologies that will transform the power sector," Deloitte, 2015. [Online]. Available: http://www2.deloitte.com/content/dam/Deloitte/us/Documents/energy-resources/us-er-energy-storage-tracking-technologies-transform-power-sector.pdf [Accessed: 09.08.2017].

[101] "Uni.system™ grid-scale energy storage system", UET UniEnergy Technologies," [Online]. Available: http://www.uetechnologies.com/images/product/UET_UniSystem_ProductSheet.pdf [Accessed: 09.03.2017].

[102] L. Sanz, D. Lloyd, E. Magdalena, J. Palma, and K. Kontturi, "Description and performance of a novel aqueous all-copper redox flow battery," *Journal of Power Sources,* vol. 268, pp. 121-128, 2014.

[103] P. Alotto, M. Guarnieri, and F. Moro, "Redox flow batteries for the storage of renewable energy: A review," *Renewable and Sustainable Energy Reviews,* vol. 29, pp. 325-335, 2014.

[104] E. Wesoff and J. St. John, "Largest capacity flow battery in North America and EU is on-line and commissioned", greentechmedia, 2015. [Online]. Available: http://www.greentechmedia.com/articles/read/Largest-Capacity-Flow-Battery-in-North-America-and-EU-is-Online-and-Commiss [Accessed: 02.08.2017].

[105] G. L. Kyriakopoulos and G. Arabatzis, "Electrical energy storage systems in electricity generation: energy policies, innovative technologies, and regulatory regimes," *Renewable and Sustainable Energy Reviews,* vol. 56, pp. 1044-1067, 2016.

[106] N. Van Der Wijst, *Finance: A quantitative introduction*. Cambridge University Press, 2013.

[107] S. B. Darling, F. You, T. Veselka, and A. Velosa, "Assumptions and the levelized cost of energy for photovoltaics," *Energy & Environmental Science,* vol. 4, no. 9, pp. 3133-3139, 2011.

[108] M. Jakob, "Energy policy: The fair cost of renewable energy," *Nature Climate Change,* vol. 2, no. 7, pp. 488-489, 2012.

[109] P. Poonpun and W. T. Jewell, "Analysis of the cost per kilowatt hour to store electricity," *IEEE Transactions on Energy Conversion,* vol. 23, no. 2, pp. 529-534, 2008.

[110] N. Singh and E. W. McFarland, "Levelized cost of energy and sensitivity analysis for the hydrogen–bromine flow battery," *Journal of Power Sources,* vol. 288, pp. 187-198, 2015.

[111] G. Díaz, J. Gómez-Aleixandre, and J. Coto, "Dynamic evaluation of the levelized cost of wind power generation," *Energy Conversion and Management,* vol. 101, pp. 721-729, 2015.

[112] "HOMER Pro version 3.7 user manual," HOMER Energy, Aug. 2016. [Online]. Available: http://www.homerenergy.com/pdf/HOMERHelpManual.pdf [Accessed: 08.08.2017].

[113] "RETScreen software online user manual: Combined heat and power project model," RETScreen International, Natural Resources Canada. [Online]. Available: http://www.mcit.gov.cy/mcit/mcit.nsf/0/EF620C37922EDAECC22575CB00457F21/$file/Retscreen Manual (CHP).pdf [Accessed: 02.08.2017].

[114] "User manual: SAM Version 2016.3.14," System Advisor Model, National Renewable Energy Laboratory, Sept. 2016. [Online]. Available: https://sam.nrel.gov/download [Accessed: 08.08.2017].

[115] N. DiOrio, "System Advisor Model battery storage," System Advisor Model, National Renewable Energy Laboratory, 2015. [Online]. Available: https://sam.nrel.gov/node/69635 [Accessed: 10.08.2017].

[116] I. Pawel, "The cost of storage–How to calculate the levelized cost of stored energy (LCOE) and applications to renewable energy generation," *Energy Procedia,* vol. 46, pp. 68-77, 2014.

[117] A. S. Mundada, K. K. Shah, and J. Pearce, "Levelized cost of electricity for solar photovoltaic, battery and cogen hybrid systems," *Renewable and Sustainable Energy Reviews,* vol. 57, pp. 692-703, 2016.

[118] M. Obi, S. Jensen, J. B. Ferris, and R. B. Bass, "Calculation of levelized costs of electricity for various electrical energy storage systems," *Renewable and Sustainable Energy Reviews,* vol. 67, pp. 908-920, 2017.

[119] H. Khorasanizadeh, K. Mohammadi, and N. Goudarzi, "Prediction of horizontal diffuse solar radiation using clearness index based empirical models; A case study," *International Journal of Hydrogen Energy,* vol. 41, no. 47, pp. 21888-21898, 2016.

[120] C. M. Fernández-Peruchena and A. Bernardos, "A comparison of one-minute probability density distributions of global horizontal solar irradiance conditioned to the optical air mass and hourly averages in different climate zones," *Solar Energy,* vol. 112, pp. 425-436, 2015.

[121] L. Wang, O. Kisi, M. Zounemat-Kermani, G. A. Salazar, Z. Zhu, and W. Gong, "Solar radiation prediction using different techniques: model evaluation and comparison," *Renewable and Sustainable Energy Reviews,* vol. 61, pp. 384-397, 2016.

[122] A. Sanfilippo, L. Martin-Pomares, N. Mohandes, D. Perez-Astudillo, and D. Bachour, "An adaptive multi-modeling approach to solar nowcasting," *Solar Energy,* vol. 125, pp. 77-85, 2016.

[123] L. Wang, W. Gong, M. Luo, W. Wang, B. Hu, and M. Zhang, "Comparison of different UV models for cloud effect study," *Energy,* vol. 80, pp. 695-705, 2015.

[124] K. Bakirci, "Models for the estimation of diffuse solar radiation for typical cities in Turkey," *Energy,* vol. 82, pp. 827-838, 2015.

[125] T. E. Boukelia, M.-S. Mecibah, and I. E. Meriche, "General models for estimation of the monthly mean daily diffuse solar radiation (Case study: Algeria)," *Energy Conversion and Management,* vol. 81, pp. 211-219, 2014.

[126] A. Peled and J. Appelbaum, "Evaluation of solar radiation properties by statistical tools and wavelet analysis," *Renewable Energy,* vol. 59, pp. 30-38, 2013.

[127] Z. Ren, W. Yan, X. Zhao, W. Li, and J. Yu, "Chronological probability model of photovoltaic generation," *IEEE Transactions on Power Systems,* vol. 29, no. 3, pp. 1077-1088, 2014.

[128] C. Tiba, A. N. Siqueira, and N. Fraidenraich, "Cumulative distribution curves of daily clearness index in a southern tropical climate," *Renewable Energy,* vol. 32, no. 13, pp. 2161-2172, 2007.

[129] T. Ayodele and A. Ogunjuyigbe, "Prediction of monthly average global solar radiation based on statistical distribution of clearness index," *Energy,* vol. 90, pp. 1733-1742, 2015.

[130] S. Buhan and Y. Özkazanç, "Wind pattern recognition and reference wind mast data correlations with NWP for improved wind-electric power forecasts," *IEEE Transactions on Industrial Informatics,* vol. 12, no. 3, pp. 991-1004, 2016.

[131] C. S. Ioakimidis, L. J. Oliveira, and K. N. Genikomsakis, "Wind power forecasting in a residential location as part of the energy box management decision tool," *IEEE Transactions on Industrial Informatics,* vol. 10, no. 4, pp. 2103-2111, 2014.

[132] M. B. Ozkan and P. Karagoz, "A novel wind power forecast model: statistical hybrid wind power forecast technique (SHWIP)," *IEEE Transactions on Industrial Informatics,* vol. 11, no. 2, pp. 375-387, 2015.

[133] S. Harrouni, A. Guessoum, and A. Maafi, "Classification of daily solar irradiation by fractional analysis of 10-min-means of solar irradiance," *Theoretical and Applied Climatology,* vol. 80, no. 1, pp. 27-36, 2005.

[134] T. Soubdhan, R. Emilion, and R. Calif, "Classification of daily solar radiation distributions using a mixture of Dirichlet distributions," *Solar Energy,* vol. 83, no. 7, pp. 1056-1063, 2009.

[135] M. Muselli, P. Poggi, G. Notton, and A. Louche, "Classification of typical meteorological days from global irradiation records and comparison between two Mediterranean coastal sites in Corsica Island," *Energy Conversion and Management,* vol. 41, no. 10, pp. 1043-1063, 2000.

[136] F. A. Potra and S. J. Wright, "Interior-point methods," *Journal of Computational and Applied Mathematics,* vol. 124, no. 1, pp. 281-302, 2000.

[137] L. L. Lai, *Intelligent system applications in power engineering: Evolutionary programming and neural networks*. John Wiley & Sons, Inc., 1998.

[138] K. Y. Lee and M. A. El-Sharkawi, *Modern heuristic optimization techniques: Theory and applications to power systems*. John Wiley & Sons, 2008.

[139] C. Bogani, M. Gasparo, and A. Papini, "Generalized pattern search methods for a class of nonsmooth optimization problems with structure," *Journal of Computational and Applied Mathematics,* vol. 229, no. 1, pp. 283-293, 2009.

[140] S. H. El-Hefnawi, "Photovoltaic diesel-generator hybrid power system sizing," *Renewable Energy,* vol. 13, no. 1, pp. 33-40, 1998.

[141] S. Rehman and L. M. Al-Hadhrami, "Study of a solar PV–diesel–battery hybrid power system for a remotely located population near Rafha, Saudi Arabia," *Energy,* vol. 35, no. 12, pp. 4986-4995, 2010.

[142] Homer Energy, [Online]. Available: http://www.homerenergy.com/software.html [Accessed: 08.08.2017].

[143] O. Erdinc and M. Uzunoglu, "Optimum design of hybrid renewable energy systems: Overview of different approaches," *Renewable and Sustainable Energy Reviews,* vol. 16, no. 3, pp. 1412-1425, 2012.

[144] L. Xu, X. Ruan, C. Mao, B. Zhang, and Y. Luo, "An improved optimal sizing method for wind-solar-battery hybrid power system," *IEEE Transactions on Sustainable Energy,* vol. 4, no. 3, pp. 774-785, 2013.

[145] S. Shaahid and M. Elhadidy, "Economic analysis of hybrid photovoltaic–diesel–battery power systems for residential loads in hot regions—A step to clean future," *Renewable and Sustainable Energy Reviews,* vol. 12, no. 2, pp. 488-503, 2008.

[146] S. Shaahid and M. Elhadidy, "Technical and economic assessment of grid-independent hybrid photovoltaic–diesel–battery power systems for commercial loads in desert environments," *Renewable and Sustainable Energy Reviews,* vol. 11, no. 8, pp. 1794-1810, 2007.

[147] S. Singh and S. C. Kaushik, "Optimal sizing of grid integrated hybrid PV-biomass energy system using artificial bee colony algorithm," *IET Renewable Power Generation,* vol. 10, no. 5, pp. 642-650, 2016.

[148] Y.-Y. Hong and R.-C. Lian, "Optimal sizing of hybrid wind/PV/diesel generation in a stand-alone power system using Markov-based genetic algorithm," *IEEE Transactions on Power Delivery,* vol. 27, no. 2, pp. 640-647, 2012.

[149] Z. Moradi-Shahrbabak, A. Tabesh, and G. R. Yousefi, "Economical design of utility-scale photovoltaic power plants with optimum availability," *IEEE Transactions on Industrial Electronics,* vol. 61, no. 7, pp. 3399-3406, 2014.

[150] F. Kazhamiaka, C. Rosenberg, and S. Keshav, "Practical strategies for storage operation in energy systems: design and evaluation," *IEEE Transactions on Sustainable Energy,* vol. 7, no. 4, pp. 1602-1610, 2016.

[151] W. Su, J. Wang, and J. Roh, "Stochastic energy scheduling in microgrids with intermittent renewable energy resources," *IEEE Transactions on Smart Grid,* vol. 5, no. 4, pp. 1876-1883, 2014.

[152] B. Zhou, X. Liu, Y. Cao, C. Li, C. Y. Chung, and K. W. Chan, "Optimal scheduling of virtual power plant with battery degradation cost," *IET Generation, Transmission & Distribution,* vol. 10, no. 3, pp. 712-725, 2016.

[153] Z. Zhang, J. Wang, and X. Wang, "An improved charging/discharging strategy of lithium batteries considering depreciation cost in day-ahead microgrid scheduling," *Energy Conversion and Management,* vol. 105, pp. 675-684, 2015.

[154] Y. Zheng, Z. Y. Dong, F. J. Luo, K. Meng, J. Qiu, and K. P. Wong, "Optimal allocation of energy storage system for risk mitigation of DISCOs with high renewable penetrations," *IEEE Transactions on Power Systems,* vol. 29, no. 1, pp. 212-220, 2014.

[155] H. de Vries, T. T. Nguyen, and B. O. het Veld, "Increasing the cycle life of lithium ion cells by partial state of charge cycling," *Microelectronics Reliability,* vol. 55, no. 11, pp. 2247-2253, 2015.

[156] S. Saxena, C. Hendricks, and M. Pecht, "Cycle life testing and modeling of graphite/$LiCoO_2$ cells under different state of charge ranges," *Journal of Power Sources,* vol. 327, pp. 394-400, 2016.

[157] A. Ahmadian, M. Sedghi, B. Mohammadi-ivatloo, A. Elkamel, M. A. Golkar, and M. W. Fowler, "Cost-benefit analysis of V2G implementation in distribution networks considering PEVs battery degradation," *IEEE Transactions on Sustainable Energy,* vol. 9, pp. 961-970, 2017.

[158] C. Bordin, H. O. Anuta, A. Crossland, I. L. Gutierrez, C. J. Dent, and D. Vigo, "A linear programming approach for battery degradation analysis and optimization in offgrid power systems with solar energy integration," *Renewable Energy,* vol. 101, pp. 417-430, 2017.

[159] A. Hoke, A. Brissette, K. Smith, A. Pratt, and D. Maksimovic, "Accounting for lithium-ion battery degradation in electric vehicle charging optimization," *IEEE Journal of Emerging and Selected Topics in Power Electronics,* vol. 2, no. 3, pp. 691-700, 2014.

[160] A. Yoshida, T. Sato, Y. Amano, and K. Ito, "Impact of electric battery degradation on cost-and energy-saving characteristics of a residential photovoltaic system," *Energy and Buildings,* vol. 124, pp. 265-272, 2016.

[161] M. G. Ippolito, M. L. Di Silvestre, E. R. Sanseverino, G. Zizzo, and G. Graditi, "Multi-objective optimized management of electrical energy storage systems in an islanded network with renewable energy sources under different design scenarios," *Energy,* vol. 64, pp. 648-662, 2014.

[162] R. K. Akikur, R. Saidur, H. W. Ping, and K. R. Ullah, "Comparative study of stand-alone and hybrid solar energy systems suitable for off-grid rural electrification: A review," *Renewable and Sustainable Energy Reviews,* vol. 27, pp. 738-752, 2013.

[163] A. T. D. Perera, V. M. Nik, D. Mauree, and J.-L. Scartezzini, "Electrical hubs: An effective way to integrate non-dispatchable renewable energy sources with minimum impact to the grid," *Applied Energy,* vol. 190, pp. 232-248, 2017.

[164] J. Sachs and O. Sawodny, "A two-stage model predictive control strategy for economic diesel-pv-battery island microgrid operation in rural areas," *IEEE Transactions on Sustainable Energy,* vol. 7, no. 3, pp. 903-913, 2016.

[165] A.-S. Hamedi and A. Rajabi-Ghahnavieh, "Explicit degradation modelling in optimal lead–acid battery use for photovoltaic systems," *IET Generation, Transmission & Distribution,* vol. 10, no. 4, pp. 1098-1106, 2016.

[166] E. Hittinger, T. Wiley, J. Kluza, and J. Whitacre, "Evaluating the value of batteries in microgrid electricity systems using an improved Energy Systems Model," *Energy Conversion and Management,* vol. 89, pp. 458-472, 2015.

[167] E. Telaretti, G. Graditi, M. Ippolito, and G. Zizzo, "Economic feasibility of stationary electrochemical storages for electric bill management applications: The Italian scenario," *Energy Policy,* vol. 94, pp. 126-137, 2016.

[168] G. Graditi, M. Ippolito, E. Telaretti, and G. Zizzo, "Technical and economical assessment of distributed electrochemical storages for load shifting applications: An Italian case study," *Renewable and Sustainable Energy Reviews,* vol. 57, pp. 515-523, 2016.

[169] C. Budischak, D. Sewell, H. Thomson, L. Mach, D. E. Veron, and W. Kempton, "Cost-minimized combinations of wind power, solar power and electrochemical storage, powering the grid up to 99.9% of the time," *Journal of Power Sources,* vol. 225, pp. 60-74, 2013.

[170] R. Rajbongshi, D. Borgohain, and S. Mahapatra, "Optimization of PV-biomass-diesel and grid base hybrid energy systems for rural electrification by using HOMER," *Energy,* vol. 126, pp. 461-474, 2017.

[171] Y. Zhang, A. Lundblad, P. E. Campana, F. Benavente, and J. Yan, "Battery sizing and rule-based operation of grid-connected photovoltaic-battery system: A case study in Sweden," *Energy Conversion and Management,* vol. 133, pp. 249-263, 2017.

[172] S. Mandelli, C. Brivio, E. Colombo, and M. Merlo, "A sizing methodology based on levelized cost of supplied and lost energy for off-grid rural electrification systems," *Renewable Energy,* vol. 89, pp. 475-488, 2016.

[173] G. Allan, M. Gilmartin, P. McGregor, and K. Swales, "Levelised costs of wave and tidal energy in the UK: Cost competitiveness and the importance of "banded" Renewables Obligation Certificates," *Energy Policy,* vol. 39, no. 1, pp. 23-39, 2011.

[174] K. Branker, M. Pathak, and J. M. Pearce, "A review of solar photovoltaic levelized cost of electricity," *Renewable and Sustainable Energy Reviews,* vol. 15, no. 9, pp. 4470-4482, 2011.

[175] W. Short, D. J. Packey, and T. Holt, *A manual for the economic evaluation of energy efficiency and renewable energy technologies*. University Press of the Pacific, 2005.

[176] Skye Instruments Ltd, "SKS 1110 Pyranometer". [Online]. Available: http://www.skyeinstruments.info/index_htm_files/Pyranometer.pdf [Accessed: 03.08.2017].

[177] G. Kidegho and M. Mbogho, "A study of an urban domestic composite load model suitable for solar PV and grid hybrid system," in *Scientific Conference Proceedings*, 2010. [Online]. Available: http://journals.jkuat.ac.ke/index.php/jscp/article/view/701 [Accessed: 10.08.2017].

[178] "Updated least cost power development plan study period: 2011-2031," The Ministry of Energy, Kenya, 2011. [Online]. Available: https://renewableenergy.go.ke/downloads/studies/LCPDP-2011-2030-Study.pdf [Accessed: 10.08.2017].

[179] "Kenya's weather and average temperatures," tripsavvy, [Online]. Available: https://www.tripsavvy.com/kenya-weather-and-average-temperatures-4071455 [Accessed: 10.08.2017].

[180] N. Moksnes, A. Korkovelos, D. Mentis, and M. Howells, "Electrification pathways for Kenya–linking spatial electrification analysis and medium to long term energy planning," *Environmental Research Letters,* vol. 12, no. 9, p. 095008, 2017.

[181] A. Rose, R. Stoner, and I. Pérez-Arriaga, "Prospects for grid-connected solar PV in Kenya: A systems approach," *Applied Energy,* vol. 161, pp. 583-590, 2016.

[182] "2006 Electricity supply statistics for South Africa," National Energy Regulator of South Africa. [Online]. Available: http://www.nersa.org.za/Admin/Document/Editor/file/News and Publications/Publications/Current Issues/Electricity Supply Statistics/Electricity supply statistics 2006.pdf [Accessed: 03.08.2017].

[183] "Electricity supply statistics 2001 for South Africa," National Electricity Regulator. [Online]. Available: http://www.nersa.org.za/Admin/Document/Editor/file/News%20and%20Publications/Publications/Archived%20Issues/Electricity%20Supply%20Statistics/ESS2001_o.pdf [Accessed: 10.08.2017].

[184] J. Ondraczek, "Are we there yet? Improving solar PV economics and power planning in developing countries: The case of Kenya," *Renewable and Sustainable Energy Reviews,* vol. 30, pp. 604-615, 2014.

[185] D. Liu, W. Xie, H. Liao, and Y. Peng, "An integrated probabilistic approach to lithium-ion battery remaining useful life estimation," *IEEE Transactions on Instrumentation and Measurement,* vol. 64, no. 3, pp. 660-670, 2015.

[186] A. Saez-de-Ibarra, E. Martinez-Laserna, D.-I. Stroe, M. Swierczynski, and P. Rodriguez, "Sizing study of second life Li-ion batteries for enhancing renewable energy grid integration," *IEEE Transactions on Industry Applications,* vol. 52, no. 6, pp. 4999-5008, 2016.

[187] A. Hassan, M. Saadawi, M. Kandil, and M. Saeed, "Modified particle swarm optimisation technique for optimal design of small renewable energy system supplying a specific load at Mansoura University," *IET Renewable Power Generation,* vol. 9, no. 5, pp. 474-483, 2015.

[188] R. M. Swanson, "A vision for crystalline silicon photovoltaics," *Progress in photovoltaics: Research and Applications,* vol. 14, no. 5, pp. 443-453, 2006.

[189] "CREST cost of energy model: Photovoltaic V1.4," National Renewable Energy Laboratory (NREL). [Online]. Available: https://financere.nrel.gov/finance/content/crest-cost-energy-models [Accessed: 03.08.2017].

[190] R. Dufo-López, E. Pérez-Cebollada, J. L. Bernal-Agustín, and I. Martínez-Ruiz, "Optimisation of energy supply at off-grid healthcare facilities using Monte Carlo simulation," *Energy Conversion and Management,* vol. 113, pp. 321-330, 2016.

[191] Prepared for the committee on climate change, "Discount rates for low-carbon and renewable generation technologies," Oxera, [Online]. Available: http://www.oxera.com/Latest-Thinking/Publications/Reports/2011/Discount-rates-for-low-carbon-and-renewable-genera.aspx [Accessed: 10.08.2017].

[192] L. Wang, G. A. Salazar, W. Gong, S. Peng, L. Zou, and A. Lin, "An improved method for estimating the Ångström turbidity coefficient β in Central China during 1961-2010," *Energy,* vol. 81, no. 1, pp. 67-73, 2015.

[193] K. Scharmer and J. Greif, *The European solar radiation atlas Vol. 1: Fundamentals and maps*, École des Mines de Paris, 2000.

[194] T. Hove and E. Manyumbu, "Estimates of the Linke turbidity factor over Zimbabwe using ground-measured clear-sky global solar radiation and sunshine records based on

a modified ESRA clear-sky model approach," *Renewable Energy,* vol. 52, pp. 190-196, 2013.

[195] F. Kasten, "The Linke turbidity factor based on improved values of the integral Rayleigh optical thickness," *Solar Energy,* vol. 56, no. 3, pp. 239-244, 1996.

[196] P. Hedelin and J. Skoglund, "Vector quantization based on Gaussian mixture models," *IEEE Transactions on Speech and Audio Processing,* vol. 8, no. 4, pp. 385-401, 2000.

[197] M.-S. Yang, C.-Y. Lai, and C.-Y. Lin, "A robust EM clustering algorithm for Gaussian mixture models," *Pattern Recognition,* vol. 45, no. 11, pp. 3950-3961, 2012.

[198] T. W. Liao, "Clustering of time series data—A survey," *Pattern Recognition,* vol. 38, no. 11, pp. 1857-1874, 2005.

[199] U. Mori, A. Mendiburu, and J. A. Lozano, "Similarity measure selection for clustering time series databases," *IEEE Transactions on Knowledge and Data Engineering,* vol. 28, no. 1, pp. 181-195, 2016.

[200] R. C. de Amorim and C. Hennig, "Recovering the number of clusters in data sets with noise features using feature rescaling factors," *Information Sciences,* vol. 324, pp. 126-145, 2015.

[201] H. Izakian, W. Pedrycz, and I. Jamal, "Fuzzy clustering of time series data using dynamic time warping distance," *Engineering Applications of Artificial Intelligence,* vol. 39, pp. 235-244, 2015.

[202] F. Petitjean, A. Ketterlin, and P. Gançarski, "A global averaging method for dynamic time warping, with applications to clustering," *Pattern Recognition,* vol. 44, no. 3, pp. 678-693, 2011.

[203] C. Zhu and D. Gao, "Multiple matrix learning machine with five aspects of pattern information," *Knowledge-Based Systems,* vol. 83, pp. 13-31, 2015.

[204] J. F. Kolen and T. Hutcheson, "Reducing the time complexity of the fuzzy c-means algorithm," *IEEE Transactions on Fuzzy Systems,* vol. 10, no. 2, pp. 263-267, 2002.

[205] C. Bouveyron, S. Girard, and C. Schmid, "High-dimensional data clustering," *Computational Statistics & Data Analysis,* vol. 52, no. 1, pp. 502-519, 2007.

[206] C. Bouveyron and C. Brunet-Saumard, "Model-based clustering of high-dimensional data: A review," *Computational Statistics & Data Analysis,* vol. 71, pp. 52-78, 2014.

[207] S. Agrawal, B. Panigrahi, and M. K. Tiwari, "Multiobjective particle swarm algorithm with fuzzy clustering for electrical power dispatch," *IEEE Transactions on Evolutionary Computation,* vol. 12, no. 5, pp. 529-541, 2008.

[208] X. Huang, Y. Ye, and H. Zhang, "Extensions of kmeans-type algorithms: A new clustering framework by integrating intracluster compactness and intercluster separation," *IEEE Transactions on Neural Networks and Learning Systems,* vol. 25, no. 8, pp. 1433-1446, 2014.

[209] "Historical data," Weatherunderground.com, [Online]. Available: https://www.wunderground.com/history/. [Accessed: 03.08.2017].

[210] "Weather glossary - terms & definitions," timeanddate.com. [Online]. Available: https://www.timeanddate.com/weather/glossary.html [Accessed: 03.08.2017].

[211] M. Asif and T. Muneer, "Energy supply, its demand and security issues for developed and emerging economies," *Renewable and Sustainable Energy Reviews,* vol. 11, no. 7, pp. 1388-1413, 2007.

[212] "Energy security," International Energy Agency, [Online]. Available: https://www.iea.org/topics/energysecurity/ [Accessed: 03.02.2017].

[213] M. A. Gonzalez-Salazar, T. Kirsten, and L. Prchlik, "Review of the operational flexibility and emissions of gas-and coal-fired power plants in a future with growing

renewables," *Renewable and Sustainable Energy Reviews,* vol. 82 part 1, pp. 1497-1513, 2017.

[214] R&D Construction Ltd, "R&D wins Renewable Project for a 2.4 Megawatt Anaerobic Digestion Plant". [Online]. Available: http://www.randdconstruction.co.uk/rd-wins-renewable-project-for-a-2-4-megawatt-anaerobic-digestion-plant [Accessed: 03.08.2017].

[215] H. Gooi, D. Mendes, K. Bell, and D. Kirschen, "Optimal scheduling of spinning reserve," *IEEE Transactions on Power Systems,* vol. 14, no. 4, pp. 1485-1492, 1999.

[216] J. A. Momoh, *Adaptive stochastic optimization techniques with applications*. CRC Press, 2015.

[217] W. Li, *Risk assessment of power systems: models, methods, and applications*. John Wiley & Sons, 2014.

[218] P. Dagnely, E. Tsiporkova, T. Tourwé, T. Ruette, K. De Brabandere, and F. Assiandi, "A semantic model of events for integrating photovoltaic monitoring data," in *Industrial Informatics (INDIN), 2015 IEEE 13th International Conference on*, 2015, pp. 24-30: IEEE.

[219] M. Liserre, R. Teodorescu, and F. Blaabjerg, "Stability of photovoltaic and wind turbine grid-connected inverters for a large set of grid impedance values," *IEEE Transactions on Power Electronics,* vol. 21, no. 1, pp. 263-272, 2006.

[220] M. Meinhardt and G. Cramer, "Past, present and future of grid connected photovoltaic- and hybrid-power-systems," in *Power Engineering Society Summer Meeting, 2000. IEEE*, 2000, vol. 2, pp. 1283-1288: IEEE.

[221] X. Qiu, T. A. Nguyen, J. D. Guggenberger, M. L. Crow, and A. C. Elmore, "A field validated model of a vanadium redox flow battery for microgrids," *IEEE Transactions on Smart Grid,* vol. 5, no. 4, pp. 1592-1601, 2014.

[222] "Flexmax 60/80: Continuous MPPT charge controllers," OutBack Power, 2017. [Online]. Available: http://www.outbackpower.com/downloads/documents/charge_controllers/flexmax_6080/specsheet.pdf [Accessed: 03.02.2017].

[223] "First AD biogas plant opens in Kenya", The Association for Decentralised Energy, 2015, [Online]. Available: http://www.theade.co.uk/first-adbiogas-plant-opens-in-kenya_3412.html [Accessed: 02.08.2017].

[224] "CREST cost of energy model: Anaerobic digestion V1.4," National Renewable Energy Laboratory (NREL). [Online]. Available: https://financere.nrel.gov/finance/content/crest-cost-energy-models [Accessed: 10.08.2017].

[225] G. Petrone, G. Spagnuolo, R. Teodorescu, M. Veerachary, and M. Vitelli, "Reliability issues in photovoltaic power processing systems," *IEEE Transactions on Industrial Electronics,* vol. 55, no. 7, pp. 2569-2580, 2008.

[226] C. S. Lai and M. D. McCulloch, "Sizing of stand-alone solar PV and storage system with anaerobic digestion biogas power plants," *IEEE Transactions on Industrial Electronics,* vol. 64, no. 3, pp. 2112-2121, 2017.

[227] "G3512E Caterpillar Gas engine technical data, Ref. Data Set DM8811-06-001," Industrial Motor Power Corporation, 2013. [Online]. Available: http://attachments.impcorporation.com/21373414/Performance Data G3512E.pdf [Accessed: 10.08.2017].

[228] T. A. Nguyen and M. Crow, "Stochastic optimization of renewable-based microgrid operation incorporating battery operating cost," *IEEE Transactions on Power Systems,* vol. 31, no. 3, pp. 2289-2296, 2016.

[229] J. C. Beddoes, K. S. Bracmort, R. T. Burns, and W. F. Lazarus, "An analysis of energy production costs from anaerobic digestion systems on US livestock production facilities," *USDA NRCS Technical Note,* no. 1, 2007.

[230] J. Wang, P. Liu, J. Hicks-Garner, E. Sherman, S. Soukiazian, M. Verbrugge*, et al.*, "Cycle-life model for graphite-$LiFePO_4$ cells," *Journal of Power Sources,* vol. 196, pp. 3942-3948, 2011.

[231] S. Watanabe, M. Kinoshita, T. Hosokawa, K. Morigaki, and K. Nakura, "Capacity fading of $LiAl_yNi_{1-x-y}Co_xO_2$ cathode for lithium-ion batteries during accelerated calendar and cycle life tests (effect of depth of discharge in charge–discharge cycling on the suppression of the micro-crack generation of $LiAl_yNi_{1-x-y}Co_xO_2$ particle)," *Journal of Power Sources,* vol. 260, pp. 50-56, 2014.

[232] T. P. Hanusa, *The lightest metals: Science and technology from Lithium to Calcium*. John Wiley & Sons, 2015.